Morten Breivik

Topics in Guided Motion Control of Marine Vehicles

Thesis for the degree of philosophiae doctor

Trondheim, June 2010

Norwegian University of Science and Technology
Faculty of Information Technology, Mathematics and Electrical Engineering
Department of Engineering Cybernetics

NTNU
Norwegian University of Science and Technology

Thesis for the degree of philosophiae doctor

Faculty of Information Technology, Mathematics and Electrical Engineering
Department of Engineering Cybernetics

ISBN 978-82-471-2084-2 (printed ver.)
ISBN 978-82-471-2085-9 (electronic ver.)
ISSN 1503-8181

ITK Report 2010-7-W

Doctoral Theses at NTNU, 2010:63

Printed by Tapir Uttrykk

This thesis is dedicated to my wife Siri as a token of my love and admiration.

Summary

A mix between a monograph and an article collection, this PhD thesis considers the concept of guided motion control for marine vehicles, in particular focusing on underactuated marine surface vehicles. The motion control scheme is defined to involve the combination of a guidance system which issues meaningful velocity commands with a velocity control system which has been specifically designed to take vehicle maneuverability and agility constraints into account when fulfilling these commands such that a given motion control objective can be achieved in a controlled and feasible manner without driving the vehicle actuators to saturation.

Furthermore, motion control scenarios are classified in a novel way according to whether they involve desired motion which has been defined a priori or not. Consequently, in addition to the classical scenarios of point stabilization, trajectory tracking, path following and maneuvering, the so-called target tracking scenario is considered. The resulting scenarios then involve target tracking, path following, path tracking and path maneuvering. In addition, it is proposed to define the control objectives associated with each scenario as work-space tasks instead of configuration-space tasks. Such a choice seems better suited for practical applications, since most vehicles operate in an underactuated configuration exposed to some kind of environmental disturbances.

The thesis also proposes a novel mechanization of constant bearing guidance, which is a classical guidance principle well-known in the guided missile literature. This suggestion is motivated by a need to solve the target tracking motion control objective for marine vehicles. The proposed implementation enables explicit specification of the transient rendezvous behavior toward the target by selection of two intuitive tuning parameters.

In addition, a singularity-free guidance law applicable to path following scenarios involving regularly parameterized paths which do not need to be arc-length parameterized is proposed. An extension to this guidance law is also suggested in order to enable off-path traversing of regularly parameterized paths for formation control purposes.

A novel velocity control system which inherently takes maneuverability, agility and actuator constraints into account is developed for the purpose of controlling underactuated marine vehicles moving at high speed. The system is derived through a design method which involves a control-oriented modeling approach and requires a minimum of system identification tests to be carried out.

The thesis also gives a novel overview of the major developments in marine control systems as seen from a Norwegian perspective. The development can be viewed as three waves of control, where the first wave concerned development of novel ship automation technology in the 1960s and 1970s, the second wave involved development of unique dynamic positioning systems in the 1970s and 1980s, while the third wave is expected to encompass the development of unmanned vehicle technology for a large number of maritime applications.

A summary of the historical development, present status and future possibilities associated with unmanned surface vehicles (USVs) is also given. Current Norwegian activities are particularly emphasized.

Furthermore, an overview of the main formation control concepts applicable to marine surface vehicles is given. A novel formation control functionality named coordinated target tracking is subsequently suggested within a leader-follower framework. Employing a guided motion control system using the suggested mechanization of constant bearing guidance, this functionality is then implemented for two different types of underactuated USVs such that they are able to move in formation with a leader vessel which can maneuver freely without being constrained to any predefined motion pattern.

In particular, excerpts from successful full-scale formation control experiments involving a manned leader vessel and the two USVs executing coordinated target tracking at high speed are presented. This functionality currently seems to be unique on a worldwide basis, providing a convenient plug-and-play formation control capability for manned leader vessels involved in maritime survey operations.

Preface

This thesis is based on research carried out in the period July 2003 through December 2009. From July 2003 through June 2006 my work was financed by a PhD scholarship sponsored by the Norwegian Research Council (NFR) through the Centre for Ships and Ocean Structures (CeSOS) at the Norwegian University of Science and Technology (NTNU) in Trondheim, Norway. From July 2006 through June 2008 I worked as a temporarily engaged assistant professor at the Department of Engineering Cybernetics (ITK) at NTNU, while I have been working partly as a temporarily appointed assistant professor at NTNU's Department of Marine Technology (IMT) and partly as a researcher at CeSOS since July 2008. In addition, I have worked as a scientific advisor for the Trondheim-based company Maritime Robotics from June 2007 through December 2008 on the NFR-sponsored project "175977: Unmanned Surface Vehicle". The financial support from these institutions is gratefully acknowledged.

I would particularly like to thank Professor Thor I. Fossen for originally convincing me to embark on a PhD study and for serving as my thesis supervisor. I consider myself very fortunate and privileged to have been brought up professionally under his wings. He has provided me with the freedom to pursue my own ideas, has given me the possibility to travel around the world, and has been very efficient and helpful in dealing with practical issues concerning financing and bureaucracy during my studies. Without his invaluable guidance and continued support, I would not have been where I am today.

I would also like to thank Professor Roger Skjetne for inspiring me to start my PhD study through his work on maneuvering theory and his advisory role during the work with my MSc thesis. Professor Asgeir J. Sørensen is also thanked for his great advice and continued support during my time at NTNU. In addition, I would like to thank Professor Torgeir Moan, the director of CeSOS, for always having an open door and his willingness to support unconventional research topics.

Furthermore, I would like to thank Professor Andrew R. Teel for inviting me to visit the Center for Control Engineering and Computation (CCEC) at the University of California, Santa Barbara (UCSB) in the period September 2005 through April 2006. The US-Norway Fulbright Foundation for Educational Exchange is gratefully acknowledged for financing my stay in the US. Special thanks is due to Maxim V. Subbotin for our joint work on guided formation control as well as the UCSB College Republicans and the International Students Association at UCSB for giving me many fun moments during my stay in California. Richard Schuh is also thanked for showing me just how hospitable Americans can be to newcomers, while Carlos Ortiz and his family always will have a special place in my heart after opening their home to me.

I've had a great time working with the crew at Maritime Robotics since 2007. This collaboration has given me invaluable insights into the relationship between theory and practice and the unique opportunity to test my motion control ideas in the real world. Many thanks are due to Vegard E. Hovstein, Arild Hepsø, Eirik E. Hovstein, Stein Johansen, Idar Petersen and Kristin Sundfør Schive.

In addition to those co-authors whose names are mentioned elsewhere in this Preface, I would especially like to acknowledge Jann Peter Strand, Renato Skejic, Alexey Pavlov, Gunnar Sand and Geir Hovland for their efforts on our joint publications.

My friends and colleagues at NTNU are thanked for providing a diverse, interesting and stimulating working environment up through the years, in particular Ivar Ihle, Johannes Tjønnås, Jostein Bakkeheim, Frank Jakobsen, Andrew Ross, Tristan Perez, Jerome Jouffroy, Jon Refsnes, Kari Unneland, Luca Pivano, Tu Duc Nguyen, Gullik Jensen, Christian Holden, Jørgen Hals, Roberto Galeazzi, Dominik Breu and Anastasios Lekkas. Thanks are also due to those who have joined for football practice each week, especially Torkel Hansen and Stefano Bertelli for organizing the training sessions.

I've also had the privilege of supervising many bright and creative MSc students on their project and thesis work, and would particularly like to mention Benjamin Golding, Jon Alme and Øivind Loe. My current group of MSc students should also be thanked for their eagerness and enthusiasm, including Jon-Erik Loberg, Øivind Kåre Kjerstad, Joakim Haugen, Vetle Vintervold and Per Nord.

The administrative staff consisting of Sigrid Bakken Wold and Karelle Gilbert at CeSOS and Tove K. B. Johnsen, Eva Amdahl and Unni Johansen at ITK are thanked for handling formal issues smoothly and efficiently.

Dr. Andrew Ross from MARINTEK, Professor Nadav Skjøndal-Bar from NTNU and Professor Craig A. Woolsey from Virginia Tech are also thanked for providing constructive comments and feedback which have improved the quality of this thesis.

Finally, I would like to thank my family for their continued support and encouragement throughout the years, especially my mother Tove and father Knut as well as my in-laws Anna and Thor. Tine is also acknowledged for helping me get the initial version of this thesis submitted on time. But most of all I am deeply grateful to my dear wife Siri without whom this thesis would not have been possible. Your love and support have carried me through the last hectic months leading up to its completion and I consider myself extremely fortunate to have met someone like you. Together we are dynamite!

Morten Breivik, May 2010

Abbreviations

AUV	Autonomous Underwater Vehicle
CB	Constant Bearing
CeSOS	Centre for Ships and Ocean Structures
CMI	Chr. Michelsen Institute
CMR	Christian Michelsen Research
COTS	Commercial Off The Shelf
DNV	Det Norske Veritas
DOF	Degree Of Freedom
DP	Dynamic Positioning
DTU	Technical University of Denmark
ECEF	Earth-Centered Earth-Fixed
ECI	Earth-Centered Inertial
GPS	Global Positioning System
IFAC	International Federation of Automatic Control
IMO	International Maritime Organization
IMT	Department of Marine Technology
ISR	Intelligence, Surveillance and Reconnaissance
ITK	Department of Engineering Cybernetics
KDA	Kongsberg Defence and Aerospace
KM	Kongsberg Maritime
KS	Kongsberg Seatex
KV	Kongsberg Weapons Factory
LOS	Line Of Sight
MARINTEK	Norwegian Marine Technology Research Institute
MC	Marine Cybernetics
MIC	Modeling, Identification and Control
MR	Maritime Robotics
MTC	Marine Technology Centre
NED	North-East-Down
NFR	Norwegian Research Council
NRK	Norwegian Broadcasting Corporation
NTH	Norwegian Institute of Technology
NTNU	Norwegian University of Science and Technology
PID	Proportional-Integral-Derivative
PN	Proportional Navigation
PP	Pure Pursuit
RIB	Rigid-Inflatable Boat
RRM	Rolls-Royce Marine

SNAME	Society of Naval Architects and Marine Engineers
SOLAS	International Convention for the Safety of Life at Sea
UAV	Unmanned Aerial Vehicle
UCSB	University of California, Santa Barbara
UGAS	Uniformly Globally Asymptotically Stable
UGES	Uniformly Globally Exponentially Stable
UGV	Unmanned Ground Vehicle
ULES	Uniformly Locally Exponentially Stable
USV	Unmanned Surface Vehicle
UUV	Unmanned Underwater Vehicle
VOC	Vessel Operational Condition
WMR	Wheeled Mobile Robot

Table of Contents

1. Introduction

This chapter provides some perspective to the work described in this thesis, presents a list of all the articles published during the course of my PhD study, states the main contributions I believe that the thesis has to offer, and finally presents an outline of the rest of the PhD thesis.

1.1. Background and Motivation

The work associated with this PhD thesis began almost immediately after I submitted my MSc thesis in June 2003 on "Nonlinear Maneuvering Control of Underactuated Ships" (Breivik 2003) at the Department of Engineering Cybernetics (Institutt for teknisk kybernetikk, ITK) at the Norwegian University of Science and Technology (Norges teknisk-naturvitenskapelige universitet, NTNU) in Trondheim, Norway.

As part of this thesis I contributed to my first conference paper on path following for ships (Fossen et al. 2003), which was the starting point of my PhD research. For the first time in my career, I went to an international conference where I had to give a presentation among fellow researchers from all around the world. It was a very useful experience to be "thrown to the lions" only a couple of months after commencing my PhD study, and it instantly made me feel part of a larger international research community. Almost needless to say, numerous conference trips followed.

Looking back at my original research plan, the main goal was stated as employing *"…nonlinear guidance and control theory together with physical intuition to try and create guidance and control systems for underactuated vessels which are applicable for industrial implementation."* My argument was that the sophisticated nonlinear motion control schemes proposed for underactuated vessels were unsuitable for practical implementation, in particular due to unrealistic assumptions about the vessel dynamics and a lack of robustness toward modeling uncertainties and environmental disturbances. I also pointed out that state-of-the-art industrial solutions mostly employed linear control strategies and thus had a considerable potential for improvement.

With this goal in sight, and influenced by the path-based maneuvering theory of my MSc thesis co-advisor Roger Skjetne (Skjetne 2005), I spent the period 2003-2005 investigating guidance and control systems for underactuated vehicles within a path following framework. This work culminated in the paper "Principles of Guidance-Based Path Following in 2D and 3D" (Breivik and Fossen 2005d), which focuses on the fundamental kinematic aspects of guidance laws designed for path following applications. Hence, I was still far from my goal of any industrial implementation.

In September 2005, I went to the University of California, Santa Barbara (UCSB) as a Fulbright scholar for 8 months. There I started looking into extending my previous work toward formation control applications involving coordinated control of multiple vehicles along predefined paths. Perhaps a sidetrack compared to my original research plan, this topic was nevertheless very hot at the time and also enabled me to participate at a workshop on group coordination and cooperative control which was held in Tromsø during the spring of 2006, see (Breivik et al. 2006b). Several papers on formation control later followed, mainly contributing at a fundamental kinematic level.

At the beginning of 2006, I published my first popularized account of marine motion control systems (Breivik 2006a), which is something I greatly enjoyed writing. I also finally started venturing outside the path-based framework I so far had been working within, and began exploring the problem of tracking a target point for which no future motion information is available. The first paper employing missile guidance concepts for marine target tracking purposes was subsequently published in the autumn of 2006, see (Breivik et al. 2006e). However, the main achievement was still at a kinematic level and not quite ready for industrial implementation.

My PhD scholarship at the Centre for Ships and Ocean Structures (CeSOS) also ended in 2006, running from July 2003 to June 2006. Having contributed to a total of 14 publications during this period, I was now in a good position to write my PhD thesis. However, fate would have it that I received an offer from ITK to be temporarily hired as an assistant professor for a period of two years, corresponding to the leave of absence of my supervisor Thor I. Fossen due to the establishment of Marine Cybernetics (MC). This pioneering company was founded in 2002 by four NTNU professors with extensive knowledge in modeling, simulation and control of marine systems, and is currently a world-leading supplier of independent testing of marine computer control systems based on hardware-in-the-loop (HIL) technology.

Submitting a preliminary PhD thesis in June 2006 as a requirement to start my new job, I began working at ITK the following month. The initial plan was to spend some more time polishing my research before finalizing my thesis, but I soon became engulfed in my new full-time position and the thesis did not materialize as originally intended.

Toward the end of 2006, my friend and colleague Tristan Perez, who at that time worked as a post-doctoral researcher at CeSOS, put me in contact with the small Trondheim-based company Maritime Robotics (MR). They were looking for collaborators from NTNU with skills in marine motion control and an interest in unmanned vehicles. After initial meetings with MR's Vegard Hovstein during the spring of 2007, I was hired as a scientific advisor from June 2007. This agreement represented

the start of a very fruitful academic-industrial cooperation as well as a unique possibility for me to finally realize my motion control ideas in practice.

I also began teaching my first course at NTNU during the spring of 2007. Titled "Guidance and Control", the course is mainly aimed at students doing their 4th year of MSc studies at ITK with a specialization in motion control. I was lucky to recruit 6 of these students for supervision in their upcoming project and thesis work, half of whom would consider problems related to unmanned surface vehicles (USVs). At the same time, I focused on developing a USV-based formation control system together with Maritime Robotics, and also continued to refine my missile guidance approach to marine motion control, see (Breivik and Fossen 2007b). However, as a result of my new and exciting challenges, the completion of my PhD thesis was postponed even further.

While supervising my MSc students during the spring of 2008, I taught the marine-oriented G&C course for a second time. During this period, I also became aware of the American fighter pilot and military strategist John Boyd and his concept of energy-maneuverability for fighter aircraft, see (Coram 2002). This concept and a further dive into literature on missile guidance and aircraft maneuverability inspired me to develop simple but robust velocity controllers for underactuated surface vessels which enabled my previously-developed guidance algorithms to finally be implemented in full scale.

Initial sea trials for the velocity controllers began in late June 2008 and successful tracking of a virtual target point moving on the sea surface was achieved with an underactuated USV one month later, see (Breivik et al. 2008c). I had finally achieved my original goal of creating nonlinear *"…guidance and control systems for underactuated vessels which are applicable for industrial implementation."* To achieve this goal, I had been forced to venture outside the marine control literature, which I felt had become stuck in its simplifying assumptions regarding vessel dynamics and environmental disturbances for the academic goal of obtaining theoretical proofs for closed-loop stability. This journey also changed my view of how control theory should be applied; focusing more on basic control-oriented models together with advanced feedback concepts rather than sophisticated model-based controllers whose performance rely heavily on uncertain feedforward terms.

My contract with ITK expired at the end of June 2008, but once again I was able to continue working at NTNU despite still not having finished my PhD thesis. While my supervisor Thor I. Fossen now returned to the university, his colleague and fellow MC co-founder Asgeir Sørensen needed to extend his leave of absence from NTNU's Department of Marine Technology (Institutt for marin teknikk, IMT) to continue as CEO of the company. As a result, I signed a new two-year contract where I was partly engaged as an assistant professor at IMT and partly as a researcher at my old PhD-

scholarship funder CeSOS, both collocated at the Marine Technology Centre (Marinteknisk senter, MTS) in Trondheim. It was naturally expected that I finalized my PhD thesis within a short time.

However, again I got caught up with my new position and found it far more interesting to pursue new challenges than writing up my thesis. I also continued to refine my algorithms for guided motion control of USVs in cooperation with MR. We soon came to the conclusion that it would be more flexible and industrially relevant to develop a formation control system based on the tracking of virtual target points defined relative to a manned leader vessel allowed to maneuver freely rather than constrained to some predefined path. Later termed coordinated target tracking, this functionality was first tried out in full scale when we hired NTNU's research vessel Gunnerus to play the role of a manned leader vessel in a sea trial toward the end of September 2008.

Figure 1: Taking some time off for a photo shoot, a content formation control designer hands over the challenging task of moving in formation with Gunnerus entirely to the USV.

Having solved some initial communication problems between the two formation members, the USV eventually began receiving reliable and timely motion data from Gunnerus, and the fun could start. For safety reasons, we were two people manning the USV during the sea trial; Arild Hepsø from MR and myself from NTNU. It was truly an exhilarating and memorable experience to be onboard the USV as it intercepted and rendezvoused with its virtual target point and continued to track this point tightly when Gunnerus began conducting unplanned port and starboard maneuvers. We could literally feel the USV living its own life as its engine noise rose and fell in synchronization with the maneuvers of its leader vessel. Partly described in (Breivik and

Evans 2009b) and (Breivik and Hovstein 2009c), these experiments seem to have been the first of their kind to be carried out in the world. In fact, I am still not aware of anyone else who has achieved target tracking for marine vehicles moving at high speed. However, my PhD thesis still represented unfinished business while new and exciting challenges constantly rose to the occasion.

Following the successful trials with the USV-based formation control system, I was asked to participate on an application to the Norwegian Research Council (Norges forskningsråd, NFR) concerning the use of unmanned aerial vehicles (UAVs) for maritime surveillance purposes in Arctic regions. Collaborating within a consortium led by the Kongsberg-based company Simicon and consisting of both end-users and technology developers, CeSOS was assigned to work on image processing and motion control problems. The application went through and the project got underway during the spring of 2009. One of the initial tasks was to properly coordinate the various work packages between the project participants. We also had to find someone suitable for working on the image processing tasks since CeSOS lacked previous experience within this highly important field. It obviously doesn't help to be in possession of sophisticated guidance and control algorithms if they are bereft of necessary motion information.

I also started teaching a new course as part of my duties as an assistant professor at IMT during the spring of 2009. Titled "Marine Control Systems", it was a more practically oriented subject than the G&C course I had previously been teaching at ITK. Also aimed at students doing their 4th year of MSc study with a specialization in marine cybernetics, the two courses were in fact taken in parallel by many due to their complementary content. Again, I was lucky to attract 5 highly motivated and skilled students to work on topics related to motion control of USVs in cooperation with Maritime Robotics. However, my PhD thesis was still left largely unattended.

During the same period, I was asked to serve as an associate editor of Norway's only technology journal Modeling, Identification and Control (MIC), which had recently risen from the ashes after almost being closed down at the beginning of its 30th year in operation. The new and dynamic editor Geir Hovland from the mechatronics group at the University of Agder (UiA) had revitalized the journal and converted it to an online, open access outlet for researchers affiliated with Nordic research institutions. Becoming responsible for the area of marine control systems and ship control, I also went on to co-edit the 30th-year anniversary issue of MIC which came out at the end of 2009. In this turn of events, I consider myself extremely fortunate. Being able to contribute to a biographical paper on Norway's grand old man in engineering cybernetics Jens Glad Balchen as well as a paper on trends in research and publication (Breivik and Sand 2009d; Breivik et al. 2009e), I finally found an outlet for my lifelong interest in technology history and the future prospects of science and research. It also didn't

exactly put a damper on my enthusiasm when Balchen's old friend and colleague Rudolf Kalman agreed to contribute with a guest editorial to the anniversary issue.

Further refinements to the USV-based formation control technology were also made during the summer of 2009. Only three days after my wedding in the middle of August, a team from the Norwegian Broadcasting Corporation (Norsk rikskringkasting, NRK) had decided to pay a visit in order to make a report on maritime robots and their potential capabilities. A whole day's worth of filming was compressed into a five-minute long feature which was sent on the Norwegian popular science show Schrødinger's Katt the following week, while I was away on my honeymoon. Needless to say, my wife did not allow me to watch this show until we had returned to Norway.

Figure 2: In August 2009, a team from the Norwegian broadcasting corporation NRK came on a visit to experience some unmanned action in the Trondheimsfjord.

Currently teaching the marine control systems course for the second time, supervising my current team of MSc students, participating in the Arctic UAV project, and fulfilling my other duties as an assistant professor at IMT and researcher at CeSOS, I have now finally prioritized the completion of my PhD thesis before it becomes too late. Considering that I have contributed to a total of 26 publications in the period July 2003 to December 2009, taught 3 different graduate-level courses a total of 7 times, and supervised a total of 12 students on their MSc thesis, it is definitely high time that my own PhD thesis soon becomes done and dusted. Having followed a highly unusual career path in this context, it has now become vital for me to obtain a PhD degree before I continue to take on new challenges. This document will hopefully help me achieve this task and also serve as a tool to put my current research efforts into a useful perspective.

1.2. List of Publications

As previously mentioned, I have contributed to a total of 26 publications in the period July 2003 to December 2009, including 2 book chapters, 3 journal papers, 1 magazine article and 20 conference papers. I am the first author of 21 of these contributions, the second author of 4, and the third author of 1.

Regarding declaration of authorship, I have done most of the work in those papers where I am the first author. My co-authors are gratefully acknowledged for providing constructive comments that have improved the content of these papers. As a second author, I have contributed strongly in all aspects of the papers, including concepts, theory, writing, illustrations, simulations, experiments, etc. Finally, as a third author I have been the one to provide constructive comments to the principal authors.

Grouped by type and sorted in reverse chronological order, a list of my contributed publications is given in the following:

Book Chapters

- [B02]: M. Breivik and T. I. Fossen. *Guidance Laws for Autonomous Underwater Vehicles*. In A. V. Inzartsev (Ed.), Underwater Vehicles, pp. 51-76. IN-TECH Education and Publishing, 2009.

- [B01]: M. Breivik, M. V. Subbotin and T. I. Fossen. *Kinematic Aspects of Guided Formation Control in 2D*. In K. Y. Pettersen, T. Gravdahl and H. Nijmeijer (Eds.), Group Coordination and Cooperative Control, Lecture Notes in Control and Information Systems, pp. 55-74. Springer-Verlag Heidelberg, 2006. doi:10.1007/11505532_4

Journal Papers

- [J03]: M. Breivik, G. Hovland and P. J. From. *Trends in Research and Publication: Science 2.0 and Open Access*. Modeling, Identification and Control, 2009. 30(3):181-190. doi:10.4173/mic.2009.3.8

- [J02]: M. Breivik and G. Sand. *Jens Glad Balchen: A Norwegian Pioneer in Engineering Cybernetics*. Modeling, Identification and Control, 2009. 30(3):101-125. doi:10.4173/mic.2009.3.2

- [J01]: M. Breivik, V. E. Hovstein, and T. I. Fossen. *Straight-Line Target Tracking for Unmanned Surface Vehicles*. Modeling, Identification and Control, 2008. 29(4):131-149. doi:10.4173/mic.2008.4.2

Magazine Articles

- [M01]: M. Breivik. *Marine Craft: 21st Century Motion Control Concepts*. Sea Technology, 2006. 47(3): 33-36.

Conference Papers

- [C20]: A. Pavlov, H. Nordahl, and M. Breivik. *MPC-Based Optimal Path Following for Underactuated Vessels*, in Proceedings of the 8th IFAC MCMC, Guarujá, Brazil, pp. 340-345, 2009.

- [C19]: J. Alme and M. Breivik. *Autotuning Aspects for Dynamic Positioning Systems*, in Proceedings of the 8th IFAC MCMC, Guarujá, Brazil, pp. 334-339, 2009.

- [C18]: R. Skejic, M. Breivik, T. I. Fossen, and O. M. Faltinsen. *Modeling and Control of Underway Replenishment Operations in Calm Water*, in Proceedings of the 8th IFAC MCMC, Guarujá, Brazil, pp. 78-85, 2009.

- [C17]: M. Breivik and V. E. Hovstein. *Guidance Systems for Motion Control of Unmanned Surface Vehicles*, in Proceedings of the NATO RTO SCI-202 Symposium, Neubiberg, Germany, 2009.

- [C16]: G. A. Jensen, M. Breivik and T. I. Fossen. *Offshore Pipelay Operations From a Control Perspective*, in Proceedings of the 28th ASME OMAE, Honolulu, Hawaii, USA, pp. 259-268, 2009. doi:10.1115/OMAE2009-79371

- [C15]: M. Breivik and T. I. Fossen. *Guidance Laws for Planar Motion Control*, in Proceedings of the 47th IEEE CDC, Cancun, Mexico, pp. 570-577, 2008.

- [C14]: M. Breivik, V. E. Hovstein, and T. I. Fossen. *Ship Formation Control: A Guided Leader-Follower Approach*, in Proceedings of the 17th IFAC World Congress, Seoul, Korea, pp. 16008-16014, 2008.

- [C13]: M. Breivik and T. I. Fossen. *Applying Missile Guidance Concepts to Motion Control of Marine Craft*, in Proceedings of the 7th IFAC CAMS, Bol, Croatia, 2007.

- [C12]: M. Breivik, M. V. Subbotin and T. I. Fossen. *Guided Formation Control for Wheeled Mobile Robots*, in Proceedings of the ICARCV'06, Singapore, pp. 1-7, 2006.

- [C11]: M. Breivik and T. I. Fossen. *Motion Control Concepts for Trajectory Tracking of Fully Actuated Ships*, in Proceedings of the 7th IFAC MCMC, Lisbon, Portugal, 2006.

- [C10]: M. Breivik, J. P. Strand and T. I. Fossen. *Guided Dynamic Positioning for Fully Actuated Marine Surface Vessels*, in Proceedings of the 7th IFAC MCMC, Lisbon, Portugal, 2006.

- [C09]: M. Breivik, M. V. Subbotin and T. I. Fossen. *Guided Formation Control for Fully Actuated Marine Surface Craft*, in Proceedings of the 7th IFAC MCMC, Lisbon, Portugal, 2006.

- [C08]: M. Breivik and T. I. Fossen. *A Unified Control Concept for Autonomous Underwater Vehicles*, in Proceedings of the ACC'06, Minneapolis, Minnesota, USA, pp. 4920-4926, 2006. doi:10.1109/ACC.2006.1657500

- [C07]: M. Breivik and T. I. Fossen. *Principles of Guidance-Based Path Following in 2D and 3D*, in Proceedings of the CDC-ECC'05, Seville, Spain, pp. 627-634, 2005. doi:10.1109/CDC.2005.1582226

- [C06]: M. Breivik and T. I. Fossen. *Guidance-Based Path Following for Autonomous Underwater Vehicles*, in Proceedings of the OCEANS'05, Washington D.C., USA, pp. 2807-2814, 2005. doi: 10.1109/OCEANS.2005.164020

- [C05]: M. Breivik and T. I. Fossen. *Guidance-Based Path Following for Wheeled Mobile Robots*, in Proceedings of the 16th IFAC World Congress, Prague, Czech Republic, pp. 13-18, 2005.

- [C04]: M. Breivik and T. I. Fossen. *A Unified Concept for Controlling a Marine Surface Vessel Through the Entire Speed Envelope*, in Proceedings of the ISIC-MED'05, Limassol, Cyprus, pp. 1518-1523, 2005. doi:10.1109/.2005.1469807

- [C03]: M. Breivik and T. I. Fossen. *Path Following for Marine Surface Vessels*, in Proceedings of the OTO'04, Kobe, Japan, pp. 2282-2289, 2004. doi:10.1109/OCEANS.2004.1406507

- [C02]: M. Breivik and T. I. Fossen. *Path Following of Straight Lines and Circles for Marine Surface Vessels*, in Proceedings of the 6th IFAC CAMS, Ancona, Italy, pp. 65-70, 2004.

- [C01]: T. I. Fossen, M. Breivik and R. Skjetne. *Line-of-Sight Path Following of Underactuated Marine Craft*, in Proceedings of the 6th IFAC MCMC, Girona, Spain, pp. 244-249, 2003.

More detailed comments about these papers and how they relate to each other are given in Chapter 6. In addition, 9 of the papers have been explicitly appended to the thesis in order to illustrate some of the main thrust of my work. These papers are [C01], [C04], [C10], [C11], [C14], [C18], [M01], [J01] and [B02].

Part of the work presented in this thesis has also been featured by NRK and reported in the research magazine Gemini, see (Schrødingers Katt 2009; Tveter 2010).

1.3. Main Contributions

The main contributions of this thesis are considered to be:

- Giving a novel overview of the major developments in marine control systems, rationalized in a Norwegian context. Proposing to view this development as three waves of control, where the first wave concerns development of groundbreaking ship automation systems in the 1960s and 1970s, the second wave involves development of novel dynamic positioning systems in the 1970s and 1980s, while the third wave is expected to encompass the development of unmanned vehicle technology for a large number of maritime applications.

- Proposing the concept of guided motion control, which is defined to involve the combination of a guidance system which issues meaningful velocity commands with a velocity control system which has been specifically designed to take vehicle maneuverability and agility constraints into account when fulfilling these commands such that a given motion control objective can be achieved in a controlled and feasible manner.

- Classifying a set of motion control scenarios according to whether they involve desired motion which has been defined a priori or not. Proposing to include the target tracking scenario in addition to the classical scenarios of point stabilization, trajectory tracking, path following and maneuvering. The resulting

scenarios then become target tracking, path following, path tracking and path maneuvering. In addition, it is proposed to define the control objectives associated with each scenario as work-space tasks instead of configuration-space tasks. Such a choice seems better suited for practical applications, where most vehicles operate in an underactuated configuration exposed to some kind of environmental disturbances.

- Proposing a novel mechanization of constant bearing guidance, which is a classical guidance principle reported in the guided missile literature. This proposition is motivated by a need to solve the target tracking motion control objective for marine vehicles. The suggested implementation makes it possible to explicitly specify the transient rendezvous behavior toward the target by selection of two intuitive tuning parameters.

- Suggesting a singularity-free guidance law applicable to path following scenarios involving regularly parameterized paths that do not need to be arc-length parameterized. Also proposing a synchronization-law extension of this guidance law to be able to handle path tracking scenarios. Interpreting the lookahead-based steering law associated with this guidance law as a saturated proportional control law, thus becoming aware of the possibilities to also include derivative and integral action depending on the considered application.

- Proposing a novel extension to the singularity-free guidance law involving two virtual particles in order to enable off-path traversing of regularly parameterized paths for formation control purposes.

- Suggesting novel velocity controllers for underactuated marine vehicles that inherently take maneuverability, agility and actuator constraints into account, derived through a novel design method which represents a control-oriented modeling approach and only requires a minimum of system identification tests to be carried out.

- Giving a summary of the historical development, present status and future possibilities associated with unmanned surface vehicles (USVs). Also giving an overview of current Norwegian efforts to develop such vehicles.

- Achieving the target tracking motion control objective for underactuated marine vehicles travelling at high speed by using the proposed guided motion control system, illustrated through full-scale experiments with underactuated USVs.

- Giving an overview of the main formation control concepts applicable to marine surface vehicles. Suggesting a novel formation control functionality denoted coordinated target tracking within a leader-follower framework, and implementing this functionality for two different types of USVs such that they are able to move in formation with a leader vessel whose future motion pattern is unknown. Presenting successful full-scale experimental results involving NTNU's research vessel Gunnerus and Maritime Robotics' two underactuated USVs when executing coordinated target tracking at high speed. This functionality currently seems to be unique in the world, providing a convenient plug-and-play formation control capability for manned leader vessels.

- Proposing a unified motion control concept suitable for controlling a marine vehicle seamlessly through its entire speed regime from full actuation at low speeds to underactuation at high speeds.

- Suggesting a modular motion control design procedure inspired by integrator backstepping and supported by nonlinear cascade theory which is suitable for both single and multiple marine vehicles.

- Contributing to cross-disciplinary work on underway replenishment operations where realistic ship-to-ship interaction effects are considered.

1.4. Thesis Outline

This PhD thesis is written as combination of a monograph and an article collection comprising a selection of 9 publications out a total contribution of 26. Focus has been put on marine surface vessel applications, which is also reflected through the choice of articles. These publications encompass content on both theory and practice as well as scale-model and full-scale experiments, and are located in appendices A-I following the introductory material contained in chapters 1-7. Making up the monograph part of the thesis, these chapters present some new results and perspectives, and also summarize the work that has been done so far by drawing a red thread through the publications. Since the introductory part is written to be more or less self-contained, some overlap with the article part will occur. However, the two parts mostly complement each other. The contents of the introductory part are outlined in the following.

Chapter 2 considers what I have termed the 3 waves of control. Rationalized in a Norwegian context, the 1st wave concerned the shipping business and resulted in development of unique ship automation systems, the 2nd wave concerned offshore activities and resulted in the development of world-leading dynamic positioning

systems, while the 3rd wave is still waiting to happen and will most certainly somehow involve unmanned vehicles.

Chapter 3 elaborates on the concept of guided motion control. Equally suitable for fully actuated and underactuated vehicles, this motion control framework considers the design of nonlinear guidance and velocity control systems which enable vehicles to accomplish a variety of motion control objectives in a feasible and controlled manner.

Chapter 4 takes a look at unmanned surface vehicles, a hitherto neglected type of unmanned vehicles which are suitable for carrying out a wide range of tasks at sea. An historical overview is given, the present status is reviewed and future challenges and possibilities are discussed. Then Norwegian efforts within the area are presented, in particular the fruitful collaboration between NTNU and the Trondheim-based company Maritime Robotics which has been ongoing since 2006.

Chapter 5 deals with the important topic of formation control, offering some general background to and motivation for its practical application. Specifically, a distinct and novel approach to formation control termed coordinated target tracking has been developed for unmanned surface vehicles. Implemented through a leader-follower framework, the scheme enables such vehicles to track the motion of a leader vessel which travels at high speed and whose future motion pattern is unknown. Excerpts from relevant full-scale experiments are included at the end of the chapter.

Chapter 6 explores the relation between my various publications and divides the performed research into two distinct periods, the first one concerning guided motion control algorithms for path following applications and the second period concerning algorithms for target tracking applications.

Finally, Chapter 7 offers some conclusions as well as views and recommendations for future work.

2. Waves of Control

Perhaps unbeknownst to many, the first theoretical analysis of the PID controller can be found in a paper concerning autopilots for ships (Minorsky 1922). Authored by the Russian-born electrical engineer Nicolas Minorsky, this paper represented a theoretical justification for the simultaneous practical work carried out by the American entrepreneur Elmer Sperry (Bennett 1984).

In 1911, Sperry had installed his first serially-produced gyrocompass aboard the US naval vessel USS Utah (Hughes 1971). The invention of the gyrocompass meant that, for the first time in history, the heading of a ship could be measured reliably. Following this technological breakthrough it did not take long until the first automatic steering device for ships was developed.

The same year as Minorsky published his paper, Sperry commenced field trials with his so-called gyropilot, a gyroscope-guided steering mechanism for ships. Popularly termed "Metal Mike", Sperry's gyropilot was used to control the Munson liner Munargo when it successfully made the roundtrip from New York to Cuba in October 1922. Captain Andrew Asborn enthusiastically characterized the performance as *"…a triumph of matter over mind,"* and also remarked that he was satisfied with a helmsman that *"…doesn't drink, smoke or kick about working overtime."* (Hughes 1971).

Although Sperry was unaware of Minorsky's work at the time, they together laid the theoretical and practical foundations for the successful application of ship autopilots in the following years. These contributions represented the starting point of a development which since has resulted in increasingly sophisticated marine control systems, until we are now at the brink of removing humans from the control loop altogether.

The next major advance in control-related ship technology did not arrive until the middle of the 1960s, when the small Norwegian company Norcontrol developed a groundbreaking mix of ship automation technology which resulted in unmanned engine rooms and radar-based anti-collision systems. Further developments were closely tied with advances in computer technology, opening up whole new vistas of possibilities and in particular enabling the introduction of nonlinear control concepts.

The rest of this chapter focuses on two major Norwegian contributions in the field of marine control systems, as well as a possible third one ascending on the horizon. For a long time, Norway has been a leading maritime nation in the world. Since the 1960s, the country has experienced two important periods with significant advances in control technology for the benefit of the marine industries, see (Breivik and Sand 2009d).

Figure 3: A fjord-based facility belonging to the Ocean Space Centre. Courtesy of Snøhetta/MIR.

As already implied, the first period concerned the shipping business and entailed development of advanced automation systems which improved the competitiveness of the Norwegian merchant fleet. Important contributions were given in the 1960s and 1970s. The second period was related to the discovery of oil and gas on the Norwegian continental shelf, and entailed the development of technology for dynamic positioning (DP) of offshore vessels required to operate in deep water and in bad weather. World-leading DP solutions were developed by Norwegians in the 1970s and 1980s.

Today, the maritime Norway once again finds itself on the threshold of a new period with extensive control-technological challenges. These challenges are particularly associated with the resource management of the country's northern maritime zones, areas that are extremely harsh and inhospitable to humans.

This characterization and classification runs analogous to the notion of the 3 waves recently put forth by the Norwegian Marine Technology Research Institute (MARINTEK). MARINTEK rationalizes in terms of its research infrastructure at Tyholt in Trondheim, stating that the 1st wave was associated with the contributions of the Towing Tank which opened in 1939. Its use gave increased insight into matters of hull design and propulsion efficiency, which significantly helped reduce fuel consumption and emissions for the shipping industry. The 2nd wave was related to the large Ocean Basin which was opened in 1980, and which has been an invaluable tool in developing technology for the purpose of offshore oil and gas activities. MARINTEK envisions the 3rd wave to concern future challenges related to managing an increasingly complex ocean space in an environmentally-friendly manner. Their proposal is to build a new research center in Trondheim termed the “Ocean Space Centre” to handle these challenges, see (Ocean Space Centre 2010). Figure 3 shows an artist’s impression of one of the center’s test facilities which is planned to be located in the Trondheimsfjord.

The following account will thus deal with the 3 waves as seen from a control perspective. The stories of the first 2 waves are taken from the biography of Jens Glad Balchen, a Norwegian research scientist and engineer who is widely regarded as the father of Engineering Cybernetics in Norway (Breivik and Sand 2009d). His participation was instrumental for both waves, and as stated by him in the biography: *"The period 1955-85 was the best in modern history. We then lay the foundations of what we have based our lives on since. It was during these years that Norway became the world's best country to live in."*

2.1. Wave 1: Ship Automation

In 1959, four young Norwegians visited the University of California, Berkeley (UC Berkeley) in the United States. Hailing from different research communities, the one thing they had in common was a vision for coupling automation technology with the Norwegian shipping industry. At this time, Norway had the fourth largest fleet in the world, but the ship owners were conservative and did not readily welcome technological changes.

Two of the Norwegians, managing director Jan Getz from the Institute for Ship Research (Skipsteknisk forskningsinstitutt, SFI) and NTNF[1] scholar Arild Økland, had a maritime background. The other two, servo enthusiasts Ibb Høivold from the Chr. Michelsen Institute (CMI) and Jens Glad Balchen from NTH[2], did not. This combination of backgrounds would prove to be very fruitful.

By chance, it was discovered that the US Maritime Administration had started an extensive investigation into ship automation technology. The ultimate goal was to develop an unmanned ship. A preliminary goal was to reduce ship crew by a third.

Already in March 1960, SFI applied to NTNF for funds to carry out a theoretical ship automation study. Being a trade institute for the shipping business, with shipbuilders, shipowners and the classification company Det Norske Veritas (DNV) as contributing

[1] In 1946, the Norwegian government established the Royal Norwegian Council for Scientific and Industrial Research (Norges teknisk-naturvitenskapelige forskningsråd, NTNF). NTNF was an independent agency tasked with promoting research for the benefit of Norwegian industry and society, both initiating and coordinating publicly funded research programs carried out by applied research institutes, universities and by the industry itself.

[2] The Norwegian Institute of Technology (Norges tekniske høgskole, NTH) was established in the city of Trondheim, Norway in 1910. NTH merged into the Norwegian University of Science and Technology (Norges teknisk-naturvitenskapelige universitet, NTNU) in 1996.

members, SFI envisioned an incremental development based on conventional automation equipment. Balchen and Høivold were a bit more ambitious and wanted to see computer-based automation technology in practical use as soon as possible.

Figure 4: Norsk Hydro's ammonia tanker M/S Haugvik was retrofitted with experimental automation technology to enable unmanned engine rooms. Courtesy of DNV.

After a visit by Høivold in the autumn of 1962, SFI invited its shipowners to place a vessel at the researchers' disposal for automation experiments. At first, no one was willing to take the risk. However, in 1963 Høivold was able to convince his new employer Norsk Hydro to make one of its ammonia tankers available, see Figure 4. As a result, NTNF granted funding for a new research project led by Høivold.

The main goal was to create an unmanned engine room onboard the M/S Haugvik. Project work was distributed among SFI, SINTEF[3], Norsk Hydro and DNV. For reasons of availability, applicability and reliability, conventional automation equipment was chosen over electronic components. In anticipation of suitable computer-based systems, a rapid development founded on well-known technology was pursued. Mixing the views of Getz and Økland with those of Balchen and Høivold, this choice proved to be a smart move and prepared the ground for the later introduction of more advanced technology.

In October 1964, an enthusiastic captain docked Haugvik by remote control. At this time, DNV had already begun evaluating the safety and reliability of the new installation. Early in 1966, the company's work resulted in a new class for automated

[3] The independent research organization SINTEF was founded in 1950 when the professors at NTH joined forces with the local municipality and industries in Trondheim. Today the largest in Scandinavia, the organization was originally formed to encourage industrially-oriented technology research at NTH.

ships, the “engine zero” (E0) class. E0 represented pioneering work and a world's first. More importantly, the class enabled industrial use of the newly developed technology.

Observing the progress of the Haugvik project, other Norwegian companies also wanted to get into the ship automation business. On the 1st of April 1965, Norsk Hydro joined forces with Kongsberg Weapons Factory (Kongsberg Våpenfabrikk, KV)[4] and the former nuclear energy-focused Noratom to establish Norcontrol.

Ibb Høivold was appointed general manager of the joint venture, which set up shop in the old naval town of Horten. The first product to be developed was a new bridge control system for E0. In 1967, the same year as the first order came, Norsk Hydro decided to withdraw as a partner. Shortly thereafter Noratom suggested a merger with Norcontrol, which went through in June 1967. The newly formed company had an impressive board, with 3 representatives from the shipping industry. Høivold became manager of the ship automation division.

Almost a year earlier, an application had been sent to NTNF for funding of a new trial project, this time for research on computerized ship automation. Jens Balchen strongly supported the project through his position in NTNF's Feedback Control Committee. Norcontrol was to be in charge, with SINTEF and SFI as collaborators. A few months before the merger with Noratom, NTNF granted money to the project. The time had come to move beyond conventional automation technology.

Soon the hunt for a test ship was underway. It turned out to be easier than with Haugvik. M/S Taimyr was a cargo liner under construction in Japan, contracted by the Norwegian shipowner Wilh. Wilhelmsen, who decided to support the new endeavor.

The project also needed a suitable computer. At this time, some researchers at the Norwegian Defence Research Establishment (Forsvarets forskningsinstitutt, FFI) had plans to commercialize promising new technology. In the autumn of 1967, Norcontrol aided in the establishment of Norsk Data (ND) by purchasing stocks and buying the new company's first computer NORD-1, a gamble which turned out to be very successful.

The Taimyr project resulted in a revolutionary mix of advanced ship automation functionality: A computer-based E0 system, a bridge control system, an automated power management system, a system for monitoring the load condition, and the world's first radar-based anti-collision system (automatic radar plotting aid, ARPA). In addition,

[4] Originally established in 1814 for defense purposes, KV was split into several smaller units in 1987 following financial troubles. Today, its remains make up one of Norway's main high-tech clusters, centered on the defense and maritime giant Kongsberg Gruppen.

the ND computer showed a remarkably good reliability with more than one year between failures.

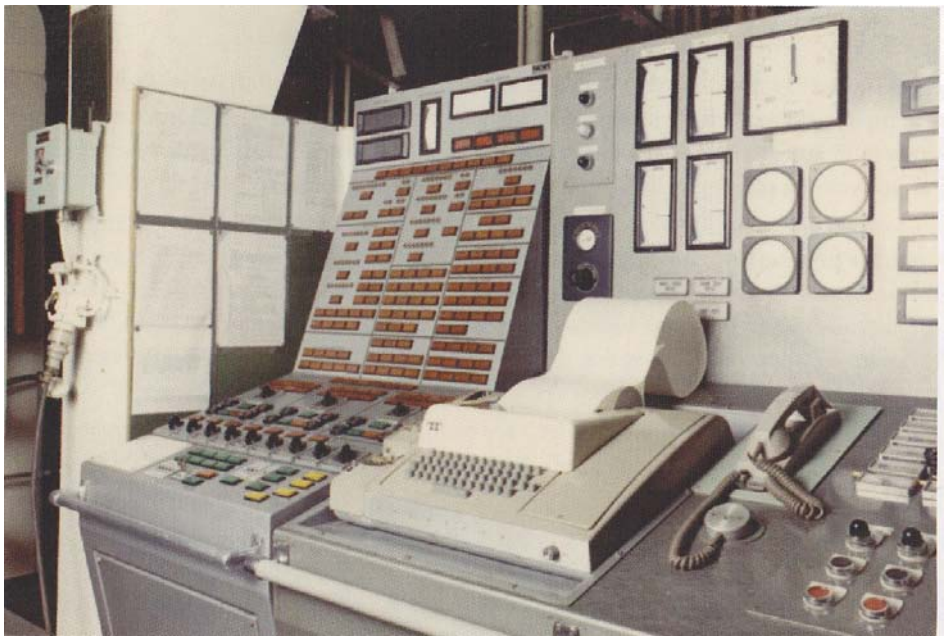

Figure 5: A prototype of a computer-based ship automation system onboard the M/S Taimyr. Courtesy of Kongsberg Maritime.

Sailing from Cape Town to various ports in Europe in 1969, Taimyr arrived in Oslo on the 2nd of October. A big press conference was held with the Norwegian broadcasting corporation NRK present, where captain Husum enthusiastically declared that: *"With our installation we sailed more safely in dense fog than without it on a clear day!"*

The project represented an astounding technological success. In the aftermath, NTNF decided to award Norcontrol exclusive rights to the developed technology. Today, the Norcontrol legacy is continued by the high-tech company Kongsberg Maritime, which constitutes one of the cornerstones of the KV-successor Kongsberg Gruppen.

More detailed accounts of these activities can be found in (Høivold 1984), (Overbye 1989), (Wicken 1994), (Høivold 2003) and (Bjerva 2006).

2.2. Wave 2: Dynamic Positioning

The concept of dynamic positioning (DP) was conceived in the early 1960s. DP technology was motivated by the need for accurate placement of ships for drilling purposes, at locations where it is practically impossible to deploy conventional jack-up barges or anchor spreads due to large water depths.

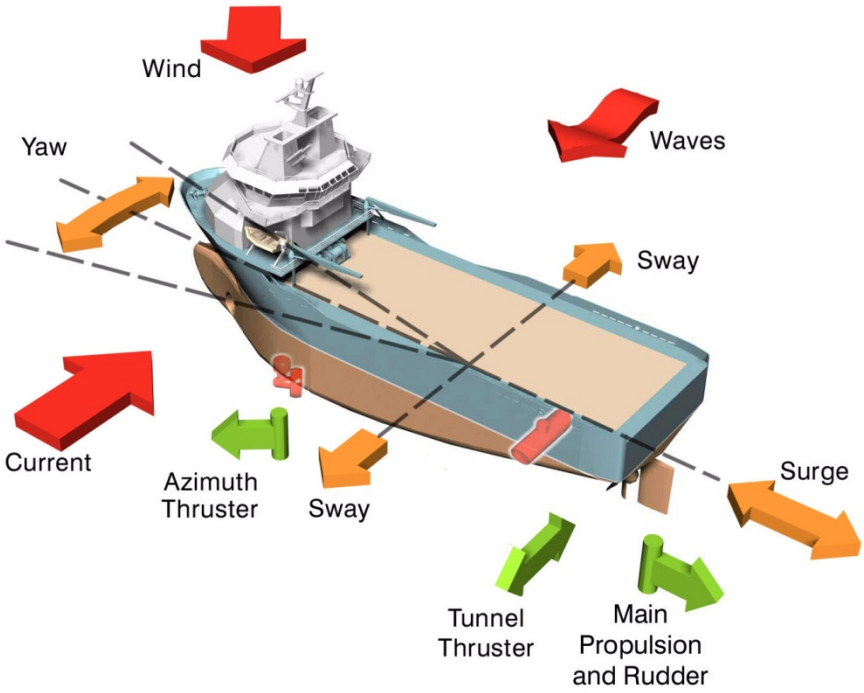

Figure 6: A DP vessel positions itself in the desired degrees of freedom (orange arrows) by counteracting the environmental forces (red arrows) through its propulsors (green arrows). Courtesy of Kongsberg Maritime.

In 1961, the American drillship Cuss 1 became the first DP-capable vessel in the world (Fäy 1990). It maintained position offshore La Jolla in California exclusively by means of four steerable propellers. The control was manual, but later that same year the Shell Oil Company introduced the first computer-based DP system for its coring vessel Eureka. However, the technology was still only in its infancy.

While on a sabbatical at the University of California, Santa Barbara (UCSB) in 1967-1968, Jens Balchen learned about a project to equip the scientific drilling vessel Glomar Challenger with a DP system (Bjørnstad 2009). He became convinced that such technology could aid in the emerging oil and gas activities on the Norwegian continental shelf. Balchen also believed that the technology had great potential for improvement. In particular, he wanted to use model-based estimation techniques to obtain enhanced navigation data from noisy measurements. The recently developed Kalman filter, which already had proven itself in the American space program, seemed a prime candidate for the job.

Back in Norway, Balchen got several of his students to explore Kalman filtering and other DP-related issues in their thesis work. From 1971, he also started lobbying KV for developing a commercial product. At first the company was not interested. It made a survey which concluded that the Norwegian market was too small for such a product.

Not unexpectedly, the lukewarm response did not deter Balchen, who continued to promote DP with great enthusiasm.

Finally, in January 1974 a joint effort involving NTH, CMI, KV and the Horten-based electronics company Simrad got underway. KV administered the project while Jens Balchen pushed it forward.

The following year, the KV subsidiary Albatross was founded to develop and deliver DP systems. The name reflected on the large seabird's ability to glide for hours without rest, rarely seen on land except for nesting. Albatross soon received its first order.

At this time, the American company Honeywell had 80 percent of the global market for dynamic positioning. A market which was quite small, with only 3 to 4 installations per year. One of Honeywell's customers was the Norwegian shipping company Stolt-Nielsen. Their multipurpose vessel M/V Seaway Falcon sported the Honeywell Automatic Station Keeping (ASK) system. However, Stolt-Nielsen was discontented with the Americans' bulky system and expensive service. As a result, the company contacted KV for their next installation. The contract was signed in November 1975.

Using a coated plywood box with a Simrad sonar screen in front, Albatross marketed its first DP product at the 1976 Offshore Technology Conference (OTC) in Houston, Texas. Later that same year, Jens Glad Balchen and his coworkers Nils Albert Jenssen and Steinar Sælid published their first academic DP paper, see (Balchen et al. 1976). Combining an entrepreneurial and customer-centered Albatross with a unique DP concept from NTH/SINTEF would soon dethrone Honeywell. The first prototype was installed on the Stolt-Nielsen diving support vessel M/V Seaway Eagle on May 17th, 1977.

As stated in (Balchen et al. 1980), a DP system should *"...be designed to keep the given vessel within specified position limits, with a minimum fuel consumption and with minimum wear and tear on the propulsion equipment."* The use of Kalman filtering helps achieve this goal. Based on a mathematical model of the vessel to be positioned, as well as the characteristics of the environmental influence of wind, waves and current, the estimator is able to distinguish between the rapidly-varying oscillations which over time cancel each other out and the slowly-varying drift pattern. Only the latter motion component is relevant for a vessel which wants to avoid unnecessary energy use.

In addition, the Kalman filter allows several different position reference systems to be used simultaneously, combining the various outputs to achieve an optimal position estimate. This property is very important since different measurement principles utilizing different transmission media yield a higher reliability than a single solution.

Honeywell's DP system mostly relied on hydroacoustics alone, which inherently made it more unreliable. And in case all the navigation systems should fail at the same time, the Kalman filter is still able to provide a rough estimate of the vessel position based on its mathematical model.

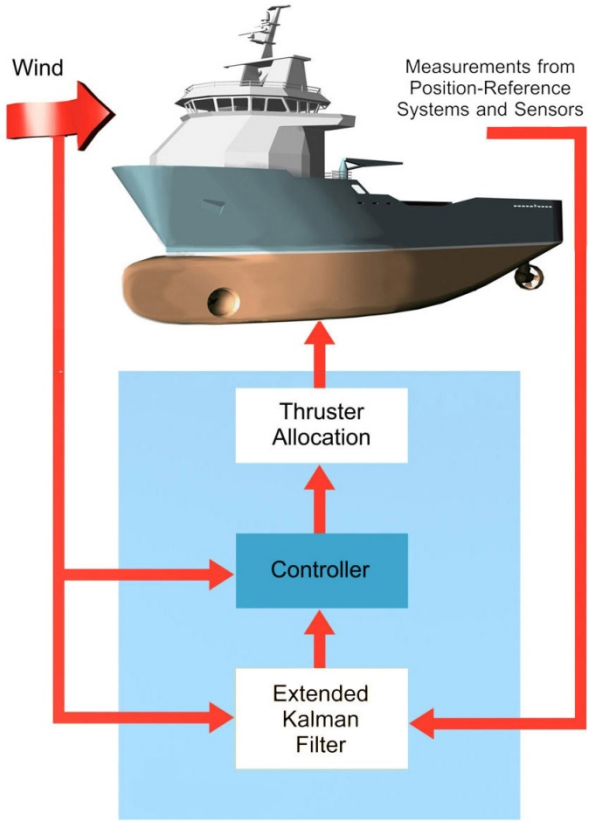

Figure 7: The control principle of a DP system. Motion data are processed through a model-based Kalman filter to extract the slowly-varying components. By comparing this information with the desired motion (feedback), and also using the predicted wind effect on the vessel (feedforward), the controller gives commands to the propellers, thrusters and rudders on how they should behave in order for the vessel to keep its desired position and orientation. Courtesy of Kongsberg Maritime.

Finally, the Kalman filter continuously predicts how the wind will affect the vessel. This information is used to proactively counteract wind disturbances by feedforward control, making it difficult for the wind to push the vessel off position. In contrast, the principle of feedback can only be applied as a response to events that have already occurred. At this time, all Albatross' competitors only employed feedback control in their DP solutions. According to Balchen, dynamic positioning without feedforward control is like steering a car by watching the centerline through a hole in the floor (Bjørnstad 2009).

In sum, the Albatross DP system was more reliable, more robust and saved more fuel than anything the competition had to offer. In addition, it was very user-friendly with a 'one button for one function' approach (Ryvik 1999). As a result, every new DP installation in 1980 was delivered by Albatross. In 1981, half of the 80 operational DP systems worldwide had been been installed by the company. Albatross then moved on to capture more than 80% of the market in the 1980s.

At the end of 1999, the Albatross positioning system came second in a vote among Norwegian engineers over the "Engineering Feat of the Century" ("Århundrets Ingeniørbragd"), a national competition arranged by the leading engineering magazine Teknisk Ukeblad. Important criteria included technical boldness, imagination, innovation and social significance. The gigantic Troll A platform, the tallest structure ever moved, was voted number one.

In time, DP functionality has evolved to include low-speed path following applications such as cable and pipe laying (Kittilsen 1994). The technology has also extended into other maritime segments to serve passenger and cargo vessels, research and survey vessels, as well as naval vessels. In 2003, over 1000 DP-capable vessels were in operation all around the world (Bray 2003).

Today, similar to Norcontrol, the heritage of Albatross is furthered by Kongsberg Maritime, one of the world's largest suppliers of maritime electronics.

2.3. Wave 3: Unmanned Vehicles

In April 2009, the Norwegian continental shelf was extended with a massive 235 000 square kilometers (Klungtveit 2009). The country's maritime zone now stretches all the way up to 84 degrees and 43 minutes north. An important challenge thus becomes how to efficiently manage such huge territorial waters, in particular since the offshore business pushes toward moving into Arctic areas as the North Sea gradually empties.

In a report prepared by Arve Johnsen, the former president of the Norwegian oil-giant Statoil, future visions of petroleum activities in the Barents Sea are considered (Johnsen 2006). One of the visions involves real-time surveillance of the ocean by means of a network of vehicles operating under water, on the surface of the sea, in the air and in space, see Figure 8.

An excerpt from the report reads: *"There is a need to develop a joint Norwegian surveillance of the northern waters. It is necessary to establish a single portal that allows users to easily access historical and real-time information about what is going on in the ocean space, on the seabed, on land, at sea level and in the airspace over the*

sea. Such monitoring will represent an efficient tool for managing the environment and the ocean resources in the north. The ambition should be that Norway becomes a vanguard nation and a driving force behind a knowledge-based management of the northern territories."

Figure 8: The Barents 2020 vision includes surveillance of the Barents Sea by means of a large network of cooperating vehicles which provide end-users with historical and real-time information about what goes on in the ocean space, constituting an efficient tool for knowledge-based management of environmental and marine resources. Courtesy of SINTEF.

However, instead of employing a majority of manned vehicles as part of the surveillance network, unmanned vehicles of all types should be considered. In environments such as the Barents Sea, it is desirable to use such robotic vehicles to perform both routine missions and dangerous operations since they never tire or complain. This way, costs can be kept down while humans are put out of harm's way.

With the current robotics revolution taking place in the US military (Singer 2009), resulting in the fact that the US Air Force currently trains more pilots for unmanned aerial vehicles (UAVs) than for manned planes (Pincus 2009), Norway is now in a unique position to capitalize on the development for civilian and marine purposes.

At present, the only major and commercially thriving Norwegian activity within unmanned vehicles seems to involve the autonomous underwater vehicle (AUV) series HUGIN. Developed in cooperation between Kongsberg Maritime and FFI, the HUGIN vehicles represent one of the most commercially successful AUV series on the world market today. These vehicles have been employed for commercial applications since 1997 and for military purposes since 2001 (Hagen et al. 2003).

Figure 9: The HUGIN AUVs currently represent the only commercially prosperous effort within unmanned vehicle technology in Norway. Courtesy of the Royal Norwegian Navy.

But with the exception of HUGIN, Norwegian initiatives toward unmanned vehicle technology have so far been driven by a small group of enthusiasts. Neither the government nor the academic or industrial sectors currently seem to have any strategic plans or goals.

However, if Norway wants to continue its leading position as a maritime nation and technology supplier, the current possibilities represented by unmanned vehicles should not be ignored. As remarked by Ibb Høivold regarding his experience from leading the pioneering developments in ship automation technology in the 1960s and 1970s (Høivold 1984): *"…even a small country, when concentrating important resources in a limited field and having a high level of education, may contribute to the application of new technology worldwide. A condition for success, however, is that the fields chosen for main efforts are fields of national importance and of international recognition. Another condition is that a cooperation can be established between research institutes, users, and producers."*

A coordinated Norwegian initiative to develop unmanned vehicles would also be unique when compared to the mainly military-motivated efforts found elsewhere in the world since it would mainly concern commercial and scientific applications. In addition, the field of unmanned vehicle technology represents a very appealing R&D area, and has the potential to attract a large number of Norwegian engineering students. Specifically, a problematic trend during recent years has been that such students shun PhD studies and instead choose well-paid jobs in the industry. However, unmanned vehicle applications should have no problems bringing them back and perhaps also contribute positively for PhD recruitment in other areas.

Figure 10: The Royal Norwegian Air Force currently operates 6 P-3 Orion multirole aircraft for maritime intelligence and surveillance purposes, especially in the northern territories. Considering the limited and expensive operational capabilities associated with these manned airplanes, a great potential exists to augment the Orions with a fleet of UAVs. Courtesy of Lockheed Martin.

In particular due to the major challenges currently faced in the Arctic, Norway now finds itself on the threshold of a new maritime technology adventure. The question then becomes whether the unique possibilities represented by unmanned vehicle technologies are recognized by the proper authorities. It is my hope that this PhD thesis can contribute to put this important topic on the agenda.

Figure 11: KV Svalbard is a Norwegian coast guard vessel which operates mostly in Arctic waters. Similar to the Orions, its capacity can be expanded through the use of unmanned surface vehicles (USVs) and unmanned underwater vehicles (UUVs). Courtesy of the Royal Norwegian Navy.

3. Guided Motion Control

"Guidance depends upon fundamental principles and involves devices that are similar for vehicles moving on land, on water, under water, in air, beyond the atmosphere within the gravitational field of earth and in space outside this field." – C. S. Draper

Guidance represents a principal methodology which transcends specific vehicle applications and which is concerned with the transient motion behavior associated with achieving motion control objectives (Draper 1971; Shneydor 1998). For this reason, guidance laws are typically stated at a kinematic level, only considering the fundamental geometric aspects of interest for a given motion control scenario.

Figure 12: The father of inertial navigation Charles Stark Draper asserted that guidance principles are fundamental and independent of any specific vehicle application.

This chapter elaborates on the concept of *guided motion control*, which is defined to involve the combination of a guidance system which issues meaningful speed and steering commands and a velocity control system which enforces these commands for a particular vehicle such that a given motion control objective can be achieved in a controlled and feasible manner.

Part of the following material represents an excerpt of already published work on this topic, in particular as found in (Breivik et al. 2008b, Appendix G) and (Breivik and Fossen 2009a, Appendix H). Emphasis is placed on the difference between target tracking and path following motion control scenarios, and the specific application under consideration involves marine vehicles moving on the ocean surface.

3.1. Motion Control Fundamentals

To enable meaningful definitions of motion control scenarios it is necessary to distinguish between different operating spaces, of which the two most fundamental are:

- The work space: Also known as the operational space in the robotics literature (Sciavicco and Siciliano 2002), it represents the physical space in which a vehicle moves. For a car, the work space is 2-dimensional (planar position), while it is 3-dimensional (spatial position) for an aircraft, see Figure 13. Thus, the work space is a position space common to all vehicles of the same category.

- The configuration space: Also known as the joint space in the robotics literature (Sciavicco and Siciliano 2002), it is constituted by the set of variables sufficient to specify all points of a rigid-body vehicle in the work space (LaValle 2006). Thus, the configuration of a car is given by its planar position and orientation, while the configuration of an aircraft is given by its spatial position and attitude. Each configuration variable is called a degree of freedom (DOF), see Figure 13.

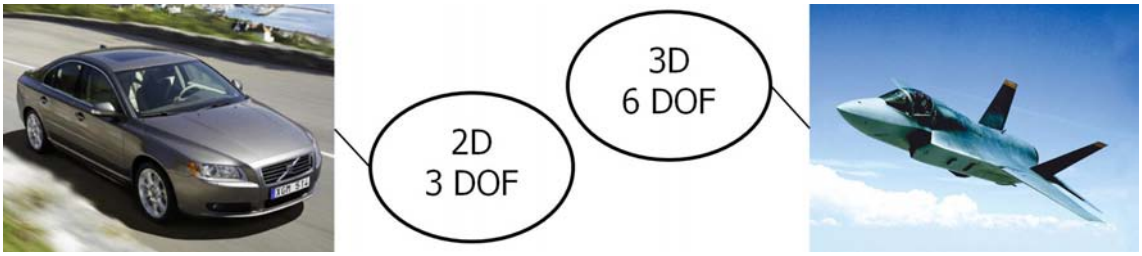

Figure 13: A road-travelling car moves around with its 3 degrees of freedom on a planar surface, while a fighter jet employs its 6 degrees of freedom to maneuver in 3-dimensional space.

It is also important to consider the actuation characteristics of a specific vehicle, which involve the type, amount and distribution of motion-inducing devices such as propellers, thrusters and control surfaces. In particular, it is common to distinguish between two qualitatively different actuation properties:

- Full actuation: A fully actuated vehicle can independently control the motion of all its degrees of freedom simultaneously.

- Underactuation: An underactuated vehicle cannot independently control the motion of all its degrees of freedom simultaneously.

Based on these definitions, it can be concluded that an underactuated vehicle is generally unable to achieve arbitrary tasks in its configuration space. However, it can still achieve meaningful tasks in its work space.

In practice, most vehicles are underactuated when moving at high speeds. Specifically, ships are typically underactuated above 1-2 m/s (3-4 knots) because the actuators that facilitate full actuation are ineffective above such speeds (Kongsberg Maritime 2006).

In the remainder of this thesis, an underactuated marine vehicle is taken to mean a vehicle which cannot control its lateral motion independently.

Figure 14: A ship rotating around its vertical axis and a surface-to-air missile just after launch. Ships maneuvering at low speed are often fully actuated, but missiles are inherently underactuated.

Motion control scenarios are traditionally divided into 4 main categories, see for example (Skjetne 2005; Aguiar and Hespanha 2007): *Point stabilization*, which involves motion toward a stationary point; *trajectory tracking*, which involves motion along a time-parameterized path; *path following*, which involves motion along a time-independent path; and *maneuvering*, which is a mix between trajectory tracking and path following where the time-parameterization of a path can be changed dynamically, for instance according to the vehicle dynamics.

In the marine control literature, these motion control scenarios are often defined by control objectives which are given as configuration-space tasks. For a marine surface vessel, such a task corresponds to achieving independent control of the vessel position and heading simultaneously. The scenarios are thus best suited for fully actuated vehicles and become impossible to fulfill for underactuated vehicles which are exposed to environmental disturbances.

One example concerns station keeping of underactuated surface vessels that do not have independent actuation in their lateral direction. The approach presented in (Pettersen and Fossen 2000) attempts to achieve independent control of the position and heading of such a vessel, but the model-scale experiments show that the ship starts oscillating around its desired configuration and thus never achieves its station-keeping objective. The reason for this behavior is that the ship is continuously exposed to small disturbances which prevent the simultaneous stabilization of both position and heading. To be able to stabilize its position, the ship must in fact turn its heading up against the mean disturbance such that it no longer experiences any lateral influence. Otherwise, if the desired heading is specified differently, the ship will neither be able to reach its desired position nor its desired heading and will consequently continue to experience an

oscillation around its desired configuration. In contrast, (Pinkster and Nienhuis 1986) defines the control objective as a work-space task where the underactuated surface vessel is supposed to converge to a desired position while the heading is left in open loop. Model-scale experiments show that the ship successfully achieves its positioning objective while the heading simultaneously converges automatically toward the mean environmental disturbance, making the ship act as a weathervane.

Hence, it is suggested that motion control objectives in general should be specified as work-space tasks and not as configuration-space tasks (Breivik and Fossen 2008c; Breivik and Fossen 2009a, Appendix H). An underactuated vehicle can then use its attitude, which corresponds to the degrees of freedom that separate the configuration space from the work space, to achieve its work-space task, especially since an arbitrary configuration is unachievable in practice. Subsequently, for those vehicles that do happen to be fully actuated, additional attitude requirements can be added to the main work-space task such that the resulting control objective corresponds to a configuration-space task.

An additional comment to the traditional motion control scenarios is that they typically only involve desired motion which has been defined a priori in some sense. They do not seem to encompass the case where no future motion information is available, such as when tracking the instantaneous position of a real or virtual target point. Such a motion control scenario should also be included in the list of relevant scenarios to consider. Hence, it is suggested to classify the motion control scenarios according to whether they are path-based or not, i.e., whether they encompass any a priori information or not.

Specifically, the following 4 motion control scenarios are suggested, where the control objective is implicitly given as a work-space task depending on the vehicle in question:

- Target tracking: The control objective is to track the position of a target which moves such that only its instantaneous motion is known, see Figure 15. In the simplified case when the target does not move, this scenario corresponds to point stabilization. For this scenario, it is impossible to separate the spatio-temporal constraint associated with the target position, i.e., to be at a certain position at a certain time, into two separate – spatial and temporal – constraints.

- Path following: The control objective is to converge to and follow a predefined geometric path, which only involves a spatial constraint. No restrictions are placed on the temporal propagation along the path.

- Path tracking: The control objective is to track the position of a target which is constrained to move along a predefined path, corresponding to the trajectory tracking scenario, see Figure 15. For this scenario, it is possible to separate the spatio-temporal constraint associated with the target position into two separate constraints, for instance such that the primary objective is to converge to and follow the path, while the secondary objective is to synchronize with the target along the path. However, by disregarding any a priori path information, this scenario can also be viewed as a target tracking scenario and handled with correspondingly appropriate methods, giving rise to maneuvers that appear to be cutting corners relative to the path.

- Path maneuvering: The control objective is to employ knowledge about vehicle maneuverability constraints to feasibly negotiate or somehow optimize the negotiation of a predefined path, for instance by traversing the path as fast as possible without derailing. As such, path maneuvering represents a subset of path following, but is less constrained than path tracking since spatial constraints typically take precedence over temporal constraints. This motion control scenario encompasses the aforementioned maneuvering scenario, and path maneuvering methods can also be used to handle path tracking scenarios.

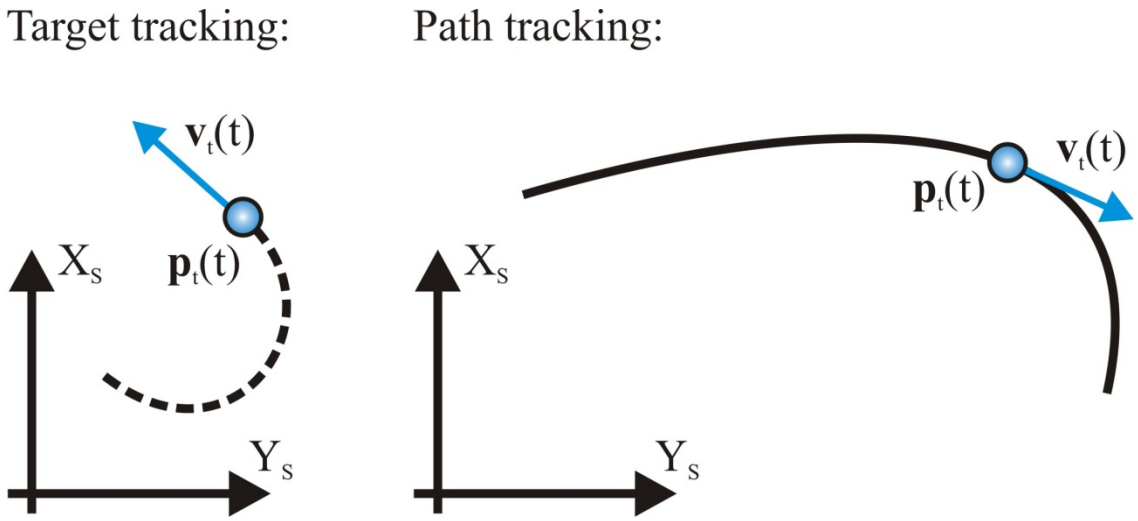

Figure 15: In a target tracking motion control scenario, no information about the future target motion is available. However, in a path tracking scenario it is known where the target will move in the future, so the motion control objective can be divided into a spatial and a temporal constraint.

In the following, planar guidance laws which solve the target tracking and path following motion control objectives will be presented. Including Figure 15, the illustrations of guidance principles in this chapter employ the marine convention of a right-handed coordinate system whose z-axis points downward into the plane.

3.2. Guidance Laws

Due to their fundamental nature, guidance laws are typically stated at a kinematic level, either just as steering laws, separate speed and steering laws, or directly prescribed as velocity assignments. Consequently, consider a kinematic vehicle represented by its planar position $\mathbf{p}(t) \triangleq [x(t), y(t)]^{\mathrm{T}} \in \mathbb{R}^2$ and velocity $\mathbf{v}(t) \triangleq \mathrm{d}\mathbf{p}(t)/\mathrm{d}t \triangleq \dot{\mathbf{p}}(t) \in \mathbb{R}^2$, stated relative to some stationary reference frame, which here is taken to mean an inertial reference frame that does not move. Then denote the speed as

$$U(t) \triangleq |\mathbf{v}(t)| = \sqrt{\dot{x}(t)^2 + \dot{y}(t)^2} \geq 0, \tag{1}$$

while the steering angle, also referred to as the course angle, is represented by

$$\chi(t) \triangleq \mathrm{atan2}(\dot{y}(t), \dot{x}(t)) \in \mathbb{S} \triangleq [-\pi, \pi], \tag{2}$$

where $\mathrm{atan2}(y, x)$ is the four-quadrant version of $\arctan(y/x) \in \langle -\pi/2, \pi/2 \rangle$. For this kinematic vehicle, guidance laws which solve the work-space motion control objectives associated with the target tracking and path following scenarios will now be presented.

3.2.1. Target Tracking

Target tracking scenarios have traditionally been considered by the guided missile community, where the motion control objective typically is to intercept a moving target in finite time. An interceptor missile nominally undergoes 3 phases during its operation; a launch phase, a midcourse phase and a terminal phase. The greatest accuracy demand is associated with the terminal phase, when the interceptor locks onto its target by using its internal homing sensors to infer the relative motion to the target such that the interceptor guidance system can compensate for the accumulated errors from the previous phases in order to achieve an intercept.

Historically, a lot of effort was put into the development of guidance laws during the Second World War, see (Locke 1955). During this period, several so-called classical guidance laws were derived for the terminal phase based on fundamental geometric considerations. Later developments have basically just involved further refinements to these laws as facilitated by increasingly advanced computer, sensor and actuator solutions. Interestingly, this evolution is completely analogous to the development of progressively sophisticated control algorithms starting with the basic PID feedback principle. In addition, the classical guidance laws have been found to be used in nature by predators hunting prey (Mizutani et al. 2003; Justh and Krishnaprasad 2006), a relation which particularly serves to underline their fundamental essence.

Specifically, I have chosen to focus on the constant bearing (CB) guidance principle in my work on target tracking. This scheme can be implemented in many different ways, but it basically tries to align the relative interceptor-target velocity vector along the relative interceptor-target position vector such that the latter is minimized. The relative position vector is also frequently referred to as the line-of-sight (LOS) vector between the interceptor and the target, see Figure 16.

The goal of CB guidance can be achieved by reducing the LOS rotation rate to zero such that the interceptor perceives the target at a constant bearing, closing in on a direct collision course. This guidance strategy is therefore often referred to as parallel navigation because consecutive LOS vectors will move in parallel to each other.

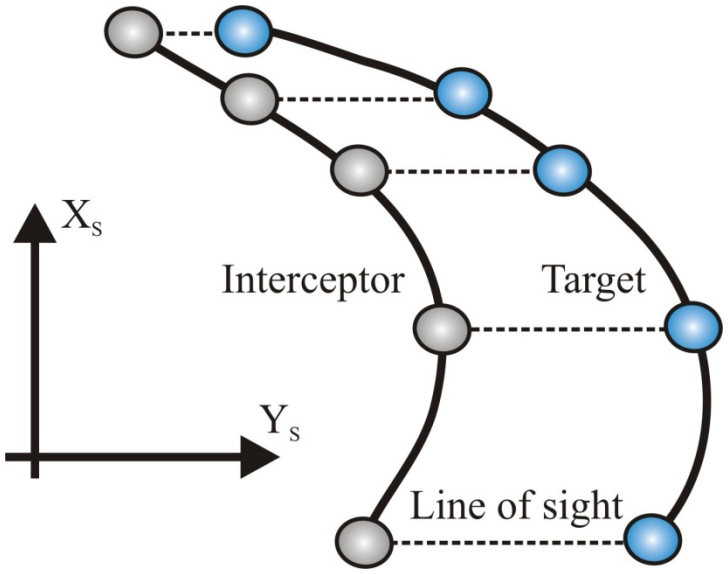

Figure 16: A possible trajectory involving an interceptor which is guided by CB guidance and which has stabilized the LOS rotation rate to zero, explaining the term parallel navigation.

Since guided missiles typically cannot control their speed and only have access to relative motion information, CB guidance is most commonly mechanized through a steering law known as proportional navigation (PN). In this law, an acceleration command which is perpendicular to the instantaneous missile velocity vector is issued to make the velocity vector rotate proportionally to the LOS rate in order to nullify it, see for instance (Shneydor 1998; Siouris 2004; Yanushevsky 2008). A multitude of variations on PN guidance have been proposed in the guided missile literature, each taking into account different assumptions about the interceptor-target scenario.

However, PN guidance is only able to achieve a collision with the target, which naturally corresponds to the control objective of a missile. This matching of target position but not speed is what is called an *intercept*, and the larger the speed difference, the more violent the collision. On the other hand, a *rendezvous* means to match both

position and speed with the target, which corresponds to the motion control objective in a target tracking scenario. Consequently, a guidance law capable of solving the rendezvous problem needs to consider both speed and steering control at the same time, and not just steering control as is the case for proportional navigation.

Motivated by the target tracking scenario, a novel CB-guidance mechanization suitable for target rendezvous was proposed in (Breivik et al. 2006d, Appendix D). This guidance law was later put into a wider context and also used in (Breivik and Fossen 2007b). The law is a direct velocity assignment assuming knowledge about the target position and velocity relative to a stationary reference frame, which is not unrealistic in a marine motion control context. Furthermore, the law has the nice feature that it makes it possible to directly shape the transient motion behavior toward the target by selection of two intuitive tuning parameters. This guidance law will be presented in the following.

Consider a target represented by its position $\mathbf{p}_t(t) \triangleq [x_t(t), y_t(t)]^T \in \mathbb{R}^2$ and velocity $\mathbf{v}_t(t) \triangleq \dot{\mathbf{p}}_t(t) \in \mathbb{R}^2$. Subsequently, define the interceptor-target LOS vector as

$$\tilde{\mathbf{p}}(t) \triangleq \mathbf{p}_t(t) - \mathbf{p}(t), \tag{3}$$

which is equivalent to the position error between the target and the interceptor. Then the control objective of a target tracking scenario can be stated as

$$\lim_{t \to \infty} \tilde{\mathbf{p}}(t) = \mathbf{0}, \tag{4}$$

thus corresponding to an asymptotic intercept, which is equivalent with a rendezvous.

Directly assigning the velocity of the kinematic interceptor as

$$\mathbf{v}(t) = \mathbf{v}_t(t) + \mathbf{v}_a(t) \tag{5}$$

means that it will close in on the target with the approach velocity $\mathbf{v}_a(t)$, see Figure 17.

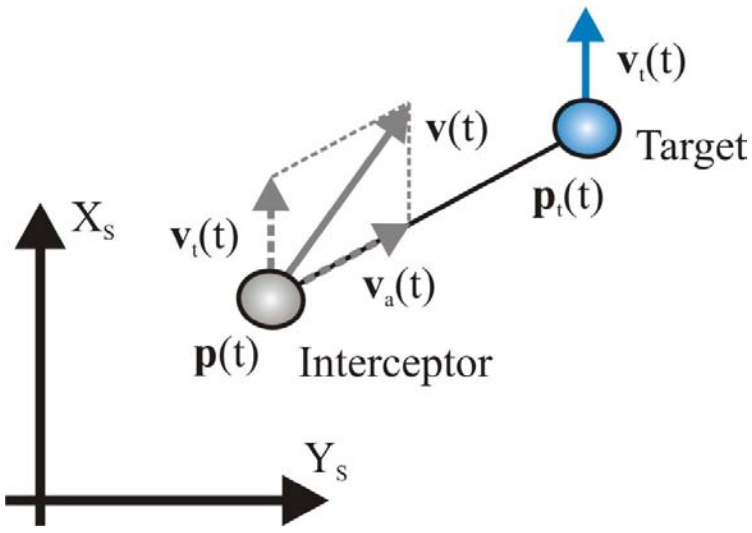

Figure 17: CB guidance mechanized by a direct velocity assignment.

Considering CB guidance, the approach velocity can be chosen as

$$\mathbf{v}_{\mathrm{a}}(t) = \kappa(t)\frac{\tilde{\mathbf{p}}(t)}{\left|\tilde{\mathbf{p}}(t)\right|}, \tag{6}$$

where $\left|\tilde{\mathbf{p}}(t)\right| \triangleq \sqrt{\tilde{\mathbf{p}}(t)^{\mathrm{T}}\tilde{\mathbf{p}}(t)} \geq 0$ is the Euclidean length of the LOS vector, and where $\kappa(t) \geq 0$ modulates the approach speed. Specifically, a rendezvous can be achieved if the approach speed is chosen proportional to the interceptor-target distance $\left|\tilde{\mathbf{p}}(t)\right|$, for example as

$$\kappa(t) = U_{\mathrm{a,max}}\frac{\left|\tilde{\mathbf{p}}(t)\right|}{\sqrt{\tilde{\mathbf{p}}(t)^{\mathrm{T}}\tilde{\mathbf{p}}(t) + \Delta_{\tilde{\mathrm{p}}}^{2}}}, \tag{7}$$

where $U_{\mathrm{a,max}} > 0$ is a parameter which specifies the maximum approach speed toward the target, while $\Delta_{\tilde{\mathrm{p}}} > 0$ can be used to tune the transient rendezvous behavior, see Figure 18. Consequently, these parameters make it possible to explicitly specify the transient rendezvous behavior for a target tracking scenario in a convenient and intuitive manner, which can be very advantageous when considering real vehicles with known velocity constraints. In this context, a fundamental assumption is that the interceptor has a speed advantage over the target, which means that the maximum vehicle speed U_{max} is larger than the maximum assigned speed $U_{\mathrm{t}}(t) + U_{\mathrm{a,max}}$ at all times.

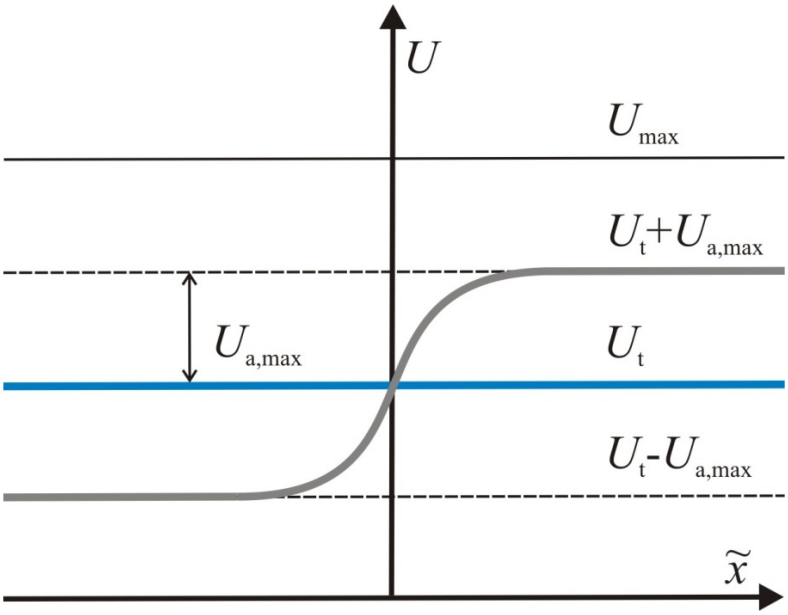

Figure 18: The speed assignment resulting from (5)-(7) for movement purely along the x-axis.

Finally note that the velocity assignment (5) simply becomes a pure pursuit (PP) guidance law if the target velocity is not employed as a kinematic feedforward, which results in a tail chase for most interceptor-target encounters. This fact also means that CB guidance equals PP guidance for a stationary target.

3.2.2. Path Following

Path following scenarios have traditionally been very popular in the marine control literature. As mentioned previously, the motion control objective is to converge to and follow a predefined geometric path without any explicit temporal constraints associated with the propagation along the path. Hence, path following basically amounts to assigning proper steering laws $\chi(t)$ as long as the speed $U(t) > 0$. As such, path following scenarios are indeed generally easier to solve than target tracking scenarios.

In the following, a guidance law developed for so-called regularly parameterized paths will be presented. The guidance law consists of a steering law assigned to the velocity vector of the kinematic vehicle and a path-constrained target which is assigned to move such that it converges with the kinematic vehicle when the latter steers as commanded.

Consequently, consider a planar path continuously parameterized by a scalar variable $\varpi \in \mathbb{R}$, such that the position of a path point is represented by $\mathbf{p}_{\mathrm{p}}(\varpi) \in \mathbb{R}^2$. The path is therefore a one-dimensional manifold which can be expressed by the set

$$\mathcal{P} \triangleq \left\{ \mathbf{p} \in \mathbb{R}^2 \mid \mathbf{p} = \mathbf{p}_{\mathrm{p}}(\varpi) \ \forall \ \varpi \in \mathbb{R} \right\}. \tag{8}$$

Regularly parameterized paths belong to the subset of $\mathcal{P}$ for which $\left| \mathbf{p}_{\mathrm{p}}'(\varpi) \right| \triangleq \left| \mathrm{d}\mathbf{p}_{\mathrm{p}}(\varpi) / \mathrm{d}\varpi \right| = \sqrt{x_{\mathrm{p}}'(\varpi)^2 + y_{\mathrm{p}}'(\varpi)^2}$ is non-zero and finite, which means that they never degenerate into a point nor have corners. These paths include both straight lines (zero curvature) and circles (constant curvature), but most have varying curvatures. In general, they are also not arc-length parameterized.

Then consider an arbitrary path point $\mathbf{p}_{\mathrm{p}}(\varpi)$ and a path-fixed reference frame associated with this point. Subsequently, define the x-axis of this frame to be aligned with the path-tangential direction at $\mathbf{p}_{\mathrm{p}}(\varpi)$, rotating it relative to the x-axis of the stationary reference frame by a positive angle

$$\chi_{\mathrm{p}}(\varpi) \triangleq \operatorname{atan2}\left(y_{\mathrm{p}}'(\varpi), x_{\mathrm{p}}'(\varpi) \right), \tag{9}$$

such that the off-path error can be expressed by

$$\boldsymbol{\varepsilon}(t) \triangleq \mathbf{R}(\chi_{\mathrm{p}})^{\mathrm{T}} (\mathbf{p}(t) - \mathbf{p}_{\mathrm{p}}(\varpi)), \tag{10}$$

where $\boldsymbol{\varepsilon}(t) = \left[s(t), e(t) \right]^{\mathrm{T}} \in \mathbb{R}^2$ represents the along-path and cross-path errors relative to $\mathbf{p}_{\mathrm{p}}(\varpi)$, decomposed in the path-fixed reference frame by

$$\mathbf{R}(\chi_{\mathrm{p}}) \triangleq \begin{bmatrix} \cos\chi_{\mathrm{p}} & -\sin\chi_{\mathrm{p}} \\ \sin\chi_{\mathrm{p}} & \cos\chi_{\mathrm{p}} \end{bmatrix}. \tag{11}$$

The path following control objective can thus be stated as

$$\lim_{t\to\infty} \boldsymbol{\varepsilon}(t) = \mathbf{0}, \tag{12}$$

which involves a collaborative effort between both $\mathbf{p}(t)$ and $\mathbf{p}_{\mathrm{p}}(\varpi)$ in order to be fulfilled. For instance, a steering law can be assigned to $\mathbf{v}(t)$ for cross-path minimization, while dynamics can be assigned to ϖ for along-path minimization.

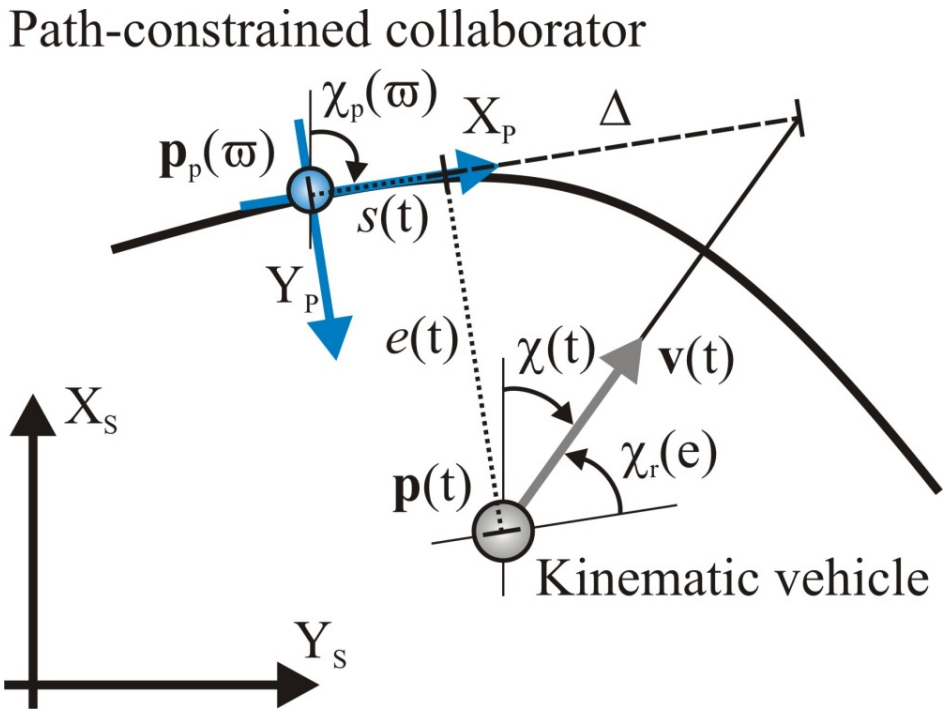

Figure 19: Lookahead-based steering combined with a path-constrained collaborator help solve the path following motion control objective associated with regularly parameterized paths.

Specifically, the steering assignment is separated into two distinct parts such that

$$\chi(\varpi, e) = \chi_{\mathrm{p}}(\varpi) + \chi_{\mathrm{r}}(e), \tag{13}$$

where

$$\chi_{\mathrm{r}}(e) \triangleq \arctan\left(-\frac{e}{\Delta}\right) \tag{14}$$

represents the path-relative steering angle which ensures that $\mathbf{v}(t)$ is directed toward a point that is located a lookahead distance $\Delta > 0$ ahead of the direct projection of $\mathbf{p}(t)$ onto the path-tangential axis at $\mathbf{p}_{\mathrm{p}}(\varpi)$, see Figure 19. Interestingly, by drawing a connection to the classical missile guidance principles, this lookahead-based steering law can be interpreted as pure pursuit of the lookahead point. Convergence to the path-tangential axis at $\mathbf{p}_{\mathrm{p}}(\varpi)$ is thus achieved as the "donkey" $\mathbf{p}(t)$ in vain chases the "carrot" located a distance Δ further ahead of the direct projection point.

At the same time, $\mathbf{p}_{\mathrm{p}}(\varpi)$ is assigned to move along the path toward the same direct projection of $\mathbf{p}(t)$ onto the path-tangential axis by

$$\dot{\varpi} = \frac{U(t)\cos\chi_{\mathrm{r}}(e) + \gamma s(t)}{\left|\mathbf{p}_{\mathrm{p}}'(\varpi)\right|}, \tag{15}$$

where the first element of the numerator represents a kinematic feedforward of the projection of $\mathbf{v}(t)$ onto the path tangent, while the second element represents a linear feedback term with $\gamma > 0$ whose purpose is to reduce the along-path error to zero.

Hence, the path-constrained attractor $\mathbf{p}_{\mathrm{p}}(\varpi)$ tracks the motion of $\mathbf{p}(t)$ which steers by the location of $\mathbf{p}_{\mathrm{p}}(\varpi)$.

The presented guidance law was first proposed in (Breivik and Fossen 2004b), following the steering law derivations for straight lines and circles in (Breivik and Fossen 2004a) and the dynamic path parameter projection algorithm suggested in (Breivik 2003). The total scheme has mainly been inspired by and derived as a combination of the approaches found in (Papoulias 1991; Hauser and Hindman 1995; Pettersen and Lefeber 2001; Rysdyk 2003; Lapierre et al. 2003). In particular, the suggested approach suffers from no kinematic singularities and ensures that the path following motion control objective is achieved for regularly parameterized paths which need not be arc-length parameterized, see (Breivik and Fossen 2009a, Appendix H) for further details.

3.2.3. Closed-Loop Stability Considerations

For a real vehicle, the velocity and steering commands presented in the previous sections cannot be attained instantaneously. Hence, consider the velocity residual

$$\tilde{\mathbf{v}} \triangleq \mathbf{v}_{\mathrm{d}} - \mathbf{v}, \tag{16}$$

where $\mathbf{v}_{\mathrm{d}} \in \mathbb{R}^2$ represents the desired vehicle velocity as prescribed by a kinematic guidance law and $\mathbf{v} \in \mathbb{R}^2$ is the actual vehicle velocity. In practice, this velocity error must be handled by a separate velocity control system, and the dynamics of the error might then be represented by the nonlinear dynamic system

$$\dot{\tilde{\mathbf{v}}} = \mathbf{f}(\tilde{\mathbf{v}}, t) \tag{17}$$

in closed loop. Assuming a certain stability property for this system, a qualitative assessment can then be made about the combined guidance and velocity control system without having to know the details behind the specific velocity control implementation. In particular, theory on nonlinear cascades can be used for this purpose, see for example (Panteley et al. 1998).

The performance of the target tracking and path following guidance laws used in combination with velocity controllers will now be evaluated analytically. It is assumed that the reader is familiar with fundamental nonlinear stability and Lyapunov theory as explained for instance in (Khalil 2001).

Starting with the target tracking scenario, define the following positive definite and radially unbounded Lyapunov function

$$V_{\mathrm{TT}} \triangleq \frac{1}{2}\tilde{\mathbf{p}}^{\mathrm{T}}\tilde{\mathbf{p}}, \tag{18}$$

and differentiate it along the trajectories of $\tilde{\mathbf{p}}$ to obtain

$$\dot{V}_{\mathrm{TT}} = \tilde{\mathbf{p}}^{\mathrm{T}}\hat{\mathbf{v}}, \tag{19}$$

where

$$\hat{\mathbf{v}} = \mathbf{v}_{\mathrm{t}} - \mathbf{v} \tag{20}$$

which can be rewritten as

$$\hat{\mathbf{v}} = \mathbf{v}_{\mathrm{t}} - \mathbf{v}_{\mathrm{d}} + \tilde{\mathbf{v}}. \tag{21}$$

Subsequently inserting the expression for $\mathbf{v}_{\mathrm{d}}$ as prescribed by (5)-(7) results in

$$\hat{\mathbf{v}} = -U_{\mathrm{a,max}}\frac{\tilde{\mathbf{p}}}{\sqrt{\tilde{\mathbf{p}}^{\mathrm{T}}\tilde{\mathbf{p}} + \Delta_{\tilde{\mathrm{p}}}^2}} + \tilde{\mathbf{v}}, \tag{22}$$

which means that

$$\dot{V}_{\mathrm{TT}} = -U_{\mathrm{a,max}}\frac{\tilde{\mathbf{p}}^{\mathrm{T}}\tilde{\mathbf{p}}}{\sqrt{\tilde{\mathbf{p}}^{\mathrm{T}}\tilde{\mathbf{p}} + \Delta_{\tilde{\mathrm{p}}}^2}} + \tilde{\mathbf{p}}^{\mathrm{T}}\tilde{\mathbf{v}}. \tag{23}$$

Assuming for a moment perfect velocity control such that $\tilde{\mathbf{v}} = \mathbf{0}$, gives

$$\dot{V}_{\mathrm{TT}} = -U_{\mathrm{a,max}}\frac{\tilde{\mathbf{p}}^{\mathrm{T}}\tilde{\mathbf{p}}}{\sqrt{\tilde{\mathbf{p}}^{\mathrm{T}}\tilde{\mathbf{p}} + \Delta_{\tilde{\mathrm{p}}}^2}} \tag{24}$$

which is negative definite since $U_{\mathrm{a,max}} > 0$ and $\Delta_{\tilde{\mathrm{p}}} > 0$. Consequently, in this case it can be conluded by standard Lyapunov arguments that the suggested target tracking guidance law renders the origin of $\tilde{\mathbf{p}}$ uniformly globally asymptotically stable (UGAS). In addition, the derivative of the Lyapunov function becomes quadratic for local motion around the origin such that

$$\dot{V}_{\mathrm{TT}} = -\frac{U_{\mathrm{a,max}}}{\Delta_{\tilde{\mathrm{p}}}}\tilde{\mathbf{p}}^{\mathrm{T}}\tilde{\mathbf{p}}, \tag{25}$$

which means that the origin is also uniformly locally exponentially stable (ULES). Hence, the closed-loop origin of a kinematic vehicle guided by (5)-(7) is in fact UGAS/ULES, also known as κ-exponential stability, see (Sørdalen and Egeland 1995).

Considering the combined closed-loop position and velocity error system gives the following nonlinear time-varying cascade

$$\Sigma_{\tilde{\mathrm{p}}} : \dot{\tilde{\mathbf{p}}} = -U_{\mathrm{a,max}} \frac{\tilde{\mathbf{p}}}{\sqrt{\tilde{\mathbf{p}}^{\mathrm{T}}\tilde{\mathbf{p}} + \Delta_{\tilde{\mathrm{p}}}^2}} + \tilde{\mathbf{v}} \tag{26}$$

$$\Sigma_{\tilde{\mathrm{v}}} : \dot{\tilde{\mathbf{v}}} = \mathbf{f}(\tilde{\mathbf{v}}, t), \tag{27}$$

where the $\Sigma_{\tilde{\mathrm{v}}}$ system is seen to linearly perturb the $\Sigma_{\tilde{\mathrm{p}}}$ system. In fact, assuming that the origin of $\tilde{\mathbf{v}}$ is UGAS/ULES after having recently showed that the unperturbed origin of $\tilde{\mathbf{p}}$ is UGAS/ULES, Theorem 7 and Lemma 8 in (Panteley et al. 1998) directly shows that the origin of the combined system also becomes UGAS/ULES.

This result is quite interesting since it shows that any velocity controller capable of rendering the velocity error system UGAS/ULES will also render the total system guided by the suggested CB guidance law UGAS/ULES. Hence, a modular approach to the motion control problem can be taken whereby the guidance law remains the same while the specific vehicle and its velocity control system can vary, see also (Breivik et al. 2006d, Appendix D; Breivik and Fossen 2007b).

The same approach can be taken to show stability for the path following scenario. Consequently, define the following positive definite and radially unbounded Lyapunov function

$$V_{\mathrm{PF}} \triangleq \frac{1}{2}\boldsymbol{\varepsilon}^{\mathrm{T}}\boldsymbol{\varepsilon}, \tag{28}$$

and differentiate it along the trajectories of $\boldsymbol{\varepsilon}$ to obtain

$$\dot{V}_{\mathrm{PF}} = \boldsymbol{\varepsilon}^{\mathrm{T}}\left(\mathbf{R}^{\mathrm{T}}(\dot{\mathbf{p}} - \dot{\mathbf{p}}_{\mathrm{p}}) + \dot{\mathbf{R}}^{\mathrm{T}}(\mathbf{p} - \mathbf{p}_{\mathrm{p}})\right), \tag{29}$$

where

$$\dot{\mathbf{R}} = \mathbf{R}\mathbf{S} \tag{30}$$

with

$$\mathbf{S} = \begin{bmatrix} 0 & -\dot{\chi}_{\mathrm{p}} \\ \dot{\chi}_{\mathrm{p}} & 0 \end{bmatrix}, \tag{31}$$

which is skew-symmetric. Continuing with

$$\dot{V}_{\mathrm{PF}} = \boldsymbol{\varepsilon}^{\mathrm{T}}\left(\mathbf{R}^{\mathrm{T}}(\mathbf{v} - \dot{\mathbf{p}}_{\mathrm{p}}) + \mathbf{S}^{\mathrm{T}}\mathbf{R}^{\mathrm{T}}(\mathbf{p} - \mathbf{p}_{\mathrm{p}})\right) \tag{32}$$

which is equal to

$$\dot{V}_{\mathrm{PF}} = \boldsymbol{\varepsilon}^{\mathrm{T}}\left(\mathbf{S}^{\mathrm{T}}\boldsymbol{\varepsilon} + \mathbf{R}^{\mathrm{T}}(\mathbf{v}_{\mathrm{d}} - \dot{\mathbf{p}}_{\mathrm{p}})\right) - \boldsymbol{\varepsilon}^{\mathrm{T}}\mathbf{R}^{\mathrm{T}}\tilde{\mathbf{v}} \tag{33}$$

where $\boldsymbol{\varepsilon}^{\mathrm{T}}\mathbf{S}^{\mathrm{T}}\boldsymbol{\varepsilon} = 0$ such that

$$\dot{V}_{\mathrm{PF}} = \boldsymbol{\varepsilon}^{\mathrm{T}}\mathbf{R}^{\mathrm{T}}(\mathbf{v}_{\mathrm{d}} - \dot{\mathbf{p}}_{\mathrm{p}}) - \boldsymbol{\varepsilon}^{\mathrm{T}}\mathbf{R}^{\mathrm{T}}\tilde{\mathbf{v}}. \tag{34}$$

Now, $\mathbf{v}_\mathrm{d}$ can be written in polar coordinate form as

$$\mathbf{v}_\mathrm{d} = \left[U\cos\chi_\mathrm{d}, U\sin\chi_\mathrm{d}\right]^\mathrm{T} \tag{35}$$

where χ_d is the desired velocity vector steering angle. Note that speed control is not explicitly considered in this case since it is sufficient that the vehicle speed $U > 0$. Subsequently, derive the first term of (34) on component form as

$$\dot{V}_\mathrm{PF} = s\left(U\cos\left(\chi_\mathrm{d} - \chi_\mathrm{p}\right) - U_\mathrm{p}\right) + eU\sin\left(\chi_\mathrm{d} - \chi_\mathrm{p}\right) - \boldsymbol{\varepsilon}^\mathrm{T}\mathbf{R}^\mathrm{T}\tilde{\mathbf{v}}, \tag{36}$$

where U_p represents the speed of the path-constrained collaborator $\mathbf{p}_\mathrm{p}(\varpi)$ and $\chi_\mathrm{d} - \chi_\mathrm{p} = \chi_\mathrm{r}$ according to the steering assignment given in (13). Hence,

$$\dot{V}_\mathrm{PF} = s\left(U\cos\chi_\mathrm{r} - U_\mathrm{p}\right) + eU\sin\chi_\mathrm{r} - \boldsymbol{\varepsilon}^\mathrm{T}\mathbf{R}^\mathrm{T}\tilde{\mathbf{v}}, \tag{37}$$

and by assigning χ_r as in (14) and $U_\mathrm{p} = \left|\mathbf{p}_\mathrm{p}'(\varpi)\right|\dot{\varpi}$ according to (15), then

$$\dot{V}_\mathrm{PF} = -\gamma s^2 - U\frac{e^2}{\sqrt{e^2+\Delta^2}} - \boldsymbol{\varepsilon}^\mathrm{T}\mathbf{R}^\mathrm{T}\tilde{\mathbf{v}} \tag{38}$$

such that the perfectly controlled system corresponds to

$$\dot{V}_\mathrm{PF} = -\gamma s^2 - U\frac{e^2}{\sqrt{e^2+\Delta^2}}, \tag{39}$$

which means that the origin of $\boldsymbol{\varepsilon}$ is UGAS since the path is regularly parameterized, $\gamma > 0$, $U > 0$ and $\Delta > 0$. Furthermore, the derivative of the Lyapunov function becomes quadratic for local motion around the origin such that

$$\dot{V}_\mathrm{PF} = -\gamma s^2 - \frac{U}{\Delta}e^2 \tag{40}$$

which means that the origin is also uniformly locally exponentially stable (ULES). Hence, the closed-loop origin of a kinematic vehicle steered by (13)-(14) and supported by (15) is in fact UGAS/ULES.

Similar to the target tracking case, the combined closed-loop position and velocity error system gives the following nonlinear time-varying cascade

$$\Sigma_\varepsilon : \dot{\boldsymbol{\varepsilon}} = \mathbf{h}(\boldsymbol{\varepsilon}, t) - \mathbf{R}^\mathrm{T}\tilde{\mathbf{v}} \tag{41}$$

$$\Sigma_{\tilde{\mathrm{v}}} : \dot{\tilde{\mathbf{v}}} = \mathbf{f}(\tilde{\mathbf{v}}, t), \tag{42}$$

where the $\Sigma_{\tilde{\mathrm{v}}}$ system is seen to perturb the Σ_ε system through the size-wise linearly-perturbing term $\mathbf{R}^\mathrm{T}\tilde{\mathbf{v}}$. Again, assuming that the origin of $\tilde{\mathbf{v}}$ is UGAS/ULES after having recently showed that the unperturbed origin of $\boldsymbol{\varepsilon}$ is UGAS/ULES, Theorem 7 and Lemma 8 in (Panteley et al. 1998) directly shows that the origin of the combined system also becomes UGAS/ULES.

3.3. Guided Motion Control of Marine Vehicles

This section considers the application of guided motion control to marine vehicles, in particular surface vehicles. First, some preliminaries regarding reference frames, motion variables, vessel types, mathematical modeling and operational conditions are reviewed. Then, aspects related to the velocity-commanding guidance system are investigated. Subsequently, a velocity control system methodology for underactuated marine vehicles is described. Finally, the guided motion control system resulting from combining the presented guidance and velocity control systems is discussed.

3.3.1. Marine Control Fundamentals

When considering motion control of marine vehicles, many factors must be taken into account. These vehicles are dynamical systems whose motion can be mathematically described by a combination of kinematics and kinetics, where:

- Kinematics purely considers the geometric aspects of motion, without reference to the forces and moments which generate such motion. No uncertainty is associated with the kinematics.

- Kinetics considers how forces and moments generate vessel motion. Uncertainty is always associated with the kinetics, both structural and parametric uncertainty. Even if structural uncertainty often is reduced to a minimum, parametric uncertainty will still represent a practical problem for most applications.

In particular, the most relevant kinematics and kinetics related to marine vehicles travelling on the ocean surface will now be explored.

Kinematics

Kinematic relationships can be described by using various types of reference frames. A total of 4 reference frames are usually employed in order to describe vehicle motion on a global scale. The first two frames are global and defined at the center of the earth, the third frame is a local geographic reference frame, while the fourth reference frame is fixed to the vehicle of interest.

The following exposition corresponds to those given in (Egeland and Gravdahl 2002; Fossen 2002). Figure 20 illustrates 3 of the reference frames, where the symbol ω_e denotes the earth's rate of rotation. Specifically, the reference frames are:

- Global reference frames:
    - ECI: Earth-Centered Inertial. This reference frame is often considered to be an inertial reference frame. It has its origin at the center of the earth. The x-axis points toward the Aries point in the Vernal Equinox direction, while the z-axis is aligned with the spin axis of the earth and points toward the celestial North Pole. The y-axis points so as to accomplish orthogonality with the other two. This reference frame is applied for orbital navigation and is represented with subscript I in Figure 20.
    - ECEF: Earth-Centered-Earth-Fixed. This reference frame has the same origin as the ECI frame, but rotates with the earth. The z-axis also points towards the North Pole. This frame is strictly speaking not an inertial reference frame, but can be regarded as such for most marine vehicle applications. It is required when considering terrestrial navigation and is represented with the subscript E in Figure 20.
- Local reference frames:
    - NED: North-East-Down. This is a local reference frame defined relative to the reference ellipsoid of the earth as described by WGS 84 (NIMA 1997). The frame has its origin at some chosen point on the earth's surface, where the x- and y-axes spans a tangent plane to the surface while the z-axis points downwards normal to the surface. Specifically, the x-axis points towards true north and the y-axis points towards east. The NED frame is employed for marine surface vehicles operating in a confined area and is represented with the subscript N in Figure 20.
    - BODY: A body-fixed reference frame which is attached to a point belonging to the vehicle under consideration. The axes are often chosen along the principal axes of inertia, hence the x-axis is longitudinal (from stern to bow) and the y-axis transversal (from port to starboard). The z-axis then points downwards, orthogonal to the plane spanned by the x- and y-axes in accordance with the right-hand rule convention. The BODY frame is illustrated in Figure 20.

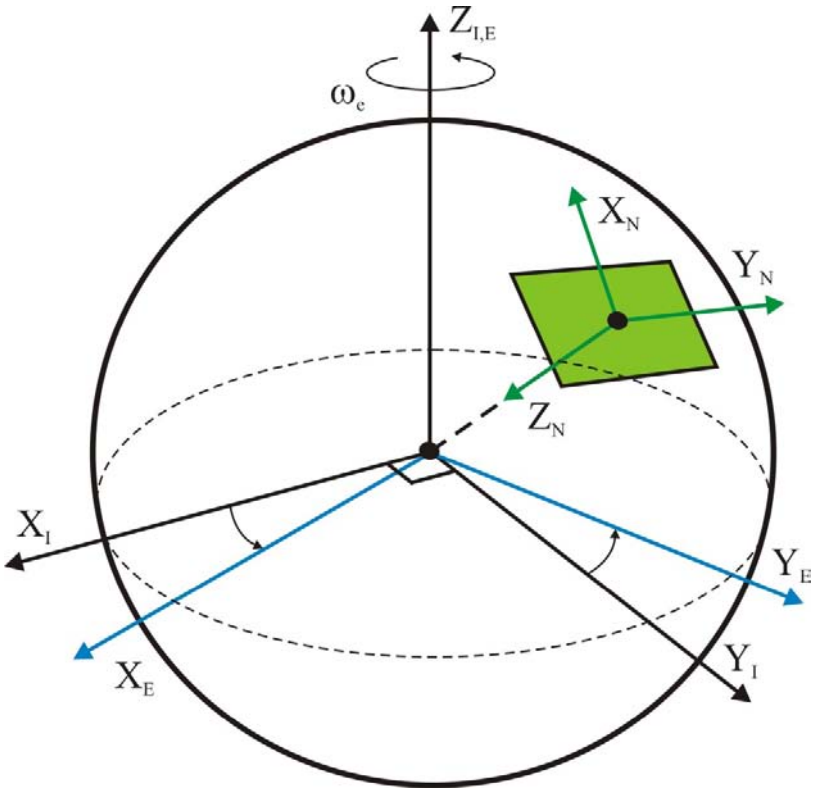

Figure 20: Illustration of the ECI (black), ECEF (blue) and NED (green) reference frames.

In particular, the relationships between the ECEF, NED and BODY frames are relevant for the applications considered in this thesis. GPS coordinates are given relative to the ECEF frame and must be transformed to a local NED frame before they can be utilized for motion control purposes. Also, BODY-fixed velocities must be transformed to the NED frame to evaluate the local motion behavior. However, prior to stating these relationships it is necessary to define some basic motion variables.

In 1950, the Society of Naval Architects and Marine Engineers (SNAME) agreed on a common nomenclature for marine motion variables, see (SNAME 1950). The BODY-fixed axes and their associated linear speeds and angular rates are shown in Figure 21, while the main BODY-fixed variables can be seen in Table 1.

In addition, the NED-relative position and orientation of a BODY frame attached to a vehicle moving in 6 DOF can be expressed by $\boldsymbol{\eta} \triangleq [x, y, z, \phi, \theta, \psi]^{\mathrm{T}} \in \mathbb{R}^3 \times \mathbb{S}^3$, where the orientation is represented by the Euler angles using the ZYX relative rotation convention, see (Fossen 2002; Sciavicco and Siciliano 2002). The BODY-fixed velocities can also be gathered in $\boldsymbol{\nu} \triangleq [u, v, w, p, q, r]^{\mathrm{T}} \in \mathbb{R}^6$, see Figure 21 and Table 1.

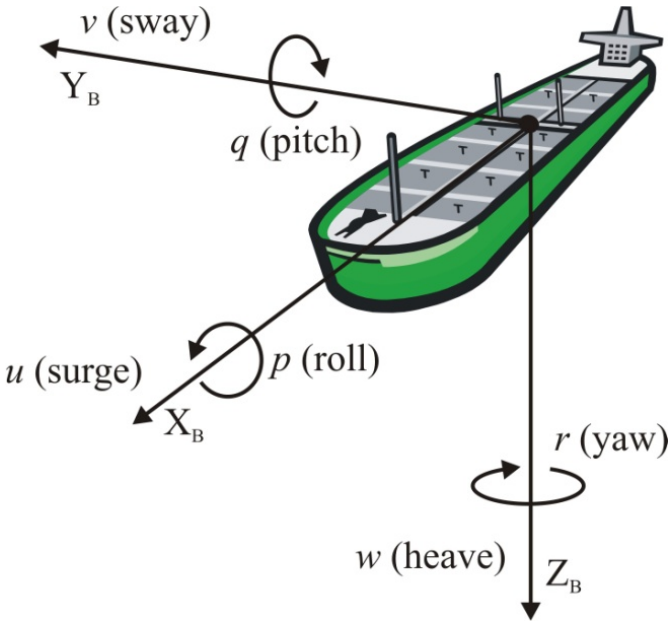

Figure 21: The BODY-fixed reference frame and its associated linear speeds and angular rates.

BODY-fixed axes:	Forces and moments:	Speeds and rates:
X-direction (surge)	X	*u*
Y-direction (sway)	Y	*v*
Z-direction (heave)	Z	*w*
X-rotation (roll)	K	*p*
Y-rotation (pitch)	M	*q*
Z-rotation (yaw)	N	*r*

Table 1: SNAME notation for BODY-fixed forces, moments, linear speeds and angular rates.

However, it is usually sufficient to consider only 3 DOF when dealing with motion on the ocean surface. Consequently, for planar purposes the generalized position vector can be redefined as $\boldsymbol{\eta} \triangleq [x, y, \psi]^{\mathrm{T}} \in \mathbb{R}^2 \times \mathbb{S}$, while the generalized velocity vector can be represented by $\boldsymbol{\nu} \triangleq [u, v, r]^{\mathrm{T}} \in \mathbb{R}^3$. In this reduced configuration space, the relationship between a velocity vector in the NED frame and a velocity vector in the BODY frame can be stated as

$$\dot{\boldsymbol{\eta}} = \mathbf{R}(\psi)\boldsymbol{\nu}, \tag{43}$$

where $\mathbf{R}(\psi) \in SO(3)$ is the rotation matrix

$$\mathbf{R}(\psi) \triangleq \begin{bmatrix} \cos\psi & -\sin\psi & 0 \\ \sin\psi & \cos\psi & 0 \\ 0 & 0 & 1 \end{bmatrix} \tag{44}$$

which represents a positive rotation about the z-axis of the NED frame by an angle ψ, see Figure 22. Details about the transformation between ECEF and NED coordinates can be found in (Fossen 2002).

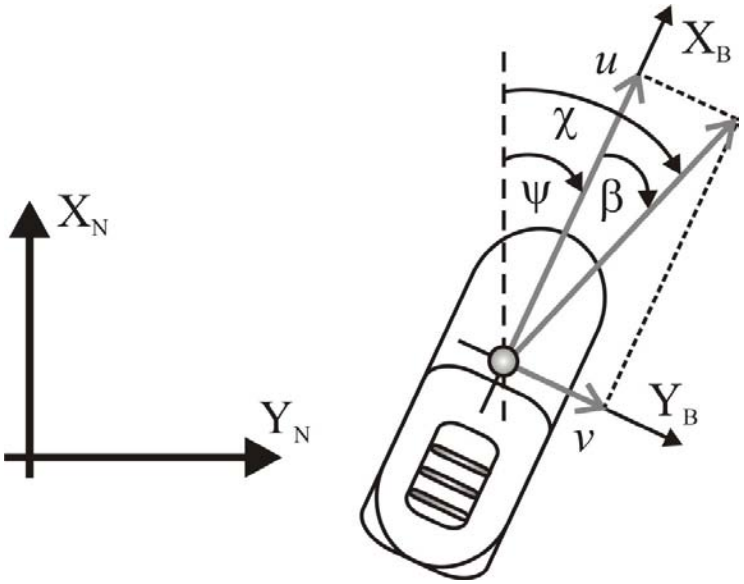

Figure 22: The heading angle ψ represents the orientation of the BODY frame relative to the NED frame, the course angle χ represents the orientation of the vessel velocity vector relative to the NED frame, while the sideslip angle β signifies the difference between the course and the heading.

The above figure also illustrates a key aspect regarding underactuated vessels, namely that the direction of the vessel velocity vector is generally not equal to the direction of the vessel heading. In (Breivik and Fossen 2004a), the relationship between the course angle χ and the heading angle ψ is defined as follows

$$\chi \triangleq \psi + \beta, \tag{45}$$

where β represents the so-called sideslip angle. The sideslip angle is uncontrollable for an underactuated vessel which is unactuated in the lateral sway direction and will only be zero when the vessel travels in a straight line without any influence from environmental disturbances. Hence, the course and heading angles will differ in practice since vessels are always affected by waves, wind and current effects and also regularly carry out nonlinear maneuvers.

These facts imply that in order to for instance achieve path following for a sway-unactuated vessel, the steering law (13) must be assigned to χ and not to ψ. However, by augmenting the steering law with an integral term (Børhaug 2008; Breivik and Fossen 2008c; Breivik and Fossen 2009a, Appendix H), path following can in fact also be achieved through a direct heading assignment. Still, the transient behavior will be worse than for a direct course assignment since the integral action necessarily always lags behind.

In practice, most commercial ship navigation packages of today provide an accurate and reliable measurement of the velocity vector, and so there are currently few reasons to assign the steering law to ψ instead of directly to χ.

Kinetics

The kinetics of a marine surface vessel describes the dynamic interaction effects related to the ambient vessel-water and vessel-air systems. These effects will influence the vessel to a varying degree depending on the vessel type. Regarding the vessel-water system, the vessel weight is always carried by a combination of hydrostatic and hydrodynamic pressure (Faltinsen 2005). The hydrostatic pressure results in a buoyancy force which is proportional to the submerged volume of the vessel, also known as the vessel displacement. In contrast, the hydrodynamic pressure depends on the fluid flow around the hull and is roughly proportional to the square of the vessel speed. Hence, by relating the amount of hull submergence to the vessel speed, something qualitatively can be said about the relative importance of the hydrostatic and hydrodynamic effects. This relationship is efficiently captured by the so-called Froude number, which is defined as the dimensionless parameter

$$Fn \triangleq \frac{U}{\sqrt{Lg}}, \tag{46}$$

where U is the vessel speed, L is the submerged length of the vessel and g is the acceleration of gravity.

According to (Faltinsen 2005), marine surface vessels can broadly be divided into 3 main categories characterized by the Froude number:

- Displacement vessels: At maximum speed, the vessel hull is mainly supported by the buoyancy force. Here, $Fn < 0.4$.

- Semi-displacement vessels: At maximum speed, the vessel hull is no longer mainly supported by hydrostatic pressure since hydrodynamic effects are starting to dominate. Here, $0.4 - 0.5 < Fn < 1.0 - 1.2$.

- Planing vessels: At maximum speed, the hydrodynamic force mainly carries the weight of the vessel. Here, $Fn > 1.0 - 1.2$.

Naturally, these categories do not only refer to an inherent vessel type, but also to different operating regimes. For example, a planing vessel starting at rest will have to move through both the displacement and semi-displacement regimes before reaching the planing regime. The pitch angle of a planing monohull starts to increase as the vessel gains speed, which relates to the fact that the planing hull form is designed to develop a dynamic lift such that its draft decreases with increasing speed. Hence, the lift reduces the wetted surface of the vessel and therefore also the drag such that the pitch angle of the vessel increases even more until a stable steady-state condition is reached. However, a displacement vessel can only operate in the displacement regime. Most large vessels

are of the displacement type, but small boats typically belong to the semi-displacement or planing categories, see Figure 23.

Figure 23: As seen to the left, a large oil tanker is an example of a displacement vessel, while a semi-displacement leisure boat is seen to the bottom right and a RIB-type planing vessel to the top right.

Finally, it is important to take into account the various constraints under which a vessel must perform a required mission. Such constraints typically include the speed range, loading conditions, sea states, water depths, temperatures, etc. In particular, it can be fruitful to view these constraints as representing the axes of a vessel operational condition (VOC) space, see (Perez et al. 2006; Nguyen et al. 2008). The main axes related to an operation within a limited geographical area are shown in Figure 24.

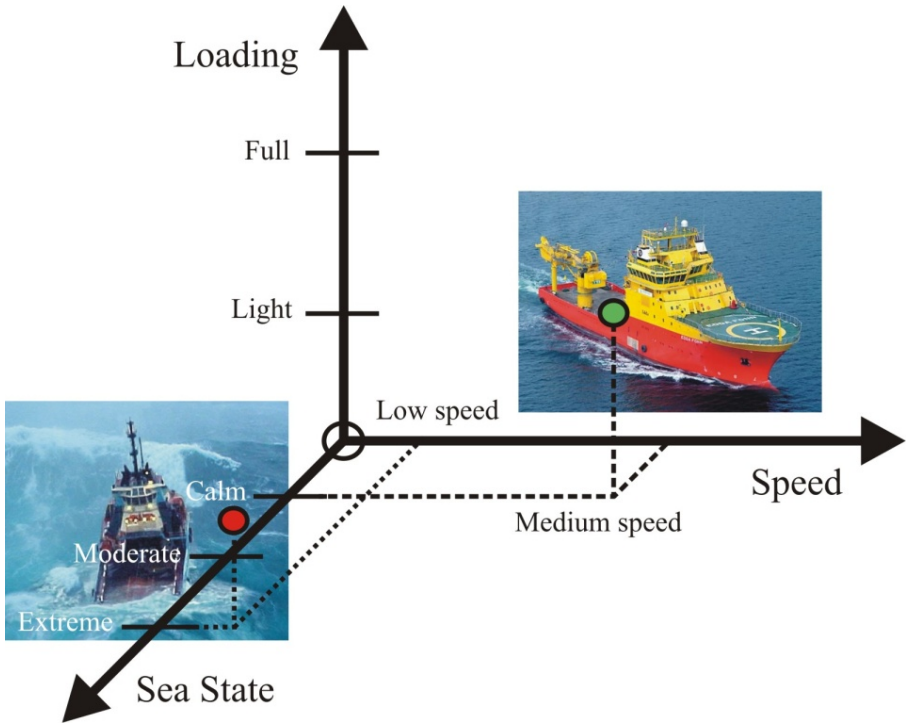

Figure 24: The main axes of speed, sea state and loading which constitute the vessel operational condition (VOC) space for confined-area operations. Adapted from (Perez et al. 2006).

3.3.2. Guidance System

The role of a guidance system is to compute meaningful command signals to a vehicle control system such that the vehicle is able to achieve a given motion control objective. In the context of guided motion control, the guidance system should compute meaningful velocity commands to the velocity control system of the vehicle.

At the core of any guidance system rests a number of guidance algorithms, which in this thesis correspond to kinematic guidance laws as presented in Section 3.2. Depending on the motion control scenario under consideration, a relevant guidance law is selected. In order to ensure feasible velocity or steering commands for a particular vehicle, the key parameters of the selected guidance law must be chosen in accordance with known vehicle maneuverability and agility constraints. For a target tracking scenario, the key parameters are $U_{\mathrm{a,max}}$ and $\Delta_{\tilde{\mathrm{p}}}$, while a path following scenario mainly involves Δ.

In addition, it is important to take into consideration whether the vehicle is fully actuated or underactuated when deciding on how to submit commands to the velocity control system. Specifically, for a sway-unactuated vehicle it can be meaningful to decompose a direct velocity assignment into speed and steering assignments in a polar coordinate fashion.

For example, consider a vehicle whose actual velocity is represented by $\mathbf{v}(t) \in \mathbb{R}^2$, while the velocity command from the guidance system is represented by $\mathbf{v}_{\mathrm{d}}(t) \in \mathbb{R}^2$. The velocity error then becomes

$$\tilde{\mathbf{v}}(t) = \mathbf{v}_{\mathrm{d}}(t) - \mathbf{v}(t) \tag{47}$$

such that the velocity control objective becomes equal to

$$\lim_{t \to \infty} \tilde{\mathbf{v}}(t) = \mathbf{0}. \tag{48}$$

Then the responsibility for achieving this objective can be divided as in Figure 25, where a surge speed controller is given the responsibility of narrowing the speed error $\tilde{U}(t)$, while a yaw rate controller is assigned to narrow the course (steering) error $\tilde{\chi}(t)$. Specifically, the speed and course errors must be employed to correspondingly compute a desired surge speed $u_{\mathrm{d}}(t)$ and yaw rate $r_{\mathrm{d}}(t)$ suitable for implementation, see (Breivik et al. 2008b, Appendix G) for further details.

Traditionally, the course error would be calculated as

$$\tilde{\chi}(t) = \chi_{\mathrm{d}}(t) - \chi(t), \tag{49}$$

which would necessitate having to deal with wraparound problems since the course angles belong to a closed and bounded set. However, this problem can be avoided by

employing a novel method of directly calculating $\tilde{\chi}(t)$ by employing cross- and inner-product information about the velocity vectors $\mathbf{v}_d(t)$ and $\mathbf{v}(t)$.

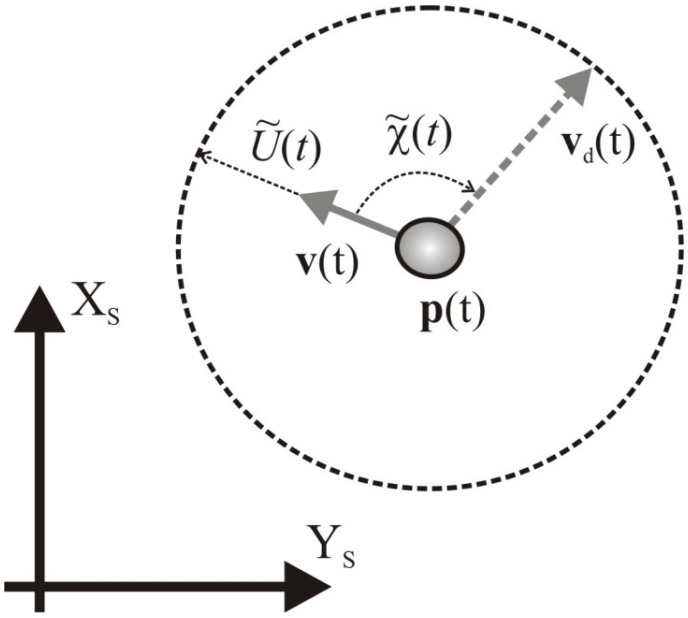

Figure 25: Decomposing the velocity error $\tilde{\mathbf{v}}(t)$ into a speed error $\tilde{U}(t)$ and a course error $\tilde{\chi}(t)$.

The approach has been inspired by the concept of cross-product steering, which is a steering principle used for intercontinental ballistic missiles, see (Battin 1982). This principle employs the notion of a velocity-to-be-gained $\mathbf{v}_g(t)$ which is equal to $\tilde{\mathbf{v}}(t)$ here. The goal is then to drive $\mathbf{v}_g(t)$ to zero, which can be done by applying the cross-product steering law $\mathbf{v}_g(t) \times \dot{\mathbf{v}}_g(t)$, thus aligning the time rate of change of the vector with the vector itself. However, this method suffers from the weakness that it will not command any action if the two vectors are aligned in parallel but opposite directions. Consequently, inner-product information must also be utilized in order to also handle this special case.

Analogously, it is possible to extract $\sin(\tilde{\chi}(t))$ information from the cross product $\mathbf{v}(t) \times \mathbf{v}_d(t)$ and $\cos(\tilde{\chi}(t))$ information from the inner product $\mathbf{v}(t)^T \mathbf{v}_d(t)$ for use in the direct calculation

$$\tilde{\chi}(t) = \operatorname{atan2}\left(\sin(\tilde{\chi}), \cos(\tilde{\chi})\right). \tag{50}$$

This method of directly calculating the steering error has also been used in the full-scale experiments reported later in this thesis, and seems to first have been suggested in (Breivik et al. 2008b, Appendix G).

3.3.3. Velocity Control System

In a guided motion control context, the purpose of a velocity control system is to make a specific vehicle feasibly achieve the desired velocity commanded by the guidance system such that the overall motion control objective is satisfied. The challenge then becomes how to design such a control system.

Most academic work on the design of nonlinear motion controllers for underactuated marine surface vessels are typically based on some variant of the kinetic model presented in (Fossen 2002). However, this model formulation is only valid for displacement vessels with a Froude number $Fn \leq 0.3$, see (Fossen 2005). In practice, it can also be quite difficult to obtain all the parameter values required to populate the model, especially with regard to hydrodynamic damping effects. Consequently, alternative control design methods which do not rely on this model should be explored, in particular when considering motion control of semi-displacement or planing vessels.

Specifically, a novel control design method also suitable for operations outside the displacement regime has been developed for the purpose of controlling the velocity of small underactuated boats. This method requires a minimum of system identification tests to be carried out for the velocity control system to perform well. In addition, the resulting system inherently takes vessel maneuverability and agility constraints into account, such that the commanded velocity from the guidance system is achieved in a controlled and feasible manner.

Early work describing the initial development of this system is reported in (Breivik et al. 2008b, Appendix G). Inspired by the definitions of maneuverability and agility which are frequently used in literature on fighter aircraft, I started exploring a more control-oriented modeling approach to nonlinear motion control than what is usually reported in the marine control literature. In the following, the fundamentals behind this approach is described together with the structure of the resulting controllers.

The terms maneuverability and agility are used to characterize close-combat fighting abilities for fighter aircraft, see Figure 26. In (Paranjape and Ananthkrishnan 2006), it is shown that these terms are in fact not uniquely defined. However, I've chosen to subscribe to the definitions given in (Beck and Cord 1995), where maneuver performance is defined as a measure of steady maneuver capability and agility is defined as a measure of the ability to transition between steady maneuvers.

Figure 26: The F-16 Fighting Falcon is a highly agile jet fighter suitable for dogfights. Courtesy of Richard Seaman.

Consequently, the relevant maneuver states of a surface vessel include the surge speed $u(t)$, the sway speed $v(t)$ and the yaw rate $r(t)$. These variables determine how fast the vessel can move on the sea surface, that is, how fast it can traverse the configuration space. The agility of a vessel then describes how fast it can transition between its maneuver states.

The most relevant maneuverability aspect for control purposes is the relationship between the actuator inputs and the maneuver states. All actuators are ultimately controlled by an electric signal, such that their capacity can be conveniently represented in the range $[-100\%,100\%]$ when abstracting away the actual signal range. For a vehicle whose actuator setup corresponds to that of having a propeller and rudder mounted at the stern, tests can be carried out in which the control signal for both actuators are applied in steps to cover their entire signal range, while simultaneously recording the steady-state response of the maneuver states. Subsequently, by using for example least-squares curve fitting to the obtained data sets, analytic relationships between the control inputs and the maneuver states can be established. The result will constitute a 5-dimensional surface in the combined input (propeller throttle, rudder angle) and output (surge speed, sway speed and yaw rate) space, which is the steady-state input-output surface that the vessel nominally will be able to traverse.

Furthermore, the tests should be carried out in ideal conditions with nominal loading and a minimum of environmental disturbances. The results can then be used to derive a feedforward controller which will be able to achieve any allowable set of speeds by simply allocating the corresponding control inputs from the maneuver map. Feedback

terms must also be added to take care of any discrepancies between the nominal maneuver map and the conditions of a situation where the environmental disturbances or loading are different. Hence, while the feedforward terms handle operations in the nominal part of the VOC space, the feedback terms enlarge this operational area by adding robustness against modeling errors, parametric uncertainties and disturbances.

One way to determine the maximum agility of a vehicle is to record the response of the maneuver states to steps in the control inputs from 0% to 100%. Such step-response analysis will determine how fast the vehicle is able to move in the maneuver space. These agility tests should be carried out for each controllable maneuver state and its corresponding control input. A function can then be defined for each of these maneuver states to encapsulate their corresponding agility. For example, $\alpha_{\mathrm{u}}(\delta)$ can represent the surge speed agility, which varies as a function of the rudder angle δ. Correspondingly, $\alpha_{\mathrm{r}}(\tau)$ can represent the yaw rate agility, which is a function of the throttle input τ. The specific values of $\alpha_{\mathrm{u}}(\delta)$ obtained through step-response tests involving zero to maximum throttle input for a set of rudder angles then represent the maximum attainable surge speed agility $\alpha_{\mathrm{u,max}}(\delta)$. Correspondingly, $\alpha_{\mathrm{r,max}}(\tau)$ will then represent the maximum attainable yaw rate agility obtained through step-response tests employing zero to maximum rudder angle for a set of throttle inputs. See (Breivik et al. 2008b, Appendix G) for more details concerning a simplified version of the agility concept.

To guarantee both static and dynamic feasibility, the desired surge speed $u_{\mathrm{d}}(t)$ and yaw rate $r_{\mathrm{d}}(t)$ supplied by the guidance system should not be used directly in the velocity control system. Instead, they should be fed into a reference filter which has been designed such that its outputs are always constrained within the range of the maneuver map and never change faster than what corresponds to the maximum agility values. Denoting the filter outputs $u_{\mathrm{r}}(t)$ and $r_{\mathrm{r}}(t)$, the control objectives of the surge speed and yaw rate controllers become to reduce $\bar{u} \triangleq u_{\mathrm{r}}(t) - u(t)$ and $\bar{r} \triangleq r_{\mathrm{r}}(t) - r(t)$ to zero.

Considering all these factors, the following surge speed controller can be employed to generate a feasible command for the propeller throttle

$$\tau_{\mathrm{c}}(u_{\mathrm{r}}, \bar{u}, \tau, \delta) = \sigma_{\tau}(u_{\mathrm{r}}, \delta) + k_{\mathrm{p},\bar{\mathrm{u}}}(\tau, \delta)\bar{u} + k_{\mathrm{i},\bar{\mathrm{u}}}(\tau, \delta)\int_0^t \bar{u}\, d\zeta, \tag{51}$$

where $\sigma_{\tau}(u_{\mathrm{r}}, \delta)$ represents the feedforward control assignment based on the maneuver map as a function of the commanded reference speed and the actual rudder angle, and where the PI feedback terms are weighted according to the actual propeller throttle and rudder angle to achieve robust and tight control even in adverse conditions.

Correspondingly, the following yaw rate controller can be employed to generate a feasible command for the rudder angle

$$\delta_{\mathrm{c}}(r_{\mathrm{r}},\bar{r},\tau,\delta)=\sigma_{\delta}(r_{\mathrm{r}},\tau)+k_{\mathrm{p},\bar{r}}(\tau,\delta)\bar{r}+k_{\mathrm{i},\bar{r}}(\tau,\delta)\int_{0}^{t}\bar{r}d\zeta. \tag{52}$$

The velocity control system is thus comprised of filters transforming the velocity commands from the guidance system into feasible reference signals that are subsequently fed to surge speed and yaw rate controllers which consist of feedforward terms based on maneuver map data as well as PI feedback terms included for robustness reasons. These controllers have proven themselves successfully in full-scale experiments with both semi-displacement and planing vessels, some of which are presented in Chapter 5. Further implementation details about this velocity control system will not be given in this thesis, where one of the main goals is rather to illustrate the fundamental aspects of the guided motion control scheme.

3.3.4. Guided Motion Control System

Summing up the material presented in this chapter, a guided motion control system in general consists of:

- A guidance system which partly is vehicle-independent through its set of guidance laws and partly vehicle-dependent through proper tuning of the guidance parameters as well as through the format in which the guidance commands are sent. The task of the guidance system is to compute feasible velocity commands whose fulfillment ensures that a specific vehicle achieves a given motion control objective.

- A velocity control system which is purely vehicle-specific. It can be designed based on maneuverability and agility test data in order to attain its commanded velocity in a controlled manner. This system relies on local actuator controllers to carry out its commands. Such controllers are not the topic of this thesis, but they are often implemented as pure feedback controllers.

In particular, a guided motion control system developed for an underactuated marine surface vehicle assigned to achieve a target tracking motion control objective can be designed and structured as shown in Figure 27. Other motion control scenarios can then be handled simply by changing the guidance law.

The velocity control system can naturally be designed through other approaches than the one suggested here. However, these can nevertheless not be based on the conveniently

analytic kinetic vessel model found in (Fossen 2002) since its formulation only describes displacement vessels operating at Froude numbers $Fn \leq 0.3$. In fact, this limitation constituted a hard practical constraint when I started considering velocity control of vessels operating at much higher Froude numbers, and it thus represented the main motivating factor for developing a more control-oriented modeling approach suitable also for semi-displacement and planing vessels. A particular advantage of this approach is that it inherently takes vehicle maneuverability and agility constraints into account and therefore also do not drive the vehicle actuators to saturation.

In conclusion, guided motion control systems as described here have so far been developed and successfully implemented on a set of 3 different vehicle platforms. These platforms and some corresponding full-scale results are described in Chapter 4 and 5 as well as in Appendix G.

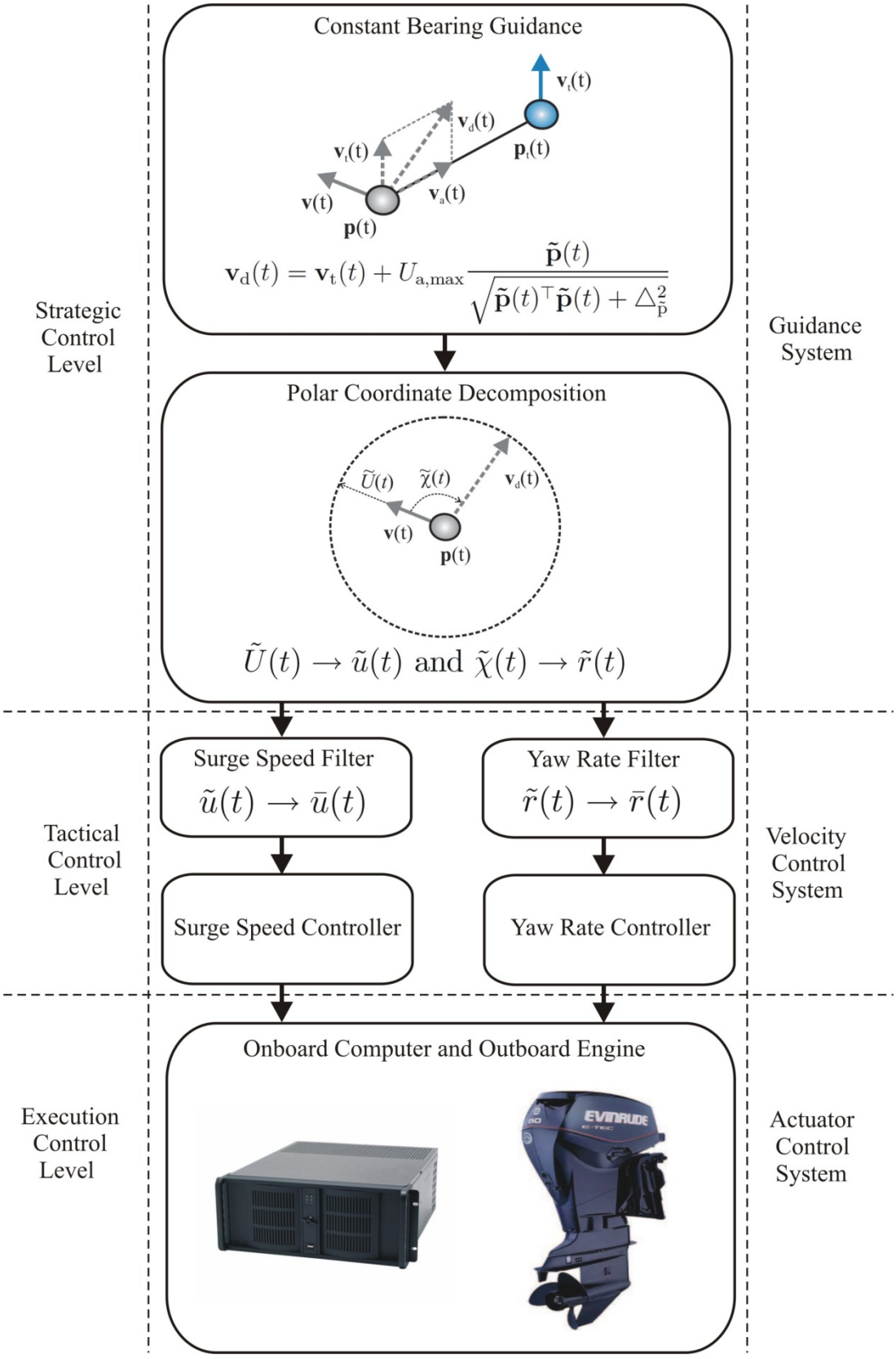

Figure 27: A guided motion control system capable of achieving high-speed target tracking for an underactuated marine surface vehicle controlled by an outboard engine.

4. Unmanned Surface Vehicles

This chapter considers several aspects related to unmanned surface vehicles (USVs). First, a brief historical overview and some motivational arguments are given. Then the present status is reviewed, before future challenges and possibilities are discussed. Finally, current Norwegian USV efforts are described.

4.1. Background and Motivation

Already in 1898, the Serbian-American inventor and engineer Nikola Tesla obtained a patent for radio-based remote control of boats (Tesla 1898). Earlier that same year he had amazed a crowd of people who witnessed a demonstration of his system in New York's Madison Square Gardens (Withington 2008). In his autobiography from 1919, Tesla would go on to predict the development of robotic vehicles *"…capable of acting as if possessed of their own intelligence, and their advent will create a revolution."* (Tesla 1919).

When people hear of unmanned vehicles today they mostly think about either unmanned aerial vehicles (UAVs), unmanned underwater vehicles (UUVs) or unmanned ground vehicles (UGVs). Little attention has so far been paid to USVs. In fact, the US Navy did not release its first USV Master Plan until 2007 (U. S. Navy 2007), where a USV is defined by:

- Unmanned: Capable of unmanned operation. Can be manned for dual use or test and evaluation. Has varying degrees of autonomy.

- Surface Vehicle: Displaces water at rest. Operates with near continuous contact with the surface of the water. Interface of the vehicle with the surface is a major design driver.

Figure 28: UAVs, UUVs and UGVs have received far more attention than USVs.

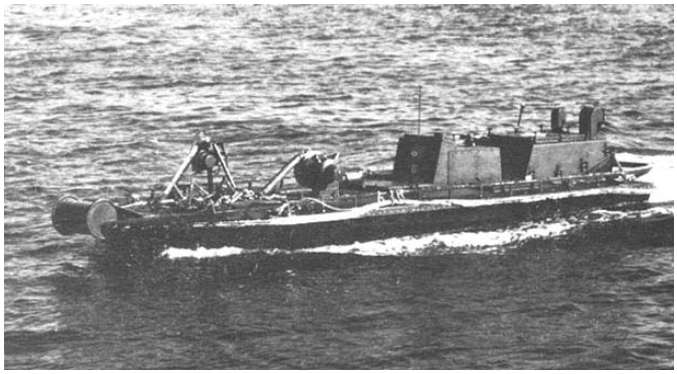

Figure 29: A remotely-controlled "chain drag" minesweeper drone (MSD) operating in Vietnam in the late 1960s. Courtesy of the US Navy.

USVs have actually been developed and operated since the Second World War, but mostly as drone boats for mine clearance and firing practice. A brief historical timeline encompass (Portmann et al. 2002):

- 1940s:
  - Laying smoke for the Normandy invasion (COMOX).
  - Mine and obstacle clearance (Demolition Rocket Craft).
  - Drone boats collecting radioactive water samples after atomic bomb blasts on the Bikini Atoll.
- 1950s:
  - Remotely operated minesweeping boats (DRONE).
  - Target boats for missile firing practice and destroyer gunnery training.
- 1960s:
  - Munitions deployment (Drone Boat).
  - Minesweeping Drone (MSD) for use in Vietnam, see Figure 29.
- 1990s:
  - Sophisticated minesweeping systems (R/C DYADS, MOSS, ALISS).
  - Autonomous features in the Remote Minehunting System (RMS).
  - Reconnaisance and surveillance missions (ASH, Roboski).

It is only during the last decade that USVs have been considered for more advanced operations, and their use harbors great potential for:

- Reduced personnel cost.
- Less need for personnel in exposed areas and thus improved personnel safety.
- Reduced risk and smaller consequences from operator errors.
- Increased operational precision.
- Widened weather window of operations.
- Flexible vehicles with reduced emissions and thus more environmentally-friendly operations.
- New vehicle designs and concepts of operation.

Like other categories of unmanned vehicles, USVs are particularly suited for so-called dirty, dull and dangerous missions:

- Dirty: Disaster monitoring, operations in polluted or NBC-exploited areas.
- Dull: Maritime surveillance, geophysical surveys, communication relays.
- Dangerous: Military observations, operations in desolate areas, anti-submarine warfare (ASW), mine countermeasures (MCM), anti-piracy operations.

USVs might also cooperate with other unmanned platforms such as UAVs and UUVs to form large communication and surveillance networks that are able to provide unique situational awareness capabilities. In fact, USVs are unique in the sense that they are able to communicate with vehicles both above and below the sea surface at the same time, capable of acting as relays between underwater vehicles and vehicles operating on land, in the air or in space. Through such cooperative behavior, unmanned vehicles can act as autonomous information gatherers feeding computer-based tools that provide historical and real-time information to end-users about what goes on in the ocean space. Such systems will enable unprecedented decision-making capabilities and constitute extremely efficient tools for knowledge-based management of environmental and marine resources, see also Section 2.3 and Figure 8.

Another important application area concerns resupply of UUVs far out at sea. Such vehicles are increasingly used to collect different types of ocean data, but have limited battery capacity and are often accompanied by large and expensive support vessels. Both time and money can be saved if the manned support vessels can be replaced by USVs. A large fleet of UUVs can thus be served by a smaller fleet of USVs, resulting in an energy-efficient and environmentally-friendly UUV support system.

Local-area positioning applications are also interesting for monitoring or search-and-rescue purposes. Such applications will benefit from USVs that can keep their position in a weather-optimal manner, reducing fuel consumption and thus prolonging the operation. While a dynamically positioned USV continuously rotates its bow against the weather, its cameras rotate in the opposite direction to keep focus on their assigned targets.

According to (Bertram 2008b), transatlantic cargo ships have reduced their crew from 250 to 15 in the period 1860 to 2000. Developments within machinery systems, navigational equipment, communication technology and positioning reference systems have contributed to a present-day situation where the bridge can be operated by a single person. This development will ultimately lead to completely unmanned cargo ships shuttling between the major ports of the world. Controlled in a master-slave fashion, such unmanned ships were already envisioned almost four decades ago (Schönknecht et al. 1973), see Figure 30.

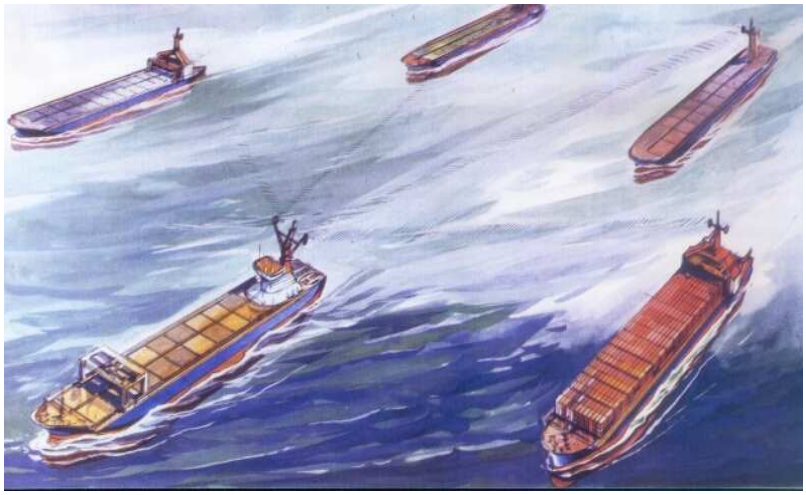

Figure 30: A formation of unmanned containerships slaved to a manned mother ship. Courtesy of (Schönknecht et al. 1973).

4.2. Current Status

A majority of USVs currently under development are found in the United States and Israel, encompassing mostly naval but also scientific applications. No applications currently seem to exist in the commercial market.

Other countries that pursue USV development include Canada (Barracuda, Dolphin, Seal), France (Argonaute, Basil, Seakeeper), Germany (Measuring Dolphin, Rescuing Dolphin), Italy (Alanis, Charlie), Japan (UMV-H, UMV-O), Norway (Mariner), Portugal (Delfim, Caravela), Sweden (Piraya, SAM), and the United Kingdom (Mimir, SASS, Springer), see also (Caccia 2006; Bertram 2008a).

The only industrial-level USVs are currently found within the naval segment, mainly applied for intelligence, surveillance, and reconnaissance (ISR) operations. These vehicles are mostly remotely operated.

Present USVs are typically also small boat-like vehicles of up to around 10 meters in length, see Figure 31. Many of them have been adapted from manned designs that were originally intended to accommodate human occupants. However, such limitations need not apply to these vehicles, which for instance can be designed as semi-submersibles for improved stealth and platform stability (Cooper et al. 2002).

Most USVs are just experimental platforms, used to test hull designs, communication and sensor systems, propulsion solutions, as well as control algorithms. Compared to the current UAV market and technology, USV development is still in its infancy.

Figure 31: Current USVs are mostly small boat-like vehicles. Many are retrofitted from manned designs. The only industry-standard USVs today are employed for naval purposes.

4.3. Future Challenges and Possibilities

Returning to the USV Master Plan, the following levels of autonomy are defined:

- Manual: Man in loop continuously or near-continuously.

- Semi-autonomous: Some vehicle behaviors are completely autonomous (e.g., transit to station, activate sensors). The vehicle refers to its operator when directed by the operator or by its own awareness of the situation (e.g., for permission to fire).

- Autonomous: The vehicle governs its own decisions and makes its own decisions from launch point to recovery point.

In the short term, remotely or semi-autonomous USVs will continue to dominate. For such applications, communications issues are of the utmost importance. A shift toward more autonomy will require the introduction of new, advanced motion control concepts, where perhaps the most important contributor in the short term is collision avoidance.

Collision avoidance requires both sense and avoid abilities:

- Sense: Access to both global (electronic charts, etc.) and local (radar, stereo vision, etc.) information about the surrounding environment.

- Avoid: Superior maneuverability and agility through powerful actuators as well as advanced motion control algorithms that are able to perform both long-term (proactive) and short-term (reactive) planning to ensure avoidance.

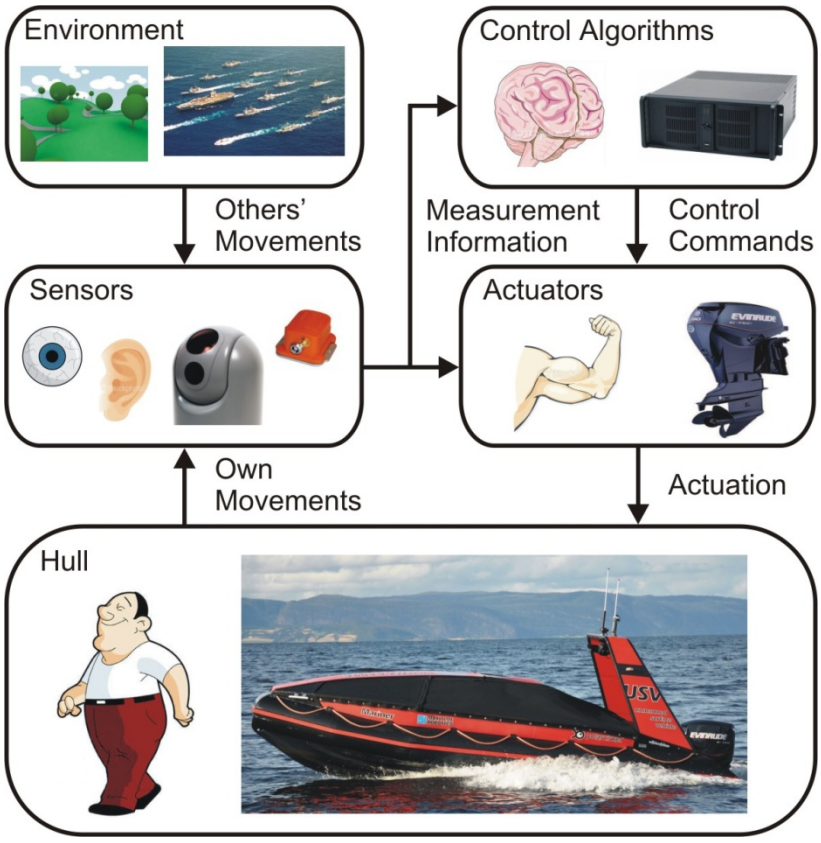

Figure 32: Analogy between a human and a USV. To be able to maneuver in a collision-free manner, the USV needs to know about its environment in addition to its own movements.

The main challenge in designing sufficiently dependable collision avoidance systems lies in the sensor solutions. It is vital to be able to develop a composite sensor suite which reliably can detect both small and large objects for all types of visibility and weather conditions. This sensor problem currently represents one of the most fiercely pursued UAV areas of research, and USVs are naturally expected to benefit from this development.

In the long term it is desirable to develop more advanced cognitive functions for the USVs such that they can make their own decisions in unfamiliar and unstructured environments. Such functionality will require the vehicles to be equipped with intelligence similar to humans. It remains, however, to clarify whether humans are so smart that they are able to understand their own intelligence and therefore manage to engineer it artificially. If not, truly autonomous USVs will never see the light of day.

Figure 33: The Norwegian rescue vessel Elias with his friends Kaptein Krutt and Sinus. It remains to be seen if similar autonomy can be achieved in reality. Courtesy of Filmkameratene/SF Norge.

Apart from the purely technological challenges, commercial USV applications fundamentally depend on the development of a legal framework which provides guidelines and renders possible unmanned operations in manned seaways.

Currently, very little has been done in this area. One of the few ongoing efforts is pursued by the standards development organization ASTM International's Committee F41 on Unmanned Maritime Vehicle Systems (UMVS), which has been addressing standards development for UUVs since 2005 and USVs since 2007.

At the moment, Chapter V of the International Convention for the Safety of Life at Sea (SOLAS), which is administered by the United Nations agency IMO (International Maritime Organization), poses the possibly strictest condition to the application of USVs: *"From the point of view of safety of life at sea, all ships shall be sufficiently and efficiently manned."*

Also, the Norwegian Maritime Directorate (NMD) demands that: *"Every maritime operation must have a captain in charge. In case of a USV, the captain can be located on the bridge of the manned mother vessel, as long as he has sensor-based and/or visual view of the operational area."*

A lot of regulatory work thus remains to be done before USVs can be turned loose on the Seven Seas, but fortunately inspiration can be sought from ongoing work concerning UAVs.

Figure 34: A two-meter long sailing buoy intended for collection of meteorological and oceanographic data in areas where traditional buoy technology falls short. Courtesy of CMR.

4.4. Norwegian Efforts

USV activities in Norway have at best been limited to the infrequent use of target drones by the Royal Norwegian Navy. No concerted effort is currently being pursued for more advanced solutions, but two separate initiatives have recently surfaced.

4.4.1. Christian Michelsen Research

The first initiative involves so-called autonomous sailing buoys (ASBs), developed by a team at the Bergen-based research organization Christian Michelsen Research (CMR). The small ASBs are equipped with a glass-fibre armed wing sail for propulsion and satellite communication through the Iridium system (Stensvold 2009), see Figure 34. Partly sponsored by NFR, the development has been going on since 2006.

4.4.2. Maritime Robotics

The second initiative concerns technology development for USVs pursued by the small privately-held and Trondheim-based company Maritime Robotics (MR). Cooperation between MR and NTNU started back in 2006 through a project partly financed by NFR. In particular, NFR's maritime innovation program MAROFF granted funds for the project "175977: Unmanned Surface Vehicle".

The initial contact between MR and NTNU concerned project and master thesis work on the development of heading autopilots and way-point navigation systems for USVs, resulting in (Beinset and Blomhoff 2007).

Figure 35: Initial sea trials with target tracking were carried out in June 2008 with a retrofitted Kaasbøll 19-feet planing monohull equipped with an Evinrude 50 E-Tec outboard engine.

I started collaborating with MR in 2007, especially on matters of formation control. Project and master thesis work on collision avoidance, dynamic positioning and low-cost navigation systems for USVs was also carried out under my supervision, resulting in (Loe 2008), (Halvorsen 2008) and (Ellingsen 2008). Currently, a group of 5 MSc students working under my supervision considers aspects of AUV-USV docking, weather-optimal positioning control for underactuated USVs, as well as path planning, path maneuvering and formation control for USVs.

Target tracking functionality was initially developed during the summer of 2008. Velocity controllers were first implemented and tested before a guidance system was added. The development platform was MR's first test vehicle as shown in Figure 35. Some of this work has been reported in (Breivik et al. 2008b, Appendix G).

The guided motion control system developed for the Kaasbøll USV was later ported to the Viknes platform and further refined before using it for formation control purposes in September 2008. NTNU's research vessel Gunnerus was then hired to play the role of a manned leader vessel to which a virtual target point was attached, translating and rotating with Gunnerus as if belonging to its extended rigid body. The task of the Viknes USV was then to track the motion of this target and thus move in formation with the leader vessel, without any a priori knowledge of Gunnerus' future motion behavior.

Some of these formation control results have been reported in (Breivik and Hovstein 2009c). As far as I am aware, these full-scale experiments were the first of their kind to

be carried out worldwide. Achieving high-speed target tracking for an underactuated USV is a challenging task that currently does not appear to have been reported elsewhere in the research literature. Additional experiments involving two USVs moving in formation with Gunnerus are reported in Chapter 5 of this thesis.

After phasing out the Kaasbøll USV, Maritime Robotics now owns and operates two leisure boats retrofitted for control purposes. The Viknes USV is based on a Viknes 830 semi-displacement hull, while the Mariner USV is based on a Polarcirkel 660 planing hull, see Table 2, Figure 36 and Figure 37. These boats represent excellent test platforms for carrying out full-scale experiments with advanced motion control system functionality. Their location in direct proximity to the Trondheimsfjord also makes for easy and convenient sea trials, see Figure 38.

USV:	**Viknes**	**Mariner**
Hull type:	Semi-displacement	Planing
Length:	8.3 m	6.6 m
Breadth:	3.0 m	2.2 m
Weight:	3300 kg	1200 kg
Engine:	Inboard Yanmar 184 hp	Outboard Evinrude E-Tec 150 hp
Top speed:	20 knots	38 knots
Navigation:	Furuno SC-50	Kongsberg Seatex Seapath 20
Role:	Multipurpose test vehicle	Early concept demonstrator

Table 2: The Maritime Robotics USV fleet consists of two significantly different types of boats, both of which provide a rapid prototyping environment with Matlab/Simulink-compliant software.

Figure 36: The Viknes USV represents a flexible test platform from which to conduct full-scale motion control experiments throughout the year. Courtesy of Maritime Robotics.

Figure 37: The Mariner USV is a high-speed test platform. Courtesy of Maritime Robotics.

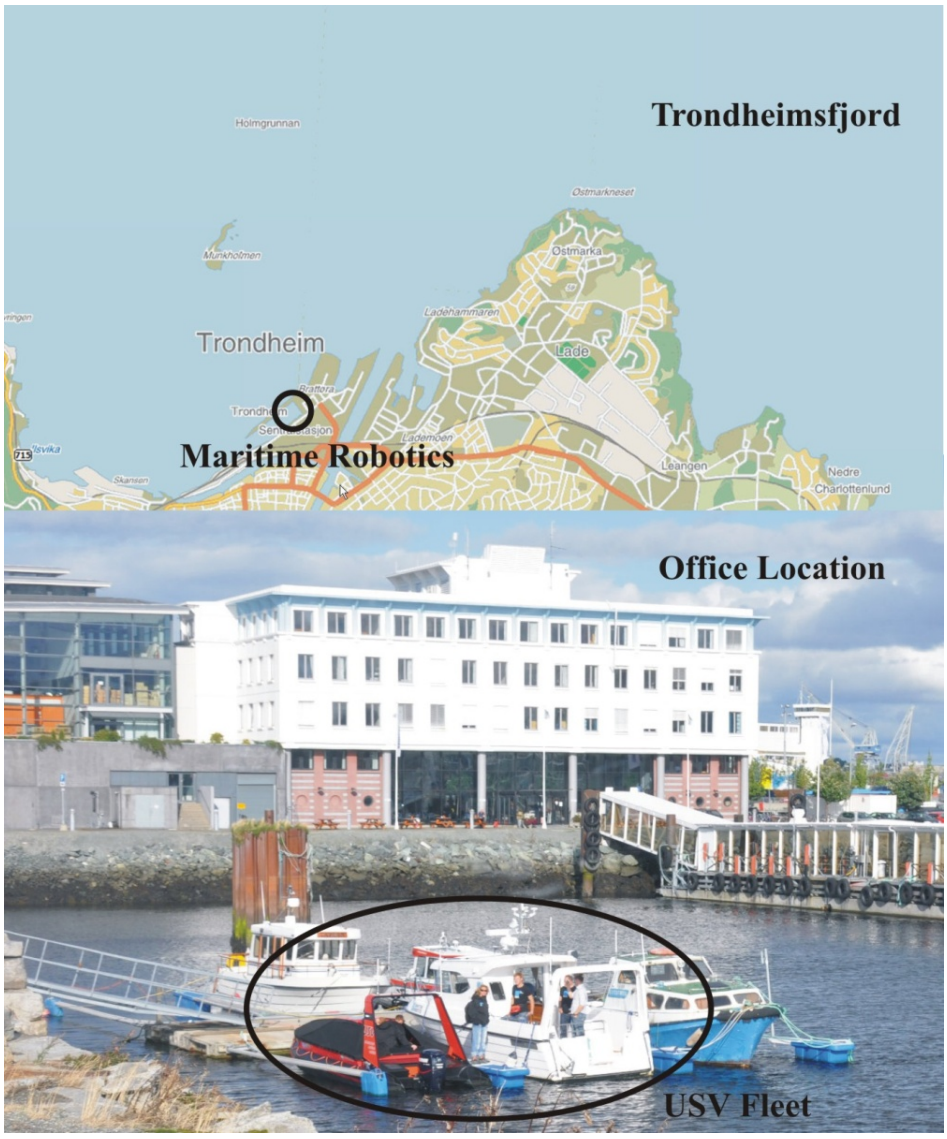

Figure 38: Maritime Robotics' offices and USV fleet is located in the immediate vicinity of the Trondheimsfjord, offering unprecedented test facilities for USV research and development.

5. Formation Control

This chapter considers the topic of formation control in a marine survey context. Starting with some motivational arguments, various formation control concepts are subsequently reviewed. A formation control scheme termed coordinated target tracking is then suggested, offering a flexible survey functionality within a leader-follower framework. Finally, some full-scale experimental results which involve a manned leader vessel followed by two unmanned surface vehicles are presented.

5.1. Motivation

Formation control technology enables multiple vehicles to purposefully collaborate with each other to solve difficult challenges and such technology plays an increasingly important role for commercial, scientific and military purposes. Today, relevant applications can be found everywhere; at sea, on land, in the air and in space.

At sea, the subject of formation control has been important for centuries. In old times, groups of warships had to be controlled during naval battles. In both world wars, it was pivotal for merchant ships to travel in convoys. Today, oceanographers utilize platoons of autonomous underwater vehicles to efficiently gather timely and spatially-distributed data for the construction of sea topography maps. Formation control is also required for underway ship replenishment operations, where various types of goods must be transported between ships moving in transit.

On land, military applications include platoons of scout vehicles, coordinated clearing of mine fields and mobile communication and sensor networks.

In the air, unmanned aerial vehicles are currently playing an increasingly important role, especially in military operations, both strategically and tactically. Flying sensor networks acting as eyes in the sky open up new possibilities for information gathering and distribution, for instance in search-and-rescue missions. More prosaic formation flying applications include aerial acrobatics, see Figure 39.

Spacewise, a recent trend is the concept of large sensor arrays consisting of multiple satellites. Spacecraft cooperate to act as a single instrument, thus achieving a level of resolution previously unheard of, and practically impossible to obtain by employing any single satellite.

Ultimately, multi-vehicle operations render possible tasks that no single vehicle can solve, as well as increase operational robustness toward individual failures.

Figure 39: The Royal Air Force aerobatic team The Red Arrows flying in formation with four Eurofighter Typhoons. Courtesy of BAE Systems.

5.2. Formation Control Concepts

Control system researchers have always been fascinated by the natural world and sought inspiration from it whenever applicable. This fact especially holds true for concepts relating to group coordination and cooperative control. The aggregate behavior observed in nature such as flocks of birds, schools of fish, herds of ungulates and swarms of bees has been and still remains the focus of a concerted effort by researchers to unlock some of the secrets of the natural world for use in artificial systems.

Specifically, the computer scientist Craig Reynolds originally proposed a distributed behavioral model for bird-like simulation entities to be able to naturally attain realistic motion patterns in animation of animal groups (Reynolds 1987). Simple motion primitives were suggested for each group member such as collision avoidance, velocity matching and neighbor tracking, resulting in an overall complex motion behavior resembling that found in nature.

In principle, this type of emergent behavior is similar to that illustrated for cellular automata in (Wolfram 2002), where the assignment of simple behavioral rules to each cell in an automaton results in an emergent and unpredictable overall complexity. However, this kind of rule-based paradigm hardly lends itself to rigid mathematical analysis, nor can it easily be applied as a constructive tool for designing cooperative behavior with guaranteed coordinated performance for vehicle systems.

Also, by applying such suggested motion primitives, the group ultimately degenerates into a steady-state condition of stationary speed and orientation if it is not roaming in a

complex environment capable of continuously exciting it. Still, this property has been put to good use with the concept of virtual leaders, which can be employed to herd and control a group by using artificial potential fields (Leonard and Fiorelli 2001). Relevant work in the vein of behavioral assignments is also reported in (Balch and Arkin 1998).

Interesting and useful as it may be, achieving cooperative control through enforcing local motion primitives does not generally guarantee a specific group behavior. However, achieving a specific group behavior is usually what formation control is all about. It is typically a high-precision engineering application which entails the assembly and maintenance of a particular geometric formation structure.

Relevant work can be found in (Lewis and Tan 1997), where the concept of a virtual structure is put forward. In this framework, the formation is considered analogous to the geometric structure of a rigid body, where the geometric constraints of the structure are enforced by feedback control of the involved vehicles. Furthermore, the design of the approach is such that if a vehicle fails, the rest will reconfigure accordingly in order to maintain the desired structure, automatically accounting for the weakest link. Similar work is also reported in (Ihle et al. 2006b), where the authors propose to use constraint forces originating from constraint functions in order to maintain a formation as a virtual structure. This approach is rooted in analytical mechanics for multi-body dynamics and facilitates a flexible and robust formation control scheme.

In addition to the behavior-based and virtual structure concepts, leader-follower schemes have also been extensively investigated in the literature, see (Breivik et al. 2008a, Appendix F) and the references therein. In this framework, a formation consists of one or more (real or virtual) leaders to which a number of followers are assigned, see Figure 40. The task of the followers is to somehow mimic the motion of the leaders such that an overall formation goal is achieved. This kind of approach is highly intuitive and has so far been employed in manned applications such as underway replenishment and aerial acrobatics. It is also particularly suitable for underactuated vehicles since underactuated followers typically will be able to follow underactuated leaders.

5.3. Coordinated Target Tracking

As previously mentioned in Chapter 4, USVs might in the future cooperate autonomously with other unmanned platforms to form large communication and surveillance networks that are able to provide unique situational awareness capabilities. However, such formation control technology is still just a dream. Still, as a means to fulfill such a dream, intermediate technologies must be developed, especially with current applications which are considered important in mind. When transitioning from remotely-controlled to self-controlled USVs, a step-by-step approach must be taken.

Figure 40: A naval battle group moving in a leader-follower formation. Courtesy of NATO.

A case in point involves marine survey operations, which today are both costly and time consuming since they are performed mostly by single vessels. For such operations, USVs can for instance be employed to augment the basic capability of a manned survey vessel by purposefully moving in formation with it, see Figure 41. The question then becomes how such functionality should be implemented.

Since the performance of behavioral methods is hard to predict and verify analytically and the virtual structure framework seems poorly suited for underactuated vehicles, the leader-follower framework is chosen as a basis from which to develop a USV-augmented formation control system. Within this framework, many authors have chosen to develop systems which rely on predefined paths which the formation must traverse. For marine control purposes, such coordinated path following solutions are reported in (Skjetne 2005; Ihle 2006a; Ghabcheloo 2007; Børhaug 2008). However, each time the mission changes or something unexpected happens, the original path must be redesigned with the new situation in mind.

It would therefore be advantageous to have access to a system where the captain of the manned survey vessel can maneuver as he pleases without being constrained to move along any predefined paths. A system where the leader vessel can augment its basic capabilities by attaching or detaching a number of follower USVs as needed, thus providing a path-independent plug-and-play functionality for maximum flexibility.

As a first step toward developing such a system, a set of separate target tracking problems can be defined. Each problem then corresponds to a specific follower vehicle and the total set of problems to the desired formation. Hence, virtual targets are defined

relative to the leader such that each follower USV will move in formation with the leader when tracking the position of its individually assigned target. A formation supervisor onboard the leader vessel can then straightforwardly attach or detach follower USVs as needed, as well as allocate meaningful formation geometries on demand. Being a surface application, the motion variables of the leader can also easily be broadcasted through radio signals to the other formation members.

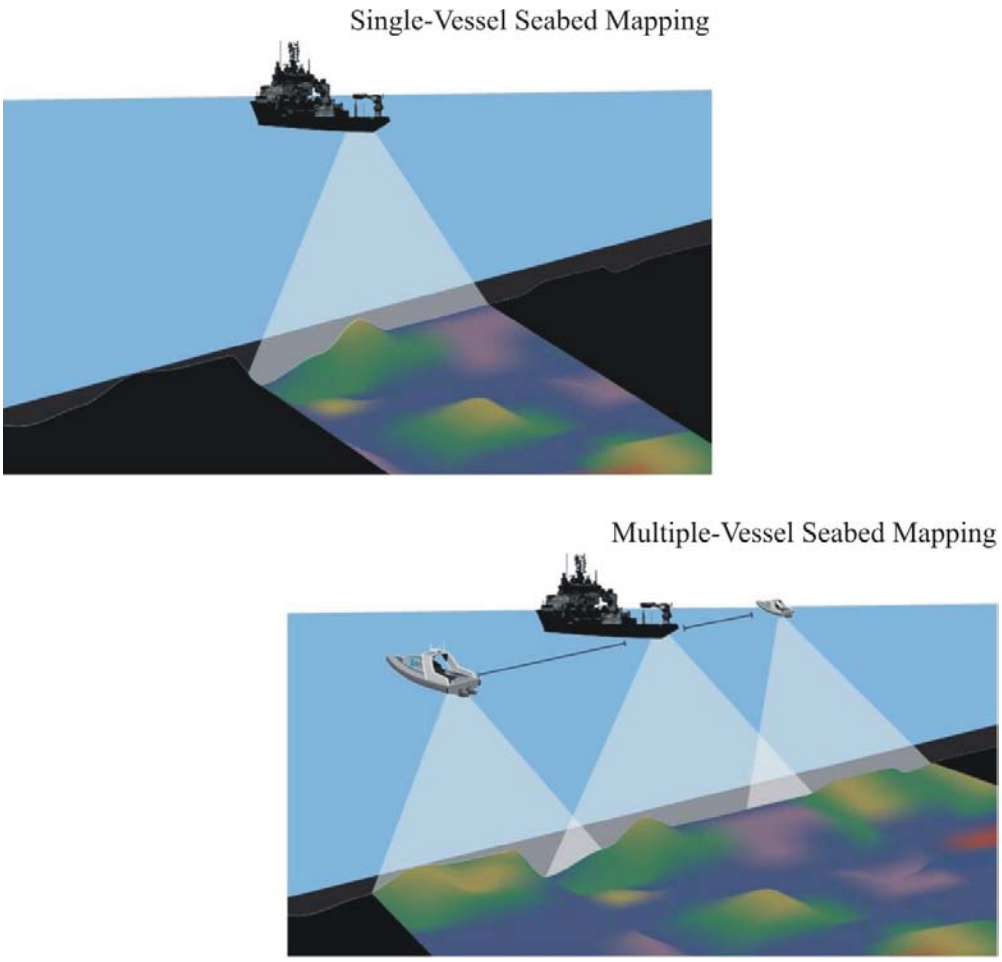

Figure 41: USV-augmented seabed mapping entails faster and cheaper operations since the capacity of the main survey vessel is significantly expanded. Courtesy of Maritime Robotics.

Termed *coordinated target tracking*, this scheme provides a simple and flexible formation control functionality which is well suited for typical marine survey applications.

A similar functionality has also been suggested in (Kyrkjebø 2007), but the proposed control approach assumes fully actuated vessels which travel at low speeds. In contrast, this thesis considers high-speed applications which involve underactuated USVs.

Finally, in (Aguiar et al. 2009) so-called cooperative target following and target tracking schemes are suggested. These approaches also consider a leader vessel whose future motion pattern is unknown, but they differ from the approach considered here since the follower vessels are tasked with moving along a path which has already been traced out by the leader. Hence, in the framework of this thesis such functionality would be classified respectively as path following or path tracking, where the path is continuously created in the wake of a leader vessel which is allowed to maneuver freely.

It actually appears that coordinated target tracking for underactuated marine vehicles travelling at high speed has not been considered in the literature before. Hence, this functionality seems to represent a truly novel contribution within the marine control community, applicable not only to marine survey operations but also to underway replenishment and similar coordinated control applications at sea. Its performance will be illustrated through excerpts from some full-scale experiments in what follows.

5.4. Full-Scale Experiments with USVs

As already mentioned in Chapter 4, the first time formation control by coordinated target tracking was achieved successfully in full scale was on the 25th of September 2008 when Maritime Robotics' Viknes USV tracked a virtual target point defined in relation to NTNU's research vessel Gunnerus. Several such tests have since been carried out, two of which will be mentioned here.

In particular, these two experiments were performed in relation with the visit by the Norwegian broadcasting corporation NRK on August 18th 2009. While Maritime Robotics contributed with their Mariner and Viknes USVs, NTNU hired a helicopter to enable filming of the full-scale demonstrations from the air and also placed Gunnerus at disposal as a leader vessel. This research vessel sports a DP system for low-speed operations and is also equipped with a remotely operated vehicle (ROV) for underwater operations, see Figure 42.

In what follows, some practical aspects are discussed before a sample of results from the demonstrations is presented.

5.4.1. Practical Aspects

Due to safety considerations and requirements from the port authorities in Trondheim, all motion control experiments in the Trondheimsfjord are performed with at least one person aboard each USV. Ironically, both USVs were thus manned during the trials.

Figure 42: NTNU's research vessel Gunnerus is a 30 m long displacement vessel capable of reaching a maximum speed of 13 knots. The phased-out Kaasbøll USV is seen in the foreground. Courtesy of Maritime Robotics.

Prior to the NRK demonstrations, guided motion control systems employing CB guidance and specifically-tailored velocity control systems had been implemented aboard each USV. However, details about the particular guidance and control system implementations will not be reported here.

While the Viknes USV is quite a sluggish boat with a semi-displacement hull and equipped with an inboard motor and a propeller + rudder configuration, the Mariner USV is a much more maneuverable vehicle with its planing hull and outboard engine configuration. Both USVs are thus unactuated in sway and cannot control their heading independently of their position at any speed. Onboard computers provide a rapid prototyping environment with Matlab/Simulink-compliant software and execution-level proportional controllers ensure that the actuators respond effectively to throttle and rudder commands, see Figure 27.

As shown in Table 2, both vehicles are also equipped with a one-stop-shop navigation package which provides all the necessary motion variables required for controlling their own motion. The leader vessel Gunnerus was configured to broadcast its motion variables via radio signals to both USVs. However, since GPS signals are only updated at 1 Hz, kinematic estimators were also developed to estimate the position in-between updates using velocity information. Alternatively, the position error would for instance increase unacceptably to 6 m between each GPS update when travelling at 6 m/s.

Finally, none of the USVs employ any kind of wave filtering due to their size and maneuverability.

5.4.2. Case 1: Surveys at Sea

Motivated by marine survey operations where USVs can be used to augment the basic capability of a manned survey vessel in a plug-and-play manner, experiments were carried out where the Maritime Robotics USVs tracked the motion of individually assigned virtual targets defined in a survey formation pattern relative to Gunnerus.

In particular, the formation positions were defined relative to Gunnerus' BODY-fixed frame in a polar coordinate fashion as specific ranges and bearings. The corresponding position and velocity of the virtual target points were then calculated online based on the Gunnerus-relative coordinates in combination with Gunnerus' own motion.

During the experiments, I was located in the Viknes USV together with Idar Petersen from Maritime Robotics, while MR's Arild Hepsø and Thomas Ianke manned the Mariner USV. MR's CEO Vegard Hovstein and his brother Eirik Hovstein had the pleasure of supervising the operations from the bridge of Gunnerus, see Figure 43.

Figure 43: MR's CEO Vegard Hovstein interviewed by the NRK reporter Christoffer Veløy during the formation control experiments. Here, the Mariner USV is assigned a location 100 m port of Gunnerus while the Viknes USV is positioned 200 m port. The helicopter is seen in the background.

Using my Dell Latitude D830 laptop running Matlab/Simulink, the Viknes USV was efficiently controlled through the full-scale demonstrations, see Figure 44.

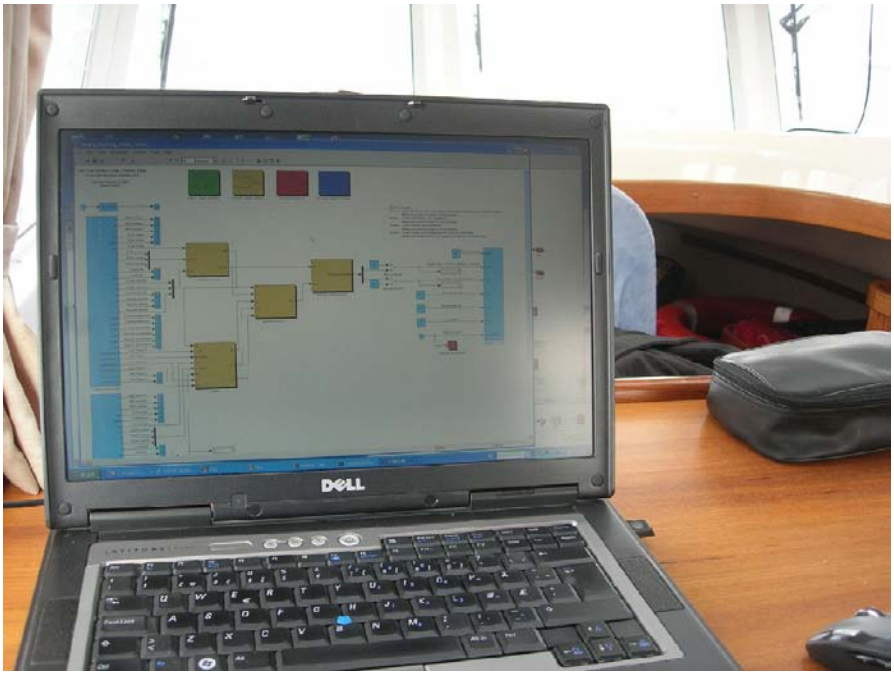

Figure 44: The vicarious digital captain of the Viknes USV during the formation control trials.

During part of the experiments, all 3 vessels travelling in formation used single-beam echo sounders to map the seabed, see Figure 45. The survey capacity of the manned leader vessel was thus tripled, as can be seen in the enlarged blue belt following the vessel traces.

Figure 45 also shows that the initial formation configuration specified the virtual target point of the Mariner USV to be located 100 m port of Gunnerus while the Viknes target point was located a further 100 m to port. Shortly after Gunnerus started its first port maneuver, the Viknes USV was assigned a new formation position 100 m starboard of the leader vessel, which for safety reasons was implemented as an initial change to a position aft of Gunnerus before ultimately assigning the target point 100 m to starboard.

Some photos taken from the helicopter during the formation control experiments can be seen in Figure 46. Gunnerus was moving at approximately 7.5 knots throughout these trials.

Finally, as can be seen in Figure 45, both USVs tightly tracked their assigned formation positions even though Gunnerus executed maneuvers that were not preplanned. These experiments clearly demonstrate the unique functionality of coordinated target tracking.

Further details regarding the experiments will be published elsewhere.

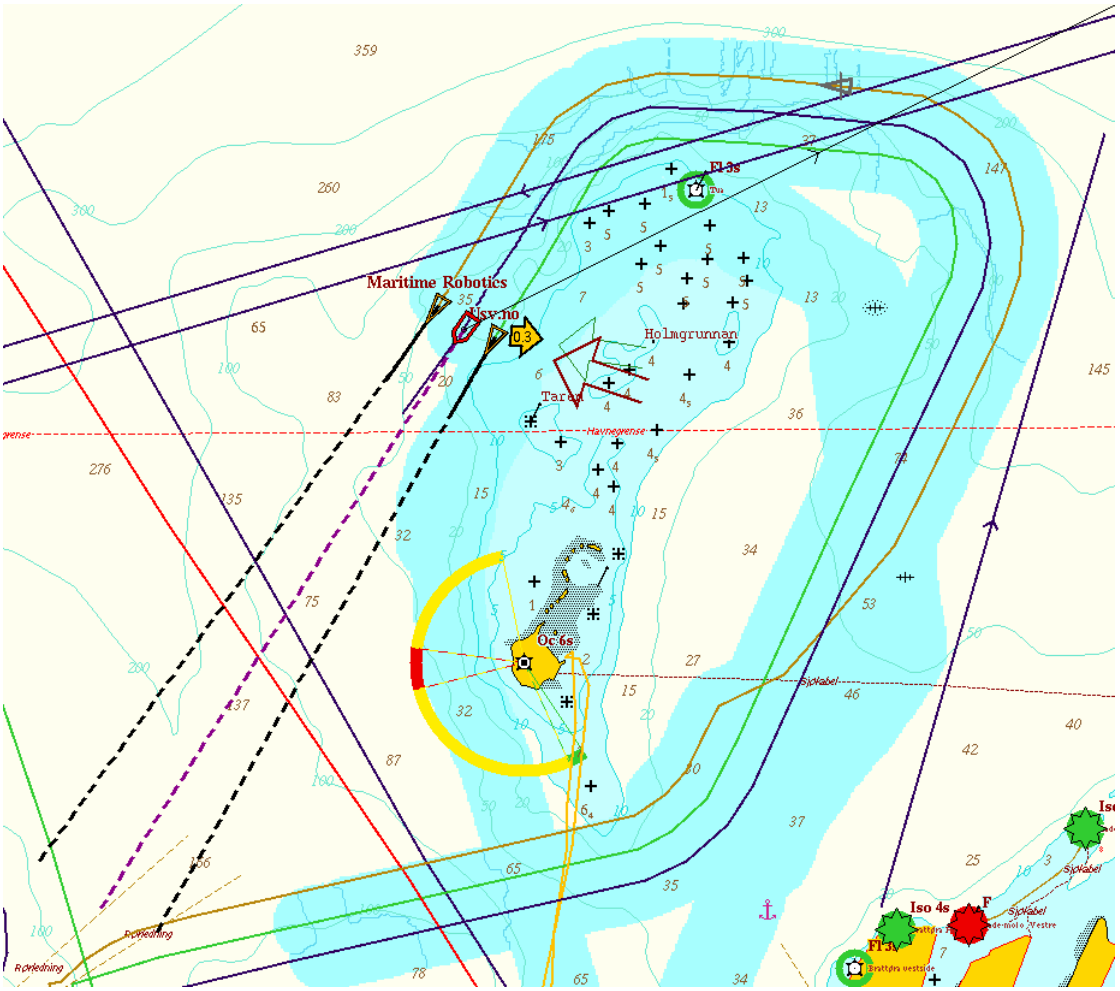

Figure 45: An excerpt from an electronic OLEX plot showing a seabed survey operation around the Munkholmen islet just outside Trondheim. While Gunnerus is represented by the blue trace, the Viknes USV leaves behind a brown trace and the Mariner USV moves in front of a green trace.

5.4.3. Case 2: Ducklings to Port

Having finished most of the demonstrations for the day, Gunnerus and the two USVs headed back to port. Just for fun's sake, it was then decided to define virtual target points located along an imagined line extending directly aft of Gunnerus through its longitudinal axis; 40 m aft for the Mariner USV and 80 m aft for the Viknes USV.

Results from the "ducklings to port" formation control maneuver can be seen in Figure 47. This demonstration was a gimmick which illustrates the diverse applicability of the coordinated target tracking formation control functionality. Hitching a ride with a leader vessel through the narrow port opening shown in Figure 48 has not been done before in Trondheim and was fun to experience.

Figure 46: The top left photo shows the two USVs both travelling in formation on Gunnerus' port side; the top right photo shows the Viknes USV changing its formation position to starboard of Gunnerus; the bottom left photo shows the new formation configuration where the two USVs travel on different sides of the leader vessel; while the bottom right photo shows that the formation geometry is kept even when Gunnerus executes a circular maneuver. Photos courtesy of NRK.

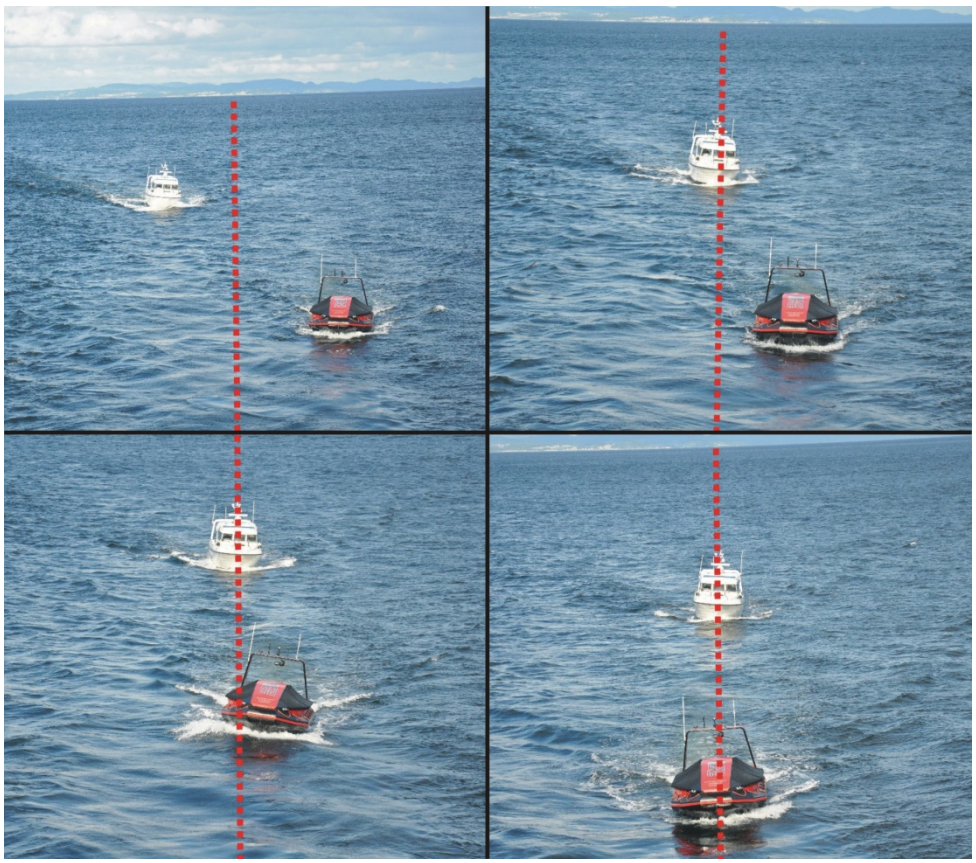

Figure 47: From top left to bottom right, the Mariner and Viknes USVs are steaming ahead to track their assigned virtual targets directly aft of Gunnerus. Photos courtesy of Maritime Robotics.

Figure 48: Ducklings following the mother duck to port, enabling the passengers to take photos.

Briefly concluding on the full-scale experiments, marine survey operations can clearly be performed cheaper and faster with USV-based formation control technology than with the methods available today. However, it remains to be seen in which application area such technology will be applied first. The technology has nevertheless arrived and will surely make for an invaluable ally in the future, especially with regards to exploration and surveillance of challenging and dangerous regions such as the Arctic.

6. The Red Thread

This chapter attempts to explore the red thread running through my work since the completion of my MSc thesis (Breivik 2003). This work can be broadly divided into two distinct periods:

- The first period comprising the years 2003-2006, when I mainly worked with problems related to path following. The core aspect of this work concerned guidance algorithms at a kinematic level. I started looking at straight lines and circles, and continued with regularly parameterized paths. The resulting control systems were mostly evaluated through simulations.

- The second period comprising the years 2006-2009, when I started venturing outside the commonly considered path-based problems in the marine control literature. Inspired by concepts applied to guided missiles and fighter aircraft, I developed guided motion control systems for target tracking of marine vehicles which so far have proven themselves through full-scale experiments with USVs.

The following two sections will further detail the work associated with these periods.

6.1. Legacy Explored: Adventures in Path Following

Having completed my MSc thesis within a path following framework, it was natural for me to continue down this road when embarking on my PhD study. In particular, this framework seemed to be very popular for motion control of underactuated vehicles.

My path following research adventure started with (Fossen et al. 2003, Appendix A), where the challenge was to make an underactuated ship follow straight-line paths. Mainly based on my MSc thesis, the paper introduced a number of novelties, including a dynamic backstepping-based control law. However, the steering law was unfortunately assigned to the vessel heading ψ instead of the course χ. Nevertheless, this subtlety did not affect the experimental results since our model ship only executed low-speed maneuvers in a test basin with no environmental disturbances.

The steering assignment was thereafter changed in (Breivik and Fossen 2004a), where the course angle was explicitly defined for motion control purposes. However, I was still thinking in a conventional autopilot-influenced way when the steering law was allocated via the transformation $\psi_d = \chi_d - \beta$, which was termed "sideslip compensation". Naturally, such a transformation would be necessary if pairing the

suggested guidance laws designed for χ with commercial-off-the-shelf (COTS) autopilots controlling ψ, but not when having full design freedom from the start. Still, I did not begin to assign steering laws directly to the course angle until my later work on USVs. The paper also suggested lookahead-based steering laws applicable to straight lines and circles.

This work was subsequently extended to regularly parameterized paths in (Breivik and Fossen 2004b), where a singularity-free guidance law was proposed for paths that need not be arc-length parameterized. In addition, sideslip compensation and the dynamic controller from (Fossen et al. 2003, Appendix A) was used to achieve path following for an underactuated marine surface vessel exposed to constant environmental disturbances. The paper also showed that it is unphysical to achieve a uniformly globally exponentially stable (UGES) closed-loop property for the path following control objective since this would require a vehicle speed proportional to the cross-path error, which is impossible in practice since all vehicles have actuator constraints. It was thus concluded that UGAS/ULES represents the best stability property a real vehicle system can hold for path following purposes.

The results from this path following paper were then employed in (Breivik and Fossen 2005a, Appendix B) to propose a novel motion control concept for unified control of a vessel through its two main modes of full actuation and underactuation. The main motivation was to avoid using two separate systems such as DP for low speeds and autopilots for high speeds by replacing them with one single system to handle all speeds seamlessly. As all other marine-related work in the path following period, the kinetic displacement model from (Fossen 2002) was used as a basis for the work. This concept would be very interesting to reconsider in a guided motion control context for USVs which are equipped such that they are fully actuated at low speeds but become underactuated at high speeds.

In (Breivik and Fossen 2005b), the so-called “guidance-based path following” approach originally developed for marine surface vessels was used to achieve path following for wheeled mobile robots (WMRs). Such systems are simpler to control since no environmental disturbances are involved. I believe it is important to illustrate results with general applicability to another audience than just the marine control community. In addition, this paper enabled my first trip to an IFAC World Congress.

Subsequently, in (Breivik and Fossen 2005c) the guidance-based path following approach was applied to a more challenging vehicle system moving in a 3-dimensional work space, namely autonomous underwater vehicles (AUVs). Sideslip compensation was extended to also include angle-of-attack compensation for an underactuated AUV. It was nice to see the general usability of the approach for a variety of vehicle systems.

The pure guidance principles were thereafter extracted from the previous papers for (Breivik and Fossen 2005d), which elaborates upon guidance-based path following in both a 2D and 3D context. This paper was a pure kinematics paper, also suggesting how the kinematic guidance laws could be used in combination with physical vehicle systems through cascade-theory arguments.

A request then came from managing editor Michele Umansky of Sea Technology Magazine to write a popularized account based on (Breivik and Fossen 2004b). I naturally accepted the enquiry and contributed with (Breivik 2006a, Appendix C), where I stated some of my thoughts on marine motion control systems. I also greatly enjoy writing non-technical papers for popular dissemination among the general public, which I believe is just as important as publishing technical papers intended for the control community. As researchers, we should not just keep to ourselves while complaining about the decreasing number of students applying for engineering educations. In addition, we should not just be reactive to technology trends originated by others, but also try to be proactive and contribute to trends that we consider important ourselves.

At this time, I was visiting the ECE department at UCSB in California and started getting interested in formation control. I had been wondering how I could extend the guidance-based framework into a formation control context when I was invited to participate at a workshop on group coordination and cooperative control to be held in the northern city of Tromsø, Norway during May 2006. Together with Max Subbotin at UCSB I then worked on extending the guidance algorithm developed for on-path traversing of regularly parameterized paths to also include off-path traversing of such paths for formation control purposes. To achieve a singularity-free solution it turned out that two virtual particles had to be used instead of just one. The main kinematics required for a 2D consideration was then published in (Breivik et al. 2006b).

Subsequently, for (Breivik and Fossen 2006c) the dust was brushed off (Breivik and Fossen 2005a, Appendix B) in order to apply the unified control concept also for AUVs. The conference participation was an interesting experience where I got food poisoned and had to be hospitalized and treated with cancer medicine to stabilize my stomach. I just barely made it back to the hotel in time to put the final touches to my presentation.

A series of 3 marine motion control papers was then written for the 7th IFAC MCMC in Lisbon, Portugal, where I simultaneously started to refer to the “guidance-based” approach as a “guided” approach since it sounded shorter and more compact. The first paper (Breivik et al. 2006d, Appendix D) represented the result of my first dive into the guided missile literature and suggested a novel DP scheme based on constant bearing

guidance, where the transient motion behavior toward the DP target could be explicitly specified through the selection of two intuitive tuning parameters. The second paper (Breivik and Fossen 2006e, Appendix E) attempted to underline the difference between traditional marine motion control designs for fully actuated marine surface vessels with that of the guided approach. This difference between the so-called "servoed" and "guided" motion control schemes was argued to relate both to a distinction in transient convergence behavior as well as to how easy the control design can be extended toward underactuated configurations. The third and final paper (Breivik et al. 2006f) applied the guided formation control concept from (Breivik et al. 2006b) to marine surface vessels.

Toward the end of 2006, the guided formation control concept was also used and illustrated for WMRs in (Breivik et al. 2006g).

6.2. A Broadened Scope: Challenges in Target Tracking

Having finished my PhD scholarship at CeSOS and started in my new position at ITK, I began departing from my previous focus on path following to spend more time on how missile guidance theory can be used to solve the target tracking motion control scenario. In 2007, an expanded version of (Breivik et al. 2006d, Appendix D) was published in (Breivik and Fossen 2007b), where several applicable missile guidance principles were presented. An overview of the history of missile guidance was also given and relevant literature was suggested for exploration by the marine control community. In addition, the fundamental guidance relations with natural and technological systems through the notions of motion camouflage and robotic interception were pointed out. Finally, the paper proposed a modular design method inspired by backstepping and cascade theory, which resulted in a classical inner-outer loop guidance and control structure.

As mentioned earlier, my collaboration with Maritime Robotics began in 2007, and later that same year we were invited to contribute to a formation control workshop at the 17th IFAC World Congress in Seoul, Korea. We were also encouraged to participate with a paper for an invited session, and contributed with (Breivik et al. 2008a, Appendix F) where the guided formation control concept was further elaborated in a path following context for marine surface vessels. Prior to the conference, we had just begun considering coordinated target tracking as a flexible alternative to coordinated path following, but no results were ready for publication at the time.

Then, following our first successful full-scale results with straight-line target tracking for underactuated USVs, (Breivik et al. 2008b, Appendix G) was published toward the end of 2008. This paper introduced a plethora of novel motion control algorithms, including a control-oriented modeling approach which inherently considers vehicle maneuverability and agility constraints for the purpose of designing an easily derivable

and physically feasible velocity control system. For the first time in my career, I had obtained full-scale results which proved the feasibility of my design methodology.

Shortly thereafter, (Breivik and Fossen 2008c) was published as a summary of my accumulated guidance algorithm knowledge, considering both path-based and target tracking motion control scenarios in 2D.

This paper was subsequently expanded into (Breivik and Fossen 2009a, Appendix H), where 3D scenarios were also considered. This book chapter is a state-of-the-art survey which tries to relate the different approaches to each other and put them into a general framework. The AUV-related title is perhaps a bit misleading since the proposed guidance algorithms are generally applicable to any type of vehicle and not just AUVs. In particular, it was important for me to publish this paper in an open access publication since I believe publicly funded research should be publicly available and not shielded behind expensive subscription solutions affordable only by the most wealthy research institutions. Interestingly, such publications have been found to be more downloaded and cited than corresponding work published through traditional channels. So far, the book chapter has been downloaded over 1000 times in the period March 2009 to May 2010. If this number is an indication of the amount of citations it can expect to receive in the following years, someone will be a happy researcher.

I subsequently collaborated on motion control concepts applicable to offshore pipelaying operations in (Jensen et al. 2009). While the pipe should follow a predefined path on the seabed, the vessel responsible for laying the pipe is faced by a target tracking motion control scenario on the ocean surface.

In the summer of 2009, I participated at a NATO conference in Munich, Germany where among 99% UAV contributors I tried to argue the case for USVs through (Breivik and Hovstein 2009c). This paper focuses on the guidance systems associated with guided motion control and presented our first full-scale formation control results using the coordinated target tracking functionality as case studies. Some of these results had previously been mentioned in CeSOS' annual report from 2008 (Breivik and Evans 2009b), but I do not consider this two-page article as one of my formal publications.

Subsequently, I contributed to 3 papers at the 8th IFAC MCMC in Guarujá, Brazil. In (Skejic et al. 2009, Appendix I), a practical guidance and control system was designed for underway replenishment operations which involve large ships that move in parallel while exposed to significant interaction effects between their hulls. This paper involved a truly cross-disciplinary effort, in accordance with the main goal of CeSOS. I also contributed to (Alme and Breivik 2009), written together with my former MSc student Jon Alme as a summary of his main thesis work. Autotuning of motion control systems

is a research area I find very interesting since it relates to the fundamental concepts of learning with a totally open mind versus just applying previously-acquired knowledge when solving a task. Finally, I collaborated on an MPC-based path following control scheme in (Pavlov et al. 2009), where interestingly closed-loop stability can be rigorously proven independent of the transient performance of the MPC optimization.

The two last papers published in the period 2003-2009 were contributions to the 30th anniversary issue of the Norwegian control journal MIC, which recently has become Nordic in scope. I was privileged to be trusted with the responsibility of writing a biography paper about Norway's cybernetics pioneer Jens Glad Balchen (Breivik and Sand 2009d) as well as contributing to a vision paper on trends in research and publication (Breivik et al. 2009e). Considering that MIC has just converted to open access, it was very interesting to explore the larger picture associated with this transformation. MIC's editor Geir Hovland also let me participate in co-editing the anniversary issue, which I believe turned out very well. Getting Rudolf Kalman to contribute with a guest editorial put the icing on the cake.

Thus ends my PhD-related publication tale. Additional papers have currently been submitted for publication, but that is another story. I sincerely thank you – the reader – for showing interest in my work on guided motion control so far.

7. Conclusions and Future Work

This chapter offers some conclusions to the work presented in this thesis and rounds off with some views and recommendations for future work.

7.1. Conclusions

This PhD thesis has considered the concept of guided motion control for marine vehicles, with a special focus on underactuated marine surface vehicles. Guided motion control has been defined to involve the combination of a guidance system which issues meaningful velocity commands with a velocity control system which has been intentionally designed to take vehicle maneuverability and agility constraints into account when fulfilling these commands such that a given motion control objective can be achieved in a controlled and feasible manner without driving the vehicle actuators to saturation.

Furthermore, motion control scenarios have been classified in a novel way according to whether they involve desired motion which has been defined a priori or not. Consequently, in addition to the classical scenarios of point stabilization, trajectory tracking, path following and maneuvering, the so-called target tracking scenario has been considered. The resulting scenarios involve target tracking, path following, path tracking and path maneuvering. In addition, it has been proposed to define the control objectives associated with each scenario as work-space tasks instead of configuration-space tasks. Such a choice seems better suited for practical applications, since most vehicles operate in an underactuated configuration exposed to some kind of environmental disturbances.

The thesis also proposed a novel mechanization of constant bearing guidance, which is a classical guidance principle well-known in the guided missile literature. This suggestion was motivated by a need to solve the target tracking motion control objective for marine vehicles. The proposed implementation enables explicit specification of the transient rendezvous behavior toward the target by selection of two intuitive tuning parameters.

In addition, a singularity-free guidance law applicable to path following scenarios involving regularly parameterized paths which do not need to be arc-length parameterized has been proposed. An extension to this guidance law was also suggested in order to enable off-path traversing of regularly parameterized paths for formation control purposes.

A novel velocity control system which inherently takes maneuverability, agility and actuator constraints into account was developed for the purpose of controlling underactuated marine vehicles moving at high speed. The system is derived through a design method which involves a control-oriented modeling approach and requires a minimum of system identification tests to be carried out.

The thesis also gave a novel overview of the major developments in marine control systems as seen from a Norwegian perspective. The development was suggested to be viewed as three waves of control, where the first wave concerned development of new ship automation technology in the 1960s and 1970s, the second wave involved development of unique dynamic positioning systems in the 1970s and 1980s, while the third wave is expected to encompass the development of unmanned vehicle technology for a large number of maritime applications.

A summary of the historical development, present status and future possibilities associated with unmanned surface vehicles (USVs) was also given. Current Norwegian activities were particularly emphasized.

Furthermore, an overview of the main formation control concepts applicable to marine surface vehicles has been given. A novel formation control functionality named coordinated target tracking was subsequently suggested within a leader-follower framework. Employing a guided motion control system using the suggested mechanization of constant bearing guidance, this functionality was then implemented for two different types of underactuated USVs based on semi-displacement and planing monohulls such that they were able to move in formation with a leader vessel which could maneuver freely without being constrained to any predefined motion pattern.

In particular, excerpts from successful full-scale formation control experiments involving a manned leader vessel and the two USVs executing coordinated target tracking at high speed were presented. This functionality currently seems to be unique on a worldwide basis, providing a convenient plug-and-play formation control capability for manned leader vessels involved in maritime survey operations.

Finally, it can be remarked that the guiding principles for developing the concept of guided motion control have been simplicity and applicability. It is believed that advanced functionality does not necessarily require a complex design. On the contrary, a practically-motivated design feasible for full-scale implementation and supported by control theory at a fundamental level typically gets the job done very well.

7.2. Future Work

As always, more doors have been opened than closed after having journeyed into the wonderful world of research. In the following, I will present some views on and recommendations for future challenges in some of the research fields I have been privileged to encounter during my PhD voyage.

7.2.1. Views and Recommendations from the MARCOW'07

In February 2007, I organized and chaired a workshop in Oppdal, Norway with the intention of gathering researchers and engineers from both academia and industry for the mutual benefit of exchanging new ideas and results in an informal environment. The main goal was to advance academic-industrial cooperation and understanding.

Named the Marine Control Workshop 2007 (MARCOW'07), the event spanned two full days filled with numerous regular presentations, three keynote presentations and two panel discussions. Academic participants came from the Norwegian University of Science and Technology (NTNU) and the Technical University of Denmark (DTU), while the industry was represented by people from Det Norske Veritas (DNV), Kongsberg Defence and Aerospace (KDA), Kongsberg Maritime (KM), Kongsberg Seatex (KS), Marine Cybernetics (MC), Maritime Robotics (MR), Rolls-Royce Marine (RRM) and SINTEF, see also (Marine Control Workshop 2007).

In particular, it is the outcome of the panel discussions that I believe are sufficiently interesting to include in this part of the thesis. Each discussion was set up with a moderator, a panel of four participants representing a mix of academic and industrial representatives, and a secretary who recorded the exchange of ideas and viewpoints.

I chose the topics of discussion based on my interests and curiosities at the time, and the ensuing debates can be read in the following two sections. This material has been taken from the panel discussion summaries given in the internally-distributed and unpublished workshop summary (Breivik 2007a).

Panel Discussion 1 – Industrial Real-Life Challenges: Beyond Stability Theory?

The moderator Asgeir Sørensen from NTNU/MC initiated the discussion by challenging the panel to comment on general aspects related to the subject matter. Per Martinsen from DNV responded by emphasizing the difficulty faced by the regulatory hierarchy when attempting to follow the current rate of technological development, adding that a solution could be to develop more high-level functional requirements (qualitative, universal guidelines) as a framework for assessing specific implementations instead of

employing a vast set of individually tailored requirements. He also said that development of new theory is important for moving forward, and that the main future challenge is to achieve proper cooperation between universities and the industry.

Bjørn Gjelstad from KM argued that it was important to have PhD students seeking new problems and new solutions, but that the current gap between basic and applied research was too large. He said that an important problem was how to bridge the gap between theory and implementation.

Jann Peter Strand from RRM agreed with the views of Bjørn Gjelstad, and added that there is a huge gap between real-life system requirements and what is currently taught at the universities. According to Strand, the understanding of key aspects such as failure impacts and failure handling is too weak. He also argued that few students truly understand what it takes to bring a physical system from prototype to final product, and claimed that many new theories emanating from academia in essence turn out to be no more than smart ways of mathematically proving the performance of concepts that the industry have used for a long time.

The moderator continued by asking Mogens Blanke from DTU if he considered the industry open enough to point out relevant research areas for the universities, i.e., if the industry is doing its part to bridge the theory-implementation gap. Blanke responded that it was difficult to say, but added that the industry generally must have resistance to wild ideas (originating from universities) and act as a corrector (to such ideas). He also remarked that Norwegian companies probably are more risk-driven and interested in advanced technology than Danish companies, and that the academic-industrial interaction within the marine segment is better in Norway than in Denmark.

The moderator then moved on to ask Bjørn Gjelstad from KM to illustrate why the ‘fantastic’ controllers of cutting-edge PhD research (mostly) were unfit for industrial implementation, where requirements encompass the delivery of several DP systems each week. Gjelstad replied that cheap and simple solutions usually got the job done, and that a number of factors destroyed the opportunity to have ‘fantastic’ controllers working; available time for sea trials, lack of available engineering skills, embedded computer capacity, quality of measurements, etc. The moderator subsequently pointed out the difference in possibilities between standardized systems associated with large production volumes and highly specialized systems associated with small production volumes. Gjelstad responded that everything was naturally a money-time question, and added that it is acceptable and feasible to spend time on tuning 40 parameters (once) for a specific series of vessels. The audience followed up by inquiring how KM tuned controllers in practice, and Gjelstad mentioned tuning in sheltered waters and consideration of vessel characteristics such as added mass and thruster forces. He also

said that vessels naturally need to be fully exposed to the environment (in order to observe their genuine performance), and that the tuning process naturally includes trial and error.

The discussion subsequently turned to the topic of asymptotic stability versus transient performance, i.e., qualitative vs. quantitative aspects. Mogens Blanke from DTU talked about the difference between linear and nonlinear control theory, and the possibility of characterizing system response for linear systems. He remarked that current control research perhaps is too focused on nonlinear aspects, and that control engineering students often lack intuition on feedback gains and tuning by relying too much on Matlab/Simulink. Jann Peter Strand from RRM added that we should not stop the design process after having obtained our Lyapunov proofs, but a member from the audience responded that we currently lack the required tools to proceed any further (i.e., to analyze nonlinear systems quantitatively). Mogens Blanke then suggested introducing performance criteria, disturbance rejection and sensitivity to nonlinear control theory.

The talk returned to the research gap between academia and industry, and the moderator said that researchers are supposed to have wild ideas and not be gagged by restrictions. Bjørn Gjelstad from KM stressed the importance of researchers that are not bound by industry comments. Mogens Blanke from DTU then made an interesting comment that hardware-wise, the industry is (and always will be) in front of academic research. Examples include computer hardware and high-powered machinery. He elaborated that universities are mostly good at inexpensive research, and that their main advantage is (what he termed) “brainware”.

The last part of the discussion dealt with topics related to intellectual property rights. A member of the audience questioned the fact that researchers cannot employ know-how achieved through restricted industry projects for educational purposes. Mogens Blanke from DTU responded that this was natural in those cases where the industry wholly paid all the research expenses. He added that university employees should (be able to) work with different companies since everybody benefits in the long term (both academia and the industry). Subsequently, Per Martinsen from DNV stated that researchers must interact with the industry such that universities do not become like science castles isolated from the rest of society. A member of the audience then said that universities have no choice but to generate income, e.g., by cooperating on industry projects. Another member of the audience stressed the importance of researcher independence and diversity of research topics, and that academic researchers should not become too industry-driven. Mogens Blanke then stated that control researchers must maintain a long-term perspective on their research since they typically work with general principles, and obtain funding from different sources as long as the ensuing research results pull in the right direction. The moderator rounded up the discussion by

remarking that the industry often encourages dissemination of research results for educational purposes, but that they naturally hesitate to publicly release information which is very important for their competitive edge.

In short: There will always be a (research) gap between academia and the industry. Academia will typically excel at inexpensive research, while the industry will excel at expensive and hardware-intensive research. A main challenge for the future is to extend the nonlinear control-theoretic toolbox to also include quantitative analysis tools in addition to the qualitative tools of today.

Panel Discussion 2 – Unmanned Technology: The Future?

The first aspect to be discussed was how the regulatory hierarchy would handle unmanned vessel technology. The moderator Morten Breivik from NTNU inquired Per Martinsen from DNV, who stated that there were no quick solutions and that currently no committees dealing with unmanned issues existed within the International Maritime Organization (IMO). However, he added that it should not be difficult to agree on relevant (qualitative) requirements for unmanned systems if needed. Martinsen also suggested that unmanned technology should be developed step-by-step, starting gradually with small projects (for proof of concept, etc.).

Figure 49: Ongoing panel discussion concerning unmanned technology. From left to right: The moderator (me), followed by the panel members Erik Kyrkjebø from NTNU/SINTEF, Asgeir Sørensen from NTNU/MC, Jerome Jouffroy from KDA and Vegard Hovstein from MR.

Motivated by the fact that the maritime community perhaps could learn from the extensive experience of the aerial community on the subject matter (regarding legislative aspects, unmanned vs. manned traffic, etc.), the moderator inquired if there was any contact between the aerial and maritime regulatory hierarchies. According to Martinsen, no such contact was currently taking place. He also could not give an estimate on how long it could take before regulations on unmanned vessels were established (due to extensive uncertainty).

The audience suggested emphasizing the human-in-the-loop aspect (neglecting autonomous capabilities at first), thus entailing requirements for remote monitoring and supervision. In response, Jerome Jouffroy from KDA commented that such an approach would still involve problems related to the issue of responsibility (of failures), since the correctness of the human response cannot surpass the correctness of the information provided by the computer-based advisory systems. Hence, humans should still be able to make decisions based on (more or less) raw sensory data, especially audiovisual data. Subsequently, Asgeir Sørensen from NTNU/MC stated that humans must participate in vehicle operations for the foreseeable future since they are unique at performing maintenance operations and at handling unanticipated incidents. He also added that it would be very difficult to introduce unmanned technology without the aid of a strong (big brother) industrial participant.

Vegard Hovstein from MR suggested to focus on unmanned technology intended for so-called 3D (dirty, dull and dangerous) environments, where human presence is considered too risky or just plainly infeasible. Erik Kyrkjebø from NTNU/SINTEF remarked that such an approach would probably work well since it inherently justifies unmanned operations. The moderator subsequently concluded the discussion by stating that unmanned technology perhaps should rely on a risk-driven development (as often witnessed historically).

In short: It will probably be a long time until unmanned vehicle technology dominates at sea. Until such a time, we should perhaps opt for “unmanned and manned – hand in hand” ☺

7.2.2. Personal Views and Recommendations

Regarding my own work, I would particularly like to extend the guided motion control framework to also include collision avoidance capabilities. In order for unmanned vehicles to operate autonomously in the future, a collision avoidance system with a robust sense and avoid functionality is an absolute requirement. Nobody will allow such vehicles to move around in a non-segregated land, sea or airspace alongside manned traffic unless the probability of collisions has been reduced to a minimum.

Figure 50: Today, the captain of a well-equipped vessel usually has at least 3 different modes of operation from which to choose. With an integrated motion control system, the dynamic positioning and autopilot functionalities could be merged into a single functionality covering all vessel speeds.

I would also like to extend my current results to develop practical solutions for path maneuvering scenarios, taking vehicle maneuverability and agility constraints into account when dynamically calculating guidance parameters such as lookahead distance and desired speed in order to traverse a given geometric path as efficiently as possible.

Developing an integrated motion control system capable of serving all needs for a specific vehicle over a VOC space as large as possible is also high on my wish list. Replacing the currently separate DP and autopilot functionality present in many vessels, the main goal of such a system would be to efficiently handle a vessel through all modes of actuation seamlessly without requiring the captain to manually switch between several different motion control systems, see Figure 50. I believe that the framework of guided motion control is particularly suited to develop such an integrated system.

On a more general level, one of the main things I have learned during the course of my work so far is that when developing practically-motivated control concepts it is important not to be confined within the constraints of the control-theoretic toolbox. When trying to think outside the box, limitations associated with obtaining analytical proofs must often be left behind. For example, it does not matter if a particular control design results in an elegant Lyapunov proof if the underlying assumptions are unrealistic or if the applied dynamic model is overly simplified or of such a nature that its parameters are very difficult or even impossible to obtain in practice. I've therefore come to believe in a more practical approach, where analytic tools such as Lyapunov theory are suited for basic proof-of-concept studies involving those parts of the total system which are simple and well-known, while more control-oriented methods are used to design controllers for those parts that are more complex and uncertain. In my own case, this division is analogous to the separation I've made between the guidance

and velocity control systems. Having obtained analytic Lyapunov proofs for the kinematics-based guidance laws, nonlinear cascade theory was used to support the notion that a well-designed velocity control system which proves itself in practice will contribute to achieving a physically-realistic overall closed-loop behavior.

In particular, I think that the time has now come to start focusing less on control designs which rely heavily on the performance of complex and model-based feedforward terms, and instead go back to the roots of the automatic control discipline where feedback terms are regarded more important to the performance of a closed-loop dynamic system, see also (Skogestad 2009). Relying on increasingly cheap, small and reliable measurement systems, a more sensor-based feedback approach should thus be pursued for the purpose of reducing both computational complexity and modeling uncertainty to a minimum, see also (Zbikowski 2004).

I also believe that the academic control community has some unique possibilities ahead regarding access to hardware and full-scale platforms on which to test and validate their control designs. Such technology will no longer be exclusively reserved for the industry. Historically, the 1950s saw increasingly cheap computer-based tools replace expensive laboratory equipment, and so the theory-practice gap between academia and the industry started widening. However, we are now in a situation where increasingly cheap computers, sensors, navigation systems, actuators, communication equipment and vehicle frames enable many research groups around the world to actually purchase and operate their own full-scale equipment. Thus, sophisticated control concepts can be put to the test in real-life experiments and not just through numerical simulations on a computer. In particular, this development will be related to and motivated by the need for increasingly advanced unmanned vehicle technologies.

I finally consider myself very lucky to live in these exciting times when technology development for unmanned vehicles has barely started. Nobody knows what it will lead to but the journey will surely be fantastic. Speaking for myself, I definitely want to be part of the development crew.

References

Aguiar, A. P. and J. P. Hespanha (2007). "Trajectory-Tracking and Path-Following of Underactuated Autonomous Vehicles with Parametric Modeling Uncertainty." IEEE Transactions on Automatic Control **52**(8): 1362-1379.

Aguiar, A., J. Almeida, M. Bayat, B. Cardeira, R. Cunha, A. Häusler, P. Maurya, A. Oliveira, A. Pascoal, A. Pereira, M. Rufino, L. Sebastião, C. Silvestre and F. Vanni (2009). Cooperative Control of Multiple Marine Vehicles: Theoretical Challenges and Practical Issues. Proceedings of the 8th IFAC MCMC. Guarujá, Brazil.

Alme, J. and M. Breivik (2009). Autotuning Aspects for Dynamic Positioning Systems. Proceedings of the 8th IFAC MCMC. Guarujá, Brazil.

Balch, T. and R. C. Arkin (1998). "Behavior-Based Formation Control for Multirobot Teams." IEEE Transactions on Robotics and Automation **14**(6): 926-939.

Balchen, J. G., N. A. Jenssen and S. Sælid (1976). Dynamic Positioning using Kalman Filtering and Optimal Control Theory. Proceedings of the IFAC/IFIP Symposium on Automation in Offshore Oilfield Operations. Bergen, Norway.

Balchen, J. G., N. A. Jenssen, E. Mathisen and S. Sælid (1980). "A Dynamic Positioning System Based on Kalman Filtering and Optimal Control." Modeling, Identification and Control **1**(3): 135-163.

Battin, R. H. (1982). "Space Guidance Evolution - A Personal Narrative." Journal of Guidance, Control, and Dynamics **5**(2): 97-110.

Beck, J. A. and T. J. Cord (1995). A Framework for Analysis of Aircraft Maneuverability. Proceedings of the AIAA Atmospheric Flight Mechanics Conference. Baltimore, Maryland, USA.

Beinset, G. and J. S. Blomhoff (2007). Controller Design for an Unmanned Surface Vessel: Design of a Heading Autopilot and Way-Point Navigation System for an Underactuated USV, MSc Thesis, Department of Engineering Cybernetics, Norwegian University of Science and Technology, Trondheim, Norway.

Bennett, S. (1984). "Nicolas Minorsky and the Automatic Steering of Ships." IEEE Control Systems Magazine **4**(4): 10-15.

Bertram, V. (2008a). Unmanned Surface Vehicles – A Survey. Copenhagen, Denmark, Skibsteknisk Selskab.

Bertram, V. (2008b). Cyber-Ships – Artificial Intelligence Technologies for Ships. Copenhagen, Denmark, Skibsteknisk Selskab.

Bjerva, K. G., Ed. (2006). Norcontrol: Maritim innovasjon siden 1965, Norcontrol/Kongsberg Maritime Pensjonistforening, Horten.

Bjørnstad, S. (2009). Shipshaped: Kongsberg Industry and Innovations in Deepwater Technology, 1975 - 2007, PhD Thesis, BI Norwegian School of Management, Oslo, Norway.

Bray, D. (2003). Dynamic Positioning, Oilfield Publications Inc.

Breivik, M. (2003). Nonlinear Maneuvering Control of Underactuated Ships, MSc Thesis, Department of Engineering Cybernetics, Norwegian University of Science and Technology, Trondheim, Norway.

Breivik, M. and T. I. Fossen (2004a). Path Following of Straight Lines and Circles for Marine Surface Vessels. Proceedings of the 6th IFAC CAMS. Ancona, Italy.

Breivik, M. and T. I. Fossen (2004b). Path Following for Marine Surface Vessels. Proceedings of the OTO'04. Kobe, Japan.

Breivik, M. and T. I. Fossen (2005a). A Unified Concept for Controlling a Marine Surface Vessel Through the Entire Speed Envelope. Proceedings of the ISIC-MED'05. Limassol, Cyprus.

Breivik, M. and T. I. Fossen (2005b). Guidance-Based Path Following for Wheeled Mobile Robots. Proceedings of the 16th IFAC World Congress. Prague, Czech Republic.

Breivik, M. and T. I. Fossen (2005c). Guidance-Based Path Following for Autonomous Underwater Vehicles. Proceedings of the OCEANS'05. Washington D.C., USA.

Breivik, M. and T. I. Fossen (2005d). Principles of Guidance-Based Path Following in 2D and 3D. Proceedings of the CDC-ECC'05. Seville, Spain.

Breivik, M. (2006a). Marine Craft: 21st Century Motion Control Concepts. Sea Technology. **47:** 33-36.

Breivik, M., M. V. Subbotin and T. I. Fossen (2006b). Kinematic Aspects of Guided Formation Control in 2D. Group Coordination and Cooperative Control. K. Y. Pettersen, T. Gravdahl and H. Nijmeijer, Springer-Verlag Heidelberg**:** 55-74.

Breivik, M. and T. I. Fossen (2006c). A Unified Control Concept for Autonomous Underwater Vehicles. Proceedings of the ACC'06. Minneapolis, Minnesota, USA.

Breivik, M., J. P. Strand and T. I. Fossen (2006d). Guided Dynamic Positioning for Fully Actuated Marine Surface Vessels. Proceedings of the 7th IFAC MCMC. Lisbon, Portugal.

Breivik, M. and T. I. Fossen (2006e). Motion Control Concepts for Trajectory Tracking of Fully Actuated Ships. Proceedings of the 7th IFAC MCMC. Lisbon, Portugal.

Breivik, M., M. V. Subbotin and T. I. Fossen (2006f). Guided Formation Control for Fully Actuated Marine Surface Craft. Proceedings of the 7th IFAC MCMC. Lisbon, Portugal.

Breivik, M., M. V. Subbotin and T. I. Fossen (2006g). Guided Formation Control for Wheeled Mobile Robots. Proceedings of the ICARCV'06. Singapore.

Breivik, M. (2007a). Workshop Summary MARCOW'07. Unpublished.

Breivik, M. and T. I. Fossen (2007b). Applying Missile Guidance Concepts to Motion Control of Marine Craft. Proceedings of the 7th IFAC CAMS. Bol, Croatia.

Breivik, M., V. E. Hovstein and T. I. Fossen (2008a). Ship Formation Control: A Guided Leader-Follower Approach. Proceedings of the 17th IFAC World Congress. Seoul, Korea.

Breivik, M., V. E. Hovstein and T. I. Fossen (2008b). "Straight-Line Target Tracking for Unmanned Surface Vehicles." Modeling, Identification and Control **29**(4): 131-149.

Breivik, M. and T. I. Fossen (2008c). Guidance Laws for Planar Motion Control. Proceedings of the 47th IEEE CDC. Cancun, Mexico.

Breivik, M. and T. I. Fossen (2009a). Guidance Laws for Autonomous Underwater Vehicles. Underwater Vehicles. A. V. Inzartsev, IN-TECH Education and Publishing**:** 51-76.

Breivik, M. and K. Evans (2009b). Formation Control of Unmanned Surface Vehicles. CeSOS Annual Report 2008, Centre for Ships and Ocean Structures**:** 30-31.

Breivik, M. and V. E. Hovstein (2009c). Guidance Systems for Motion Control of Unmanned Surface Vehicles. Proceedings of the NATO RTO SCI-202 Symposium. Neubiberg, Germany.

Breivik, M. and G. Sand (2009d). "Jens Glad Balchen: A Norwegian Pioneer in Engineering Cybernetics." Modeling, Identification and Control **30**(3): 101-125.

Breivik, M., G. Hovland and P. J. From (2009e). "Trends in Research and Publication: Science 2.0 and Open Access." Modeling, Identification and Control **30**(3): 181-190.

Børhaug, E. (2008). Nonlinear Control and Synchronization of Mechanical Systems, PhD Thesis, Department of Engineering Cybernetics, Norwegian University of Science and Technology, Trondheim, Norway.

Caccia, M. (2006). Autonomous Surface Craft: Prototypes and Basic Research Issues. Proceedings of the MED'06. Ancona, Italy.

Cooper, S. L., D. A. Newborn and M. R. Norton (2002). New Paradigms in Boat Design: An Exploration into Unmanned Surface Vehicles. Proceedings of the AUVSI Unmanned Systems. Lake Buena Vista, Florida, USA.

Coram, R. (2002). Boyd: The Fighter Pilot Who Changed the Art of War, Little, Brown and Company.

Draper, C. S. (1971). "Guidance is forever." Navigation **18**(1): 26-50.

Egeland, O. and J. T. Gravdahl (2002). Modeling and Simulation for Automatic Control, Marine Cybernetics.

Ellingsen, H. (2008). Development of a Low-Cost Integrated Navigation System for USVs, MSc Thesis, Department of Engineering Cybernetics, Norwegian University of Science and Technology, Trondheim, Norway.

Faltinsen, O. M. (2005). Hydrodynamics of High-Speed Marine Vehicles, Cambridge University Press.

Fossen, T. I. (2002). Marine Control Systems: Guidance, Navigation and Control of Ships, Rigs and Underwater Vehicles, Marine Cybernetics.

Fossen, T. I., M. Breivik and R. Skjetne (2003). Line-of-Sight Path Following of Underactuated Marine Craft. Proceedings of the 6th IFAC MCMC. Girona, Spain.

Fossen, T. I. (2005). "A Nonlinear Unified State-Space Model for Ship Maneuvering and Control in a Seaway." Journal of Bifurcation and Chaos **15**(9): 2717-2746.

Fäy, H. (1990). Dynamic Positioning Systems: Principles, Design and Applications, Éditions Technip, Paris.

Ghabcheloo, R. (2007). Coordinated Path Following of Multiple Autonomous Vehicles, PhD Thesis, Instituto Superior Técnico, Universidade Técnica de Lisboa, Portugal.

Hagen, P. E., N. J. Størkersen and K. Vestgård (2003). The HUGIN AUVs – Multi-Role Capability for Challenging Underwater Survey Operations. EEZ International.

Halvorsen, H. (2008). Dynamic Positioning for Unmanned Surface Vehicles, MSc Thesis, Department of Engineering Cybernetics, Norwegian University of Science and Technology, Trondheim, Norway.

Hauser, J. and R. Hindman (1995). Maneuver Regulation from Trajectory Tracking: Feedback Linearizable Systems. Proceedings of the IFAC Symposium on Nonlinear Control System Design. Tahoe City, California, USA.

Hughes, T. P. (1971). Elmer Sperry: Inventor and Engineer, The Johns Hopkins Press.

Høivold, I. (1984). "Norwegian Research and Development in the Field of Ship Automation." Modeling, Identification and Control **5**(3): 171-178.

Høivold, I. (2003). Uten nisselue: Historien om Norcontrol. Unpublished personal memoirs.

Ihle, I.-A. F. (2006a). Coordinated Control of Marine Craft, PhD Thesis, Department of Engineering Cybernetics, Norwegian University of Science and Technology, Trondheim, Norway.

Ihle, I.-A. F., J. Jouffroy and T. I. Fossen (2006b). "Formation Control of Marine Surface Craft: A Lagrangian Approach." IEEE Journal of Oceanic Engineering **31**(4): 922-934.

Jensen, G. A., M. Breivik and T. I. Fossen (2009). Offshore Pipelay Operations From a Control Perspective. Proceedings of the 28th ASME OMAE. Honolulu, Hawaii, USA.

Johnsen, A. (2006). "Barents 2020: Et virkemiddel for en framtidsrettet nordområdepolitikk." Retrieved March 25, 2010, from http://www.aksjonsprogrammet.no/vedlegg/Barents%202020.pdf.

Justh, E. W. and P. S. Krishnaprasad (2006). "Steering Laws for Motion Camouflage." Proceedings of the Royal Society A **462**(2076): 3629–3643.

Khalil, H. K. (2001). Nonlinear Systems, Prentice Hall, 3rd edition.

Kittilsen, F. (1994). Simrad Albatross: En stødig lausunge fra Kongsberg. Bladet Forskning. **2**(7).

Klungtveit, H. S. (2009). "Såååå stort er Norge nå." Retrieved March 25, 2010, from http://www.dagbladet.no/2009/04/15/nyheter/nordomradene/norge/kart/geografi/5755268/.

Kongsberg Maritime (2006). Kongsberg K-Pos DP Dynamic Positioning System, Report No. 301093/B.

Kyrkjebø, E. (2007). Motion Coordination of Mechanical Systems: Leader-Follower Synchronization of Euler-Lagrange Systems using Output Feedback Control, PhD Thesis, Department of Engineering Cybernetics, Norwegian University of Science and Technology, Trondheim, Norway.

Lapierre, L., D. Soetanto and A. Pascoal (2003). Nonlinear Path Following with Applications to the Control of Autonomous Underwater Vehicles. Proceedings of the 42nd IEEE CDC. Maui, Hawaii, USA.

LaValle, S. M. (2006). Planning Algorithms, Cambridge University Press.
Leonard, N. E. and E. Fiorelli (2001). Virtual Leaders, Artificial Potentials and Coordinated Control of Groups. Proceedings of the 40th IEEE CDC. Orlando, Florida, USA.

Lewis, M. A. and K.-H. Tan (1997). "High Precision Formation Control of Mobile Robots Using Virtual Structures." Autonomous Robots **4**: 387-403.

Locke, A. S. (1955). Guidance, D. Van Nostrand Company, Inc.

Loe, Ø. A. G. (2008). Collision Avoidance for Unmanned Surface Vehicles, MSc Thesis, Department of Engineering Cybernetics, Norwegian University of Science and Technology, Trondheim, Norway.

Marine Control Workshop. (2007). Retrieved March 25, 2010, from http://www.cesos.ntnu.no/marcow/.

Minorsky, N. (1922). "Directional Stability of Automatically Steered Bodies." Journal of the American Society for Naval Engineers **34**(2): 280-309.

Mizutani, A., J. S. Chahl and M. V. Srinivasan (2003). "Motion Camouflage in Dragonflies." Nature **423**: 604.

Nguyen, T. D., A. J. Sørensen and S. T. Quek (2008). "Multi-Operational Controller Structure for Station Keeping and Transit Operations of Marine Vessels." IEEE Transactions on Control Systems Technology **16**(3): 491-498.

NIMA (1997). Department of Defense World Geodetic System 1984, Its Definition and Relationships With Local Geodetic Systems, Technical Report TR8350.2.

Ocean Space Centre. (2010). Retrieved March 25, 2010, from http://www.oceanspacecentre.no/.

Overbye, S. (1989). Fra forskning til industri: Utviklingen av skipsautomatiseringsbedriften Norcontrol, MSc Thesis, University of Oslo, Oslo, Norway.

Panteley, E., E. Lefeber, A. Loría and H. Nijmeijer (1998). Exponential Tracking of a Mobile Car Using a Cascaded Approach. Proceedings of the IFAC Workshop on Motion Control. Grenoble, France.

Papoulias, F. A. (1991). "Bifurcation Analysis of Line of Sight Vehicle Guidance Using Sliding Modes." International Journal of Bifurcation and Chaos **1**(4): 849–865.

Paranjape, A. A. and N. Ananthkrishnan (2006). "Combat Aircraft Agility Metrics - A Review." Journal of Aerospace Sciences and Technologies **58**(2): 1-12.

Pavlov, A., H. Nordahl and M. Breivik (2009). MPC-Based Optimal Path Following for Underactuated Vessels. Proceedings of the 8th IFAC MCMC. Guarujá, Brazil.

Perez, T., A. J. Sørensen and M. Blanke (2006). Marine Vessel Models in Changing Operational Conditions (A Tutorial). Proceedings of the 14th IFAC SYSID. Newcastle, Australia.

Pettersen, K. Y. and T. I. Fossen (2000). "Underactuated Dynamic Positioning of Ships - Experimental Results." IEEE Transactions on Control Systems Technology **8**(5): 856-863.

Pettersen, K. Y. and E. Lefeber (2001). Way-Point Tracking Control of Ships. Proceedings of the 40th IEEE CDC. Orlando, Florida, USA.

Pincus, W. (2009). "Air Force Training More Pilots for Drones Than for Manned Planes." Retrieved March 25, 2010, from http://www.washingtonpost.com/wp-dyn/content/article/2009/08/10/AR2009081002712.html.

Pinkster, J. A. and U. Nienhuis (1986). Dynamic Positioning of Large Tankers at Sea. Proceedings of the 18th OTC. Houston, Texas.

Portmann, H. H., S. L. Cooper, M. R. Norton and D. A. Newborn (2002). Unmanned Surface Vehicles: Past, Present, and Future. Unmanned Systems. **SEPT/OCT:** 32-37.

Reynolds, C. W. (1987). "Flocks, Herds, and Schools: A Distributed Behavioral Model." Computer Graphics **21**(4): 25-34.

Rysdyk, R. (2003). UAV Path Following for Constant Line-of-Sight. Proceedings of the 2nd AIAA Unmanned Unlimited. San Diego, California, USA.

Ryvik, H. (1999). "Stødig på alle hav." Retrieved March 25, 2010, from http://web.tu.no/nyheter/arkiv/?id=1999/33/s2425/s2425.html.

Schrødingers Katt. (2009). "Førerløse båter." Retrieved March 25, 2010, from http://www1.nrk.no/nett-tv/indeks/182279.

Schönknecht, R., J. Lüsch, M. Schelzel and H. Obenaus (1973). Schiffe und Schiffahrt von Morgen, VEB Verlag Technik Berlin.

Sciavicco, L. and B. Siciliano (2002). Modelling and Control of Robot Manipulators, Springer-Verlag London Ltd.

Shneydor, N. A. (1998). Missile Guidance and Pursuit: Kinematics, Dynamics and Control, Horwood Publishing Ltd.

Singer, P. W. (2009). Wired for War: The Robotics Revolution and Conflict in the 21st Century, Penguin.

Siouris, G. M. (2004). Missile Guidance and Control Systems, Springer-Verlag New York, Inc.

Skejic, R., M. Breivik, T. I. Fossen and O. M. Faltinsen (2009). Modeling and Control of Underway Replenishment Operations in Calm Water. Proceedings of the 8th IFAC MCMC. Guarujá, Brazil.

Skjetne, R. (2005). The Maneuvering Problem, PhD Thesis, Department of Engineering Cybernetics, Norwegian University of Science and Technology, Trondheim, Norway.

Skogestad, S. (2009). "Feedback: Still the Simplest and Best Solution." Modeling, Identification and Control **30**(3): 149-155.

SNAME (1950). Nomenclature for Treating the Motion of a Submerged Body Through a Fluid, Technical and Research Bulletin No. 1-5.

Stensvold, T. (2009). "Seiler inn vær og klimadata." Retrieved March 25, 2010, from http://www.tu.no/miljo/article230559.ece.

Sørdalen, O. J. and O. Egeland (1995). "Exponential Stabilization of Nonholonomic Chained Systems." IEEE Transactions on Automatic Control **40**(1): 35–49.

Tesla, N. (1898). Method of and Apparatus for Controlling Mechanism of Moving Vessels or Vehicles. U. S. Patent Office. **613809**.

Tesla, N. (1919). My Inventions: The Autobiography of Nikola Tesla, Experimenter Publishing Company, Inc.

Tveter, N. (2010). "Førerløse båter: Selvstyrte roboter til sjøs." Retrieved March 25, 2010, from http://www.ntnu.no/gemini/2010-01/22-25.htm.

U. S. Navy. (2007). "The Navy Unmanned Surface Vehicle (USV) Master Plan." Retrieved March 25, 2010, from http://www.news.navy.mil/navydata/technology/usvmppr.pdf.

Wicken, O., Ed. (1994). Elektronikkentreprenørene, AdNotam Gyldendal.

Withington, T. (2008). "No Crew Onboard!" Armada International **32**(3): 18-26.

Wolfram, S. (2002). A New Kind of Science, Wolfram Media Incorporated.

Yanushevsky, R. (2008). Modern Missile Guidance, CRC Press.

Zbikowski, R. (2004). "Sensor-Rich Feedback Control." IEEE Instrumentation & Measurement Magazine **7**(3): 19-26.

A. Line-of-Sight Path Following of Underactuated Marine Craft

LINE-OF-SIGHT PATH FOLLOWING OF UNDERACTUATED MARINE CRAFT

Thor I. Fossen [*,1] **Morten Breivik** [*] **Roger Skjetne** [*]

[*] *Centre of Ships and Ocean Structures (CESOS), Norwegian University of Science and Technology (NTNU), NO-7491 Trondheim, Norway. E-mails: tif@itk.ntnu.no, mortebre@itk.ntnu.no, skjetne@ieee.org*

Abstract: A 3 degrees of freedom (surge, sway, and yaw) nonlinear controller for path following of marine craft using only two controls is derived using nonlinear control theory. Path following is achieved by a geometric assignment based on a line-of-sight projection algorithm for minimization of the cross-track error to the path. The desired speed along the path can be specified independently. The control laws in surge and yaw are derived using backstepping. This results in a dynamic feedback controller where the dynamics of the uncontrolled sway mode enters the yaw control law. UGAS is proven for the tracking error dynamics in surge and yaw while the controller dynamics is bounded. A case study involving an experiment with a model ship is included to demonstrate the performance of the controller and guidance systems.

Keywords: Ship steering, Line-of-Sight guidance, Path following, Maneuvering, Nonlinear control, Underactuated control, Experimental results

1. INTRODUCTION

In many applications offshore it is of primary importance to steer a ship, a submersible or a rig along a desired *path* with a prescribed *speed* (Fossen 1994, 2002). The path is usually defined in terms of *way-points* using the *Cartesian* coordinates $(x_k, y_k) \in \mathbb{R}^2$. In addition, each way-point can include turning information usually specified by a circle arc connecting the way-point before and after the way-point of interest. Desired vessel speed $u_d \in \mathbb{R}$ is also associated with each way-point implying that the speed must be changed along the path between the way-points. The path following problem can be formulated as two control objectives (Skjetne *et al.* 2002). The first objective is to reach and follow a desired path (x_d, y_d). This is referred to as the *geometric assignment.* In this paper a *line-of-sight* (LOS) projection algorithm is used for this purpose. The desired geometric path consists of straight line segments connected by way-points. The second control objective, *speed assignment*, is defined in terms of a prescribed speed u_d along the body-fixed x-axis of the ship. This speed will be identical to the path speed once the ship has converged to the path. Hence, the desired speed profile can be assigned dynamically.

1.1 Control of Underactuated Ships

For floating rigs and supply vessels, trajectory tracking in *surge*, *sway*, and *yaw* (3 DOF) is easily achieved since independent control forces and moments are simultaneously available in all degrees of freedom. For slow speed, this is referred to as dynamic positioning (DP) where the ship is controlled by means of tunnel thrusters, azimuths, and main propellers; see Fossen (2002). Conventional ships, on the other hand, are usually equipped with one or two main propellers for forward speed control and rudders for turning control.

[1] Supported by the Norwegian Research Council through the Centre of Ships and Ocean Structures, Centre of Excellence at NTNU.

The minimum configuration for way-point tracking control is one main propeller and a single rudder. This means that only two controls are available, thus rendering the ship underactuated for the task of 3 DOF tracking control.

Recently, underactuated tracking control in 3 DOF has been addressed by Pettersen and Nijmeijer (1999, 2001), Jiang and Nijmeijer (1999), Sira-Ramirez (1999), Jiang (2002), Do *et al.* (2002), and Lefeber *et al.* (2003). These designs deals with simultaneous tracking control in all three modes (x, y, ψ) using only two controls. One of the main problems with this approach is that integral action, needed for compensation of slowly-varying disturbances due to wind, waves, and currents, can only be assigned to two modes (surge and yaw); see Pettersen and Fossen (2000). Consequently, robustness to environmental disturbances is one limiting factor for these methods. In addition, requirements for a persistently exciting reference yaw velocity results in unrealistic topological restrictions on which type of paths that can be tracked by these controllers (Lefeber *et al.* 2003).

Conventional way-point guidance systems are usually designed by reducing the output space from 3 DOF position and heading to 2 DOF heading and surge (Healey and Marco 1992). In its simplest form this involves the use of a classical autopilot system where the commanded yaw angle ψ_d is generated such that the *cross-track error* is minimized. This can be done in a multivariable controller, for instance $\mathcal{H}_\infty$ or LQG, or by including an additional tracking error control-loop in the autopilot; see Holzhüter and Schultze (1996), and Holzhüter (1997). A path following control system is usually designed such that the ship moves forward with reference speed u_d at the same time as the cross-track error to the path is minimized. As a result, ψ_d and u_d are tracked using only two controls. The desired path can be generated using a route management system or by specifying way-points (Fossen 2002). If weather data are available, the optimal route can be generated such that the effects of wind and water resistance are minimized.

1.2 Main Contribution

The main contribution of this paper is a ship maneuvering design involving a LOS guidance system and a nonlinear feedback tracking controller. The desired output is reduced from (x_d, y_d, ψ_d) to ψ_d and u_d using a LOS projection algorithm. The tracking task $\psi(t) \to \psi_d(t)$ is then achieved using only one control (normally the rudder), while tracking of the speed assignment u_d is performed by the remaining control (the main propeller). Since we are dealing with segments of straight lines, the LOS projection algorithm will guarantee that the task of path following is satisfied.

First, a LOS guidance procedure is derived. This includes a projection algorithm and a way-point switching algorithm. To avoid large bumps in ψ_d when switching, and to provide the necessary derivatives of ψ_d to the controller, the commanded LOS heading is fed through a reference model. Secondly, a nonlinear 2 DOF tracking controller is derived using the backstepping technique. Three stabilizing functions $\alpha = [\alpha_1, \alpha_2, \alpha_3]^\top$ are defined where α_1 and α_3 are specified to satisfy the tracking objectives in the controlled surge and yaw modes. The stabilizing function α_2 in the uncontrolled sway mode is left as a free design variable. By assigning dynamics to α_2, the resulting controller becomes a dynamic feedback controller so that $\alpha_2(t) \to v(t)$ (sway velocity) during path following. This is a new idea that adds to the extensive theory of backstepping. The presented design technique results in a robust controller for underactuated ships since integral action can be implemented for both path following and speed control.

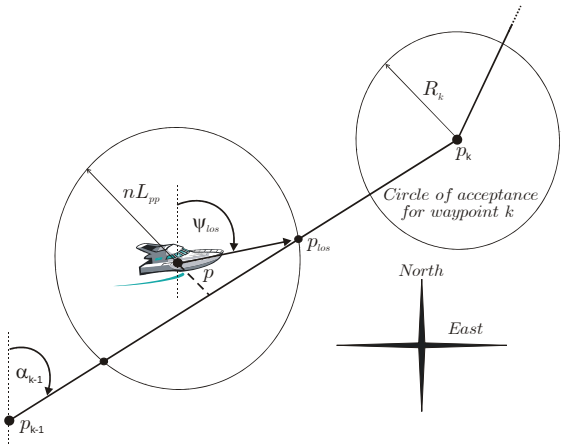

Fig. 1. The Line-of-Sight guidance principle.

1.3 Problem Statement

The problem statement is stated as a maneuvering problem with the following two objectives (Skjetne *et al.* 2002):

LOS Geometric Task: Force the vessel position $p = [x, y]^\top$ to converge to a desired path by forcing the yaw angle ψ to converge to the LOS angle:

$$\psi_{\text{los}} = \text{atan2}\left(y_{\text{los}} - y, x_{\text{los}} - x\right) \tag{1}$$

where the LOS position $p_{\text{los}} = [x_{\text{los}}, y_{\text{los}}]^\top$ is the point along the path which the vessel should be pointed at; see Figure 1. Note that utilizing the four quadrant inverse tangent function $\text{atan2}(y, x)$ ensures the mapping $\psi_{\text{los}} \in \langle -\pi, \pi \rangle$.

Dynamic Task: Force the speed u to converge to a desired speed assignment u_d, that is:

$$\lim_{t \to \infty} \left[u(t) - u_d(t)\right] = 0 \tag{2}$$

where u_d is the desired speed composed along the body-fixed x-axis.

2. LINE-OF-SIGHT GUIDANCE SYSTEM

The desired geometric path considered here is composed by a collection of way-points in a way-point

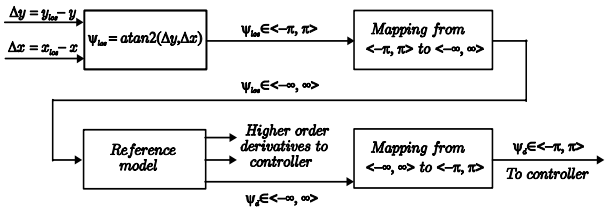

Fig. 2. LOS guidance system.

table. The LOS position $p_{\rm los}$ is located somewhere along the straight line segment connecting the previous p_{k-1} and current p_k way-points. Let the ship's current horizontal position p be the center of a circle with radius of n ship lengths (nL_{pp}). This circle will intersect the current straight line segment at two points where $p_{\rm los}$ is selected as the point closest to the next way-point. To calculate $p_{\rm los}$, two equations with two unknowns must be solved online. These are:

$$(y_{\rm los}-y)^2+(x_{\rm los}-x)^2=(nL_{pp})^2 \tag{3}$$

$$\frac{y_{\rm los}-y_{k-1}}{x_{\rm los}-x_{k-1}}=\frac{y_k-y_{k-1}}{x_k-x_{k-1}}=\tan(\alpha_{k-1}) \tag{4}$$

The first equation is recognized as the theorem of *Pythagoras*, while the second equation states that the slope of the path between the previous and current way-point is constant.

Selecting way-points in the way-point table relies on a switching algorithm. A criteria for selecting the next way-point, located at $p_{k+1}=[x_{k+1},y_{k+1}]^\top$, is for the ship to be within a *circle of acceptance* of the current way-point p_k. Hence, if at some instant of time t the ship position $p(t)$ satisfies:

$$(x_k-x(t))^2+(y_k-y(t))^2\le R_k^2, \tag{5}$$

the next way-point is selected from the way-point table. R_k denotes the radius of the circle of acceptance for the current way-point. It is imperative that the circle enclosing the ship has a sufficient radius such that the solutions to (3) exist. Therefore, $nL_{pp}\ge R_k$, for all k is a necessary bound.

The signals ψ_d, $\dot\psi_d$, and $\ddot\psi_d$ are required by the controller. To provide these signals, a reference model is implemented. This will generate the necessary signals as well as smoothing the discontinuous way-point switching to prevent rapid changes in the desired yaw angle fed to the controller. However, since the atan2-function is discontinuous at the $-\pi/\pi$-junction, the reference model cannot be applied directly to its output. This is solved by constructing a mapping $\Psi_d:\langle-\pi,\pi\rangle\to\langle-\infty,\infty\rangle$ and sandwiching the reference filter between Ψ_d and Ψ_d^{-1}; see Fig. 2. Details about the mappings can be found in Breivik (2003).

3. LINE-OF-SIGHT CONTROL DESIGN

A conventional tracking control system for 3 DOF is usually implemented using a standard PID autopilot in series with a LOS algorithm as shown in Figure 3. Hence, a state-of-the-art autopilot system can be modified to take the LOS reference angle as input. This adds flexibility since the default commercial autopilot system of the ship can be used together with the LOS guidance system. The speed can be adjusted manually by the Captain or automatically using the path speed profile. A model-based nonlinear controller that solves the control objective as stated in Section 1.3 is derived next. The basis is a 3 DOF ship maneuvering model.

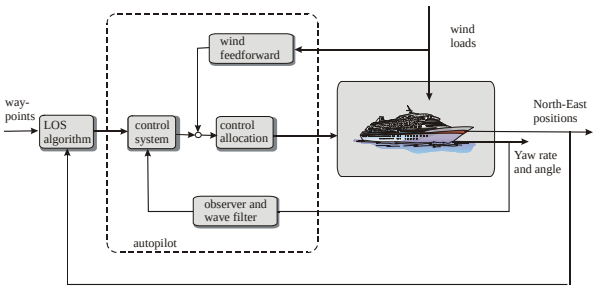

Fig. 3. Conventional autpilot with a LOS projection algorithm for way-point tracking.

3.1 Surge, Sway, and Yaw Equations of Motion

Consider the 3 DOF nonlinear maneuvering model in the form (Fossen 2002):

$$\dot\eta=R(\psi)\nu \tag{6}$$

$$M\dot\nu+N(\nu)\nu=\begin{bmatrix}\tau_1\\0\\\tau_3\end{bmatrix} \tag{7}$$

where $\eta=[x,y,\psi]^\top$, $\nu=[u,v,r]^\top$ and:

$$R(\psi)=\begin{bmatrix}\cos\psi&-\sin\psi&0\\\sin\psi&\cos\psi&0\\0&0&1\end{bmatrix} \tag{8}$$

The matrices M and N are defined as:

$$M=\begin{bmatrix}m_{11}&0&0\\0&m_{22}&m_{23}\\0&m_{32}&m_{33}\end{bmatrix}$$

$$=\begin{bmatrix}m-X_{\dot u}&0&0\\0&m-Y_{\dot v}&mx_g-Y_{\dot r}\\0&mx_g-N_{\dot v}&I_z-N_{\dot r}\end{bmatrix}$$

$$N(\nu)=\begin{bmatrix}n_{11}&0&0\\0&n_{22}&n_{23}\\0&n_{32}&n_{33}\end{bmatrix}=\begin{bmatrix}-X_u&0&0\\0&-Y_v&mu-Y_r\\0&-N_v&mx_gu-N_r\end{bmatrix}$$

Symmetrization of the System Inertia Matrix: If $M\ne M^\top$, the inertia matrix can be made symmetric by acceleration feedback; see Fossen *et al.* (2002) and Lindegaard (2003). This is necessary in a Lyapunov stability analysis for a kinetic energy function to be applied. For low-speed applications like DP, a symmetric system inertia matrix M is an accurate assumption. However, for craft operating at high speed, this assumption is not valid since M is largely nonsymmetric due to hydrodynamically added mass.

Acceleration feedback is implemented by the inner feedback loop:

$$\tau_3=(m_{32}-m_{23})\dot v+\tau_3^* \tag{9}$$

where the sway acceleration $\dot{v}$ is assumed to be measured. The new control variable τ_3^* is then used for maneuvering control. The resulting model is:

$$\dot{\eta} = R(\psi)\nu \tag{10}$$

$$M^*\dot{\nu} + N(\nu)\nu = \begin{bmatrix} \tau_1 \\ 0 \\ \tau_3^* \end{bmatrix} \tag{11}$$

where

$$M^* = \begin{bmatrix} m_{11} & 0 & 0 \\ 0 & m_{22} & m_{23} \\ 0 & m_{23} & m_{33} \end{bmatrix} = (M^*)^\top > 0 \tag{12}$$

Consequently, the following control design can be based on a symmetric representation of M.

3.2 Control Design

The design is based on the model (6)–(7) where M is symmetric or at least made symmetric by acceleration feedback. Define the error signals $z_1 \in \mathbb{R}$ and $z_2 \in \mathbb{R}^3$ according to:

$$z_1 \triangleq \psi - \psi_d \tag{13}$$

$$z_2 \triangleq [z_{2,1}, z_{2,2}, z_{2,3}]^\top = \nu - \alpha \tag{14}$$

where ψ_d and its derivatives are provided by the guidance system, $u_d \in \mathcal{L}_\infty$ is the desired speed, and $\alpha = [\alpha_1, \alpha_2, \alpha_3]^\top \in \mathbb{R}^3$ is a vector of stabilizing functions to be specified later. Next, let:

$$h = [0, 0, 1]^\top \tag{15}$$

such that:

$$\begin{aligned} \dot{z}_1 &= r - r_d = h^\top \nu - r_d \\ &= \alpha_3 + h^\top z_2 - r_d \end{aligned} \tag{16}$$

where $r_d = \dot{\psi}_d$ and:

$$M\dot{z}_2 = M\dot{\nu} - M\dot{\alpha} = \tau - N\nu - M\dot{\alpha}. \tag{17}$$

Motivated by backstepping; see Fossen (2002, Ch. 7), we consider the control Lyapunov function (CLF):

$$V = \frac{1}{2}z_1^2 + \frac{1}{2}z_2^\top M z_2, \qquad M = M^\top > 0. \tag{18}$$

Differentiating V along the trajectories of z_1 and z_2, yields:

$$\begin{aligned} \dot{V} &= z_1\dot{z}_1 + z_2^\top M\dot{z}_2 \\ &= z_1(\alpha_3 + h^\top z_2 - r_d) + z_2^\top(\tau - N\nu - M\dot{\alpha}). \end{aligned}$$

Choosing the virtual control α_3 as:

$$\alpha_3 = -cz_1 + r_d \tag{19}$$

while α_1 and α_2 are yet to be defined, gives:

$$\begin{aligned} \dot{V} &= -cz_1^2 + z_1 h^\top z_2 + z_2^\top(\tau - N\nu - M\dot{\alpha}) \\ &= -cz_1^2 + z_2^\top(hz_1 + \tau - N\nu - M\dot{\alpha}). \end{aligned} \tag{20}$$

Suppose we can assign:

$$\tau = \begin{bmatrix} \tau_1 \\ 0 \\ \tau_3 \end{bmatrix} = M\dot{\alpha} + N\nu - Kz_2 - hz_1 \tag{21}$$

where $K = \mathrm{diag}(k_1, k_2, k_3) > 0$. This results in:

$$\dot{V} = -cz_1^2 - z_2^\top K z_2 < 0, \quad \forall z_1 \neq 0, z_2 \neq 0, \tag{22}$$

and by standard Lyapunov arguments, this guarantees that (z_1, z_2) is bounded and converges to zero.

However, notice from (21) that we can only prescribe values for τ_1 and τ_3, that is:

$$\begin{aligned} \tau_1 &= m_{11}\dot{\alpha}_1 + n_{11}u - k_1(u - \alpha_1) \\ \tau_3 &= m_{32}\dot{\alpha}_2 + m_{33}\dot{\alpha}_3 + n_{32}v + n_{33}r - k_3(r - \alpha_3) - z_1 \end{aligned}$$

Choosing $\alpha_1 = u_d$ solves the dynamic task and gives the closed-loop:

$$m_{11}(\dot{u} - \dot{u}_d) + k_1(u - u_d) = 0. \tag{23}$$

in surge. The remaining equation ($\tau_2 = 0$) in (21) results in a dynamic equality constraint:

$$m_{22}\dot{\alpha}_2 + m_{23}\dot{\alpha}_3 + n_{22}v + n_{23}r - k_2(v - \alpha_2) = 0. \tag{24}$$

Substituting $\dot{\alpha}_3 = c^2 z_1 - cz_{2,3} + \dot{r}_d$, $v = \alpha_2 + z_{2,2}$, and $r = \alpha_3(z_1, r_d) + z_{2,3}$ into (24), gives:

$$m_{22}\dot{\alpha}_2 = -n_{22}\alpha_2 + \gamma(z_1, z_2, r_d, \dot{r}_d) \tag{25}$$

where:

$$\begin{aligned} \gamma(z_1, z_2, r_d, \dot{r}_d) = (n_{23}c - m_{23}c^2)z_1 + (k_2 - n_{22})z_{2,2} \\ + (m_{23}c - n_{23})z_{2,3} - m_{23}\dot{r}_d - n_{23}r_d. \end{aligned}$$

The variable α_2 becomes a dynamic state of the controller according to (25). Furthermore, $n_{22} > 0$ implies that (25) is a stable differential equation driven by the converging error signals (z_1, z_2) and the bounded reference signals $(r_d, \dot{r}_d)$. Since $z_{2,2}(t) \to 0$, we get that $|\alpha_2(t) - v(t)| \to 0$ as $t \to \infty$. The main result is summarized by Theorem 1:

Theorem 1. (LOS Path Following). The LOS maneuvering problem for the 3 DOF underactuated vessel model (6)–(7) is solved using the control laws:

$$\begin{aligned} \tau_1 &= m_{11}\dot{u}_d + n_{11}u - k_1(u - u_d) \\ \tau_3 &= m_{32}\dot{\alpha}_2 + m_{33}\dot{\alpha}_3 + n_{32}v + n_{33}r - k_3(r - \alpha_3) - z_1 \end{aligned}$$

where $k_1 > 0$, $k_3 > 0$, $z_1 \triangleq \psi - \psi_d$, $z_2 \triangleq [u - u_d, v - \alpha_2, r - \alpha_3]^\top$, and:

$$\alpha_3 = -cz_1 + r_d, \qquad c > 0 \tag{26}$$

$$\dot{\alpha}_3 = -c(r - r_d) + \dot{r}_d. \tag{27}$$

The reference signals u_d, $\dot{u}_d$, ψ_d, r_d, and $\dot{r}_d$ are provided by the LOS guidance system, while α_2 is found by numerical integration of:

$$m_{22}\dot{\alpha}_2 = -n_{22}\alpha_2 + (k_2 - n_{22})z_{2,2} - m_{23}\dot{\alpha}_3 - n_{23}r$$

where $k_2 > 0$. This results in a UGAS equilibrium point $(z_1, z_2) = (0, 0)$, while $\alpha_2 \in \mathcal{L}_\infty$ satisfies:

$$\lim_{t\to\infty} |\alpha_2(t) - v(t)| = 0 \tag{28}$$

Remark 1: Notice that the smooth reference signal $\psi_d \in \mathcal{L}_\infty$ must be differentiated twice to produce r_d and $\dot{r}_d$, while $u_d \in \mathcal{L}_\infty$ must be differentiated once to give $\dot{u}_d$. This is most easily achieved by using reference models represented by low-pass filters; see Fossen (2002), Ch. 5.

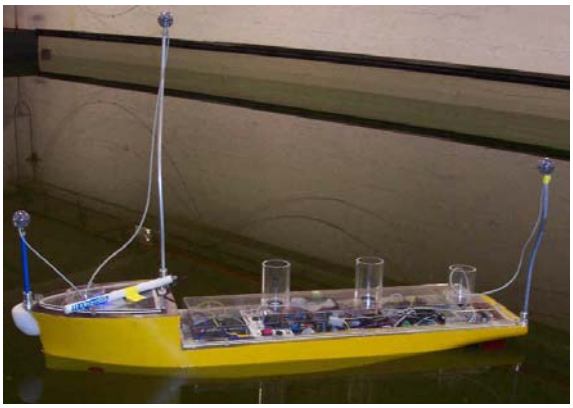

Fig. 4. CyberShip 2 in action at the MCLab.

PROOF. The closed-loop equations become:

$$\begin{bmatrix} \dot{z}_1 \\ \dot{z}_2 \end{bmatrix} = \begin{bmatrix} -c & h^\top \\ -M^{-1}h & -M^{-1}K \end{bmatrix} \begin{bmatrix} z_1 \\ z_2 \end{bmatrix} \tag{29}$$

$$m_{22}\dot{\alpha}_2 = -n_{22}\alpha_2 + \gamma(z_1, z_2, r_d, \dot{r}_d). \tag{30}$$

From the Lyapunov arguments (18) and (22), the equilibrium $(z_1, z_2) = (0, 0)$ of the z-subsystem is proved UGAS. Moreover, the unforced α_2-subsystem ($\gamma = 0$) is clearly exponentially stable. Since $(z_1, z_2) \in \mathcal{L}_\infty$ and $(r_d, \dot{r}_d) \in \mathcal{L}_\infty$, then $\gamma \in \mathcal{L}_\infty$. This implies that the α_2-subsystem is input-to-state stable from γ to α_2. This is seen by applying for instance $V_2 = \frac{1}{2}m_{22}\alpha_2^2$ which differentiated along solutions of α_2 gives $\dot{V}_2 \leq -\frac{1}{2}n_{22}\alpha_2^2$ for all $|\alpha_2| \geq \frac{2}{n_{22}}|\gamma(z_1, z_2, r_d, \dot{r}_d)|$. By standard comparison functions, it is straight-forward to show that for all $|\alpha_2(t)| \geq \frac{2}{n_{22}}|\gamma(z_1(t), z_2(t), r_d(t), \dot{r}_d(t))|$ then

$$|\alpha_2(t)| \leq |\alpha_2(0)|\, e^{-\frac{n_{22}}{4}t}. \tag{31}$$

Hence, α_2 converges to the bounded set $\{\alpha_2 : |\alpha_2| \leq \frac{2}{n_{22}}||\gamma(z_1, z_2, r_d, \dot{r}_d)||\}$. Since $z_{2,2}(t) \to 0$ as $t \to \infty$, we get the last limit.

4. CASE STUDY: EXPERIMENT PERFORMED WITH THE CS2 MODEL SHIP

The proposed controller and guidance system were tested out at the *Marine Cybernetics Laboratory* (MCLab) located at the Norwegian University of Science and Technology. MCLab is an experimental laboratory for testing of scale models of ships, rigs, underwater vehicles and propulsion systems. The software is developed by using rapid prototyping techniques and automatic code generation under *Matlab/Simulink*^{TM} and *RT-Lab*^{TM}. The target PC onboard the model scale vessels runs the *QNX*^{TM} real-time operating system, while experimental results are presented in real-time on a host PC using *Labview*^{TM}.

In the experiment, *CyberShip 2* (CS2) was used. It is a 1:70 scale model of an offshore supply vessel with a mass of 15 kg and a length of 1.255 m. The maximum surge force is approx. 2.0 N, while the maximum yaw moment is about 1.5 Nm. The MCLab tank is $L \times B \times D$ = 40 m $\times$ 6.5 m $\times$ 1.5 m.

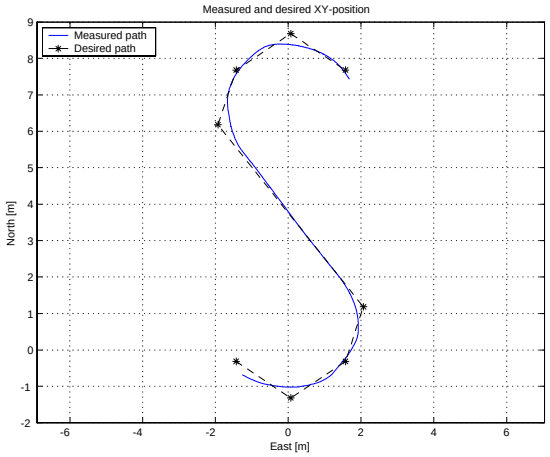

Fig. 5. xy-plot of the measured and desired geometrical path during the experiment.

Figure 4 shows CS2. Three spheres can be seen mounted on the ship, ensuring that its position and orientation can be identified by infrared cameras. Two *Qualisys*^{TM} infrared cameras mounted on a towing carriage currently supply the position and orientation estimates in 6 DOF, but due to a temporary bad calibration, the camera measurements vanished when the ship assumed certain yaw angles and regions of the tank. This affected the results of the experiment and also limited the available space for maneuvering. Nevertheless, good results were obtained. The cameras operate at 10 Hz.

The desired path consists of a total of 8 way-points:

$$\begin{array}{ll} wpt_1 = (0.372, -0.181) & wpt_5 = (6.872, -0.681) \\ wpt_2 = (-0.628, 1.320) & wpt_6 = (8.372, -0.181) \\ wpt_3 = (0.372, 2.820) & wpt_7 = (9.372, 1.320) \\ wpt_4 = (1.872, 3.320) & wpt_8 = (8.372, 2.820) \end{array}$$

representing an S-shape. CS2 was performing the maneuver with a constant surge speed of 0.1 m/s. By assuming equal *Froude numbers*, this corresponds to a surge speed of 0.85 m/s for the full scale supply ship. A higher speed was not attempted because the consequence of vanishing position measurements at higher speed is quite severe. The controller used:

$$M = \begin{bmatrix} 25.8 & 0 & 0 \\ 0 & 33.8 & 1.0115 \\ 0 & 1.0115 & 2.76 \end{bmatrix} \quad N(\nu) = \begin{bmatrix} 2 & 0 & 0 \\ 0 & 7 & 0.1 \\ 0 & 0.1 & 0.5 \end{bmatrix}$$

$$c = 0.75,\ k_1 = 25,\ k_2 = 10,\ k_3 = 2.5$$

In addition, a reference model consisting of three 1st-order low-pass filters in cascade delivered continuos values of ψ_d, r_d, and $\dot{r}_d$. The ship's initial states were:

$$(x_0, y_0, \psi_0) = (-0.69 \text{ m}, -1.25 \text{ m},\ 1.78 \text{ rad})$$
$$(u_0, v_0, r_0) = (0.1 \text{ m/s},\ 0 \text{ m/s},\ 0 \text{ rad/s})$$

Both the ship enclosing circle and the radius of acceptance for all way-points was set to one ship length. Figure 5 shows an xy-plot of the CS2's position together with the desired geometrical path consisting of straight line segments. The ship is seen to follow

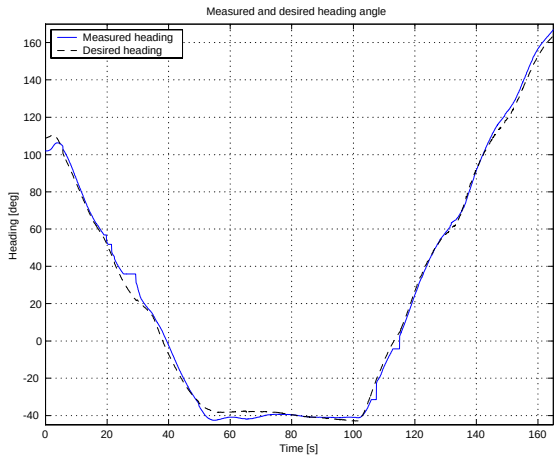

Fig. 6. The actual yaw angle of the ship tracks the desired LOS angle well.

the path very well. To illustrate the effect of the positioning reference system dropping out from time to time, Figure 6 is included. It shows the actual heading angle of CS2 alongside the desired LOS angle. The discontinuities in the actual heading angle is due to the camera measurements dropping out. When the measurements return, the heading angle of the ship is seen to converge nicely to the desired angle.

5. CONCLUSIONS

A nonlinear guidance system that reduces the output space from 3 DOF to 2 DOF was developed by using a LOS projection algorithm. Moreover, a nonlinear controller for maneuvering of underactuated marine craft utilizing dynamic feedback has been developed with a vectorial backstepping approach. UGAS is proven for the controlled error states, and boundedness is proven for a controller dynamic state that will track the sway velocity. The design technique is robust since integral action can easily be implemented. Note that the controller also can be utilized for a fully actuated ship since the control law is derived without assuming a specific control allocation scheme. Hence, the controller and control allocation blocks can be replaced by other algorithms in a modular design. Experiments with a model ship document the performance of the guidance and control systems.

REFERENCES

Breivik, M. (2003). Nonlinear Maneuvering Control of Underactuated Ships. MSc thesis. Dept. of Eng. Cybernetics, Norwegian University of Science and Technology.

Do, K. D., Z. P. Jiang and J. Pan (2002). Underactuated Ship Global Tracking under Relaxed Conditions. *IEEE Transactions on Automatic Control* **TAC-47**(9), 1529–1535.

Fossen, T. I. (1994). *Guidance and Control of Ocean Vehicles*. John Wiley and Sons Ltd. ISBN 0-471-94113-1.

Fossen, T. I. (2002). *Marine Control Systems: Guidance, Navigation and Control of Ships, Rigs and Underwater Vehicles*. Marine Cybernetics AS. Trondheim, Norway. ISBN 82-92356-00-2.

Fossen, T. I., K. P. Lindegaard and R. Skjetne (2002). Inertia Shaping Techniques for Marine Vessels using Acceleration Feedback. In: *Proceedings of the IFAC World Congress*. Elsevier Science. Barcelona.

Healey, A. J. and D. B. Marco (1992). Slow Speed Flight Control of Autonomous Underwater Vehicles: Experimental Results with the NPS AUV II. In: *Proceedings of the 2nd International Offshore and Polar Engineering Conference (ISOPE)*. San Francisco, CA. pp. 523–532.

Holzhüter, T. (1997). LQG Approach for the High-Precision Track Control of Ships. *IEE Proceedings on Control Theory and Applications* **144**(2), 121–127.

Holzhüter, T. and R. Schultze (1996). On the Experience with a High-Precision Track Controller for Commercial Ships. *Control Engineering Practise* **CEP-4**(3), 343–350.

Jiang, Z. P. (2002). Global Tracking Control of Underactuated Ships by Lyapunov's Direct Method. *Automatica* **AUT-38**(2), 301–309.

Jiang, Z.-P. and H. Nijmeijer (1999). A Recursive Technique for Tracking Control of Nonholonomic Systems in Chained Form. *IEEE Transactions on Automatic Control* **TAC-4**(2), 265–279.

Lefeber, A.A.J., K. Y. Pettersen and H. Nijmeijer (2003). Tracking Control of an Underactuated Ship. *IEEE Transactions on Control Systems Technology* **TCST-11**(1), 52–61.

Lindegaard, K.-P. (2003). Acceleration Feedback in Dynamic Positioning Systems. PhD thesis. Department of Engineering Cybernetics, Norwegian University of Science and Technology. Trondheim.

Pettersen, K. Y. and H. Nijmeijer (1999). Tracking Control of an Underactuated Surface Vessel. In: *Proceedings of the IEEE Conference on Decision and Control*. Phoenix, AZ. pp. 4561–4566.

Pettersen, K. Y. and H. Nijmeijer (2001). Underactuated Ship Tracking Control. *International Journal of Control* **IJC-74**, 1435–1446.

Pettersen, K. Y. and T. I. Fossen (2000). Underactuated Dynamic Positioning of a Ship - Experimental Results. *IEEE Transactions on Control Systems Technology* **TCST-8**(5), 856–863.

Sira-Ramirez, H. (1999). On the Control of the Underactuated Ship: A Trajectory Planning Approach. In: *IEEE Conference on Decision and Control*. Phoenix, AZ.

Skjetne, R., T. I. Fossen and P. V. Kokotovic (2002). Output Maneuvering for a Class of Nonlinear Systems. In: *Proc. of the IFAC World Congress*. Barcelona.

B. A Unified Concept for Controlling a Marine Surface Vessel Through the Entire Speed Envelope

A Unified Concept for Controlling a Marine Surface Vessel Through the Entire Speed Envelope

Morten Breivik*,[1]
*Centre for Ships and Ocean Structures (CESOS)
Norwegian University of Science and Technology (NTNU)
NO-7491 Trondheim, Norway
E-mail: morten.breivik@ieee.org

Thor I. Fossen*,†
†Department of Engineering Cybernetics (ITK)
Norwegian University of Science and Technology (NTNU)
NO-7491 Trondheim, Norway
E-mail: fossen@ieee.org

***Abstract*— This paper addresses the problem of creating a controller structure for the automatic control of a marine surface vessel through its entire speed regime without resorting to heuristics and switching between fundamentally different controllers. Hence, a single controller structure is proposed for the purpose. Its core is a nonlinear, model-based velocity and heading controller which relies on a key guidance-based path following concept necessary to ensure geometric path convergence. The scheme renders all regular paths feasible, and ensures that a vessel which is fully actuated at low speeds, but becomes underactuated at high speeds, is able to converge to and follow a desired geometric path independent of the current vessel speed.**

I. Introduction

It is a fundamental necessity to be able to automatically control a marine surface vessel through its entire speed regime, i.e. through all the stages from low-speed positioning to high-speed maneuvers. Traditionally, such a problem has been solved by constructing dedicated controllers for each distinct part of the speed envelope. The desired functionality is then achieved by designing a high-level decision-making system to intelligently switch between the different controllers, resulting in a hybrid and discontinous system. Usually, a nonlinear, model-based controller is designed for low-speed applications, and it is assumed that the vessel in question is fully actuated for the purpose, i.e. independently actuated in all degrees-of-freedom (DOFs) simultaneously. For high-speed applications, a linear heading controller based on the Nomoto model is usually designed, together with an independent speed controller. At high speeds, the vessel is for all practical purposes underactuated, i.e. it lacks the capability to command independent accelerations in all DOFs simultaneously.

Being able to design a single controller structure, i.e. without heuristics and hybrid switching, to cover the entire speed envelope of a marine surface vessel, would be very desirable from both a theoretical and industrial point of view. Theoretically, for obvious reasons such as stability results. Industrially, for reasons such as reduced complexity of implementation, easier code verification and maintenance procedures, and possibly increased safety of operation.

In practice, the only relevant type of vessels to consider are the ones which become underactuated in the sway direction (lateral direction) at high speeds. These are typically equipped with a number of tunnel thrusters both fore and aft, designed to assist at low-speed maneuvers, which are rendered inoperable at high speeds mainly due to the relative water speed past their outlets. Under such circumstances the only means of actuation are the main propulsors located aft. An example of such a vessel is a tugboat from Rolls-Royce Marine, which is illustrated in Figure 1.

A. Previous Work

An interesting paper which treats the desired control topic is [1], where a hybrid switching design between a dynamic positioning controller for low speeds and a track-keeping controller for high speeds is considered for minehunters in the Italian Navy. A similar hybrid procedure is presented in [2], where the application is high-speed craft powered mainly by waterjets. Hybrid designs for offshore supply vessels are mentioned in [3]. However, compared to traditional industrial control schemes where the helmsman is required to exert manual control during part of the speed envelope, the designs presented in these papers represent a step forward.

B. Main Contribution

This paper presents a single controller structure capable of controlling a marine surface vessel through its entire speed envelope. The core of the structure consists of a nonlinear, model-based velocity and heading controller which relies on a key guidance-based path following concept necessary to guarantee geometric path convergence. The scheme is a natural extension of the path following approach in [4] where the individual designs for the fully actuated and the underactuated vessels have been fusioned into one, seamless, continous design without any heuristics involved. The paper contains a lucid exposition of the proposed approach, which has an intuitive physical interpretation.

[1]This work was supported by the Research Council of Norway through the Centre for Ships and Ocean Structures at NTNU.

II. Problem Statement

The primary objective in guidance-based path following is to ensure that a vehicle converges to and follows a desired geometric path, without any temporal requirements. The secondary objective is to ensure that the vehicle complies with a desired dynamic behaviour. By using the convenient task classification scheme of [5], the guidance-based path following problem can thus be expressed by the following two task objectives:

Geometric Task: Make the position of the vehicle converge to and follow a desired geometric path.

Dynamic Task: Make the speed of the vehicle converge to and track a desired speed assignment.

III. Guidance System Design

This section develops the guidance laws required to solve the planar guidance-based path following problem in question. Throughout the section we will consistently employ the notion of an *ideal particle*, which is to be interpreted as a planar position variable without dynamics, i.e. it can instantly attain any assigned motion behaviour. The developed guidance laws can subsequently be extended to any desirable dynamics case since they are generically valid.

A. Assumptions

The following assumptions are made:

- **A.1** The desired geometric path is regularly parametrized.
- **A.2** The speed of the ideal particle is lower-bounded, i.e. $U_d(t) \in [U_{d,\min}, \infty\rangle \ \forall t \geq 0$.
- **A.3** The guidance variable is positive and upper-bounded, i.e. $\triangle(t) \in \langle 0, \triangle_{\max}] \ \forall t \geq 0$.

B. Guidance Law Design

Denote the inertial position and velocity vectors of the ideal particle by $\mathbf{p} = [x, y]^\top \in \mathbb{R}^2$ and $\mathbf{v} = \dot{\mathbf{p}} = [\dot{x}, \dot{y}]^\top \in \mathbb{R}^2$, respectively. Denote the size of the velocity vector by $U = |\mathbf{v}|_2 = (\mathbf{v}^\top \mathbf{v})^{\frac{1}{2}}$ (the speed) and its orientation by $\chi = \arctan(\frac{\dot{y}}{\dot{x}})$ (the azimuth angle). Since it is assumed that both U and χ can attain any desirable value instantaneously, they are rewritten as U_d and χ_d. Then consider a geometric path continuosly parametrized by a scalar variable $\theta \in \mathbb{R}$, and denote the inertial position of a point belonging to the path as $\mathbf{p}_d(\theta) \in \mathbb{R}^2$. The desired geometric path can consequently be expressed by the set:

$$\mathcal{P} = \left\{ \mathbf{p} \in \mathbb{R}^2 \mid \mathbf{p} = \mathbf{p}_d(\theta) \ \forall \theta \in \mathbb{R} \right\}, \tag{1}$$

where $\mathcal{P} \subset \mathbb{R}^2$. For a given θ, define a local reference frame at $\mathbf{p}_d(\theta)$ and name it the Path Parallel (PP) frame. The PP frame is rotated an angle:

$$\chi_t(\theta) = \arctan\left(\frac{y_d'(\theta)}{x_d'(\theta)} \right) \tag{2}$$

relative to the inertial frame, where the notation $x_d'(\theta) = \frac{dx_d}{d\theta}(\theta)$ has been utilized. Consequently, the x-axis of the PP frame is aligned with the tangent vector to the path at $\mathbf{p}_d(\theta)$, see Figure 2. The error vector between $\mathbf{p}$ and $\mathbf{p}_d(\theta)$ expressed in the PP frame is given by:

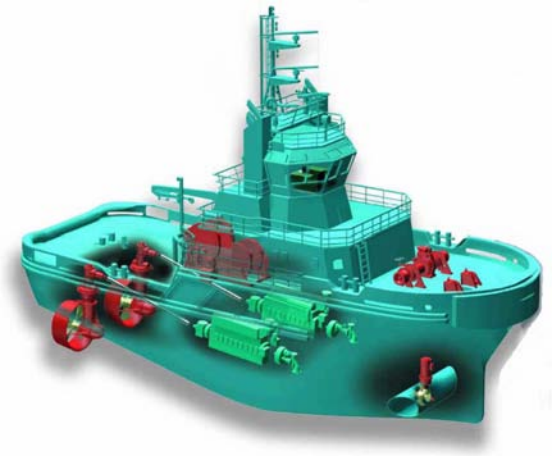

Fig. 1. A principle drawing of a tugboat with two main azimuth thrusters aft and one tunnel thruster in the bow. Courtesy of Rolls-Royce Marine, http://www.rolls-royce.com/marine/.

$$\boldsymbol{\varepsilon} = \mathbf{R}_t^\top (\mathbf{p} - \mathbf{p}_d(\theta)), \tag{3}$$

where:

$$\mathbf{R}_t(\chi_t) = \begin{bmatrix} \cos\chi_t & -\sin\chi_t \\ \sin\chi_t & \cos\chi_t \end{bmatrix} \tag{4}$$

is the rotation matrix from the inertial frame to the PP frame, $\mathbf{R}_t \in SO(2)$. The error vector $\boldsymbol{\varepsilon} = [s, e]^\top \in \mathbb{R}^2$ consists of the *along-track error* s and the *cross-track error* e, see Figure 2. Also, recognize the concept of the *off-track error*, represented by $|\boldsymbol{\varepsilon}|_2 = \sqrt{\boldsymbol{\varepsilon}^\top \boldsymbol{\varepsilon}} = \sqrt{s^2 + e^2}$.

Define the positive definite and radially unbounded Control Lyapunov Function (CLF):

$$V_{\boldsymbol{\varepsilon}} = \frac{1}{2} \boldsymbol{\varepsilon}^\top \boldsymbol{\varepsilon} = \frac{1}{2}(s^2 + e^2), \tag{5}$$

and differentiate it with respect to time along the trajectories of $\boldsymbol{\varepsilon}$ to obtain:

$$\dot{V}_{\boldsymbol{\varepsilon}} = s(U_d \cos(\chi_d - \chi_t) - U_{PP}) + eU_d \sin(\chi_d - \chi_t). \tag{6}$$

We can clearly consider the path tangential speed U_{PP} as a virtual input for stabilizing s, so by choosing:

$$U_{PP} = U_d \cos(\chi_d - \chi_t) + \gamma s, \tag{7}$$

where $\gamma > 0$ becomes a constant gain parameter in the guidance law, we achieve:

$$\dot{V}_{\boldsymbol{\varepsilon}} = -\gamma s^2 + eU_d \sin(\chi_d - \chi_t). \tag{8}$$

From (8) we see that $(\chi_d - \chi_t)$ can be considered a virtual input for stabilizing e. Denote this angular difference by $\chi_r = \chi_d - \chi_t$, i.e. the relative angle between the desired azimuth angle and the azimuth angle of the path tangential. Obviously, such a variable should depend on the cross-track

error itself, such that $\chi_r = \chi_r(e)$. An attractive choice for $\chi_r(e)$ could be the physically motivated:

$$\chi_r(e) = \arctan\left(-\frac{e}{\triangle}\right), \tag{9}$$

where $\triangle > 0$ becomes a time-varying guidance variable utilized to shape the convergence behaviour towards the path tangential, i.e. $\triangle = \triangle(t)$ satisfying A.3. It is often referred to as the *lookahead distance* in literature dealing with path following along straight lines [6], and the physical interpretation can be derived from Figure 2. Other sigmoidal shaping functions are also possible candidates for $\chi_r(e)$. The desired azimuth angle is thus given by:

$$\chi_d(\theta, e) = \chi_t(\theta) + \chi_r(e) \tag{10}$$

with $\chi_t(\theta)$ as in (2) and $\chi_r(e)$ as in (9). We also need to state the relationship between θ and U_{PP}:

$$\begin{aligned} \dot{\theta} &= \frac{U_{PP}}{\sqrt{x_d'^2 + y_d'^2}} \\ &= \frac{U_d \cos\chi_r + \gamma s}{\sqrt{x_d'^2 + y_d'^2}}, \end{aligned} \tag{11}$$

which is non-singular for all paths satisfying assumption A.1. Hence, the derivative of the CLF finally becomes:

$$\begin{aligned} \dot{V}_{\boldsymbol{\varepsilon}} &= -\gamma s^2 + e U_d \sin\chi_r \\ &= -\gamma s^2 - U_d \frac{e^2}{\sqrt{e^2 + \triangle^2}}, \end{aligned} \tag{12}$$

which is negative definite under assumptions A.2 and A.3. The last transition is made by utilizing trigonometric relationships from Figure 2. Note that the speed by definition cannot be negative.

Elaborating on these results, we find that the error system can be represented by the states $\boldsymbol{\varepsilon}$ and θ. It can be rendered autonomous by reformulating its time dependence through the introduction of an extra state:

$$\dot{l} = 1, \; l_0 = t_0 \geq 0, \tag{13}$$

see e.g. [7]. The new and extended system can be represented by the state vector $\mathbf{x} = \left[\boldsymbol{\varepsilon}^\top, \theta, l\right]^\top \in \mathbb{R}^2 \times \mathbb{R} \times \mathbb{R}_{\geq 0}$, with the dynamics:

$$\dot{\mathbf{x}} = \mathbf{f}(\mathbf{x}). \tag{14}$$

The time variable for this new system is denoted t with initial time $t = 0$, such that $l(t) = t + t_0$. We can now utilize set-stability analysis for time-invariant systems in order to be able to conclude on the task objectives in the problem statement. Hence, define the closed, but non-compact set:

$$\mathcal{G} = \left\{\mathbf{x} \in \mathbb{R}^2 \times \mathbb{R} \times \mathbb{R}_{\geq 0} \mid \boldsymbol{\varepsilon} = \mathbf{0}\right\}, \tag{15}$$

which represents the dynamics of the extended system when the ideal particle has converged to the path. Also, let:

$$\begin{aligned} |\mathbf{x}|_{\mathcal{G}} &= \inf\left\{\mathbf{x} - \mathbf{y} \mid \mathbf{y} \in \mathcal{G}\right\} && (16) \\ &= |(\boldsymbol{\varepsilon}, 0, 0)|_2 && (17) \\ &= (\boldsymbol{\varepsilon}^\top \boldsymbol{\varepsilon})^{\frac{1}{2}} && (18) \end{aligned}$$

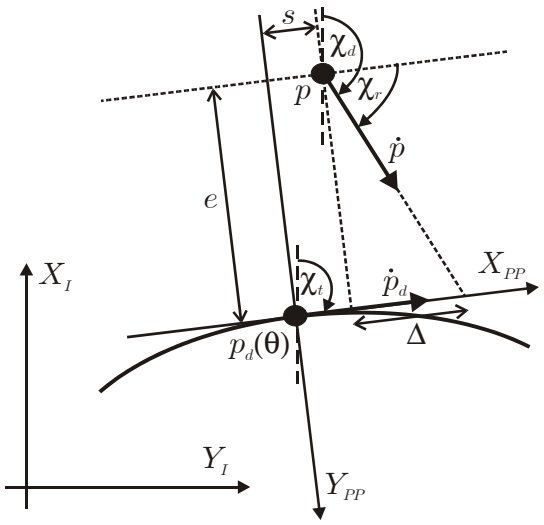

Fig. 2. The geometric relationships between the relevant parameters and variables utilized in the guidance-based path following scheme.

represent a function measuring the distance from $\mathbf{x}$ to the set $\mathcal{G}$, i.e. the previously mentioned off-track error. The goal is consequently to make $|\mathbf{x}|_{\mathcal{G}}$ converge to zero since it is equivalent to solving the geometric task of the guidance-based path following problem. The following proposition can now be stated:

Proposition 1: The error set $\mathcal{G}$ is rendered uniformly globally asymptotically and locally exponentially stable (UGAS/ULES) under assumptions A.1-A.3 if χ_r is equal to (9) and θ is updated by (11).

Proof: [Indication] By establishing that (14) is forward complete and $\mathcal{G}$ is forward invariant, we can derive our stability results by simply considering $V_{\boldsymbol{\varepsilon}} = \frac{1}{2}\boldsymbol{\varepsilon}^\top\boldsymbol{\varepsilon} = \frac{1}{2}|\mathbf{x}|^2_{\mathcal{G}}$, see e.g. [5]. Hence, by standard Lyapunov arguments the error set $\mathcal{G}$ is rendered UGAS under assumptions A.1-A.3 when (9) and (11) are satisfied. Furthermore, $\dot{V}_{\boldsymbol{\varepsilon}} \leq -\gamma s^2 - \frac{U_{d,\min}}{\triangle_{\max}} e^2$ for the error dynamics at $\boldsymbol{\varepsilon} = \mathbf{0}$, which proves ULES. ■

By choosing the speed of the ideal particle equal to:

$$U_d = \kappa\sqrt{e^2 + \triangle^2}, \tag{19}$$

where $\kappa > 0$ is a constant gain parameter, we obtain:

$$\dot{V}_{\boldsymbol{\varepsilon}} = -\gamma s^2 - \kappa e^2, \tag{20}$$

which results in the following proposition:

Proposition 2: The error set $\mathcal{G}$ is rendered uniformly globally exponentially stable (UGES) under assumptions A.1 and A.3 if χ_r is equal to (9), θ given by (11) and U_d satisfies (19).

Proof: [Indication] The first part of the proof is identical to that of Proposition 1. Hence, we conclude by standard Lyapunov arguments that the error set $\mathcal{G}$ is rendered UGES. ■

Although very powerful, this result is clearly not achievable by physical systems since these exhibit natural limitations on their maximum attainable speed. In this regard, Proposition 1 states the best possible stability property a planar physical system like a marine surface vessel can hold.

IV. Control System Design

The 3 DOF kinematics and kinetics of a marine surface vessel can be represented by [8]:

$$\dot{\boldsymbol{\eta}} = \mathbf{R}(\psi)\boldsymbol{\nu} \tag{21}$$

and:

$$\mathbf{M}\dot{\boldsymbol{\nu}} + \mathbf{C}(\boldsymbol{\nu})\boldsymbol{\nu} + \mathbf{D}(\boldsymbol{\nu})\boldsymbol{\nu} = \boldsymbol{\tau} + \mathbf{R}(\psi)^\top \mathbf{b}, \tag{22}$$

where $\boldsymbol{\eta} = [x, y, \psi]^\top \in \mathbb{R}^3$ represents the earth-fixed position and heading, $\boldsymbol{\nu} = [u, v, r]^\top \in \mathbb{R}^3$ represents the vessel-fixed velocities, $\mathbf{R}(\psi) \in SO(3)$ is the rotation matrix from the earth-fixed local geographic reference frame (NED) to the vessel-fixed reference frame (BODY), $\mathbf{M}$ is the vessel inertia matrix, $\mathbf{C}(\boldsymbol{\nu})$ is the centrifugal and coriolis matrix, and $\mathbf{D}(\boldsymbol{\nu})$ is the hydrodynamic damping matrix. The system matrices in (22) are assumed to satisfy the properties $\mathbf{M} = \mathbf{M}^\top > 0$, $\mathbf{C} = -\mathbf{C}^\top$ and $\mathbf{D} > 0$. Furthermore, $\boldsymbol{\tau}$ represents the vessel-fixed propulsion forces and moments, and $\mathbf{b}$ describes the low frequency environmental forces acting on the vessel.

A. Control Law Design

A nonlinear, model-based velocity and heading controller is designed by using the backstepping technique. The output-to-be-controlled has been redefined from position and heading to velocity and heading, so by feeding the controller with the appropriate reference signals, positional convergence is ensured such that the path following task objectives are satisfied. This approach resembles the real-life action of a helmsman onboard a vessel more closely than direct position control in the sense that he uses the vessel velocity to maneuver. He does not think in terms of controlling the position directly, but in his mind feeds the position error signal back through the velocity assignment, ensuring position control indirectly through direct velocity control. Such a technique is equally favourable for fully actuated and underactuated vessels, hence the chosen controller assumes the form of a velocity and heading controller.

Start by defining the projection vector $\mathbf{h}$:

$$\mathbf{h} = [0, 0, 1]^\top, \tag{23}$$

then the error variables $z_1 \in \mathbb{R}$ and $\mathbf{z}_2 \in \mathbb{R}^3$ according to:

$$\begin{aligned} z_1 &= \psi - \psi_d = \mathbf{h}^\top \boldsymbol{\eta} - \psi_d & (24)\\ \mathbf{z}_2 &= [z_{2,1}, z_{2,2}, z_{2,3}]^\top = \boldsymbol{\nu} - \boldsymbol{\alpha}, & (25) \end{aligned}$$

where $\boldsymbol{\alpha} = [\alpha_1, \alpha_2, \alpha_3]^\top \in \mathbb{R}^3$ is a vector of stabilizing functions to be specified later.

Step 1:

Define the first Control Lyapunov Function (CLF) as:

$$V_1 = \frac{1}{2} k_1 z_1^2, \tag{26}$$

where $k_1 > 0$. Differentiating V_1 with respect to time along the z_1-dynamics yields:

$$\begin{aligned} \dot{V}_1 &= k_1 z_1 \dot{z}_1 \\ &= k_1 z_1 (\mathbf{h}^\top \dot{\boldsymbol{\eta}} - \dot{\psi}_d) \\ &= k_1 z_1 (\mathbf{h}^\top \boldsymbol{\nu} - \dot{\psi}_d), \end{aligned} \tag{27}$$

since $\dot{\boldsymbol{\eta}} = \mathbf{R}\boldsymbol{\nu}$ and $\mathbf{h}^T \mathbf{R} \boldsymbol{\nu} = \mathbf{h}^T \boldsymbol{\nu}$. By using (25), we obtain:

$$\begin{aligned} \dot{V}_1 &= k_1 z_1 (\mathbf{h}^\top (\mathbf{z}_2 + \boldsymbol{\alpha}) - \dot{\psi}_d) \\ &= k_1 z_1 \mathbf{h}^\top \mathbf{z}_2 + k_1 z_1 (\alpha_3 - \dot{\psi}_d). \end{aligned} \tag{28}$$

This motivates the choice of the stabilizing function α_3 as:

$$\alpha_3 = \dot{\psi}_d - z_1, \tag{29}$$

which results in:

$$\dot{V}_1 = -k_1 z_1^2 + k_1 z_1 \mathbf{h}^\top \mathbf{z}_2. \tag{30}$$

Step 2:

Augment the first CLF to obtain:

$$V_2 = V_1 + \frac{1}{2} \mathbf{z}_2^\top \mathbf{M} \mathbf{z}_2 + \frac{1}{2} \tilde{\mathbf{b}}^\top \boldsymbol{\Gamma}^{-1} \tilde{\mathbf{b}}, \tag{31}$$

where $\tilde{\mathbf{b}} \in \mathbb{R}^3$ is an adaptation error defined as $\tilde{\mathbf{b}} = \hat{\mathbf{b}} - \mathbf{b}$ with $\hat{\mathbf{b}}$ being the estimate of $\mathbf{b}$, and by assumption $\dot{\mathbf{b}} = \mathbf{0}$. $\boldsymbol{\Gamma} = \boldsymbol{\Gamma}^\top > 0$ is the adaptation gain matrix.

Differentiating V_2 along the trajectories of z_1, $\mathbf{z}_2$ and $\tilde{\mathbf{b}}$, we obtain:

$$\dot{V}_2 = -k_1 z_1^2 + k_1 z_1 \mathbf{h}^\top \mathbf{z}_2 + \mathbf{z}_2^\top \mathbf{M} \dot{\mathbf{z}}_2 + \tilde{\mathbf{b}}^\top \boldsymbol{\Gamma}^{-1} \dot{\tilde{\mathbf{b}}}, \tag{32}$$

since $\mathbf{M} = \mathbf{M}^\top$ and $\dot{\tilde{\mathbf{b}}} = \dot{\hat{\mathbf{b}}}$. The fact that:

$$\begin{aligned} \mathbf{M}\dot{\mathbf{z}}_2 &= \mathbf{M}(\dot{\boldsymbol{\nu}} - \dot{\boldsymbol{\alpha}}) \\ &= \boldsymbol{\tau} + \mathbf{R}^\top \mathbf{b} - \mathbf{C}(\boldsymbol{\nu})\boldsymbol{\nu} - \mathbf{D}(\boldsymbol{\nu})\boldsymbol{\nu} - \mathbf{M}\dot{\boldsymbol{\alpha}} \end{aligned} \tag{33}$$

yields:

$$\begin{aligned} \dot{V}_2 &= -k_1 z_1^2 + \mathbf{z}_2^\top (\mathbf{h} k_1 z_1 + \boldsymbol{\tau} + \mathbf{R}^\top \mathbf{b} - \mathbf{C}(\boldsymbol{\nu})\boldsymbol{\nu}) + \\ &\quad \mathbf{z}_2^\top (-\mathbf{D}(\boldsymbol{\nu})\boldsymbol{\nu} - \mathbf{M}\dot{\boldsymbol{\alpha}}) + \tilde{\mathbf{b}}^\top \boldsymbol{\Gamma}^{-1} \dot{\hat{\mathbf{b}}}. \end{aligned} \tag{34}$$

By rewriting $\mathbf{C}(\boldsymbol{\nu}) = \mathbf{C}$ and $\mathbf{D}(\boldsymbol{\nu}) = \mathbf{D}$ for notational brevity, and utilizing the fact that $\boldsymbol{\nu} = \mathbf{z}_2 + \boldsymbol{\alpha}$ and $\mathbf{b} = \hat{\mathbf{b}} - \tilde{\mathbf{b}}$, we obtain:

$$\begin{aligned} \dot{V}_2 &= -k_1 z_1^2 - \mathbf{z}_2^\top \mathbf{C} \mathbf{z}_2 - \mathbf{z}_2^\top \mathbf{D} \mathbf{z}_2 + \\ &\quad \mathbf{z}_2^\top (\mathbf{h} k_1 z_1 + \boldsymbol{\tau} + \mathbf{R}^\top \hat{\mathbf{b}} - \mathbf{C}\boldsymbol{\alpha} - \mathbf{D}\boldsymbol{\alpha} - \mathbf{M}\dot{\boldsymbol{\alpha}}) + \\ &\quad \tilde{\mathbf{b}}^\top \boldsymbol{\Gamma}^{-1} (\dot{\hat{\mathbf{b}}} - \boldsymbol{\Gamma} \mathbf{R} \mathbf{z}_2), \end{aligned} \tag{35}$$

where $\mathbf{z}_2^\top \mathbf{C} \mathbf{z}_2 = 0$ since $\mathbf{C}$ is skew-symmetric [8]. By assigning:

$$\boldsymbol{\tau} = \mathbf{M}\dot{\boldsymbol{\alpha}} + \mathbf{C}\boldsymbol{\alpha} + \mathbf{D}\boldsymbol{\alpha} - \mathbf{R}^\top \hat{\mathbf{b}} - \mathbf{h} k_1 z_1 - \mathbf{K}_2 \mathbf{z}_2, \tag{36}$$

where $\mathbf{K}_2 = diag(k_{2,1}, k_{2,2}, k_{2,3}) > 0$, and by choosing:

$$\dot{\hat{\mathbf{b}}} = \mathbf{\Gamma R z}_2, \tag{37}$$

we finally obtain:

$$\dot{V}_2 = -k_1 z_1^2 - \mathbf{z}_2^\top (\mathbf{D} + \mathbf{K}_2)\mathbf{z}_2. \tag{38}$$

We choose $\alpha_1 = u_d$, but currently postpone the choice of α_2. Choosing α_2 is vital to the desirable system behaviour, but since equation (36) is valid as long as α_2, $\dot{\alpha}_2 \in \mathcal{L}_\infty$, it is already possible to summarize the control law design by the following proposition:

Proposition 3: For smooth reference trajectories ψ_d, $\dot{\psi}_d$, $\ddot{\psi}_d \in \mathcal{L}_\infty$, u_d, $\dot{u}_d \in \mathcal{L}_\infty$ and α_2, $\dot{\alpha}_2 \in \mathcal{L}_\infty$, the origin of the error system $\left[z_1, \mathbf{z}_2^\top, \tilde{\mathbf{b}}^\top\right]^\top$ becomes UGAS/ULES by choosing the control and disturbance adaptation laws as in (36) and (37), respectively.

Proof: [Indication] The proof can be straightforwardly carried out by utilizing Theorem A.5 from [8]. ■

B. A Unified Control Law Concept

The control vector of a fully actuated vessel is given by:

$$\boldsymbol{\tau} = [\tau_1, \tau_2, \tau_3]^\top, \tag{39}$$

where τ_1 represents the force input in surge, τ_2 represents the force input in sway, and τ_3 represents the moment input in yaw. On the other hand, the control vector of a sway-underactuated vessel is given by:

$$\boldsymbol{\tau} = [\tau_1, 0, \tau_3]^\top. \tag{40}$$

Equation (36) is kept valid in the fully actuated case by assigning the required expressions to all of $\boldsymbol{\tau}$. In the underactuated case it can still be kept valid by assigning the required expressions to τ_1 and τ_3, while simultaneously imposing dynamics on the sway stabilizing function α_2 such that (36) is satisfied [9]. An analysis of the resulting α_2-subsystem reveals that the stabilizing function, and hence also the sway speed, remains bounded. This is an inherent feature of the ambient water-vessel system due to the desirable property of hydrodynamic damping.

Elaborating on the facts above, imagine a weighting variable $\sigma \in [0, 1]$ with the following properties:

- $\sigma = 1$ indicates a fully actuated vessel.
- $\sigma = 0$ indicates an underactuated vessel.

Such a variable could be implemented as a sigmoidal function, ensuring a smooth transition between a fully actuated and an underactuated vessel. A natural choice would be to make it dependent of the instantaneous vessel speed, i.e. $\sigma = \sigma(U)$. Now, consider a vessel with a transitional speed zone between full actuation and underactuation represented by a lower limit of U_f corresponding to a speed where it is still fully actuated, and an upper limit of U_u corresponding to a speed where it has become underactuated. Then the choice of σ could be:

$$\sigma(U) = 1 - \frac{1}{2}\left(\tanh\left(\frac{U - \frac{U_f + U_u}{2}}{\triangle_\sigma}\right) + 1\right), \tag{41}$$

where $U = \sqrt{u^2 + v^2} \geq 0$ is the instantaneous vessel speed, and $\triangle_\sigma > 0$ shapes the steepness of the transitional zone from full actuation to underactuation. By denoting the sway control force for a fully actuated vessel as $\tau_{2,f}$ and for an underactuated vessel as $\tau_{2,u}$ $(= 0)$, the actual sway control force enforced at any time can be represented by:

$$\tau_2 = \sigma\tau_{2,f} + (1 - \sigma)\tau_{2,u}. \tag{42}$$

Likewise, the actual sway stabilizing function can be represented by:

$$\alpha_2 = \sigma\alpha_{2,f} + (1 - \sigma)\alpha_{2,u}, \tag{43}$$

where the stabilizing function for a fully actuated vessel is given by $\alpha_{2,f} = v_d$ and for an underactuated vessel by $\alpha_{2,u}$, which is calculated from the assigned dynamics given by (36) as mentioned previously.

As defined in [10], the course angle χ is the orientation of the velocity vector of a vessel, the heading angle ψ is the orientation of the vessel itself, while the sideslip angle β is the difference between the course angle and the heading angle. The desired heading angle is thus computed by:

$$\psi_d = \chi_d - \beta, \tag{44}$$

where the desired course angle χ_d is given by (10). Higher order derivatives are generated by processing ψ_d through a reference model which is adjusted to the closed loop vessel dynamics. This expression holds unaffected of the given actuator capability of the vessel in question, and represents a guidance system with convergence to a desired geometric path as its primary task objective.

The desired surge and sway speeds are calculated by:

$$u_d = U_d \cos\beta_d \tag{45}$$

$$v_d = U_d \sin\beta_d, \tag{46}$$

where U_d is the desired linear speed of the vessel, while β_d represents the desired sideslip angle given by:

$$\beta_d = \chi_d - \psi_c, \tag{47}$$

where ψ_c is the commanded heading of a fully actuated vessel, which has the capability to control the course and heading independently. It can be given directly by a human operator or through a high-level decision making system.

To sum up, the velocity and heading controller relies upon the guidance-based path following approach to guarantee positional convergence [4], while the speed-weighted sway force (42) and stabilizing function (43) are crucial for the validity of (36) and (37), i.e. that the controller structure is equally effective for both fully actuated and underactuated marine surface vessels, seamlessly across the entire speed regime.

V. Case Study: Automatic Control Through the Key Part of the Speed Envelope

For the sake of illustration, a simulation is performed with a vessel executing a straight line maneuver while being exposed to a constant environmental force acting from the north, size $1\ N$. The vessel data is taken from Cybership 2, a 1:70 scale model of an offshore supply vessel, with a mass of $m = 23.8\ kg$ and a length of $L = 1.255\ m$ [5]. A full scale vessel typically becomes underactuated at speeds between $3-4\ knots$, i.e. $1.5-2\ m/s$, which corresponds to $0.2-0.27\ m/s$ for the model ship Cybership 2 when assuming equal Froude numbers. Hence, the transition variable σ is modelled after (41), with $U_f = 0.15$, $U_u = 0.25$ and $\triangle_\sigma = 0.05$.

The initial vessel states are chosen as $\boldsymbol{\eta}_0 = [-10\ (m), 3\ (m), 0\ (rad)]^\top$ and $\boldsymbol{\nu}_0 = [0.1\ (m/s), 0\ (m/s), 0\ (rad/s)]^\top$. The desired vessel speed U_d is equal to the initial vessel speed for the first 200 seconds, at which time it is raised to $0.3\ m/s$. Hence, the vessel is subjected to two key speeds from its speed envelope, experiencing both full actuation and underactuation during the run. The initial path parametrization variable is set to $\theta_0 = 0$, the guidance parameter $\gamma = 100$ and the lookahead distance in the guidance law is chosen to be $\triangle = 3L$. The controller gains are chosen as $k_1 = 10$ and $\mathbf{K}_2 = 10\mathbf{I}$, while $\boldsymbol{\Gamma} = \mathbf{I}$.

Figure 3 shows that the vessel heading is tangential to the path during the early part of the run, changing towards the environmental disturbance (weathervaning) as the vessel becomes underactuated due to its speed change. Figure 4 illustrates that the cross-track error converges to zero independent of the instantaneous actuator capability of the vessel.

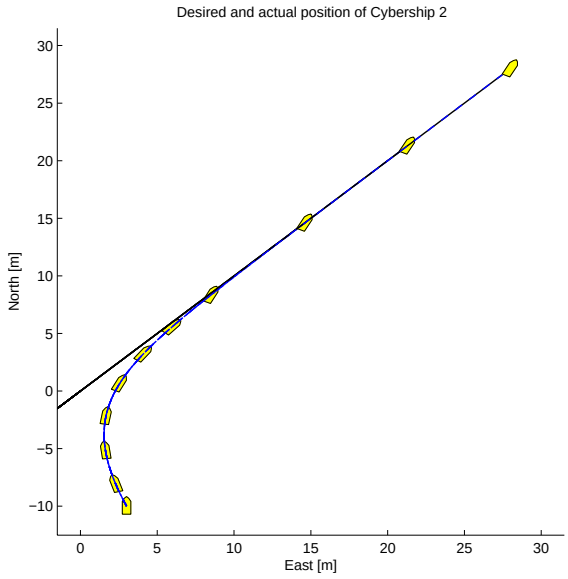

Fig. 3. Cybership 2 converges naturally to the desired geometric path.

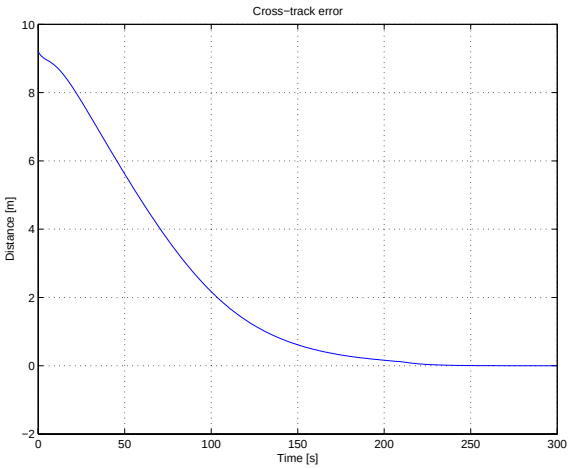

Fig. 4. The cross-track error converges to zero.

VI. Conclusions

A single controller structure has been proposed for the automatic control of a marine surface vessel through its entire speed envelope. The design is made possible by a nonlinear, model-based velocity and heading controller relying on a guidance-based path following concept necessary to ensure geometric path convergence. It guarantees that a vessel which is fully actuated at low speeds, but becomes underactuated at high speeds, is able to converge to and follow a desired geometric path independent of its speed. The result seems interesting from both a theoretical and industrial viewpoint, and the concept could contribute to reducing heuristics usually involved in industrial implementations. Simulation results successfully demonstrate the capability of the proposed guidance and control scheme.

References

[1] D. Bertin and L. Branca, "Operational and design aspects of a precision minewarfare autopilot," in *Proceedings of the Warship 2000, London, UK*, 2000.

[2] C. G. Källström, "Autopilot and track-keeping algorithms for high-speed craft," *Control Engineering Practice*, vol. 8, pp. 185–190, 2000.

[3] J. P. Strand, T. Lauvdal, and A. K. Ådnanes, "Compact azipod propulsion on DP supply vessels," in *Proceedings of the Dynamic Positioning Conference, Houston, Texas, USA*, 2001.

[4] M. Breivik and T. I. Fossen, "Path following for marine surface vessels," in *Proceedings of the OTO'04, Kobe, Japan*, 2004.

[5] R. Skjetne, "The maneuvering problem," Ph.D. dissertation, Norwegian University of Science and Technology, Trondheim, Norway, 2005.

[6] F. A. Papoulias, "Bifurcation analysis of line of sight vehicle guidance using sliding modes," *International Journal of Bifurcation and Chaos*, vol. 1, no. 4, pp. 849–865, 1991.

[7] A. Teel, E. Panteley, and A. Loría, "Integral characterization of uniform asymptotic and exponential stability with applications," *Mathematics of Control, Signals, and Systems*, vol. 15, pp. 177–201, 2002.

[8] T. I. Fossen, *Marine Control Systems: Guidance, Navigation and Control of Ships, Rigs and Underwater Vehicles*, 1st ed. Marine Cybernetics, Trondheim, Norway, 2002.

[9] T. I. Fossen, M. Breivik, and R. Skjetne, "Line-of-sight path following of underactuated marine craft," in *Proceedings of the 6th IFAC MCMC, Girona, Spain*, 2003.

[10] M. Breivik and T. I. Fossen, "Path following of straight lines and circles for marine surface vessels," in *Proceedings of the 6th IFAC CAMS, Ancona, Italy*, 2004.

C. Marine Craft: 21st Century Motion Control Concepts

Big thanks to Sue Ingle Owen at Sea Technology Magazine for helping me obtain permission to reprint this article as part of my PhD thesis.

Marine Craft: 21st Century Motion Control Concepts

The Introduction of Sophisticated Control Concepts Will Help Push the Limits of Possibility Within Marine Operations

By Morten Breivik
Ph.D. Candidate
Centre for Ships and Ocean Structures
Norwegian University of Science and Technology
Trondheim, Norway

Whether one is considering commercial, military or scientific applications, the discipline of motion control is increasingly important to the operational envelope of marine craft. It is the continuing development within sensor, actuator and computer technology that facilitates this trend. As the application of advanced control concepts ultimately relies on digital access, researchers realize that it is their own imaginations that represent the limits of what can be achieved.

Tracking and Following

The most basic form of marine craft motion control is related to the ability to accurately maneuver along a given path. Vessels with dynamic positioning capability usually employ the concept of trajectory tracking, which basically boils down to chasing a time-varying reference position. However, if the reference position just traces out the pattern of a pre-designed geometric curve, the tracking concept is a bad idea. This relates to the fact that when given the freedom to design a path, this scheme inherently mixes space and time assignments into one single assignment, suggesting that a vessel is located at a specific point in space at a specific, pre-assigned instant in time. If, for some reason, the original time-parameterization of the path becomes dynamically infeasible—for instance pertaining to changes in the weather or the propulsion capability of a vessel—it must be temporarily reparameterized to avoid saturating the actuators and rendering the path-vessel system unstable. This does not seem like an intuitive way to act, and clearly does not correspond to the way in which a human pilot would adapt to changing conditions. A human does not aim to track a conceptual point in front of his vehicle, especially if he realizes that it would risk lives or damage the vehicle.

Then there is the concept of path following. This entails the separate construction of the geometric curve and the dynamic assignment, where the task objective is first and foremost to follow the path. Thus, if the dynamic assignment cannot be satisfied, the vessel will still be able to follow the path, representing a more flexible and robust approach than the tracking concept. This also corresponds well with how a human driving a car chooses to negotiate a road. His main concern is to stay on the road, while continually adjusting the vehicle speed according to the traffic situation and road conditions. Consequently, the path-following concept appears as the most favorable for motion control systems providing accurate and safe maneuvering of marine craft.[1]

Vessel Actuation Capability

A vital aspect that must be taken into account when designing motion control systems is the vessel actuation capability. Basically, there are two categories to consider: fully actuated and underactuated vessels.

Fully actuated vessels are independently actuated in all of the relevant degrees-of-freedom (DOFs) simultaneously, while underactuated vessels are not. Underactuated vessels lack the capability to command independent accelerations in the necessary DOFs synchronously. Fully actuated vessels are able to execute any conceivable maneuver, independently controlling their position and orientation. Underactuated vessels, on the other hand, are subject to strict motion constraints where the vessel orientation must be utilized to direct the linear velocity vector in a meaningful direction. This stems from the fact that the linear velocity and orientation of these vessels are inextricably linked and cannot be controlled independently.

In fact, most mechanical vehicle systems are underactuated—cars are intrinsically underactuated, as are aircraft and missiles. Marine craft are often fully actuated when operating at low speeds, but become underactuated at high speeds. This also characterizes living creatures—most birds and fish are inherently underactuated, while humans are fully actuated when walking, but become underactuated when running.

Marine surface vessels are typically equipped with a number of tunnel thrusters both fore and aft, designed to assist with low-speed maneuvers. However, these are rendered ineffective at high speeds. Under such circumstances, the only means of actuation are the main propulsors located aft. Hence, most surface craft are uncontrollable in the lateral direction when operating at high speeds. For offshore supply vessels, this involves speeds above three to four knots.

Universal Motion Controllers

To be able to design advanced motion controllers for marine craft, a mathematical model which captures the essential dynamic behavior of the vehicle in question is required. Such

Reprinted from **Sea Technology** *magazine.*
For more information about the magazine, visit www.sea-technology.com

Marine operations from shipping and offshore to fisheries and aquaculture.

models have recently been unified into a state-of-the-art model which suits the need of control system designers.[2] So-called model-based controllers take advantage of the information embedded in these models.

It goes without saying that it is a fundamental necessity to be able to control a marine craft through its entire speed regime, from low-speed positioning to high-speed maneuvering. Traditionally, such a problem has been solved by constructing dedicated motion controllers for each distinct part of the speed envelope. Considering marine surface vessels, a nonlinear, model-based position and heading controller is usually designed for low-speed applications (dynamic positioning), where it is assumed that the vessel in question is fully actuated. On the other hand, a linear heading controller based on the classic Nomoto model is usually designed (together with an independent speed controller) for high-speed applications (autopilot), where the vessel is assumed to be underactuated. However, as these controllers are structurally different, heuristics are utilized to switch between them. This ultimately leads to an overly complex and error-prone motion control system. Consequently, it is desirable to develop a single motion controller to cover the entire operational speed envelope, as this would reduce implementation, validation and maintenance efforts, and remove the complexity associated with heuristic implementations. It could ultimately lead to increased safety of operation.

In fact, such a motion controller has recently been proposed.[3] The core of the control structure consists of a nonlinear, model-based velocity and heading controller. The output-to-be-controlled is redefined from position and heading (which is only applicable to fully actuated vessels) to velocity and heading (which is equally applicable to both fully actuated and underactuated vessels). By feeding this controller with the appropriate guidance commands, the path-following task objectives can be satisfied. This approach is inspired by the real-life behavior of a helmsman, who employs the vessel velocity to maneuver. He never thinks in terms of directly controlling the vessel position, but in his mind he feeds any position error back through the velocity assignment, indirectly ensuring position control through direct velocity control.

Vessel Control Hierarchy

A complete motion control system for a marine craft primarily involves three levels of control: low, intermediate and high. The two former levels are tactical levels, while the latter is a strategic level of control. The different levels of the control hierarchy require different bandwidths.

Low-level control is related to the local control of vessel actuators, such as tunnel thrusters, azimuth thrusters, water jets, rudders and propellers.[4] Thus, this module is responsible for controlling the actuators that deliver the forces and moments which enable a marine craft to position and orient itself. This is the tactical level with the greatest bandwidth demand. Humans never participate di-rectly at this level.

Intermediate-level control, the area that has received the greatest research attention over the years, is related to calculating the necessary forces and moments that a vessel must utilize in order for it to execute a desired maneuver. Hence, motion controllers are intermediate-level controllers. The commands issued by these controllers are supplied as reference signals to the low-level controllers via an actuator distribution scheme, known as control allocation. Humans can participate directly at this level of control.

High-level control involves calculating the reference signals that are fed to the motion controllers, and has not been researched to the same extent as the tactical levels of control. Currently, humans participate directly at this level of control most of the time. Constituting the strategic level, it is essentially the brain of all the nested control loops which form the motion control system of a marine craft. Relevant tasks of this module are to design the nominal path to be traveled, consider the dynamic interaction between the path and the vessel itself, provide collision avoidance toward both static and dynamic targets, arrange formation control in relation to other craft and guarantee synchronization to some de-sired phenomena. The autonomous part of the strategic level is usually termed the guidance system.

Co-Control and Autonomy

The term co-control can be applied when humans who pilot mechanical vehicle systems are assisted by digitally implemented motion controllers. One example is fly-by-wire aircraft, where the extensive use of digital computer technology opens up the possibility for completely autonomous operation.

Autonomy inherently implies that the human role will be substantially reduced at the strategic level of control, in addition to already being all but absent at the tactical levels. Perhaps some day humans will be issuing

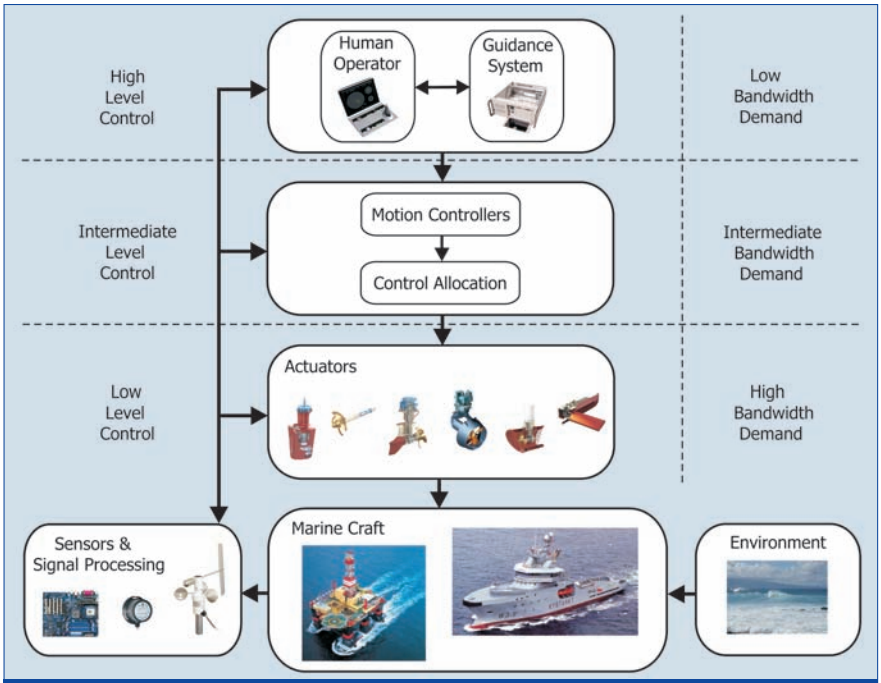

Vessel control hierarchy—the fundamental components of a vessel motion control system.

mission primitives such as "I want my shipping fleet to operate in order to maximize my profitability." However, co-control will most likely remain the preferred paradigm for passenger vessels and similar operations in the foreseeable future.

The aircraft industry undoubtedly leads the development within autonomous unmanned vehicles. The research on unmanned aerial vehicles (UAVs) is substantial, both technologically and judicially.

It is, then, imperative to determine the status of UAVs vis-à-vis manned aircraft when figuring out in what kind of airspace specific UAVs should be allowed to operate. Consequently, relevant performance evaluation schemes are called for. The marine industry should pay close attention to this development and follow suit wherever applicable.

Into the Future

Traditionally, the marine industry has been relatively conservative with regard to developing and utilizing new motion control technology. It is still lagging significantly behind the aircraft industry both in terms of applying advanced motion control concepts and at the maturity level of corresponding formal legislation. However, the offshore industry currently represents a main driving force for adopting increasingly sophisticated functionality.

A noteworthy result of this fact is the recent establishment of Marine Cybernetics, a Norwegian company whose primary service is to develop and provide standardized procedures for testing and certifying increasingly digital marine control systems.[5] It is telling that such procedures have been standard in the aircraft industry for years, while only now are being introduced for the marine market. Nevertheless, the underlying trend is positive, and the day might actually dawn when the aircraft industry will start to adopt marine concepts.

Currently, the Centre for Ships and Ocean Structures at the Norwegian University of Science and Technology is actively pursuing novel motion control research by integrating state-of-the-art theory from the fields of hydrodynamics, structural mechanics and automatic control.

The ultimate goal of this interdisciplinary endeavor is to develop safe, reliable, fault-tolerant and cost-effective motion control systems for marine craft that significantly enlarge their operational envelope.

Acknowledgements

The author of this article would like to take this opportunity to thank colleagues from both academia and industry for their constructive comments.

The work discussed herein was supported by the Research Council of Norway through actions conducted by the Centre for Ships and Ocean Structures. /st/

References

1. Breivik, M. and T. I. Fossen, "Path-Following for Marine Surface Vessels," *Proceedings of the MTS/IEEE Oceans/Techno-Ocean Conference*, Kobe, Japan, pp. 2,282-2,289, 2004.
2. Fossen, T. I., "A Non-Linear Unified State-Space Model for Ship Maneuvering and Control in a Seaway," *International Journal of Bifurcation and Chaos*, vol. 15, no. 9, pp. 2,717-2,746, 2005.
3. Breivik, M. and T. I. Fossen, "A Unified Concept for Controlling a Marine Surface Vessel Through the Entire Speed Envelope," *Proceedings of the 13th Mediterranean Conference on Control and Automation*, Limassol, Cyprus, pp. 1,518-1,523, 2005.
4. Smogeli, Ø. N., A. J. Sørensen and T. I. Fossen, "Design of a Hybrid Power/Torque Thruster Controller with Thrust Loss Estimation," *Proceedings of the International Federation of Automatic Control Conference on Control Applications in Marine Systems*, Ancona, Italy, pp. 409-414, 2004.
5. Skjetne, R. and O. Egeland, "Hardware-in-the-Loop Testing of Marine Control Systems," *Proceedings of the Scandinavian Conference on Simulation and Modeling*, Trond-heim, Norway, pp. 305-314, 2005.

Visit our Web site at www.sea-technology.com, and click on the title of this article in the Table of Contents to be linked with the respective company's Web site.

Morten Breivik is a Ph.D. student at the Centre for Ships and Ocean Structures at the Norwegian University of Science and Technology. His main research interests are advanced guidance and control concepts for motion control of mechanical systems, with application to marine systems.

D. Guided Dynamic Positioning for Fully Actuated Marine Surface Vessels

Note that the use of the term “PN guidance” in this paper is erroneous. The correct term would have been “CB guidance” since PN guidance is just a particular mechanization of the CB guidance principle.

GUIDED DYNAMIC POSITIONING FOR FULLY ACTUATED MARINE SURFACE VESSELS

Morten Breivik[1,3] **Jann Peter Strand**[2] **Thor I. Fossen**[1]

Abstract: This paper addresses the topic of dynamic positioning (DP) for fully actuated marine surface vessels. The concept of guided DP is developed by employing a modular motion control design procedure. In any DP application, the main objective is to track a planar target point while attaining a certain vessel heading. As such, this work considers both the case where the target point moves along a fully known path, as well as the case where only instantaneous target point information is available.

Keywords: Guided dynamic positioning, Fully actuated vessels, Modular design concept

1. INTRODUCTION

The concept of dynamic positioning (DP) was originally conceived in the 1960s, when drillships in the offshore oil and gas industry had to be positioned at locations where it was impossible to deploy conventional anchors due to large water depths. Hence, DP entails that surface vessels maintain their position exclusively by means of active propulsors and thrusters. Traditionally, DP-capable vessels have mainly been found within the offshore segment of the marine industries, with applications including deep-water drilling, diving support, pipelaying, anchor handling, and (heavy-lift) crane operations. However, recent years has seen an upsurge of vessels that serve other marine segments also acquire DP capabilities. Examples include passenger and cargo vessels, research and survey vessels, as well as naval vessels. Today, DP applications encompass not only station keeping, but also low-speed maneuvering operations. A basic overview of a DP system can be found in (Holvik 1998), while (Bray 2003) thoroughly treats all practical aspects related to DP of surface vessels.

The first DP-capable vessels that appeared at the beginning of the 1960s were controlled manually, but were soon retrofitted with analogue controllers for increased operational precision through automatic control. Subsequently, due to significant advances within digital computer technology, digitally implemented controllers rapidly replaced their analogue counterparts. These early controllers were based on the classical proportional-integral-derivative (PID) principle, controlling each of the 3 horizontal degrees of freedom (DOFs) independently. In the 1970s, more sophisticated linear controllers based on optimal control theory were introduced, steadily enhanced through the 1980s (Sælid *et al.* 1983) and 1990s (Sørensen *et al.* 1996) by the introduction of new state estimation and wave filtering techniques. However, linear controllers can only ensure local stability properties, so inspired by work performed in the field of robotics, nonlinear control theory was utilized in the late 1990s to guarantee global stability results (Fossen 2002).

The main focus concerning DP technology is related to practical aspects such as control allocation, power management, and signal processing. Less attention has been paid to the fundamental and underlying principles of motion control associated with the DP controllers, resulting for instance in the fact that state-of-the-art implementations are not readily extendable to handle underactuated vessels. Consequently, the focus and main contribution of this paper is a motion control concept named *guided dynamic positioning*, which is inspired by theory from both path following

[1] {Centre for Ships and Ocean Structures, Department of Engineering Cybernetics}, Norwegian University of Science and Technology (NTNU), NO-7491 Trondheim, Norway. E-mails: {morten.breivik, fossen}@ieee.org.

[2] Rolls-Royce Marine AS, P.O. Box 826, NO-6001 Aalesund, Norway. E-mail: jann_peter.strand@rolls-royce.com.

[3] Supported by the Research Council of Norway through the Centre for Ships and Ocean Structures at NTNU.

and missile guidance. This concept not only entails helmsman-like motion behavior, but also straightforward extension toward underactuated operations.

2. GUIDED DYNAMIC POSITIONING

Here, the concept of guided dynamic positioning is developed by means of a backstepping-inspired and cascaded-based design procedure. The motion control scenario entails tracking a stationary or time-varying *target point* in the plane while attaining a desired vessel heading. The consideration involves both the case where the target point moves along a path that is fully known, as well as the case where only instantaneous information about the target point is available. Since this work only treats fundamental aspects, specific issues pertaining to control allocation, state estimation, or wave filtering are disregarded. However, standard solutions to such topics are readily applicable for fully actuated vessels that employ the proposed DP scheme. In what follows, the time derivative (of a vector) $\mathbf{x}(t)$ is denoted $\dot{\mathbf{x}}$, the partial derivative of $\mathbf{x}(\varpi(t))$ is denoted $\mathbf{x}'$ $\left(= \frac{\partial \mathbf{x}}{\partial \varpi}(\varpi(t))\right)$, while $|\cdot|$ represents the Euclidean vector norm and the induced matrix norm.

2.1 Dynamic Model of a Marine Surface Vessel

A 3 degree-of-freedom (DOF) dynamic model of the horizontal surge, sway, and yaw modes can be found in (Fossen 2002), and consists of the kinematics

$$\dot{\boldsymbol{\eta}} = \mathbf{R}(\psi)\boldsymbol{\nu}, \tag{1}$$

and the kinetics

$$\mathbf{M}\dot{\boldsymbol{\nu}} + \mathbf{C}(\boldsymbol{\nu})\boldsymbol{\nu} + \mathbf{D}(\boldsymbol{\nu})\boldsymbol{\nu} = \boldsymbol{\tau} + \mathbf{R}(\psi)^\top \mathbf{b}, \tag{2}$$

where $\boldsymbol{\eta} = [x, y, \psi]^\top \in \mathbb{R}^2 \times \mathcal{S}$ represents the earth-fixed position and heading (with $\mathcal{S} = [-\pi, \pi]$), $\boldsymbol{\nu} = [u, v, r]^\top \in \mathbb{R}^3$ represents the vessel-fixed velocity, $\mathbf{R}(\psi) \in SO(3)$ is the transformation matrix

$$\mathbf{R}(\psi) = \begin{bmatrix} \cos\psi & -\sin\psi & 0 \\ \sin\psi & \cos\psi & 0 \\ 0 & 0 & 1 \end{bmatrix} \tag{3}$$

that transforms from the vessel-fixed BODY frame (**B**) to the earth-fixed NED frame (**N**), $\mathbf{M}$ is the inertia matrix, $\mathbf{C}(\boldsymbol{\nu})$ is the centrifugal and coriolis matrix, while $\mathbf{D}(\boldsymbol{\nu})$ is the hydrodynamic damping matrix. The system matrices satisfy the properties $\mathbf{M} = \mathbf{M}^\top > 0$, $\mathbf{C} = -\mathbf{C}^\top$ and $\mathbf{D} > 0$. The vessel-fixed propulsion forces and moment is represented by $\boldsymbol{\tau} = [\tau_{\mathrm{X}}, \tau_{\mathrm{Y}}, \tau_{\mathrm{N}}]^\top \in \mathbb{R}^3$, corresponding to a fully actuated vessel. Full actuation means that all 3 DOFs can be independently controlled simultaneously, i.e., the direction of the linear velocity is independent of the heading of the vessel. This is not the case for an underactuated craft, where the orientation of the linear velocity is inherently coupled (in a sense locked) to the heading. Finally, $\mathbf{b}$ represents the low-frequency earth-fixed environmental forces that act on the vessel.

2.2 Motion Control Scenario

In our scenario, the dynamic positioning problem for a fully actuated marine surface vessel can be stated by

$$\lim_{t\to\infty} (\boldsymbol{\eta}(t) - \boldsymbol{\eta}_{\mathrm{d}}(t)) = \mathbf{0}, \tag{4}$$

where $\boldsymbol{\eta}_{\mathrm{d}}(t) = \left[\mathbf{p}_{\mathrm{t}}^\top(t), \psi_{\mathrm{d}}(t)\right]^\top \in \mathbb{R}^2 \times \mathcal{S}$ represents the earth-fixed position and heading associated with the target point. We consider both the case where $\mathbf{p}_{\mathrm{t}}(t)$ is stationary (i.e., point stabilization) and time-varying (i.e., trajectory tracking), while $\psi_{\mathrm{d}}(t)$ can be chosen arbitrarily (e.g., as an auxiliary task objective).

2.3 Motion Control Design

We now employ a backstepping-inspired and cascaded-based design approach to develop the concept of guided dynamic positioning, and consider both the case where the target point moves along a path that is fully known (Case A), as well as the case where only instantaneous information about the target point is available (Case B). Due to the modular nature of the suggested scheme, we first design a motion controller (control loop) by means of integrator backstepping. A key feature is that this controller applies to both case A and B, by feeding it with the respectively appropriate reference signals. These signals (guidance loop) are specifically designed for each case.

2.3.1. Control Loop Design Since the position of a vessel can be controlled through its linear velocity, we redefine the output space of the controller from the nominal 3 DOF position and heading to the 3 DOF linear velocity and heading (Fossen *et al.* 2003). Consequently, consider the positive definite and radially unbounded Control Lyapunov Function (CLF)

$$V_{\mathrm{g}} = \frac{1}{2}(z_\psi^2 + \mathbf{z}_\nu^\top \mathbf{M}\mathbf{z}_\nu + \tilde{\mathbf{b}}^\top \boldsymbol{\Gamma}^{-1}\tilde{\mathbf{b}}) \tag{5}$$

where we have

$$z_\psi = \psi - \psi_{\mathrm{d}} \tag{6}$$

and

$$\mathbf{z}_\nu = \boldsymbol{\nu} - \boldsymbol{\alpha}, \tag{7}$$

where $\boldsymbol{\alpha} = [\alpha_u, \alpha_v, \alpha_r]^\top \in \mathbb{R}^3$ is a so-called vector of stabilizing functions (virtual inputs that become reference signals) yet to be designed. Also,

$$\tilde{\mathbf{b}} = \hat{\mathbf{b}} - \mathbf{b} \tag{8}$$

represents an adaptation error where $\hat{\mathbf{b}}$ is the estimate of $\mathbf{b}$, and by assumption $\dot{\mathbf{b}} = \mathbf{0}$. Finally, $\boldsymbol{\Gamma} = \boldsymbol{\Gamma}^\top > 0$ is the so-called adaptation gain matrix.

Then, differentiate the CLF with respect to time to ultimately obtain the negative semi-definite

$$\dot{V}_{\mathrm{g}} = -k_\psi z_\psi^2 - \mathbf{z}_\nu^\top (\mathbf{D} + \mathbf{K}_\nu)\mathbf{z}_\nu \tag{9}$$

by choosing the virtual input $\mathbf{h}^\top \boldsymbol{\alpha} = \alpha_{\mathrm{r}}$ as

$$\alpha_{\mathrm{r}} = \dot{\psi}_{\mathrm{d}} - k_\psi z_\psi, \tag{10}$$

where $k_\psi > 0$ is a constant, and

$$\mathbf{h} = [0, 0, 1]^\top ; \tag{11}$$

by choosing the control input as

$$\boldsymbol{\tau} = \mathbf{M}\dot{\boldsymbol{\alpha}} + \mathbf{C}\boldsymbol{\alpha} + \mathbf{D}\boldsymbol{\alpha} - \mathbf{R}^\top \hat{\mathbf{b}} - \mathbf{h}z_\psi - \mathbf{K}_\nu \mathbf{z}_\nu \tag{12}$$

where $\mathbf{K}_\nu = \mathbf{K}_\nu^\top > 0$ is a constant matrix; and by choosing the disturbance adaptation update law as

$$\dot{\hat{\mathbf{b}}} = \boldsymbol{\Gamma}\mathbf{R}\mathbf{z}_\nu. \tag{13}$$

Considering the vector $\mathbf{z}_\mathrm{g} = \left[z_\psi, \mathbf{z}_\nu^\top, \tilde{\mathbf{b}}^\top\right]^\top$, we can now state the following fundamental proposition

Proposition 1. The equilibrium point $\mathbf{z}_\mathrm{g} = \mathbf{0}$ is rendered uniformly globally asymptotically and locally exponentially stable (UGAS/ULES) by adhering to (10), (12) and (13) under the assumption that $\boldsymbol{\alpha}$ and $\dot{\boldsymbol{\alpha}}$ are uniformly bounded.

PROOF. The proposed result follows by straightforward application of Theorem 1 in (Fossen *et al.* 2001).

It is interesting to note that this motion controller cannot achieve anything meaningful unless it is fed sensible reference signals, i.e., unless $\boldsymbol{\alpha}_\mathrm{v} = [\alpha_\mathrm{u}, \alpha_\mathrm{v}]^\top \in \mathbb{R}^2$ is purposefully defined. However, therein lies also its strength, i.e., its universal applicability; to achieve whatever the design of $\boldsymbol{\alpha}_\mathrm{v}$ implies. We now proceed to design the reference signals solving case A and B.

2.3.2. Case A: Tracking a Target Along a Path Here, we consider the case where the motion control designer is granted the freedom to design the path (trajectory) that is to be traversed, as well as the motion of a target point that is to be tracked along the path. The theory is taken from the path following part of (Breivik and Fossen 2006). Consequently, consider a (planar) path continuously parameterized by a scalar variable $\varpi \in \mathbb{R}$, such that the position of a point belonging to the path is represented by $\mathbf{p}_\mathrm{p}(\varpi) \in \mathbb{R}^2$. Thus, the path is a one-dimensional manifold expressible by the set

$$\mathcal{P} = \left\{\mathbf{p} \in \mathbb{R}^2 \mid \mathbf{p} = \mathbf{p}_\mathrm{p}(\varpi)\ \forall \varpi \in \mathbb{R}\right\}. \tag{14}$$

Then, consider a time-varying target point $\mathbf{p}_\mathrm{t}(t) = \mathbf{p}_\mathrm{p}(\varpi_\mathrm{t}(t))$ traversing the path by adhering to a chosen speed profile $U_\mathrm{t}(\varpi_\mathrm{t})$, implemented through

$$\dot{\varpi}_\mathrm{t} = \frac{U_\mathrm{t}(\varpi_\mathrm{t})}{\left|\mathbf{p}_\mathrm{p}'(\varpi_\mathrm{t})\right|}, \tag{15}$$

since $|\dot{\mathbf{p}}_\mathrm{t}| = \left|\mathbf{p}_\mathrm{p}'(\varpi_\mathrm{t})\right| \dot{\varpi}_\mathrm{t} = U_\mathrm{t}(\varpi_\mathrm{t})$, where $U_\mathrm{t}(\varpi_\mathrm{t}) \in [U_{\mathrm{t,min}}, U_{\mathrm{t,max}}]$, $U_{\mathrm{t,min}} > 0$.

2.3.2.1. Guidance Loop Design We now design the required *orientation* of $\boldsymbol{\alpha}_\mathrm{v}$ (given that $|\boldsymbol{\alpha}_\mathrm{v}| > 0$) such that a vessel controlled by (12) and (13) achieves path following. Consequently, consider the positive definite and radially unbounded CLF

$$V_\varepsilon = \frac{1}{2}\boldsymbol{\varepsilon}^\top \boldsymbol{\varepsilon}, \tag{16}$$

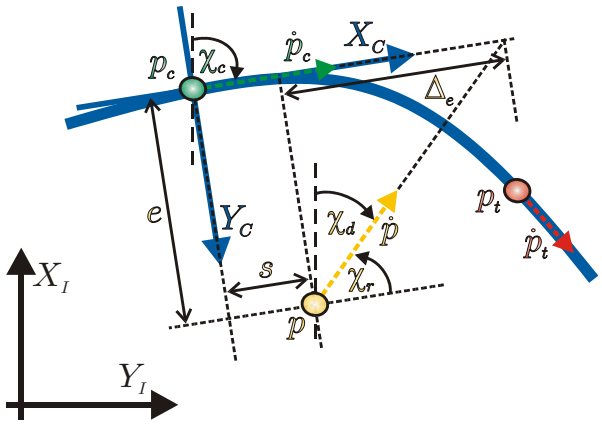

Fig. 1. The basic geometry behind tracking along a planar path. The vessel is shown in orange, the collaborator in green, and the target point in red.

with

$$\boldsymbol{\varepsilon} = \mathbf{R}_\mathrm{C}^\top(\mathbf{p} - \mathbf{p}_\mathrm{c}) \tag{17}$$

where $\mathbf{p}_\mathrm{c} = \mathbf{p}_\mathrm{p}(\varpi_\mathrm{c})$ represents a *collaborator* point that acts cooperatively with the marine craft as an intermediate path attractor, and whose sole purpose is to ensure that the vessel can converge to the path even if it has not converged to the target point. For a given ϖ_c, define a path-tangential reference frame at $\mathbf{p}_\mathrm{c}$ termed the COLLABORATOR frame (**C**). To arrive at **C**, the INERTIAL frame (**I**) must be positively rotated

$$\chi_\mathrm{c} = \arctan\left(\frac{y_\mathrm{p}'(\varpi_\mathrm{c})}{x_\mathrm{p}'(\varpi_\mathrm{c})}\right), \tag{18}$$

which can be represented by the rotation matrix

$$\mathbf{R}_\mathrm{C} = \begin{bmatrix} \cos\chi_\mathrm{c} & -\sin\chi_\mathrm{c} \\ \sin\chi_\mathrm{c} & \cos\chi_\mathrm{c} \end{bmatrix}, \tag{19}$$

$\mathbf{R}_\mathrm{C} \in SO(2)$. Hence, equation (17) represents the error vector between the vessel and its collaborator decomposed in **C**. The local coordinates $\boldsymbol{\varepsilon} = [s, e]^\top$ consist of the along-track error s and the cross-track error e. It is clear that path following can be achieved by driving $\boldsymbol{\varepsilon}$ to zero, see Figure 1. Thus, differentiate the CLF in (16) along the trajectories of $\boldsymbol{\varepsilon}$ to obtain

$$\begin{aligned}
\dot{V}_\varepsilon &= \boldsymbol{\varepsilon}^\top \dot{\boldsymbol{\varepsilon}} \\
&= \boldsymbol{\varepsilon}^\top (\mathbf{S}_\mathrm{C}^\top \mathbf{R}_\mathrm{C}^\top (\mathbf{p} - \mathbf{p}_\mathrm{c}) + \mathbf{R}_\mathrm{C}^\top (\dot{\mathbf{p}} - \dot{\mathbf{p}}_\mathrm{c})) \\
&= \boldsymbol{\varepsilon}^\top \left(\mathbf{S}_\mathrm{C}^\top \boldsymbol{\varepsilon} + \mathbf{R}_\mathrm{C}^\top \mathbf{H}\dot{\boldsymbol{\eta}} - \mathbf{v}_\mathrm{c}\right) \\
&= \boldsymbol{\varepsilon}^\top \left(\mathbf{R}_\mathrm{C}^\top \mathbf{H}\mathbf{R}\boldsymbol{\nu} - \mathbf{v}_\mathrm{c}\right)
\end{aligned}$$

where $\mathbf{S}_\mathrm{C} = -\mathbf{S}_\mathrm{C}^\top \Rightarrow \boldsymbol{\varepsilon}^\top \mathbf{S}_\mathrm{C}^\top \boldsymbol{\varepsilon} = 0$, and where

$$\mathbf{H} = \begin{bmatrix} 1 & 0 & 0 \\ 0 & 1 & 0 \end{bmatrix}. \tag{20}$$

Also, $\mathbf{v}_\mathrm{c} = [U_\mathrm{c}, 0]^\top$, where $U_\mathrm{c} = |\dot{\mathbf{p}}_\mathrm{c}|$, represents the linear velocity of the collaborator decomposed in **C**. Furthermore, we have that

$$\begin{aligned}
\dot{V}_\varepsilon &= \boldsymbol{\varepsilon}^\top \left(\mathbf{R}_\mathrm{C}^\top \mathbf{H}\mathbf{R}\boldsymbol{\alpha} - \mathbf{v}_\mathrm{c}\right) + \boldsymbol{\varepsilon}^\top \mathbf{R}_\mathrm{C}^\top \mathbf{H}\mathbf{R}\mathbf{z}_\nu \\
&= \boldsymbol{\varepsilon}^\top \left(\mathbf{R}_\mathrm{C}^\top \mathbf{H}\mathbf{R}\mathbf{H}^\top \mathbf{H}\boldsymbol{\alpha} - \mathbf{v}_\mathrm{c}\right) + \boldsymbol{\varepsilon}^\top \mathbf{R}_\mathrm{C}^\top \mathbf{H}\mathbf{R}\mathbf{H}^\top \mathbf{H}\mathbf{z}_\nu,
\end{aligned}$$

since $\boldsymbol{\nu} = \mathbf{z}_\nu + \boldsymbol{\alpha}$ and $\mathbf{H}^\top\mathbf{H} = \mathbf{I}_{3\times 3}$ (identity matrix). Defining $\mathbf{H}\mathbf{R}\mathbf{H}^\top = \mathbf{R}_{\rm B}$, i.e.,

$$\mathbf{R}_{\rm B} = \begin{bmatrix} \cos\psi & -\sin\psi \\ \sin\psi & \cos\psi \end{bmatrix}, \tag{21}$$

leads to

$$\dot{V}_\varepsilon = \boldsymbol{\varepsilon}^\top \left(\mathbf{R}_{\rm C}^\top \mathbf{R}_{\rm B}\mathbf{H}\boldsymbol{\alpha} - \mathbf{v}_{\rm c}\right) + \boldsymbol{\varepsilon}^\top \mathbf{R}_{\rm C}^\top \mathbf{R}_{\rm B}\mathbf{H}\mathbf{z}_\nu,$$

where $\mathbf{R}_{\rm B}\mathbf{H}\boldsymbol{\alpha} = \mathbf{R}_{\rm B}\boldsymbol{\alpha}_{\rm v,B}$ with $\boldsymbol{\alpha}_{\rm v,B} = \boldsymbol{\alpha}_{\rm v} = [\alpha_{\rm u}, \alpha_{\rm v}]^\top$. Now, $\mathbf{R}_{\rm B}\boldsymbol{\alpha}_{\rm v,B} = \mathbf{R}_{\rm DV}\boldsymbol{\alpha}_{\rm v,DV} = \boldsymbol{\alpha}_{\rm v,I}$ represents the desired linear velocity decomposed in **I**, while $\boldsymbol{\alpha}_{\rm v,DV} = [U_{\rm d}, 0]^\top$, where $U_{\rm d} = |\boldsymbol{\alpha}_{\rm v}|$, represents the desired linear velocity decomposed in a DESIRED VELOCITY frame (**DV**). This frame is aligned with $\boldsymbol{\alpha}_{\rm v,I}$, whose orientation we want to design so as to achieve path following. Hence, we get

$$\begin{aligned}\dot{V}_\varepsilon &= \boldsymbol{\varepsilon}^\top \left(\mathbf{R}_{\rm C}^\top \mathbf{R}_{\rm DV}\boldsymbol{\alpha}_{\rm v,DV} - \mathbf{v}_{\rm c}\right) + \boldsymbol{\varepsilon}^\top \mathbf{R}_{\rm C}^\top \mathbf{R}_{\rm B}\mathbf{H}\mathbf{z}_\nu \\ &= \boldsymbol{\varepsilon}^\top \left(\mathbf{R}_{\rm R}\boldsymbol{\alpha}_{\rm v,DV} - \mathbf{v}_{\rm c}\right) + \boldsymbol{\varepsilon}^\top \mathbf{R}_{\rm C}^\top \mathbf{R}_{\rm B}\mathbf{H}\mathbf{z}_\nu,\end{aligned}$$

where $\mathbf{R}_{\rm C}^\top(\chi_{\rm c})\mathbf{R}_{\rm DV}(\chi_{\rm d}) = \mathbf{R}_{\rm R}(\chi_{\rm d} - \chi_{\rm c})$, i.e., the relative orientation between **C** and **DV**.

Thus, $U_{\rm c}$ and $(\chi_{\rm d} - \chi_{\rm c})$ can be considered as virtual inputs for driving $\boldsymbol{\varepsilon}$ to zero, given that $U_{\rm d} > 0$. Denote the angular difference by $\chi_{\rm r} = \chi_{\rm d} - \chi_{\rm c}$, and expand the CLF derivative to obtain

$$\dot{V}_\varepsilon = s(U_{\rm d}\cos\chi_{\rm r} - U_{\rm c}) + eU_{\rm d}\sin\chi_{\rm r} + \boldsymbol{\varepsilon}^\top \mathbf{R}_{\rm C}^\top \mathbf{R}_{\rm B}\mathbf{H}\mathbf{z}_\nu,$$

where $U_{\rm c}$ can be chosen as

$$U_{\rm c} = U_{\rm d}\cos\chi_{\rm r} + \gamma s \tag{22}$$

with $\gamma > 0$ constant, while $\chi_{\rm r}$ can be selected as

$$\chi_{\rm r} = \arctan\left(-\frac{e}{\triangle_{\rm e}}\right) \tag{23}$$

with $\triangle_{\rm e} > 0$ (not necessarily constant; a variable that is often referred to as a lookahead distance in literature treating planar path following along straight lines), giving

$$\dot{V}_\varepsilon = -\gamma s^2 - U_{\rm d}\frac{e^2}{\sqrt{e^2 + \triangle_{\rm e}^2}} + \boldsymbol{\varepsilon}^\top \mathbf{R}_{\rm C}^\top \mathbf{R}_{\rm B}\mathbf{H}\mathbf{z}_\nu. \tag{24}$$

Consequently

$$\dot{\varpi}_{\rm c} = \frac{U_{\rm c}}{|\mathbf{p}_{\rm c}'|} \tag{25}$$

and

$$\chi_{\rm d} = \chi_{\rm c} + \chi_{\rm r}, \tag{26}$$

with $U_{\rm c}$ as in (22), $\chi_{\rm c}$ as in (18), and $\chi_{\rm r}$ as in (23). Equations (25) and (26) indicate that the collaborator point continuously leads the vessel, while the desired linear velocity of the vessel must point at the path-tangential associated with the collaborator, in the direction of forward motion. Specifically, the desired linear velocity $\boldsymbol{\alpha}_{\rm v}$ must be computed by

$$\begin{aligned}\boldsymbol{\alpha}_{\rm v} &= \mathbf{R}_{\rm B}^\top \mathbf{R}_{\rm DV}\boldsymbol{\alpha}_{\rm v,DV} \\ &= \begin{bmatrix} U_{\rm d}\cos(\chi_{\rm d} - \psi) \\ U_{\rm d}\sin(\chi_{\rm d} - \psi) \end{bmatrix}.\end{aligned} \tag{27}$$

Then, write the system dynamics of $\boldsymbol{\varepsilon}$ and $\mathbf{z}_{\rm g}$ as

$$\Sigma_{\rm A.1} : \dot{\boldsymbol{\varepsilon}} = \mathbf{f}_{\rm A.1}(t, \boldsymbol{\varepsilon}) + \mathbf{g}_{\rm A.1}(t, \boldsymbol{\varepsilon}, \mathbf{z}_{\rm g})\mathbf{z}_{\rm g} \tag{28}$$

$$\Sigma_{\rm A.2} : \dot{\mathbf{z}}_{\rm g} = \mathbf{f}_{\rm A.2}(t, \mathbf{z}_{\rm g}), \tag{29}$$

which is a pure cascade where the control subsystem perturbs the guidance subsystem through the matrix

$$\mathbf{g}_{\rm A.1}(t, \boldsymbol{\varepsilon}, \mathbf{z}_{\rm g}) = \left[\mathbf{0}_{2\times 1}, \mathbf{R}_{\rm C}^\top \mathbf{R}_{\rm B}\mathbf{H}, \mathbf{0}_{2\times 3}\right]. \tag{30}$$

Also, consider the following assumptions

Assumption 2. $\left|\mathbf{p}_{\rm p}'\right| \in \left[\left|\mathbf{p}_{\rm p}'\right|_{\min}, \left|\mathbf{p}_{\rm p}'\right|_{\max}\right] \; \forall \varpi \in \mathbb{R}$

Assumption 3. $\triangle_{\rm e} \in [\triangle_{\rm e,\,min}, \infty\rangle$, $\triangle_{\rm e,\,min} > 0$

Assumption 4. $U_{\rm d} \in [U_{\rm d,min}, \infty\rangle$, $U_{\rm d,min} > 0$,

where Assumption 2 means that the path must be regularly parameterized. Then, by considering $\boldsymbol{\xi} = \left[\boldsymbol{\varepsilon}^\top, \mathbf{z}_{\rm g}^\top\right]^\top$, we arrive at the following proposition

Proposition 5. The equilibrium point $\boldsymbol{\xi} = \mathbf{0}$ is rendered uniformly globally asymptotically and locally exponentially stable (UGAS/ULES) under assumptions (2-4) when applying (12-13) with (10) and (27).

PROOF. Since the origin of system $\Sigma_{\rm A.2}$ is shown to be UGAS/ULES in Proposition 1, the origin of the unperturbed system $\Sigma_{\rm A.1}$ (i.e., when $\mathbf{z}_{\rm g} = \mathbf{0}$) is trivially shown to be UGAS/ULES by applying standard Lyapunov theory to (16) and (24), and the interconnection term satisfies $\left|\mathbf{g}_{\rm A.1}(t, \boldsymbol{\varepsilon}, \mathbf{z}_{\rm g})\right| = 1$, the proposed result follows directly from Theorem 7 and Lemma 8 of (Panteley *et al.* 1998).

Note that the stability result of Proposition 5 is also known as global κ-exponential stability, as defined in (Sørdalen and Egeland 1995).

2.3.2.2. Synchronization Loop Design Here, we determine the required *size* of $\boldsymbol{\alpha}_{\rm v}$ (i.e., $U_{\rm d}$) such that a vessel controlled by (12) and (13) with reference signals given by (10) and (27) synchronizes with the target point. Consequently, consider

$$V_{\tilde{\varpi}} = \frac{1}{2}\tilde{\varpi}^2, \tag{31}$$

where

$$\tilde{\varpi} = \varpi_{\rm c} - \varpi_{\rm t}, \tag{32}$$

and differentiate the CLF to ultimately obtain

$$\dot{V}_{\tilde{\varpi}} = -k_{\tilde{\varpi}}\frac{\tilde{\varpi}^2}{\sqrt{\tilde{\varpi}^2 + \triangle_{\tilde{\varpi}}^2}} + \tilde{\varpi}z_{\rm c} \tag{33}$$

where

$$k_{\tilde{\varpi}} = \sigma\frac{U_{\rm t}}{|\mathbf{p}_{\rm t}'|}, \sigma \in \langle 0, 1] \tag{34}$$

and $z_{\rm c} = \dot{\varpi}_{\rm c} - \alpha_{\rm c}$. Here, $\alpha_{\rm c}$ represents the desired speed of the collaborator when the marine craft has converged to the path, chosen as

$$\alpha_{\rm c} = \frac{U_{\rm t}}{|\mathbf{p}_{\rm t}'|}\left(1 - \sigma\frac{\tilde{\varpi}}{\sqrt{\tilde{\varpi}^2 + \triangle_{\tilde{\varpi}}^2}}\right) \tag{35}$$

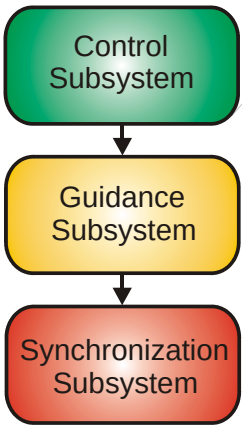

Fig. 2. The modular, cascaded nature of the motion control concept developed for DP by case A.

such that $U_{\rm d}$ satisfies Assumption 4 since $U_{\rm d} = \alpha_{\rm c}\,|\mathbf{p}_{\rm c}'|$, and where $\triangle_{\tilde{\varpi}} \in [\triangle_{\tilde{\varpi},\,\min}, \infty\rangle\,, \triangle_{\tilde{\varpi},\,\min} > 0$. Then, expand $z_{\rm c}$ to get

$$z_{\rm c} = \frac{U_{\rm d}(\cos\chi_{\rm r} - 1) + \gamma s}{|\mathbf{p}_{\rm c}'|} \tag{36}$$

where

$$(\cos\chi_{\rm r} - 1) = \frac{\triangle_{\rm e} - \sqrt{e^2 + \triangle_{\rm e}^2}}{\sqrt{e^2 + \triangle_{\rm e}^2}} \tag{37}$$

such that the system dynamics of $\tilde{\varpi}$ and $\boldsymbol{\xi}$ become

$$\Sigma_{\rm A.3} : \dot{\tilde{\varpi}} = f_{\rm A.3}(t, \tilde{\varpi}) + \mathbf{g}_{\rm A.3}(t, \tilde{\varpi}, \boldsymbol{\xi})^{\top}\boldsymbol{\xi} \tag{38}$$

$$\Sigma_{\rm A.4} : \dot{\boldsymbol{\xi}} = \mathbf{f}_{\rm A.4}(t, \boldsymbol{\xi}), \tag{39}$$

which is a cascaded system where the synchronization subsystem is perturbed through the well-defined

$$\mathbf{g}_{\rm A.3}(t, \tilde{\varpi}, \boldsymbol{\xi}) = \frac{1}{|\mathbf{p}_{\rm c}'|}\left[\gamma, U_{\rm d}\frac{\triangle_{\rm e} - \sqrt{e^2 + \triangle_{\rm e}^2}}{e\sqrt{e^2 + \triangle_{\rm e}^2}}, \mathbf{0}_{1\times 7}\right]^{\top}. \tag{40}$$

Note that the cascade structure is completely modular in the sense that the control subsystem ($\mathbf{z}_{\rm g}$) excites the guidance subsystem ($\boldsymbol{\varepsilon}$), which in turn excites the synchronization subsystem ($\tilde{\varpi}$), see Figure 2.

By considering the state vector $\boldsymbol{\zeta} = \left[\tilde{\varpi}, \boldsymbol{\xi}^{\top}\right]^{\top}$, we can now state the main result associated with dynamic positioning by case A through the following theorem

Theorem 6. (Case A). The equilibrium point $\boldsymbol{\zeta} = \mathbf{0}$ is rendered UGAS/ULES under assumptions (2-3) when applying (12-13) with (10) and (27) employing (35).

PROOF. Since the origin of system $\Sigma_{\rm A.4}$ is shown to be UGAS/ULES in Proposition 5, the origin of the unperturbed system $\Sigma_{\rm A.3}$ (i.e., when $\boldsymbol{\xi} = \mathbf{0}$) is trivially shown to be UGAS/ULES by applying standard Lyapunov theory to (31) and (33), and the interconnection term satisfies $|\mathbf{g}_{\rm A.3}(t, \tilde{\varpi}, \boldsymbol{\xi})| < |\mathbf{p}_{\rm p}'|_{\min}^{-1}\left(\gamma^2 + \left(\frac{U_{\rm t,max}}{\triangle_{\rm e,min}}\right)^2\right)^{1/2}$, the proposed result follows directly from Theorem 7 and Lemma 8 of (Panteley *et al.* 1998).

2.3.3. Case B: Tracking a Target Instantaneously It is not always possible, or even desirable, to design a spatial path that should be traversed. In a number of applications, the target point to be tracked is instantaneously calculated by a strategic motion planning component in the vessel DP control hierarchy. This is for instance the case in (Sørensen *et al.* 2001), where the main concern is the ability of the DP-controlled surface vessel to minimize bending stresses along a so-called marine riser, which basically is a pipe that is connected between the vessel and a point on the sea floor. Hence, we now focus on how to track a target point that is only available instantaneously, i.e., for which no future trajectory information exists. This objective encompass both point stabilization and trajectory tracking, where the former constitutes a special, degenerative case of the latter.

The suggested approach is inspired by theory from terminal missile guidance (Adler 1956), where the objective is to hit a physical target in finite time, subject to a number of real-life constraints. However, for our purposes we recognize the analogy of hitting a virtual target asymptotically, i.e., the concept of *asymptotic interception*. Specifically, we consider constant-bearing navigation by proportional navigation (PN) guidance as a suitable strategy to achieve asymptotic collision with a (virtual) target point that is to be tracked. In fact, proportional navigation is so fundamental that the claim could be made that PN is to guidance what PID is to control. The underlying guidance principle simply tries to align the relative linear velocity between the pursuer and its target along the line of sight (LOS) between them, thus achieving a collision. See Figure 3 for a simple illustration of the involved relationship. An alternative would be to align the linear velocity of the pursuer along the LOS, which is known as pure pursuit (PP) guidance, but this strategy very often results in a tail chase (equivalent to a predator chasing a prey in the animal world). In any case, if information about the linear velocity of the target is available (as is the case for our application; we decide the target motion), there is no reason why it should not be utilized to achieve PN instead of PP. In retrospect, we recognize that the guidance design of the previous section involved a type of PN guidance, where the responsibility for achieving an asymptotic intercept was shared between the vessel (pursuer) and its path-restricted collaborator (intermediate target).

We now proceed to develop the PN-associated guidance laws by Lyapunov theory. Consequently, consider the positive definite and radially unbounded CLF

$$V_{\tilde{\rm p}} = \frac{1}{2}\tilde{\mathbf{p}}^{\top}\tilde{\mathbf{p}}, \tag{41}$$

where

$$\tilde{\mathbf{p}} = \mathbf{p} - \mathbf{p}_{\rm t} \tag{42}$$

is the line-of-sight vector between the pursuer (surface vessel) and the target. Then, differentiate the CLF along the dynamics of $\tilde{\mathbf{p}}$ to obtain

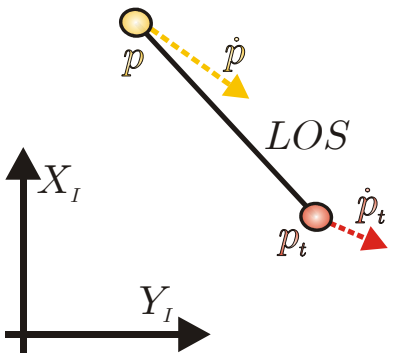

Fig. 3. The basic geometry behind tracking instantaneously. The vessel is shown in orange, while the target point is shown in red. LOS = line of sight.

$$\dot{V}_{\tilde{\mathrm{p}}} = \tilde{\mathbf{p}}^\top \dot{\tilde{\mathbf{p}}} = \tilde{\mathbf{p}}^\top (\dot{\mathbf{p}} - \dot{\mathbf{p}}_{\mathrm{t}}) = \tilde{\mathbf{p}}^\top (\mathbf{v} - \dot{\mathbf{p}}_{\mathrm{t}}) = \tilde{\mathbf{p}}^\top (\boldsymbol{\alpha}_{\mathrm{v,I}} - \dot{\mathbf{p}}_{\mathrm{t}}) + \tilde{\mathbf{p}}^\top \mathbf{z}_{\mathrm{v,I}}$$

since $\mathbf{z}_{\mathrm{v,I}} = \mathbf{v} - \boldsymbol{\alpha}_{\mathrm{v,I}}$, where $\boldsymbol{\alpha}_{\mathrm{v,I}} = \mathbf{R}_{\mathrm{B}} \boldsymbol{\alpha}_{\mathrm{v,B}}$ as in case A. Hence, by implementing PN guidance through

$$\boldsymbol{\alpha}_{\mathrm{v,I}} = \dot{\mathbf{p}}_{\mathrm{t}} - \kappa \frac{(\mathbf{p} - \mathbf{p}_{\mathrm{t}})}{|\mathbf{p} - \mathbf{p}_{\mathrm{t}}|}, \tag{43}$$

where

$$\kappa = U_{\mathrm{a}} \frac{|\mathbf{p} - \mathbf{p}_{\mathrm{t}}|}{\sqrt{\tilde{\mathbf{p}}^\top \tilde{\mathbf{p}} + \triangle_{\tilde{\mathrm{p}}}^2}} \tag{44}$$

with U_{a} representing the approach speed of the vessel toward the target (satisfying Assumption 4), and $\triangle_{\tilde{\mathrm{p}}} \in [\triangle_{\tilde{\mathrm{p}},\,\min}, \infty\rangle$, $\triangle_{\tilde{\mathrm{p}},\,\min} > 0$, we ultimately obtain

$$\dot{V}_{\tilde{\mathrm{p}}} = -U_{\mathrm{a}} \frac{\tilde{\mathbf{p}}^\top \tilde{\mathbf{p}}}{\sqrt{\tilde{\mathbf{p}}^\top \tilde{\mathbf{p}} + \triangle_{\tilde{\mathrm{p}}}^2}} + \tilde{\mathbf{p}}^\top \mathbf{R}_{\mathrm{B}} \mathbf{H} \mathbf{z}_{\nu}. \tag{45}$$

Hence, write the system dynamics of $\tilde{\mathbf{p}}$ and $\mathbf{z}_{\mathrm{g}}$ as

$$\Sigma_{\mathrm{B.1}} : \dot{\tilde{\mathbf{p}}} = \mathbf{f}_{\mathrm{B.1}}(t, \tilde{\mathbf{p}}) + \mathbf{g}_{\mathrm{B.1}}(t, \tilde{\mathbf{p}}, \mathbf{z}_{\mathrm{g}}) \mathbf{z}_{\mathrm{g}} \tag{46}$$

$$\Sigma_{\mathrm{B.2}} : \dot{\mathbf{z}}_{\mathrm{g}} = \mathbf{f}_{\mathrm{B.2}}(t, \mathbf{z}_{\mathrm{g}}), \tag{47}$$

which is a pure cascade where the control subsystem perturbs the guidance subsystem through the matrix

$$\mathbf{g}_{\mathrm{B.1}}(t, \tilde{\mathbf{p}}, \mathbf{z}_{\mathrm{g}}) = [\mathbf{0}_{2\times 1}, \mathbf{R}_{\mathrm{B}} \mathbf{H}, \mathbf{0}_{2\times 3}]. \tag{48}$$

Considering $\boldsymbol{\phi} = \left[\tilde{\mathbf{p}}^\top, \mathbf{z}_{\mathrm{g}}^\top\right]^\top$, we finally arrive at

Theorem 7. (Case B). The equilibrium point $\boldsymbol{\phi} = \mathbf{0}$ is rendered UGAS/ULES when applying (12-13) with the reference signals (10) and (43).

PROOF. Similar to that of Proposition 5.

3. CONCLUSIONS

This paper addressed the topic of dynamic positioning for fully actuated marine surface vessels. The concept of guided DP was developed by means of a modular motion control design procedure. For vessels tracking a planar target point, this work considered both the case where the target point moves along a path that is fully known in advance, as well as the case where only instantaneous information of the target point is available. A salient feature is that guided DP readily extends to underactuated vessels since it redefines the control output space to linear velocity and heading, where the heading either can be controlled independently (full actuation) or required to direct the linear velocity (underactuation). Thus, only a basic redesign of the guidance subsystem is required. For a scenario involving straight-line motion and no environmental disturbances, a redesign is unnecessary when aligning the desired heading with the desired linear velocity.

REFERENCES

Adler, F. P. (1956). Missile guidance by three-dimensional proportional navigation. *Journal of Applied Physics* **27**(5), 500–507.

Bray, D. (2003). *Dynamic Positioning*. Oilfield Publications Inc.

Breivik, M. and T. I. Fossen (2006). Motion control concepts for trajectory tracking of fully actuated ships. In: *Proceedings of the 7th IFAC MCMC, Lisbon, Portugal*.

Fossen, T. I. (2002). *Marine Control Systems: Guidance, Navigation and Control of Ships, Rigs and Underwater Vehicles*. Marine Cybernetics.

Fossen, T. I., A. Loría and A. Teel (2001). A theorem for ugas and ules of (passive) nonautonomous systems: Robust control of mechanical systems and ships. *International Journal of Robust and Nonlinear Control* **11**, 95–108.

Fossen, T. I., M. Breivik and R. Skjetne (2003). Line-of-sight path following of underactuated marine craft. In: *Proceedings of the 6th IFAC MCMC, Girona, Spain*.

Holvik, J. (1998). Basics of dynamic positioning. In: *Proceedings of the Dynamic Positioning Conference, Houston, Texas, USA*.

Panteley, E., E. Lefeber, A. Loría and H. Nijmeijer (1998). Exponential tracking of a mobile car using a cascaded approach. In: *Proceedings of the IFAC Workshop on Motion Control, Grenoble, France*.

Sørdalen, O. J. and O. Egeland (1995). Exponential stabilization of nonholonomic chained systems. *IEEE Transactions on Automatic Control* **40**(1), 35–49.

Sørensen, A. J., B. Leira, J. P. Strand and C. M. Larsen (2001). Optimal setpoint chasing in dynamic positioning of deep-water drilling and intervention vessels. *International Journal of Robust and Nonlinear Control* **11**, 1187–1205.

Sørensen, A. J., S. I. Sagatun and T. I. Fossen (1996). Design of a dynamic positioning system using model-based control. *Control Engineering Practice* **4**(3), 359–368.

Sælid, S., N. A. Jenssen and J. G. Balchen (1983). Design and analysis of a dynamic positioning system based on kalman filtering and optimal control. *IEEE Transactions on Automatic Control* **28**(3), 331–339.

E. Motion Control Concepts for Trajectory Tracking of Fully Actuated Ships

MOTION CONTROL CONCEPTS FOR TRAJECTORY TRACKING OF FULLY ACTUATED SHIPS

Morten Breivik[1,2] **Thor I. Fossen**[1]

Abstract: This paper develops and compares two different motion control concepts for fully actuated ships in a trajectory tracking scenario. The first concept, named servoed motion control, is identical to a standard solution found in the established ship control literature on dynamic positioning. The scheme is easy to derive and analyze by traditional nonlinear control theory, but not readily extendable to underactuated ships, while also exhibiting erratic transient convergence behavior. The second concept, named guided motion control, represents a novel approach inspired by literature on missile guidance, path following, and formation control. The guided concept is more complex to derive and analyze, but is readily extendable to underactuated ships, and displays gentle transient convergence behavior.

Keywords: Ship motion control, Fully actuated ships, Trajectory tracking scenario, Servoed motion control, Guided motion control

1. INTRODUCTION

Motion control is a fundamental enabling technology for any ship application. Whether humans or computers act as motion controllers, a ship requires such a tactical level to translate strategic motion planning commands into physically realistic movements of the ship hull. Today, co-control is probably the most common configuration for industrial applications, i.e., that humans maneuver ships through sail-by-wire technology, where computers are responsible for (tactical-level) motion control while humans take care of the (strategic-level) motion planning. However, sensitivity toward human casualties when operating in so-called dirty, dull, and dangerous environments will gradually enforce full autonomy requirements. Likewise, full autonomy is attractive through prospects of increased operational cost saving, endurance, precision, reliability, and safety within marine business areas such as shipping, offshore, and fisheries and aquaculture. But full autonomy requires extraordinary features, not least at the tactical level of motion control. Hence, this work considers two qualitatively different motion control concepts, and debates their distinctive qualities.

The main contribution of this paper is the development of a motion control concept denoted *guided motion control*. In a three-step, backstepping-inspired, cascaded-based design, a novel motion controller is developed that draws on control, guidance, and synchronization concepts. The approach is inspired by schemes from research areas such as missile guidance, path following, and formation control. For a trajectory tracking scenario concerning fully actuated ships, the guided concept is contrasted toward what we have called the servoed motion control concept, which represents a standard solution in the established literature on nonlinear motion control for fully actuated ships.

Since the goal of this work is to emphasize and illustrate fundamental aspects of motion control, a simplified ship model that does not consider environmental disturbances is employed. Hence, the paper should be regarded purely as a motion control concept study.

Notation: The time derivative of (a vector) $\mathbf{x}(t)$ is denoted $\dot{\mathbf{x}}$, the partial derivative of $\mathbf{x}(\varpi(t))$ is denoted $\mathbf{x}'$ $\left(= \frac{\partial \mathbf{x}}{\partial \varpi}(\varpi(t))\right)$, while $|\cdot|$ represents the Euclidean vector norm as well as the induced matrix norm.

[1] {Centre for Ships and Ocean Structures, Department of Engineering Cybernetics}, Norwegian University of Science and Technology (NTNU), NO-7491 Trondheim, Norway. E-mails: {morten.breivik, fossen}@ieee.org.

[2] Supported by the Research Council of Norway through the Centre for Ships and Ocean Structures at NTNU.

2. MOTION CONTROL CONCEPTS

This section develops two different motion control concepts that can be applied for fully actuated ships in a trajectory tracking scenario. The applied ship model is simplified such that we can concentrate on the fundamental aspects of motion control. However, any standard solutions to bias counteraction, wave filtering, and control allocation are readily applicable for fully actuated ships that employ one of the motion control concepts under consideration.

2.1 Dynamic Ship Model

A 3 degree-of-freedom (DOF) dynamic model of a ship (surface vessel; surge, sway, and yaw modes) can be found in (Fossen 2002), and is composed of the kinematics

$$\dot{\boldsymbol{\eta}} = \mathbf{R}(\psi)\boldsymbol{\nu}, \tag{1}$$

and the (purposefully simplified) kinetics

$$\mathbf{M}\dot{\boldsymbol{\nu}} + \mathbf{C}(\boldsymbol{\nu})\boldsymbol{\nu} + \mathbf{D}(\boldsymbol{\nu})\boldsymbol{\nu} = \boldsymbol{\tau}, \tag{2}$$

where $\boldsymbol{\eta} = [x, y, \psi]^\top \in \mathbb{R}^2 \times \mathcal{S}$ represents the earth-fixed position and heading (with $\mathcal{S} = [-\pi, \pi]$), $\boldsymbol{\nu} = [u, v, r]^\top \in \mathbb{R}^3$ represents the vessel-fixed velocity, $\mathbf{R}(\psi) \in SO(3)$ is the transformation matrix

$$\mathbf{R}(\psi) = \begin{bmatrix} \cos\psi & -\sin\psi & 0 \\ \sin\psi & \cos\psi & 0 \\ 0 & 0 & 1 \end{bmatrix} \tag{3}$$

that transforms from the vessel-fixed BODY frame (**B**) to the earth-fixed NED frame (**N**), $\mathbf{M}$ is the inertia matrix, $\mathbf{C}(\boldsymbol{\nu})$ is the centrifugal and coriolis matrix, while $\mathbf{D}(\boldsymbol{\nu})$ is the hydrodynamic damping matrix. The system matrices satisfy the properties $\mathbf{M} = \mathbf{M}^\top > 0$, $\mathbf{C} = -\mathbf{C}^\top$ and $\mathbf{D} > 0$. The vessel-fixed propulsion forces and moment is represented by $\boldsymbol{\tau} = [\tau_{\mathrm{X}}, \tau_{\mathrm{Y}}, \tau_{\mathrm{N}}]^\top \in \mathbb{R}^3$. A fully actuated ship can independently control all 3 DOFs simultaneously, which means that the direction of the linear velocity is independent of the heading. This is not the case for an underactuated ship, where the orientation of the linear velocity is coupled, in a sense locked, to the heading of the ship.

2.2 Trajectory Tracking Scenario

A fundamental assumption of this paper is that the motion control designer is granted the freedom to design the path (trajectory) that is to be traversed, as well as the motion of a target point that is to be tracked along the path. Consequently, consider a (planar) path continuously parameterized by a scalar variable $\varpi \in \mathbb{R}$, such that the position of a point belonging to the path is represented by $\mathbf{p}_{\mathrm{p}}(\varpi) \in \mathbb{R}^2$. Thus, the path is a one-dimensional manifold that can be expressed by the set

$$\mathcal{P} = \left\{ \mathbf{p} \in \mathbb{R}^2 \mid \mathbf{p} = \mathbf{p}_{\mathrm{p}}(\varpi)\ \forall \varpi \in \mathbb{R} \right\}. \tag{4}$$

Then, consider a time-varying target point $\mathbf{p}_{\mathrm{t}}(t) = \mathbf{p}_{\mathrm{p}}(\varpi_{\mathrm{t}}(t))$ traversing the path by adhering to a chosen speed profile $U_{\mathrm{t}}(\varpi_{\mathrm{t}})$, implemented through

$$\dot{\varpi}_{\mathrm{t}} = \frac{U_{\mathrm{t}}(\varpi_{\mathrm{t}})}{\left|\mathbf{p}'_{\mathrm{p}}(\varpi_{\mathrm{t}})\right|}, \tag{5}$$

since $|\dot{\mathbf{p}}_{\mathrm{t}}| = \left|\mathbf{p}'_{\mathrm{p}}(\varpi_{\mathrm{t}})\right| \dot{\varpi}_{\mathrm{t}} = U_{\mathrm{t}}(\varpi_{\mathrm{t}})$, where $U_{\mathrm{t}}(\varpi_{\mathrm{t}}) \in [U_{\mathrm{t,min}}, U_{\mathrm{t,max}}]$, $U_{\mathrm{t,min}} > 0$. The path, as well as the speed profile of the target point, is typically designed (by offline optimization) based on information like the nominal actuator configuration of the ship in question, weather forecasts, static obstacles, etc. A trajectory tracking (path tracking) scenario entails that the spatial and temporal assignments are linked as one single assignment, requiring that the ship is located at a certain point along the path at a certain time. The target point drives the ship-path system forward (as an independent, time-varying attractor moving along the path) by propagating without concern for the tracking ship. Thus, the ship-path system is inherently open loop, and the target may leave the ship behind if something should alter the propulsive capability of the ship.

2.2.1. Problem Statement In our scenario, the trajectory tracking problem for a fully actuated ship can be stated by

$$\lim_{t\to\infty} \left(\boldsymbol{\eta}(t) - \boldsymbol{\eta}_{\mathrm{d}}(t)\right) = \mathbf{0}, \tag{6}$$

where $\boldsymbol{\eta}_{\mathrm{d}}(t) = \left[\mathbf{p}_{\mathrm{t}}^\top(t), \psi_{\mathrm{d}}(t)\right]^\top$, and where $\psi_{\mathrm{d}}(t)$ can be any arbitrary heading, satisfying for instance some auxiliary task objective.

2.3 Servoed Motion Control

Fully actuated ships nominally imply low-speed dynamic positioning (DP) applications. This relates to the fact that the ability to produce a transversal (sway) force is lost when moving too fast. The DP literature has become rich and varied, and during the last decade nonlinear control theory has been applied to create motion controllers ensuring global stability properties. These controllers are inspired by work performed in the robotics community, which is readily extendable to ships when formulating their dynamic model within the Euler-Lagrange framework (Fossen 2002). The concept of this section has been termed servoed motion control due to the underlying control design principle, which resembles that of basic servomechanisms. Hence, the control objective is identical to the problem statement, and straightforwardly achieved in one single design step. Unfortunately, a consequence of employing such a servoed design principle is that the resulting motion controllers cannot be readily modified to handle underactuated vehicles.

The derived motion controller is backstepping-based (Krstić *et al.* 1995), and standard in the DP control literature (Fossen 2002). Consequently, consider the

positive definite and radially unbounded Control Lyapunov Function (CLF)

$$V_{\rm s} = \frac{1}{2}(\mathbf{z}_\eta^\top \mathbf{z}_\eta + \mathbf{z}_\nu^\top \mathbf{M}\mathbf{z}_\nu), \tag{7}$$

where we have defined

$$\mathbf{z}_\eta = \mathbf{R}^\top(\boldsymbol{\eta} - \boldsymbol{\eta}_{\rm d}) \tag{8}$$

with $\mathbf{R} = \mathbf{R}(\psi)$, and

$$\mathbf{z}_\nu = \boldsymbol{\nu} - \boldsymbol{\alpha}, \tag{9}$$

where $\boldsymbol{\alpha} = [\alpha_u, \alpha_v, \alpha_r]^\top \in \mathbb{R}^3$ is a so-called vector of stabilizing functions (virtual inputs that become reference signals) yet to be designed. Then, differentiate the CLF along the trajectories of $\mathbf{z}_\eta$ and $\mathbf{z}_\nu$ to obtain

$$\begin{aligned}
\dot{V}_{\rm s} &= \mathbf{z}_\eta^\top \dot{\mathbf{z}}_\eta + \mathbf{z}_\nu^\top \mathbf{M}\dot{\mathbf{z}}_\nu \\
&= \mathbf{z}_\eta^\top(\dot{\mathbf{R}}^\top(\boldsymbol{\eta} - \boldsymbol{\eta}_{\rm d}) + \mathbf{R}^\top(\dot{\boldsymbol{\eta}} - \dot{\boldsymbol{\eta}}_{\rm d})) + \\
&\quad \mathbf{z}_\nu^\top \mathbf{M}(\dot{\boldsymbol{\nu}} - \dot{\boldsymbol{\alpha}}) \\
&= \mathbf{z}_\eta^\top(\mathbf{S}^\top \mathbf{R}^\top(\boldsymbol{\eta} - \boldsymbol{\eta}_{\rm d}) + \mathbf{R}^\top \dot{\boldsymbol{\eta}} - \mathbf{R}^\top \dot{\boldsymbol{\eta}}_{\rm d}) + \\
&\quad \mathbf{z}_\nu^\top(\mathbf{M}\dot{\boldsymbol{\nu}} - \mathbf{M}\dot{\boldsymbol{\alpha}}) \\
&= \mathbf{z}_\eta^\top(\mathbf{S}^\top \mathbf{z}_\eta + \boldsymbol{\nu} - \mathbf{R}^\top \dot{\boldsymbol{\eta}}_{\rm d}) + \\
&\quad \mathbf{z}_\nu^\top(\boldsymbol{\tau} - \mathbf{C}(\boldsymbol{\nu})\boldsymbol{\nu} - \mathbf{D}(\boldsymbol{\nu})\boldsymbol{\nu} - \mathbf{M}\dot{\boldsymbol{\alpha}})
\end{aligned}$$

since $\dot{\mathbf{R}} = \mathbf{R}\mathbf{S}$ with $\mathbf{S} = -\mathbf{S}^\top$. Furthermore, recognizing that $\mathbf{z}_\eta^\top \mathbf{S}^\top \mathbf{z}_\eta = 0$ and $\boldsymbol{\nu} = \mathbf{z}_\nu + \boldsymbol{\alpha}$, we get

$$\begin{aligned}
\dot{V}_{\rm s} &= \mathbf{z}_\eta^\top(\boldsymbol{\alpha} - \mathbf{R}^\top \dot{\boldsymbol{\eta}}_{\rm d}) + \\
&\quad \mathbf{z}_\nu^\top(\boldsymbol{\tau} - \mathbf{C}(\boldsymbol{\nu})\boldsymbol{\nu} - \mathbf{D}(\boldsymbol{\nu})\boldsymbol{\nu} - \mathbf{M}\dot{\boldsymbol{\alpha}} + \mathbf{z}_\eta),
\end{aligned}$$

which results in

$$\begin{aligned}
\dot{V}_{\rm s} &= -\mathbf{z}_\eta^\top \mathbf{K}_\eta \mathbf{z}_\eta - \mathbf{z}_\nu^\top \mathbf{C}(\boldsymbol{\nu})\mathbf{z}_\nu - \mathbf{z}_\nu^\top \mathbf{D}(\boldsymbol{\nu})\mathbf{z}_\nu + \\
&\quad \mathbf{z}_\nu^\top(\boldsymbol{\tau} - \mathbf{C}(\boldsymbol{\nu})\boldsymbol{\alpha} - \mathbf{D}(\boldsymbol{\nu})\boldsymbol{\alpha} - \mathbf{M}\dot{\boldsymbol{\alpha}} + \mathbf{z}_\eta)
\end{aligned}$$

when choosing the virtual input as

$$\boldsymbol{\alpha} = \mathbf{R}^\top \dot{\boldsymbol{\eta}}_{\rm d} - \mathbf{K}_\eta \mathbf{z}_\eta, \tag{10}$$

where $\mathbf{K}_\eta = \mathbf{K}_\eta^\top > 0$ is a constant matrix. Finally, since $\mathbf{z}_\nu^\top \mathbf{C}(\boldsymbol{\nu})\mathbf{z}_\nu = 0$, and by selecting the control input as

$$\boldsymbol{\tau} = \mathbf{M}\dot{\boldsymbol{\alpha}} + \mathbf{C}(\boldsymbol{\nu})\boldsymbol{\alpha} + \mathbf{D}(\boldsymbol{\nu})\boldsymbol{\alpha} - \mathbf{z}_\eta - \mathbf{K}_\nu \mathbf{z}_\nu, \tag{11}$$

where $\mathbf{K}_\nu = \mathbf{K}_\nu^\top > 0$ is a constant matrix, we obtain the quadratically negative definite

$$\dot{V}_{\rm s} = -\mathbf{z}_\eta^\top \mathbf{K}_\eta \mathbf{z}_\eta - \mathbf{z}_\nu^\top(\mathbf{D}(\boldsymbol{\nu}) + \mathbf{K}_\nu)\mathbf{z}_\nu. \tag{12}$$

By considering the state vector $\mathbf{z}_{\rm s} = \left[\mathbf{z}_\eta^\top, \mathbf{z}_\nu^\top\right]^\top$, we can now state the following theorem

Theorem 1. (Servoed Motion Control). The equilibrium point $\mathbf{z}_{\rm s} = \mathbf{0}$ is rendered uniformly globally exponentially stable (UGES) by adhering to (10) and (11) when $\boldsymbol{\eta}_{\rm d}$, $\dot{\boldsymbol{\eta}}_{\rm d}$ and $\ddot{\boldsymbol{\eta}}_{\rm d}$ are uniformly bounded.

PROOF. By standard Lyapunov theory, (7) and (12) show that the origin of $\mathbf{z}_{\rm s}$ is UGES.

Consequently, the trajectory tracking problem as stated in (6) has been solved in one design step.

2.4 Guided Motion Control

This section solves the trajectory tracking problem in three distinct design steps by a backstepping-inspired, cascaded-based procedure that is influenced by ideas from missile guidance (Shneydor 1998), path following (Breivik and Fossen 2005), and formation control (Breivik *et al.* 2006). The underlying concept is named guided motion control since it allows the transient convergence behavior to be manipulated through guidance laws. An advantage of employing a guided design principle is that the resulting motion control structure can be readily modified to also handle underactuated vehicles.

2.4.1. Step 1: Control Loop Design Since the position of a ship can be controlled through its linear velocity, we redefine the output space from the 3 DOF position and heading to the 3 DOF linear velocity and heading. Again, we design the controller by using the backstepping approach. Consequently, consider the positive definite and radially unbounded CLF

$$V_{\rm g} = \frac{1}{2}(z_\psi^2 + \mathbf{z}_\nu^\top \mathbf{M}\mathbf{z}_\nu) \tag{13}$$

where we have

$$z_\psi = \psi - \psi_{\rm d} \tag{14}$$

and

$$\mathbf{z}_\nu = \boldsymbol{\nu} - \boldsymbol{\alpha}, \tag{15}$$

where $\boldsymbol{\alpha}$ is yet to be designed. Subsequently, differentiate the CLF with respect to time to obtain

$$\begin{aligned}
\dot{V}_{\rm g} &= z_\psi \dot{z}_\psi + \mathbf{z}_\nu^\top \mathbf{M}\dot{\mathbf{z}}_\nu \\
&= z_\psi(\dot{\psi} - \dot{\psi}_{\rm d}) + \mathbf{z}_\nu^\top \mathbf{M}(\dot{\boldsymbol{\nu}} - \dot{\boldsymbol{\alpha}}) \\
&= z_\psi(\mathbf{h}^\top \dot{\boldsymbol{\eta}} - \dot{\psi}_{\rm d}) + \mathbf{z}_\nu^\top(\mathbf{M}\dot{\boldsymbol{\nu}} - \mathbf{M}\dot{\boldsymbol{\alpha}})
\end{aligned}$$

where

$$\mathbf{h} = [0, 0, 1]^\top. \tag{16}$$

Then, recognizing that $\mathbf{h}^\top \dot{\boldsymbol{\eta}} = \mathbf{h}^\top \mathbf{R}\boldsymbol{\nu} = \mathbf{h}^\top \boldsymbol{\nu}$ and $\boldsymbol{\nu} = \mathbf{z}_\nu + \boldsymbol{\alpha}$, we obtain

$$\begin{aligned}
\dot{V}_{\rm g} &= z_\psi(\mathbf{h}^\top \boldsymbol{\alpha} - \dot{\psi}_{\rm d}) + \\
&\quad \mathbf{z}_\nu^\top(\boldsymbol{\tau} - \mathbf{C}(\boldsymbol{\nu})\boldsymbol{\nu} - \mathbf{D}(\boldsymbol{\nu})\boldsymbol{\nu} - \mathbf{M}\dot{\boldsymbol{\alpha}} + \mathbf{h}z_\psi),
\end{aligned}$$

which results in

$$\begin{aligned}
\dot{V}_{\rm g} &= -k_\psi z_\psi^2 - \mathbf{z}_\nu^\top \mathbf{C}(\boldsymbol{\nu})\mathbf{z}_\nu - \mathbf{z}_\nu^\top \mathbf{D}(\boldsymbol{\nu})\mathbf{z}_\nu + \\
&\quad \mathbf{z}_\nu^\top(\boldsymbol{\tau} - \mathbf{C}(\boldsymbol{\nu})\boldsymbol{\alpha} - \mathbf{D}(\boldsymbol{\nu})\boldsymbol{\alpha} - \mathbf{M}\dot{\boldsymbol{\alpha}} + \mathbf{h}z_\psi)
\end{aligned}$$

when choosing the virtual input $\mathbf{h}^\top \boldsymbol{\alpha} = \alpha_{\rm r}$ as

$$\alpha_{\rm r} = \dot{\psi}_{\rm d} - k_\psi z_\psi, \tag{17}$$

where $k_\psi > 0$ is a constant. Since $\mathbf{z}_\nu^\top \mathbf{C}(\boldsymbol{\nu})\mathbf{z}_\nu = 0$, and by selecting the control input as

$$\boldsymbol{\tau} = \mathbf{M}\dot{\boldsymbol{\alpha}} + \mathbf{C}(\boldsymbol{\nu})\boldsymbol{\alpha} + \mathbf{D}(\boldsymbol{\nu})\boldsymbol{\alpha} - \mathbf{h}z_\psi - \mathbf{K}_\nu \mathbf{z}_\nu, \quad (18)$$

where $\mathbf{K}_\nu = \mathbf{K}_\nu^\top > 0$ is a constant matrix, we finally obtain the quadratically negative definite

$$\dot{V}_{\mathrm{g}} = -k_\psi z_\psi^2 - \mathbf{z}_\nu^\top (\mathbf{D}(\boldsymbol{\nu}) + \mathbf{K}_\nu)\mathbf{z}_\nu. \quad (19)$$

Considering the state vector $\mathbf{z}_{\mathrm{g}} = \left[z_\psi, \mathbf{z}_\nu^\top\right]^\top$, the following proposition can now be stated

Proposition 2. The equilibrium point $\mathbf{z}_{\mathrm{g}} = \mathbf{0}$ is rendered uniformly globally exponentially stable (UGES) by adhering to (17) and (18) under the assumption that $\boldsymbol{\alpha}$ and $\dot{\boldsymbol{\alpha}}$ are uniformly bounded.

PROOF. By standard Lyapunov theory, (13) and (19) show that the origin of $\mathbf{z}_{\mathrm{g}}$ is UGES.

Unlike the result in Theorem 1, Proposition 2 does not mean that the trajectory tracking problem as stated in (6) has been solved. In fact, the controller that has been developed here cannot achieve anything meaningful unless it is fed sensible reference signals, i.e., unless $\boldsymbol{\alpha}_{\mathrm{v}} = [\alpha_{\mathrm{u}}, \alpha_{\mathrm{v}}]^\top \in \mathbb{R}^2$ is purposefully defined for the problem at hand. This, then, represents the challenge for the final two design steps.

2.4.2. Step 2: Guidance Loop Design Here, we design the required *orientation* of $\boldsymbol{\alpha}_{\mathrm{v}}$ ($|\boldsymbol{\alpha}_{\mathrm{v}}| > 0$) such that a ship controlled by (18) achieves path following. The design is inspired by the concept of guidance-based path following as found in (Breivik and Fossen 2005). Consequently, consider the positive definite and radially unbounded CLF

$$V_{\boldsymbol{\varepsilon}} = \frac{1}{2}\boldsymbol{\varepsilon}^\top \boldsymbol{\varepsilon}, \quad (20)$$

with

$$\boldsymbol{\varepsilon} = \mathbf{R}_{\mathrm{C}}^\top (\mathbf{p} - \mathbf{p}_{\mathrm{c}}) \quad (21)$$

where $\mathbf{p}_{\mathrm{c}} = \mathbf{p}_{\mathrm{p}}(\varpi_{\mathrm{c}})$ represents a *collaborator* point that acts cooperatively with the ship as an intermediate path attractor, and whose sole purpose is to ensure that the ship can converge to the path even if it has not converged to the target point. For a given ϖ_{c}, define a path-tangential reference frame at $\mathbf{p}_{\mathrm{c}}$ termed the COLLABORATOR frame (**C**). To arrive at **C**, the INERTIAL frame (**I**) must be positively rotated an angle

$$\chi_{\mathrm{c}} = \arctan\left(\frac{y_{\mathrm{p}}'(\varpi_{\mathrm{c}})}{x_{\mathrm{p}}'(\varpi_{\mathrm{c}})}\right), \quad (22)$$

which can be represented by the rotation matrix

$$\mathbf{R}_{\mathrm{C}} = \begin{bmatrix} \cos\chi_{\mathrm{c}} & -\sin\chi_{\mathrm{c}} \\ \sin\chi_{\mathrm{c}} & \cos\chi_{\mathrm{c}} \end{bmatrix}, \quad (23)$$

$\mathbf{R}_{\mathrm{C}} \in SO(2)$. Hence, equation (21) represents the error vector between the ship and its collaborator decomposed in **C**. The local coordinates $\boldsymbol{\varepsilon} = [s, e]^\top$ consist of the along-track error s and the cross-track error e. It is clear that path following can be achieved by driving $\boldsymbol{\varepsilon}$ to zero. Thus, differentiate the CLF in (20) along the trajectories of $\boldsymbol{\varepsilon}$ to obtain

$$\begin{aligned}\dot{V}_{\boldsymbol{\varepsilon}} &= \boldsymbol{\varepsilon}^\top \dot{\boldsymbol{\varepsilon}} \\ &= \boldsymbol{\varepsilon}^\top (\mathbf{S}_{\mathrm{C}}^\top \mathbf{R}_{\mathrm{C}}^\top (\mathbf{p} - \mathbf{p}_{\mathrm{c}}) + \mathbf{R}_{\mathrm{C}}^\top (\dot{\mathbf{p}} - \dot{\mathbf{p}}_{\mathrm{c}})) \\ &= \boldsymbol{\varepsilon}^\top \left(\mathbf{S}_{\mathrm{C}}^\top \boldsymbol{\varepsilon} + \mathbf{R}_{\mathrm{C}}^\top \mathbf{H}\dot{\boldsymbol{\eta}} - \mathbf{v}_{\mathrm{c}}\right) \\ &= \boldsymbol{\varepsilon}^\top \left(\mathbf{R}_{\mathrm{C}}^\top \mathbf{H}\mathbf{R}\boldsymbol{\nu} - \mathbf{v}_{\mathrm{c}}\right)\end{aligned}$$

where $\mathbf{S}_{\mathrm{C}} = -\mathbf{S}_{\mathrm{C}}^\top \Rightarrow \boldsymbol{\varepsilon}^\top \mathbf{S}_{\mathrm{C}}^\top \boldsymbol{\varepsilon} = 0$, and where

$$\mathbf{H} = \begin{bmatrix} 1 & 0 & 0 \\ 0 & 1 & 0 \end{bmatrix}. \quad (24)$$

Also, $\mathbf{v}_{\mathrm{c}} = [U_{\mathrm{c}}, 0]^\top$, where $U_{\mathrm{c}} = |\dot{\mathbf{p}}_{\mathrm{c}}|$, represents the linear velocity of the collaborator decomposed in **C**. Furthermore, we have that

$$\begin{aligned}\dot{V}_{\boldsymbol{\varepsilon}} &= \boldsymbol{\varepsilon}^\top \left(\mathbf{R}_{\mathrm{C}}^\top \mathbf{H}\mathbf{R}\boldsymbol{\alpha} - \mathbf{v}_{\mathrm{c}}\right) + \boldsymbol{\varepsilon}^\top \mathbf{R}_{\mathrm{C}}^\top \mathbf{H}\mathbf{R}\mathbf{z}_\nu \\ &= \boldsymbol{\varepsilon}^\top \left(\mathbf{R}_{\mathrm{C}}^\top \mathbf{H}\mathbf{R}\mathbf{H}^\top \mathbf{H}\boldsymbol{\alpha} - \mathbf{v}_{\mathrm{c}}\right) + \boldsymbol{\varepsilon}^\top \mathbf{R}_{\mathrm{C}}^\top \mathbf{H}\mathbf{R}\mathbf{H}^\top \mathbf{H}\mathbf{z}_\nu,\end{aligned}$$

since $\boldsymbol{\nu} = \mathbf{z}_\nu + \boldsymbol{\alpha}$ and $\mathbf{H}^\top\mathbf{H} = \mathbf{I}_{3\times 3}$ (identity matrix). Defining $\mathbf{H}\mathbf{R}\mathbf{H}^\top = \mathbf{R}_{\mathrm{B}}$, i.e.,

$$\mathbf{R}_{\mathrm{B}} = \begin{bmatrix} \cos\psi & -\sin\psi \\ \sin\psi & \cos\psi \end{bmatrix}, \quad (25)$$

leads to

$$\dot{V}_{\boldsymbol{\varepsilon}} = \boldsymbol{\varepsilon}^\top \left(\mathbf{R}_{\mathrm{C}}^\top \mathbf{R}_{\mathrm{B}}\mathbf{H}\boldsymbol{\alpha} - \mathbf{v}_{\mathrm{c}}\right) + \boldsymbol{\varepsilon}^\top \mathbf{R}_{\mathrm{C}}^\top \mathbf{R}_{\mathrm{B}}\mathbf{H}\mathbf{z}_\nu,$$

where $\mathbf{R}_{\mathrm{B}}\mathbf{H}\boldsymbol{\alpha} = \mathbf{R}_{\mathrm{B}}\boldsymbol{\alpha}_{\mathrm{v,B}}$ with $\boldsymbol{\alpha}_{\mathrm{v,B}} = \boldsymbol{\alpha}_{\mathrm{v}} = [\alpha_{\mathrm{u}}, \alpha_{\mathrm{v}}]^\top$. Now, $\mathbf{R}_{\mathrm{B}}\boldsymbol{\alpha}_{\mathrm{v,B}} = \mathbf{R}_{\mathrm{DV}}\boldsymbol{\alpha}_{\mathrm{v,DV}} = \boldsymbol{\alpha}_{\mathrm{v,I}}$ represents the desired linear velocity decomposed in **I**, while $\boldsymbol{\alpha}_{\mathrm{v,DV}} = [U_{\mathrm{d}}, 0]^\top$, where $U_{\mathrm{d}} = |\boldsymbol{\alpha}_{\mathrm{v}}|$, represents the desired linear velocity decomposed in a DESIRED VELOCITY frame (**DV**). This frame is aligned with $\boldsymbol{\alpha}_{\mathrm{v,I}}$, whose orientation we want to design so as to achieve path following. Hence, we get

$$\begin{aligned}\dot{V}_{\boldsymbol{\varepsilon}} &= \boldsymbol{\varepsilon}^\top \left(\mathbf{R}_{\mathrm{C}}^\top \mathbf{R}_{\mathrm{DV}}\boldsymbol{\alpha}_{\mathrm{v,DV}} - \mathbf{v}_{\mathrm{c}}\right) + \boldsymbol{\varepsilon}^\top \mathbf{R}_{\mathrm{C}}^\top \mathbf{R}_{\mathrm{B}}\mathbf{H}\mathbf{z}_\nu \\ &= \boldsymbol{\varepsilon}^\top \left(\mathbf{R}_{\mathrm{R}}\boldsymbol{\alpha}_{\mathrm{v,DV}} - \mathbf{v}_{\mathrm{c}}\right) + \boldsymbol{\varepsilon}^\top \mathbf{R}_{\mathrm{C}}^\top \mathbf{R}_{\mathrm{B}}\mathbf{H}\mathbf{z}_\nu,\end{aligned}$$

where $\mathbf{R}_{\mathrm{C}}^\top(\chi_{\mathrm{c}})\mathbf{R}_{\mathrm{DV}}(\chi_{\mathrm{d}}) = \mathbf{R}_{\mathrm{R}}(\chi_{\mathrm{d}} - \chi_{\mathrm{c}})$, i.e., the relative orientation between **C** and **DV**.

Thus, U_{c} and $(\chi_{\mathrm{d}} - \chi_{\mathrm{c}})$ can be considered as virtual inputs for driving $\boldsymbol{\varepsilon}$ to zero, given that $U_{\mathrm{d}} > 0$. Denote the angular difference by $\chi_{\mathrm{r}} = \chi_{\mathrm{d}} - \chi_{\mathrm{c}}$, and expand the CLF derivative to obtain

$$\dot{V}_{\boldsymbol{\varepsilon}} = s(U_{\mathrm{d}}\cos\chi_{\mathrm{r}} - U_{\mathrm{c}}) + eU_{\mathrm{d}}\sin\chi_{\mathrm{r}} + \boldsymbol{\varepsilon}^\top \mathbf{R}_{\mathrm{C}}^\top \mathbf{R}_{\mathrm{B}}\mathbf{H}\mathbf{z}_\nu,$$

where U_{c} can be chosen as

$$U_{\mathrm{c}} = U_{\mathrm{d}}\cos\chi_{\mathrm{r}} + \gamma s \quad (26)$$

with $\gamma > 0$ constant, while χ_{r} can be selected as

$$\chi_{\mathrm{r}} = \arctan\left(-\frac{e}{\triangle_{\mathrm{e}}}\right) \quad (27)$$

with $\triangle_{\mathrm{e}} > 0$ (not necessarily constant), giving

$$\dot{V}_{\boldsymbol{\varepsilon}} = -\gamma s^2 - U_{\mathrm{d}}\frac{e^2}{\sqrt{e^2 + \triangle_{\mathrm{e}}^2}} + \boldsymbol{\varepsilon}^\top \mathbf{R}_{\mathrm{C}}^\top \mathbf{R}_{\mathrm{B}}\mathbf{H}\mathbf{z}_\nu. \quad (28)$$

Consequently

$$\dot{\varpi}_{\mathrm{c}} = \frac{U_{\mathrm{c}}}{|\mathbf{p}_{\mathrm{c}}'|} \tag{29}$$

and

$$\chi_{\mathrm{d}} = \chi_{\mathrm{c}} + \chi_{\mathrm{r}}, \tag{30}$$

with U_{c} as in (26), χ_{c} as in (22), and χ_{r} as in (27). Equations (29) and (30) indicate that the collaborator point continuously leads the ship, while the desired linear velocity of the ship must point at the collaborator's path-tangential, in the direction of forward motion. Specifically, the desired linear velocity $\boldsymbol{\alpha}_{\mathrm{v}}$ must be computed by

$$\begin{aligned}\boldsymbol{\alpha}_{\mathrm{v}} &= \mathbf{R}_{\mathrm{B}}^{\top}\mathbf{R}_{\mathrm{DV}}\boldsymbol{\alpha}_{\mathrm{v,DV}} \\ &= \begin{bmatrix} U_{\mathrm{d}}\cos(\chi_{\mathrm{d}} - \psi) \\ U_{\mathrm{d}}\sin(\chi_{\mathrm{d}} - \psi) \end{bmatrix}.\end{aligned} \tag{31}$$

Then, write the system dynamics of $\boldsymbol{\varepsilon}$ and $\mathbf{z}_{\mathrm{g}}$ as

$$\Sigma_1 : \dot{\boldsymbol{\varepsilon}} = \mathbf{f}_1(t, \boldsymbol{\varepsilon}) + \mathbf{g}_1(t, \boldsymbol{\varepsilon}, \mathbf{z}_{\mathrm{g}})\mathbf{z}_{\mathrm{g}} \tag{32}$$

$$\Sigma_2 : \dot{\mathbf{z}}_{\mathrm{g}} = \mathbf{f}_2(t, \mathbf{z}_{\mathrm{g}}), \tag{33}$$

which is a pure cascade where the control subsystem perturbs the guidance subsystem through the interconnection matrix

$$\mathbf{g}_1(t, \boldsymbol{\varepsilon}, \mathbf{z}_{\mathrm{g}}) = \left[\mathbf{0}_{2\times 1}, \mathbf{R}_{\mathrm{C}}^{\top}\mathbf{R}_{\mathrm{B}}\mathbf{H}\right]. \tag{34}$$

Also, consider the following assumptions

Assumption 3. $\left|\mathbf{p}_{\mathrm{p}}'\right| \in \left[\left|\mathbf{p}_{\mathrm{p}}'\right|_{\min}, \left|\mathbf{p}_{\mathrm{p}}'\right|_{\max}\right] \; \forall \varpi \in \mathbb{R}$

Assumption 4. $\triangle_{\mathrm{e}} \in [\triangle_{\mathrm{e,\,min}}, \infty\rangle$, $\triangle_{\mathrm{e,\,min}} > 0$

Assumption 5. $U_{\mathrm{d}} \in [U_{\mathrm{d,min}}, \infty\rangle$, $U_{\mathrm{d,min}} > 0$

By considering the state vector $\boldsymbol{\xi} = \left[\boldsymbol{\varepsilon}^{\top}, \mathbf{z}_{\mathrm{g}}^{\top}\right]^{\top}$, we arrive at the following proposition

Proposition 6. The equilibrium point $\boldsymbol{\xi} = \mathbf{0}$ is rendered uniformly globally asymptotically and locally exponentially stable (UGAS/ULES) under assumptions (3-5) when applying (18) with the reference signals (17) and (31).

PROOF. Since the origin of system Σ_2 is shown to be UGES in Proposition 2, the origin of the unperturbed system Σ_1 (i.e., when $\mathbf{z}_{\mathrm{g}} = \mathbf{0}$) is trivially shown to be UGAS/ULES by applying standard Lyapunov theory to (20) and (28) (actually, it is uniformly semi-globally exponentially stable, i.e., USGES), and the interconnection term satisfies $\left|\mathbf{g}_1(t, \boldsymbol{\varepsilon}, \mathbf{z}_{\mathrm{g}})\right| = 1$, the proposed result follows directly from Theorem 7 and Lemma 8 of (Panteley *et al.* 1998).

This result means that path following is achieved globally, uniformly in time. Note that the established stability property of Proposition 6 also is known as global κ-exponential stability (Sørdalen and Egeland 1995). Finally, note that by choosing

$$U_{\mathrm{d}} = \kappa\sqrt{e^2 + \triangle_{\mathrm{e}}^2}, \tag{35}$$

where $\kappa > 0$, the origin of $\boldsymbol{\xi}$ can be shown to be UGES. Although very powerful, such a result is clearly not physically achievable due to natural speed limitations. Consequently, Proposition 6 states the best possible stability property achievable for any vehicle.

2.4.3. Step 3: Synchronization Loop Design In this final design step, we determine the required *size* of $\boldsymbol{\alpha}_{\mathrm{v}}$, i.e., U_{d}, such that a ship controlled by (18) with reference signals given by (17) and (31) achieves synchronization with the target point. This synchronization loop design is inspired by the formation control approach of (Breivik *et al.* 2006). Consequently, consider the positive definite and radially unbounded CLF

$$V_{\tilde{\varpi}} = \frac{1}{2}\tilde{\varpi}^2, \tag{36}$$

where

$$\tilde{\varpi} = \varpi_{\mathrm{c}} - \varpi_{\mathrm{t}}, \tag{37}$$

and differentiate the CLF with respect to time to get

$$\begin{aligned}\dot{V}_{\tilde{\varpi}} &= \tilde{\varpi}\dot{\tilde{\varpi}} \\ &= \tilde{\varpi}(\dot{\varpi}_{\mathrm{c}} - \dot{\varpi}_{\mathrm{t}}) \\ &= \tilde{\varpi}(z_{\mathrm{c}} + \alpha_{\mathrm{c}} - \dot{\varpi}_{\mathrm{t}})\end{aligned}$$

where $z_{\mathrm{c}} = \dot{\varpi}_{\mathrm{c}} - \alpha_{\mathrm{c}}$, and α_{c} represents the desired speed of the collaborator when the ship has converged to the path, i.e., when $\boldsymbol{\xi} = \mathbf{0}$. Hence, we have that

$$\dot{V}_{\tilde{\varpi}} = \tilde{\varpi}\left(\frac{U_{\mathrm{d}}}{|\mathbf{p}_{\mathrm{c}}'|} - \frac{U_{\mathrm{t}}}{|\mathbf{p}_{\mathrm{t}}'|}\right) + \tilde{\varpi}z_{\mathrm{c}},$$

which is equal to

$$\dot{V}_{\tilde{\varpi}} = -k_{\tilde{\varpi}}\frac{\tilde{\varpi}^2}{\sqrt{\tilde{\varpi}^2 + \triangle_{\tilde{\varpi}}^2}} + \tilde{\varpi}z_{\mathrm{c}} \tag{38}$$

when choosing

$$U_{\mathrm{d}} = |\mathbf{p}_{\mathrm{c}}'|\left(\frac{U_{\mathrm{t}}}{|\mathbf{p}_{\mathrm{t}}'|} - k_{\tilde{\varpi}}\frac{\tilde{\varpi}}{\sqrt{\tilde{\varpi}^2 + \triangle_{\tilde{\varpi}}^2}}\right), \tag{39}$$

where $\triangle_{\tilde{\varpi}} \in [\triangle_{\tilde{\varpi},\,\min}, \infty\rangle$, $\triangle_{\tilde{\varpi},\,\min} > 0$, and where

$$k_{\tilde{\varpi}} = \sigma\frac{U_{\mathrm{t}}}{|\mathbf{p}_{\mathrm{t}}'|},\ \sigma \in \langle 0, 1] \tag{40}$$

ensures that U_{d} satisfies Assumption 5 by leading to

$$U_{\mathrm{d}} = U_{\mathrm{t}}\left(1 - \sigma\frac{\tilde{\varpi}}{\sqrt{\tilde{\varpi}^2 + \triangle_{\tilde{\varpi}}^2}}\right)\frac{|\mathbf{p}_{\mathrm{c}}'|}{|\mathbf{p}_{\mathrm{t}}'|}. \tag{41}$$

Then, expand z_{c} to get

$$\begin{aligned}z_{\mathrm{c}} &= \dot{\varpi}_{\mathrm{c}} - \alpha_{\mathrm{c}} \\ &= \frac{U_{\mathrm{d}}(\cos\chi_{\mathrm{r}} - 1) + \gamma s}{|\mathbf{p}_{\mathrm{c}}'|}\end{aligned} \tag{42}$$

where

$$(\cos\chi_{\mathrm{r}} - 1) = \frac{\triangle_{\mathrm{e}} - \sqrt{e^2 + \triangle_{\mathrm{e}}^2}}{\sqrt{e^2 + \triangle_{\mathrm{e}}^2}} \tag{43}$$

such that the system dynamics of $\tilde{\varpi}$ and $\boldsymbol{\xi}$ can be written as

$$\Sigma_3 : \dot{\tilde{\varpi}} = f_3(t, \tilde{\varpi}) + \mathbf{g}_3(t, \tilde{\varpi}, \boldsymbol{\xi})^\top \boldsymbol{\xi} \tag{44}$$

$$\Sigma_4 : \dot{\boldsymbol{\xi}} = \mathbf{f}_4(t, \boldsymbol{\xi}), \tag{45}$$

which we recognize as a cascade where the control and guidance subsystems perturb the synchronization subsystem through the interconnection vector

$$\mathbf{g}_3(t, \tilde{\varpi}, \boldsymbol{\xi}) = \frac{1}{|\mathbf{p}_{\mathrm{c}}'|} \left[\gamma, U_{\mathrm{d}} \frac{\triangle_{\mathrm{e}} - \sqrt{e^2 + \triangle_{\mathrm{e}}^2}}{e\sqrt{e^2 + \triangle_{\mathrm{e}}^2}}, \mathbf{0}_{1\times 4} \right]^\top, \tag{46}$$

which is well-defined since

$$\lim_{e \to 0} \frac{\triangle_{\mathrm{e}} - \sqrt{e^2 + \triangle_{\mathrm{e}}^2}}{e\sqrt{e^2 + \triangle_{\mathrm{e}}^2}} = 0. \tag{47}$$

Note that the cascade is pure in the sense that the control subsystem excites the guidance subsystem, which in turn excites the synchronization subsystem.

Considering the state vector $\boldsymbol{\zeta} = \left[\tilde{\varpi}, \boldsymbol{\xi}^\top\right]^\top$, the following theorem can now be stated

Theorem 7. (Guided Motion Control). The equilibrium point $\boldsymbol{\zeta} = \mathbf{0}$ is rendered UGAS/ULES under assumptions (3-4) when applying (18) with reference signals (17) and (31) employing (41).

PROOF. Since the origin of system Σ_4 is shown to be UGAS/ULES in Proposition 6, the origin of the unperturbed system Σ_3 (i.e., when $\boldsymbol{\xi} = \mathbf{0}$) is trivially shown to be UGAS/ULES by applying standard Lyapunov theory to (36) and (38), and the interconnection term satisfies $|\mathbf{g}_3(t, \tilde{\varpi}, \boldsymbol{\xi})| < |\mathbf{p}_{\mathrm{p}}'|_{\min}^{-1} \left(\gamma^2 + \left(\frac{U_{\mathrm{t,max}}}{\triangle_{\mathrm{e,min}}}\right)^2\right)^{1/2}$, the proposed result follows directly from Theorem 7 and Lemma 8 of (Panteley *et al.* 1998).

Consequently, the trajectory tracking problem as stated in (6) has been solved in three design steps.

3. DISCUSSION

What can be gained by the more complex and involved control design and analysis associated with the guided approach? A very important aspect is that the guided scheme readily extends to underactuated ships since it redefines the output space to the linear velocity and heading, where the heading either can be controlled independently (fully actuated case) or must be dedicated to control the direction of the linear velocity (underactuated case). Hence, leaving the control subsystem unchanged, a basic redesign of the guidance and synchronization subsystems is all that is required. In fact, for straight-line paths no redesign is necessary if the desired heading is assigned as the desired orientation of the linear velocity. Such extendability also suggests a unified motion controller capable of handling a ship seamlessly between its actuation regimes. Furthermore, the servoed approach does not exploit any available path information, by only considering the target point. A consequence is degraded transient convergence behavior, which becomes erratic and unnatural. This aspect contrasts starkly with the guided approach, where a collaborator point guides the ship gently toward the path. In real life, this difference affects wear and tear of the actuators, as well as fuel consumption. Additionally, the commanded control input of the servoed scheme grows unbounded with the ship-target error, rendering the ship-path system unstable if the ship cannot keep up with the target. This problem does not affect the guided approach, whose commanded control input saturates at a tunable threshold, rendering the ship-path system stable even though the ship-target system may become unstable. Such a path following feature distinguishes the guided approach, and probably extends well to real-life demands of limited propulsion capacity. The stability properties of Theorems 1 and 7 also reflect this reasoning, where the former looks more impressive, but where the latter represent the physically attainable alternative.

4. CONCLUSIONS

This paper treated the topic of motion control for fully actuated ships in a trajectory tracking scenario by developing and discussing two fundamentally different motion control concepts. The servoed concept corresponds to standard DP controllers found in the established ship control literature, while the guided concept represents a novel scheme inspired by research within missile guidance, path following, and formation control.

REFERENCES

Breivik, M. and T. I. Fossen (2005). Guidance-based path following in 2D and 3D. In: *Proceedings of the 44th IEEE CDC, Seville, Spain.*

Breivik, M., M. V. Subbotin and T. I. Fossen (2006). Kinematic aspects of guided formation control in 2D. In: *Group Coordination and Cooperative Control* (K. Y. Pettersen, J. T. Gravdahl and H. Nijmeijer, Eds.). pp. 55–74. Springer-Verlag.

Fossen, T. I. (2002). *Marine Control Systems: Guidance, Navigation and Control of Ships, Rigs and Underwater Vehicles*. Marine Cybernetics.

Krstić, M., I. Kanellakopoulos and P. V. Kokotović (1995). *Nonlinear and Adaptive Control Design*. John Wiley & Sons Inc.

Panteley, E., E. Lefeber, A. Loría and H. Nijmeijer (1998). Exponential tracking of a mobile car using a cascaded approach. In: *Proceedings of the IFAC Workshop on Motion Control, Grenoble, France*.

Shneydor, N. A. (1998). *Missile Guidance and Pursuit: Kinematics, Dynamics and Control*. Horwood Publishing.

Sørdalen, O. J. and O. Egeland (1995). Exponential stabilization of nonholonomic chained systems. *IEEE Transactions on Automatic Control* **40**(1), 35–49.

F. Ship Formation Control: A Guided Leader-Follower Approach

Ship Formation Control: A Guided Leader-Follower Approach ⋆

Morten Breivik * **Vegard E. Hovstein** ** **Thor I. Fossen** *

* *{Centre for Ships and Ocean Structures, Department of Engineering Cybernetics}, Norwegian University of Science and Technology, NO-7491 Trondheim, Norway.*
E-mails: {morten.breivik, fossen}@ieee.org
** *Maritime Robotics, NO-7010, Trondheim, Norway.*
E-mail: vegard.hovstein@maritimerobotics.com

Abstract: This paper considers the topic of formation control for fully actuated ships. Within a leader-follower framework, a so-called guided formation control scheme is developed by means of a modular design procedure inspired by concepts from integrator backstepping and cascade theory. Control, guidance, and synchronization laws ensure that each individual formation member is able to converge to and maintain its assigned formation position such that the overall formation is able to assemble and maintain itself while traversing an arbitrary, regularly parameterized path that is chosen by a formation control designer. A key novelty of the approach is the derivation of guidance laws that are applicable to off-path traversing of curved paths. The helmsman-like transient motion behavior associated with the scheme is illustrated through a computer simulation involving three fully actuated ships.

1. INTRODUCTION

Formation control technology plays an increasingly important role for commercial, scientific, and military purposes. Today, relevant applications can be found everywhere; at sea, on land, in the air, and in space. At sea, the subject of formation control has been important for centuries. In old times, groups of warships had to be controlled during naval battles. In both world wars, it was pivotal for merchant ships to travel in convoys. Current applications include underway ship replenishment, towing of large structures at sea, and surveying of hydrocarbons. In the future, more sophisticated concepts will emerge, facilitated by new sensor, communication, and computer technology. Formations will become increasingly autonomous, consisting of fully autonomous marine craft that must operate in so-called dirty, dull, and dangerous environments. The vessels can act as scouts, nodes in communication and sensor networks, or elements within battlegroups. Ultimately, multi-vehicle operations render possible tasks that no single vehicle can solve, as well as increase operational robustness toward individual failures.

A main pillar in the Norwegian economy is oil and gas production. Hence, a principal motivation for Norwegian research efforts concerns the commercial offshore market, where formation control technology is expected to play a key role in future hydrocarbon exploration and exploitation. Such technology can contribute to reduced personnel costs, increased personnel safety, extended weather window (of operations), increased operational precision, and more environmentally friendly operations.

⋆ This work was supported by the Norwegian Research Council through the Centre for Ships and Ocean Structures and through the MAROFF grant 175977: Unmanned Surface Vehicle.

1.1 Previous Work

Research within formation control theory can be divided into two main categories; the analytic and the algorithmic. The analytic category represents those approaches that are most readily analyzed by mathematical tools, and include both leader-follower methods and virtual structure schemes. Conversely, the algorithmic category represents those approaches that are not easily analyzed mathematically, but have to be numerically simulated by means of a computer in order to investigate their emergent behavior. So-called behavior-based methods belong to this category.

During recent years, the marine control community has focused considerably on formation control concepts. Most of the work seems to have been performed within a leader-follower framework, e.g., in (Encarnação and Pascoal 2001), where an autonomous underwater vehicle (AUV) tracks the planar projection of a surface craft onto its nominal path, while the surface craft follows its own path at sea; in (Skjetne *et al.* 2002), where formation control of multiple so-called maneuvering systems yields a robust scheme with dynamic adjustment to the weakest link of the formation; in (Lapierre *et al.* 2003), where coordination of two AUVs is achieved by augmenting a path parameter synchronization algorithm to the controller of the follower vehicle; in (Aguiar *et al.* 2006), where multiple AUVs are coordinated along spatial paths despite communication constraints; in (Kyrkjebø and Pettersen 2006), where surface vessels are synchronized through a leader-follower scheme; and in (Pavlov *et al.* 2007), where formation control of underactuated surface vessels moving along straight lines are considered. Work related to virtual structures is reported in (Fiorelli *et al.* 2004), where cooperative control of AUVs is achieved through the use of virtual leaders and artificial potentials, considering the formation as a

rigid-body geometric structure; and in (Ihle *et al.* 2005), where the approach is rooted in analytical mechanics for multi-body dynamics, facilitating a flexible and robust formation control scheme where the geometric constraints of a virtual structure are enforced by feedback control. Also, research in the vein of behavioral methods can be found in (Arrichiello *et al.* 2006), where marine surface vessels move in formation while avoiding collisions with environmental obstacles. Finally, the anthologies (Kumar *et al.* 2005) and (Pettersen *et al.* 2006) report state-of-the-art concepts for a broad number of formation control scenarios.

1.2 Main Contribution

The main contribution of this paper is a concept named *guided formation control*. Developed within a leader-follower framework, the scheme is based on principles from integrator backstepping design (Krstić *et al.* 1995) as well as theory for nonlinear time-varying cascades (Panteley *et al.* 1998). The proposed design procedure for each individual ship is completely modular, and consists of three distinct steps where control, guidance, and synchronization laws are sequentially derived. A key novelty of the approach is the derivation of the required guidance laws for off-path traversing of curved paths. These laws also ensure that each formation member displays helmsman-like motion behavior during the transient formation assembly phase. The guided approach can be used with both centralized and decentralized formation control strategies, and is illustrated through a decentralized strategy where no inter-vessel communication is required.

2. GUIDED FORMATION CONTROL

In what follows, when considering a vector $\mathbf{x}$ that is parameterized by a time-varying scalar variable ϖ (i.e., $\mathbf{x}(\varpi(t))$), the time derivative of $\mathbf{x}$ is denoted $\dot{\mathbf{x}}$, while the partial derivative with respect to ϖ is denoted $\mathbf{x}' = \frac{\partial \mathbf{x}}{\partial \varpi}$. Also, $|\cdot|$ represents both the Euclidean vector norm and the induced matrix norm.

2.1 Ship Dynamic Model

A 3 degree-of-freedom (DOF) dynamic model of the horizontal surge, sway, and yaw modes can be found in (Fossen 2002), and consists of the kinematics

$$\dot{\boldsymbol{\eta}} = \mathbf{R}(\psi)\boldsymbol{\nu}, \tag{1}$$

and the kinetics

$$\mathbf{M}\dot{\boldsymbol{\nu}} + \mathbf{C}(\boldsymbol{\nu})\boldsymbol{\nu} + \mathbf{D}(\boldsymbol{\nu})\boldsymbol{\nu} = \boldsymbol{\tau} + \mathbf{R}(\psi)^\top \mathbf{b}, \tag{2}$$

where $\boldsymbol{\eta} \triangleq [x, y, \psi]^\top \in \mathbb{R}^3$ represents the earth-fixed position and heading; $\boldsymbol{\nu} \triangleq [u, v, r]^\top \in \mathbb{R}^3$ represents the vessel-fixed velocity; $\mathbf{R}(\psi) \in SO(3)$ is the transformation matrix

$$\mathbf{R}(\psi) \triangleq \begin{bmatrix} \cos\psi & -\sin\psi & 0 \\ \sin\psi & \cos\psi & 0 \\ 0 & 0 & 1 \end{bmatrix} \tag{3}$$

that transforms from the vessel-fixed BODY frame to the earth-fixed NED frame; $\mathbf{M}$ is the inertia matrix; $\mathbf{C}(\boldsymbol{\nu})$ is the centrifugal and coriolis matrix; while $\mathbf{D}(\boldsymbol{\nu})$ is the hydrodynamic damping matrix. The system matrices satisfy the properties $\mathbf{M} = \mathbf{M}^\top > 0$, $\mathbf{C} = -\mathbf{C}^\top$ and $\mathbf{D} > 0$. The vessel-fixed propulsion forces and moment is represented by $\boldsymbol{\tau} \triangleq [\tau_{\mathrm{X}}, \tau_{\mathrm{Y}}, \tau_{\mathrm{N}}]^\top \in \mathbb{R}^3$, corresponding to a fully actuated ship. Full actuation means that all 3 DOFs can be controlled independently at the same time, i.e., the linear velocity is independent of the vessel heading. Finally, $\mathbf{b}$ represents low-frequency, earth-fixed environmental disturbances.

2.2 Formation Control Scenario

This work considers formation control within a leader-follower framework, where a formation structure is defined relative to a virtual formation leader. It is assumed that the formation control designer can choose both the path to be traversed by the leader, the temporal motion of the leader, as well as the geometric formation structure defined relative to the leader.

Consequently, consider a planar path continuously parameterized by a scalar variable $\varpi \in \mathbb{R}$, such that the position of a point belonging to the path is represented by $\mathbf{p}_{\mathrm{p}}(\varpi) \in \mathbb{R}^2$. Thus, the path is a one-dimensional manifold that can be expressed by the set

$$\mathcal{P} \triangleq \left\{ \mathbf{p} \in \mathbb{R}^2 \mid \mathbf{p} = \mathbf{p}_{\mathrm{p}}(\varpi)\ \forall \varpi \in \mathbb{R} \right\}. \tag{4}$$

Then, represent the virtual formation leader by $\mathbf{p}_{\mathrm{l}}(t) \triangleq \mathbf{p}_{\mathrm{p}}(\varpi_{\mathrm{l}}(t))$. The leader traverses the path by adhering to the speed profile $U_{\mathrm{l}}(\varpi_{\mathrm{l}})$, implemented through

$$\dot{\varpi}_{\mathrm{l}} = \frac{U_{\mathrm{l}}(\varpi_{\mathrm{l}})}{\left|\mathbf{p}'_{\mathrm{p}}(\varpi_{\mathrm{l}})\right|}, \tag{5}$$

since $|\dot{\mathbf{p}}_{\mathrm{l}}| = \left|\mathbf{p}'_{\mathrm{p}}(\varpi_{\mathrm{l}})\right| \dot{\varpi}_{\mathrm{l}} = U_{\mathrm{l}}(\varpi_{\mathrm{l}})$, where $U_{\mathrm{l}}(\varpi_{\mathrm{l}}) \in [U_{\mathrm{l,min}}, U_{\mathrm{l,max}}]$, $U_{\mathrm{l,min}} > 0$ (non-negative by definition).

Furthermore, consider a formation consisting of n members, each uniquely identified through the index set $\mathcal{I} = \{1, ..., n\}$. The assigned formation position for member i is represented by $\mathbf{p}_{\mathrm{f,i}}(t)$, which is related to the formation leader through a chosen geometric assignment (defined in local, path-tangential coordinates relative to the leader). By design, we ensure that no formation positions are identical, i.e., $\mathbf{p}_{\mathrm{f,i}} \neq \mathbf{p}_{\mathrm{f,j}}\ \forall i \neq j$, where $i, j \in \mathcal{I}$.

Problem Statement The formation control problem for fully actuated ships can be stated by

$$\lim_{t\to\infty} \left(\boldsymbol{\eta}_{\mathrm{i}}(t) - \boldsymbol{\eta}_{\mathrm{f,i}}(t)\right) = \mathbf{0}\ \forall i \in \mathcal{I}, \tag{6}$$

where $\boldsymbol{\eta}_{\mathrm{i}}(t)$ represents the ith formation member, and $\boldsymbol{\eta}_{\mathrm{f,i}}(t) \triangleq \left[\mathbf{p}_{\mathrm{f,i}}^\top(t), \psi_{\mathrm{d,i}}(t)\right]^\top \in \mathbb{R}^3$, where $\psi_{\mathrm{d,i}}(t)$ can be any arbitrary desirable heading (typically the path-tangential orientation at $\mathbf{p}_{\mathrm{l}}(t)$) satisfying some auxiliary task objective. See Figure 1 for an illustration of the formation control concept under consideration.

2.3 Motion Control of Individual Formation Members

This section develops the control, guidance and synchronization laws that each formation member must employ in order to converge to its assigned position in the formation. The underlying concept is adapted from (Breivik *et al.* 2006), and entails a modular three-step, backstepping-inspired and cascaded-based design procedure.

Step 1: Control Loop Design Since the position of a vessel can be controlled through its linear velocity, we redefine the output space from the nominal 3 DOF position and heading to the 3 DOF linear velocity and heading (Fossen *et al.* 2003). Consequently, consider the positive definite and radially unbounded Control Lyapunov Function (CLF)

$$V_{\mathrm{g}} \triangleq \frac{1}{2}(z_\psi^2 + \mathbf{z}_\nu^\top \mathbf{M}\mathbf{z}_\nu + \tilde{\mathbf{b}}^\top \mathbf{\Gamma}^{-1}\tilde{\mathbf{b}}) \tag{7}$$

where we have

$$z_\psi \triangleq \psi - \psi_{\mathrm{d}} \tag{8}$$

and

$$\mathbf{z}_\nu \triangleq \boldsymbol{\nu} - \boldsymbol{\alpha}, \tag{9}$$

where $\boldsymbol{\alpha} \triangleq [\alpha_{\mathrm{u}}, \alpha_{\mathrm{v}}, \alpha_{\mathrm{r}}]^\top \in \mathbb{R}^3$ is a so-called vector of stabilizing functions (virtual inputs that become reference signals) yet to be designed. Also,

$$\tilde{\mathbf{b}} \triangleq \hat{\mathbf{b}} - \mathbf{b} \tag{10}$$

represents an adaptation error where $\hat{\mathbf{b}}$ is the estimate of $\mathbf{b}$, and by assumption $\dot{\mathbf{b}} = \mathbf{0}$. Finally, $\mathbf{\Gamma} = \mathbf{\Gamma}^\top > 0$ is the so-called adaptation gain matrix.

Subsequently, differentiate the CLF with respect to time to obtain

$$\begin{aligned}\dot{V}_{\mathrm{g}} &= z_\psi \dot{z}_\psi + \mathbf{z}_\nu^\top \mathbf{M}\dot{\mathbf{z}}_\nu + \tilde{\mathbf{b}}^\top \mathbf{\Gamma}^{-1}\dot{\tilde{\mathbf{b}}} \\ &= z_\psi(\dot{\psi} - \dot{\psi}_{\mathrm{d}}) + \mathbf{z}_\nu^\top \mathbf{M}(\dot{\boldsymbol{\nu}} - \dot{\boldsymbol{\alpha}}) + \tilde{\mathbf{b}}^\top \mathbf{\Gamma}^{-1}\dot{\hat{\mathbf{b}}},\end{aligned}$$

which is equal to

$$\dot{V}_{\mathrm{g}} = z_\psi(\mathbf{h}^\top \dot{\boldsymbol{\eta}} - \dot{\psi}_{\mathrm{d}}) + \mathbf{z}_\nu^\top(\mathbf{M}\dot{\boldsymbol{\nu}} - \mathbf{M}\dot{\boldsymbol{\alpha}}) + \tilde{\mathbf{b}}^\top \mathbf{\Gamma}^{-1}\dot{\hat{\mathbf{b}}}$$

by introducing

$$\mathbf{h} \triangleq [0, 0, 1]^\top. \tag{11}$$

Furthermore, recognizing that $\mathbf{h}^\top \dot{\boldsymbol{\eta}} = \mathbf{h}^\top \mathbf{R}\boldsymbol{\nu} = \mathbf{h}^\top \boldsymbol{\nu}$ and $\boldsymbol{\nu} = \mathbf{z}_\nu + \boldsymbol{\alpha}$, we obtain

$$\begin{aligned}\dot{V}_{\mathrm{g}} = z_\psi(\mathbf{h}^\top \boldsymbol{\alpha} - \dot{\psi}_{\mathrm{d}}) + \mathbf{z}_\nu^\top(\boldsymbol{\tau} - \mathbf{C}\boldsymbol{\nu} - \mathbf{D}\boldsymbol{\nu} - \mathbf{M}\dot{\boldsymbol{\alpha}}) + \\ \mathbf{z}_\nu^\top(\mathbf{R}^\top \mathbf{b} + \mathbf{h}z_\psi) + \tilde{\mathbf{b}}^\top \mathbf{\Gamma}^{-1}\dot{\hat{\mathbf{b}}},\end{aligned}$$

which results in

$$\begin{aligned}\dot{V}_{\mathrm{g}} = -k_\psi z_\psi^2 - \mathbf{z}_\nu^\top \mathbf{C}\mathbf{z}_\nu - \mathbf{z}_\nu^\top \mathbf{D}\mathbf{z}_\nu + \\ \mathbf{z}_\nu^\top(\boldsymbol{\tau} - \mathbf{C}\boldsymbol{\alpha} - \mathbf{D}\boldsymbol{\alpha} - \mathbf{M}\dot{\boldsymbol{\alpha}}) + \\ \mathbf{z}_\nu^\top(\mathbf{R}^\top \hat{\mathbf{b}} + \mathbf{h}z_\psi) + \tilde{\mathbf{b}}^\top \mathbf{\Gamma}^{-1}(\dot{\hat{\mathbf{b}}} - \mathbf{\Gamma}\mathbf{R}\mathbf{z}_\nu)\end{aligned}$$

since $\mathbf{b} = \hat{\mathbf{b}} - \tilde{\mathbf{b}}$, and when choosing the virtual input $\mathbf{h}^\top \boldsymbol{\alpha} = \alpha_{\mathrm{r}}$ as

$$\alpha_{\mathrm{r}} = \dot{\psi}_{\mathrm{d}} - k_\psi z_\psi, \tag{12}$$

where $k_\psi > 0$ is a constant. Since $\mathbf{z}_\nu^\top \mathbf{C}\mathbf{z}_\nu = 0$, by selecting the control input

$$\boldsymbol{\tau} = \mathbf{M}\dot{\boldsymbol{\alpha}} + \mathbf{C}\boldsymbol{\alpha} + \mathbf{D}\boldsymbol{\alpha} - \mathbf{R}^\top \hat{\mathbf{b}} - \mathbf{h}z_\psi - \mathbf{K}_\nu \mathbf{z}_\nu \tag{13}$$

where $\mathbf{K}_\nu = \mathbf{K}_\nu^\top > 0$ is a constant matrix, and by choosing the disturbance adaptation update law

$$\dot{\hat{\mathbf{b}}} = \mathbf{\Gamma}\mathbf{R}\mathbf{z}_\nu, \tag{14}$$

we finally obtain the negative semi-definite

$$\dot{V}_{\mathrm{g}} = -k_\psi z_\psi^2 - \mathbf{z}_\nu^\top(\mathbf{D} + \mathbf{K}_\nu)\mathbf{z}_\nu. \tag{15}$$

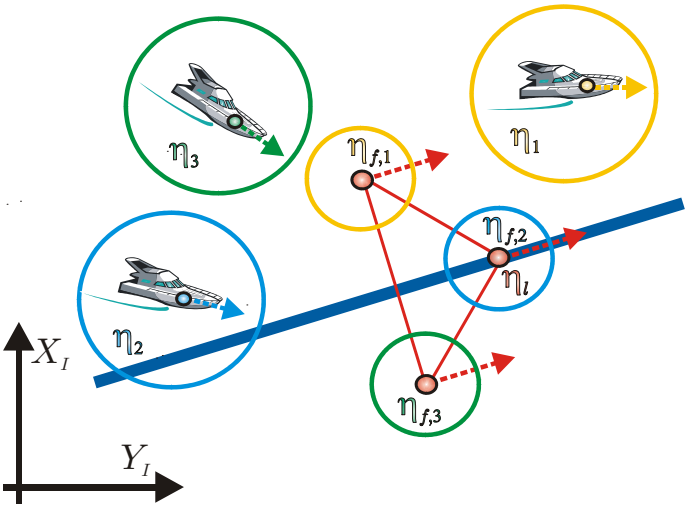

Fig. 1. A formation control scenario where 3 ships assemble and maintain a V-shaped formation along a straight-line path.

Considering the state vector $\mathbf{z}_{\mathrm{g}} \triangleq \left[z_\psi, \mathbf{z}_\nu^\top, \tilde{\mathbf{b}}^\top\right]^\top$, the following proposition can now be stated:

Proposition 1. The equilibrium point $\mathbf{z}_{\mathrm{g}} = \mathbf{0}$ is rendered uniformly globally asymptotically and locally exponentially stable (UGAS/ULES) by adhering to (12), (13) and (14) under the assumption that $\boldsymbol{\alpha}$ and $\dot{\boldsymbol{\alpha}}$ are uniformly bounded.

Proof. The proposed result follows by straightforward application of Theorem 1 in (Fossen *et al.* 2001). ■

Note that the stability property of Proposition 1 is known as global κ-exponential stability, as originally defined in (Sørdalen and Egeland 1995). In fact, global κ-exponential stability is the best stability property a physical system like a ship can achieve due to the limitations on its propulsion system. Also, note that the developed controller cannot achieve anything meaningful motionwise unless it is fed sensible reference signals, i.e., unless $\boldsymbol{\alpha}_{\mathrm{v}} \triangleq [\alpha_{\mathrm{u}}, \alpha_{\mathrm{v}}]^\top \in \mathbb{R}^2$ is purposefully defined. This task is the responsibility of the final two design steps.

Step 2: Guidance Loop Design We now design the required *orientation* of $\boldsymbol{\alpha}_{\mathrm{v}}$ such that a ship controlled by (13) and (14) attains its assigned formation position relative to the path (even though it may not be synchronized with the leader). This part contributes a key novelty to the scheme by deriving guidance laws that facilitate (singularity-free) off-path traversing of curved paths.

Consequently, consider the positive definite and radially unbounded CLF

$$V_{\tilde{\varepsilon}} \triangleq \frac{1}{2}\tilde{\boldsymbol{\varepsilon}}^\top \tilde{\boldsymbol{\varepsilon}}, \tag{16}$$

with

$$\tilde{\boldsymbol{\varepsilon}} \triangleq \boldsymbol{\varepsilon} - \boldsymbol{\varepsilon}_{\mathrm{f}} \tag{17}$$

and

$$\boldsymbol{\varepsilon} \triangleq \mathbf{R}_{\mathrm{C}}^\top(\mathbf{p} - \mathbf{p}_{\mathrm{c}}), \tag{18}$$

where $\mathbf{p}_{\mathrm{c}} \triangleq \mathbf{p}_{\mathrm{p}}(\varpi_{\mathrm{c}})$ represents a (virtual) *collaborator* point that cooperates with the ship as an intermediate path

attractor, such that the ship can converge to its assigned formation position relative to the path $\boldsymbol{\varepsilon}_\mathrm{f}$ irrespective of whether it has synchronized with the formation leader or not. Furthermore, the path-tangential reference frame at $\mathbf{p}_\mathrm{c}$ is termed the COLLABORATOR frame (**C**). To arrive at **C**, the INERTIAL frame (**I**) must be positively rotated an angle

$$\chi_\mathrm{c} \triangleq \arctan\left(\frac{y'_\mathrm{p}(\varpi_\mathrm{c})}{x'_\mathrm{p}(\varpi_\mathrm{c})}\right), \tag{19}$$

which can be represented by the rotation matrix

$$\mathbf{R}_\mathrm{C} \triangleq \begin{bmatrix} \cos\chi_\mathrm{c} & -\sin\chi_\mathrm{c} \\ \sin\chi_\mathrm{c} & \cos\chi_\mathrm{c} \end{bmatrix}, \tag{20}$$

$\mathbf{R}_\mathrm{C} \in SO(2)$. Hence, equation (18) represents the error vector between the ship and its collaborator decomposed in **C**. The local coordinates $\boldsymbol{\varepsilon} \triangleq [s, e]^\top$ consist of the *along-track error* s and the *cross-track error* e. By driving $\tilde{\boldsymbol{\varepsilon}}$ to zero, $\boldsymbol{\varepsilon}$ becomes equal to $\boldsymbol{\varepsilon}_\mathrm{f}$ such that the ship attains its assigned path-relative formation position. It is assumed that $\boldsymbol{\varepsilon}_\mathrm{f}$, $\dot{\boldsymbol{\varepsilon}}_\mathrm{f}$ and $\ddot{\boldsymbol{\varepsilon}}_\mathrm{f}$ are uniformly bounded, and typically $\dot{\boldsymbol{\varepsilon}}_\mathrm{f} = \ddot{\boldsymbol{\varepsilon}}_\mathrm{f} = \mathbf{0}$.

Now, differentiate the CLF in (16) along the trajectories of $\tilde{\boldsymbol{\varepsilon}}$ to obtain

$$\begin{aligned}
\dot{V}_{\tilde{\varepsilon}} &= \tilde{\boldsymbol{\varepsilon}}^\top \dot{\tilde{\boldsymbol{\varepsilon}}} \\
&= \tilde{\boldsymbol{\varepsilon}}^\top (\mathbf{S}_\mathrm{C}^\top \mathbf{R}_\mathrm{C}^\top (\mathbf{p} - \mathbf{p}_\mathrm{c}) + \mathbf{R}_\mathrm{C}^\top (\dot{\mathbf{p}} - \dot{\mathbf{p}}_\mathrm{c}) - \dot{\boldsymbol{\varepsilon}}_\mathrm{f}) \\
&= \tilde{\boldsymbol{\varepsilon}}^\top \left(\mathbf{S}_\mathrm{C}^\top \boldsymbol{\varepsilon} + \mathbf{R}_\mathrm{C}^\top \mathbf{v}^\mathrm{I} - \mathbf{v}_\mathrm{c}^\mathrm{C} - \dot{\boldsymbol{\varepsilon}}_\mathrm{f}\right) \\
&= \tilde{\boldsymbol{\varepsilon}}^\top \left(\mathbf{S}_\mathrm{C}^\top \tilde{\boldsymbol{\varepsilon}} + \mathbf{S}_\mathrm{C}^\top \boldsymbol{\varepsilon}_\mathrm{f} + \mathbf{R}_\mathrm{C}^\top \mathbf{v}^\mathrm{I} - \mathbf{v}_\mathrm{c}^\mathrm{C} - \dot{\boldsymbol{\varepsilon}}_\mathrm{f}\right) \\
&= \tilde{\boldsymbol{\varepsilon}}^\top \left(\mathbf{R}_\mathrm{C}^\top \mathbf{v}^\mathrm{I} - \mathbf{v}_\mathrm{c}^\mathrm{C} + \mathbf{S}_\mathrm{C}^\top \boldsymbol{\varepsilon}_\mathrm{f} - \dot{\boldsymbol{\varepsilon}}_\mathrm{f}\right),
\end{aligned}$$

where $\dot{\mathbf{R}}_\mathrm{C} = \mathbf{R}_\mathrm{C}\mathbf{S}_\mathrm{C}$ with $\mathbf{S}_\mathrm{C} = -\mathbf{S}_\mathrm{C}^\top \Rightarrow \tilde{\boldsymbol{\varepsilon}}^\top \mathbf{S}_\mathrm{C}^\top \tilde{\boldsymbol{\varepsilon}} = 0$, $\mathbf{v}^\mathrm{I} \triangleq \dot{\mathbf{p}}$ represents the linear velocity of the ship decomposed in **I**, and $\mathbf{v}_\mathrm{c}^\mathrm{C} \triangleq \mathbf{R}_\mathrm{C}^\top \dot{\mathbf{p}}_\mathrm{c} = [U_\mathrm{c}, 0]^\top$ ($U_\mathrm{c} = |\dot{\mathbf{p}}_\mathrm{c}|$) represents the linear velocity of the collaborator decomposed in **C**. Furthermore,

$$\begin{aligned}
\dot{V}_{\tilde{\varepsilon}} = \tilde{\boldsymbol{\varepsilon}}^\top &\left(\mathbf{R}_\mathrm{C}^\top \boldsymbol{\alpha}_\mathrm{v}^\mathrm{I} - \mathbf{v}_\mathrm{c}^\mathrm{C} + \mathbf{S}_\mathrm{C}^\top \boldsymbol{\varepsilon}_\mathrm{f} - \dot{\boldsymbol{\varepsilon}}_\mathrm{f}\right) + \\
&\tilde{\boldsymbol{\varepsilon}}^\top \mathbf{R}_\mathrm{C}^\top \mathbf{z}_\mathrm{v}^\mathrm{I}
\end{aligned} \tag{21}$$

when we employ $\mathbf{z}_\mathrm{v}^\mathrm{I} \triangleq \mathbf{v}^\mathrm{I} - \boldsymbol{\alpha}_\mathrm{v}^\mathrm{I}$, where $\boldsymbol{\alpha}_\mathrm{v}^\mathrm{I}$ represents the desired (ideal) linear velocity of the ship decomposed in **I**.

We now introduce a (virtual) *mediator* point located at $\mathbf{p}_\mathrm{m}$, which is defined such that when the ship converges to its assigned formation position relative to the path, the mediator converges to the path. Hence, $\boldsymbol{\varepsilon}_\mathrm{m} = \tilde{\boldsymbol{\varepsilon}}$. The relationship between the ship, the mediator, and the collaborator is illustrated in Figure 2, and can be expressed by

$$\begin{aligned}
\boldsymbol{\varepsilon} &= \boldsymbol{\varepsilon}_\mathrm{m} + \boldsymbol{\varepsilon}_\mathrm{f} && (22)\\
&= \mathbf{R}_\mathrm{C}^\top (\mathbf{p}_\mathrm{m} - \mathbf{p}_\mathrm{c}) + \boldsymbol{\varepsilon}_\mathrm{f} && (23)\\
&= \mathbf{R}_\mathrm{C}^\top (\mathbf{p} - \mathbf{p}_\mathrm{c}) && (24)
\end{aligned}$$

such that

$$\mathbf{p}_\mathrm{m} = \mathbf{p} - \mathbf{R}_\mathrm{C}\boldsymbol{\varepsilon}_\mathrm{f}, \tag{25}$$

which is used to compute (and continuously update) the location of the mediator.

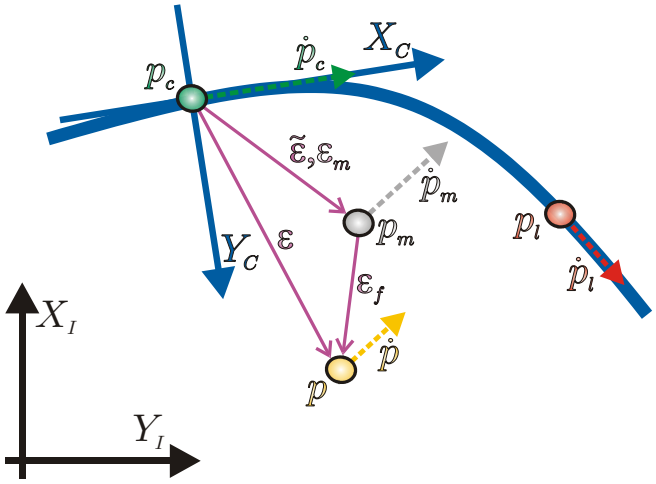

Fig. 2. The geometric relationship between the formation member ($\mathbf{p}$; orange), the mediator ($\mathbf{p}_\mathrm{m}$; grey), the collaborator ($\mathbf{p}_\mathrm{c}$; green), and the virtual leader ($\mathbf{p}_\mathrm{l}$; red). All the involved participants are virtual, except the formation member (ship). The role of the mediator is to facilitate (singularity-free) off-path traversing of curved paths.

Hence,

$$\dot{\mathbf{p}}_\mathrm{m} = \dot{\mathbf{p}} - \dot{\mathbf{R}}_\mathrm{C}\boldsymbol{\varepsilon}_\mathrm{f} - \mathbf{R}_\mathrm{C}\dot{\boldsymbol{\varepsilon}}_\mathrm{f},$$

which is equal to

$$\mathbf{v}_\mathrm{m}^\mathrm{I} = \mathbf{v}^\mathrm{I} - \mathbf{R}_\mathrm{C}\mathbf{S}_\mathrm{C}\boldsymbol{\varepsilon}_\mathrm{f} - \mathbf{R}_\mathrm{C}\dot{\boldsymbol{\varepsilon}}_\mathrm{f}, \tag{26}$$

entailing that

$$\boldsymbol{\alpha}_\mathrm{v,m}^\mathrm{I} = \boldsymbol{\alpha}_\mathrm{v}^\mathrm{I} - \mathbf{R}_\mathrm{C}\mathbf{S}_\mathrm{C}\boldsymbol{\varepsilon}_\mathrm{f} - \mathbf{R}_\mathrm{C}\dot{\boldsymbol{\varepsilon}}_\mathrm{f}, \tag{27}$$

or rather, that

$$\boldsymbol{\alpha}_\mathrm{v}^\mathrm{I} = \boldsymbol{\alpha}_\mathrm{v,m}^\mathrm{I} + \mathbf{R}_\mathrm{C}(\mathbf{S}_\mathrm{C}\boldsymbol{\varepsilon}_\mathrm{f} + \dot{\boldsymbol{\varepsilon}}_\mathrm{f}), \tag{28}$$

which we duly insert into (21) to achieve

$$\dot{V}_{\tilde{\varepsilon}} = \tilde{\boldsymbol{\varepsilon}}^\top \left(\mathbf{R}_\mathrm{C}^\top \boldsymbol{\alpha}_\mathrm{v,m}^\mathrm{I} - \mathbf{v}_\mathrm{c}^\mathrm{C}\right) + \tilde{\boldsymbol{\varepsilon}}^\top \mathbf{R}_\mathrm{C}^\top \mathbf{z}_\mathrm{v}^\mathrm{I} \tag{29}$$

since $\mathbf{S}_\mathrm{C} = -\mathbf{S}_\mathrm{C}^\top$. We note that $\boldsymbol{\alpha}_\mathrm{v,m}^\mathrm{I}$ represents the desired linear velocity of the mediator (that corresponds to the desired linear velocity of the ship) decomposed in **I**.

Subsequently, define $\boldsymbol{\alpha}_\mathrm{v,m}^\mathrm{I} \triangleq \mathbf{R}_\mathrm{DV}\boldsymbol{\alpha}_\mathrm{v,m}^\mathrm{DV}$, where $\boldsymbol{\alpha}_\mathrm{v,m}^\mathrm{DV} = [U_\mathrm{d,m}, 0]^\top$ ($U_\mathrm{d,m} = |\boldsymbol{\alpha}_\mathrm{v,m}^\mathrm{I}|$) represents the desired linear velocity of the mediator decomposed in a DESIRED VELOCITY frame (**DV**), i.e., decomposed along the desired velocity itself. Thus,

$$\begin{aligned}
\dot{V}_{\tilde{\varepsilon}} &= \tilde{\boldsymbol{\varepsilon}}^\top \left(\mathbf{R}_\mathrm{C}^\top \mathbf{R}_\mathrm{DV} \boldsymbol{\alpha}_\mathrm{v,m}^\mathrm{DV} - \mathbf{v}_\mathrm{c}^\mathrm{C}\right) + \tilde{\boldsymbol{\varepsilon}}^\top \mathbf{R}_\mathrm{C}^\top \mathbf{z}_\mathrm{v}^\mathrm{I} \\
&= \tilde{\boldsymbol{\varepsilon}}^\top \left(\mathbf{R}_\mathrm{R} \boldsymbol{\alpha}_\mathrm{v,m}^\mathrm{DV} - \mathbf{v}_\mathrm{c}^\mathrm{C}\right) + \tilde{\boldsymbol{\varepsilon}}^\top \mathbf{R}_\mathrm{C}^\top \mathbf{z}_\mathrm{v}^\mathrm{I}
\end{aligned}$$

where $\mathbf{R}_\mathrm{C}^\top \mathbf{R}_\mathrm{DV} \triangleq \mathbf{R}_\mathrm{R}$ represents the relative orientation between **C** and **DV**. Denote the corresponding angular difference by $\chi_\mathrm{r} \triangleq \chi_\mathrm{d} - \chi_\mathrm{c}$, and expand the CLF derivative to obtain

$$\dot{V}_{\tilde{\varepsilon}} = \tilde{s}(U_\mathrm{d,m}\cos\chi_\mathrm{r} - U_\mathrm{c}) + \tilde{e}U_\mathrm{d,m}\sin\chi_\mathrm{r} + \tilde{\boldsymbol{\varepsilon}}^\top \mathbf{R}_\mathrm{C}^\top \mathbf{z}_\mathrm{v}^\mathrm{I}.$$

Hence, U_c and χ_r can be considered as virtual inputs for driving $\tilde{\boldsymbol{\varepsilon}}$ to zero, given that $U_\mathrm{d,m} > 0$. Then, choose U_c as

$$U_\mathrm{c} = U_\mathrm{d,m}\cos\chi_\mathrm{r} + \gamma\tilde{s} \tag{30}$$

with $\gamma > 0$ constant, and χ_r as the helmsman-like

$$\chi_\mathrm{r} = \arctan\left(-\frac{\tilde{e}}{\triangle_{\tilde{e}}}\right) \tag{31}$$

with $\triangle_{\tilde{e}} > 0$ (not necessarily constant; a variable that is often referred to as a lookahead distance in literature treating planar path following along straight lines, see, e.g., (Papoulias 1991)), giving

$$\dot{V}_{\tilde{\varepsilon}} = -\gamma \hat{s}^2 - U_{\mathrm{d,m}} \frac{\tilde{e}^2}{\sqrt{\tilde{e}^2 + \triangle_{\tilde{e}}^2}} + \tilde{\boldsymbol{\varepsilon}}^\top \mathbf{R}_{\mathrm{C}}^\top \mathbf{z}_{\mathrm{v}}^{\mathrm{I}}, \tag{32}$$

which means that

$$\dot{\varpi}_{\mathrm{c}} = \frac{U_{\mathrm{c}}}{|\mathbf{p}_{\mathrm{c}}'|} \tag{33}$$

and

$$\chi_{\mathrm{d}} = \chi_{\mathrm{c}} + \chi_{\mathrm{r}}, \tag{34}$$

with U_{c} as in (30), χ_{c} as in (19), and χ_{r} as in (31). Equations (33) and (34) indicate that the collaborator continuously leads the mediator (which moves according to the ship), while the desired linear velocity of the mediator must point toward the path-tangential associated with the collaborator, in the direction of forward motion.

Summing up the design so far, we have introduced two virtual participants whose purposes are to guide the ship toward its assigned path-relative formation position. The use of the collaborator and the mediator ensure that possible kinematic singularities related to curved paths are avoided. They both move according to the ship, but their locations are used to calculate the desired orientation of the ship linear velocity required for converging to the specified formation position relative to the path.

In particular, the desired linear velocity of the ship is calculated from

$$\boldsymbol{\alpha}_{\mathrm{v}}^{\mathrm{I}} = \mathbf{R}_{\mathrm{DV}} \boldsymbol{\alpha}_{\mathrm{v,m}}^{\mathrm{DV}} + \mathbf{R}_{\mathrm{C}} (\mathbf{S}_{\mathrm{C}} \boldsymbol{\varepsilon}_{\mathrm{f}} + \dot{\boldsymbol{\varepsilon}}_{\mathrm{f}}) \tag{35}$$

since

$$\boldsymbol{\alpha}_{\mathrm{v}}^{\mathrm{I}} = \mathbf{R}_{\mathrm{DB}} \boldsymbol{\alpha}_{\mathrm{v}}^{\mathrm{DB}}, \tag{36}$$

where $\boldsymbol{\alpha}_{\mathrm{v}}^{\mathrm{DB}} = [U_{\mathrm{d}}, 0]^\top$ ($U_{\mathrm{d}} = |\boldsymbol{\alpha}_{\mathrm{v}}^{\mathrm{I}}|$) represents the desired linear velocity of the ship decomposed in a DESIRED BODY frame (**DB**), and

$$\mathbf{R}_{\mathrm{DB}} \triangleq \begin{bmatrix} \cos\chi_{\mathrm{d}} & -\sin\chi_{\mathrm{d}} \\ \sin\chi_{\mathrm{d}} & \cos\chi_{\mathrm{d}} \end{bmatrix} \tag{37}$$

represents the associated rotation matrix. Furthermore, define

$$\mathbf{H} \triangleq \begin{bmatrix} 1 & 0 & 0 \\ 0 & 1 & 0 \end{bmatrix}, \tag{38}$$

giving

$$\mathbf{R}_{\mathrm{B}} \triangleq \mathbf{H} \mathbf{R}(\psi) \mathbf{H}^\top \tag{39}$$

$$= \begin{bmatrix} \cos\psi & -\sin\psi \\ \sin\psi & \cos\psi \end{bmatrix}, \tag{40}$$

which can be used to state the relationship

$$\boldsymbol{\alpha}_{\mathrm{v}}^{\mathrm{I}} = \mathbf{R}_{\mathrm{B}} \boldsymbol{\alpha}_{\mathrm{v}}, \tag{41}$$

i.e.,

$$\boldsymbol{\alpha}_{\mathrm{v}} = \mathbf{R}_{\mathrm{B}}^\top \boldsymbol{\alpha}_{\mathrm{v}}^{\mathrm{I}}. \tag{42}$$

Hence, we also get

$$\mathbf{z}_{\mathrm{v}}^{\mathrm{I}} = \mathbf{R}_{\mathrm{B}} \mathbf{H} \mathbf{z}_{\nu}, \tag{43}$$

such that the system dynamics of $\tilde{\boldsymbol{\varepsilon}}$ and $\mathbf{z}_{\mathrm{g}}$ can be expressed as

$$\Sigma_1 : \dot{\tilde{\boldsymbol{\varepsilon}}} = \mathbf{f}_1(t, \tilde{\boldsymbol{\varepsilon}}) + \mathbf{g}_1(t) \mathbf{z}_{\mathrm{g}} \tag{44}$$

$$\Sigma_2 : \dot{\mathbf{z}}_{\mathrm{g}} = \mathbf{f}_2(t, \mathbf{z}_{\mathrm{g}}), \tag{45}$$

which is a pure cascade where the control subsystem ($\mathbf{z}_{\mathrm{g}}$) perturbs the guidance subsystem ($\tilde{\boldsymbol{\varepsilon}}$) through the interconnection matrix

$$\mathbf{g}_1(t) = \left[\mathbf{0}_{2\times 1}, \mathbf{R}_{\mathrm{C}}^\top \mathbf{R}_{\mathrm{B}} \mathbf{H}, \mathbf{0}_{2\times 3} \right]. \tag{46}$$

Now, consider the following assumptions:

A.1 $|\mathbf{p}_{\mathrm{p}}'| \in \left[|\mathbf{p}_{\mathrm{p}}'|_{\min}, \infty \right\rangle \; \forall \varpi \in \mathbb{R}$, $|\mathbf{p}_{\mathrm{p}}'|_{\min} > 0$

A.2 $\triangle_{\tilde{\mathrm{e}}} \in [\triangle_{\tilde{\mathrm{e}},\,\min}, \infty\rangle$, $\triangle_{\tilde{\mathrm{e}},\,\min} > 0$

A.3 $U_{\mathrm{d,m}} \in [U_{\mathrm{d,m,min}}, \infty\rangle$, $U_{\mathrm{d,m,min}} > 0$

Assumption A.1 means that the geometric path must be regularly parameterized, assumption A.2 implies that the linear velocity of the mediator must be directed toward the path-tangential, while assumption A.3 represents a minimum-speed requirement for the desired mediator linear velocity.

By contemplating $\boldsymbol{\xi} \triangleq \left[\tilde{\boldsymbol{\varepsilon}}^\top, \mathbf{z}_{\mathrm{g}}^\top \right]^\top$, we arrive at:

Proposition 2. The equilibrium point $\boldsymbol{\xi} = \mathbf{0}$ is rendered uniformly globally asymptotically and locally exponentially stable (UGAS/ULES) under assumptions A.1-A.3 when applying (13-14) with the reference signals (12) and (42).

Proof. Since the origin of system Σ_2 is shown to be UGAS/ULES in Proposition 1, the origin of the unperturbed system Σ_1 (i.e., when $\mathbf{z}_{\mathrm{g}} = \mathbf{0}$) is trivially shown to be UGAS/ULES by applying standard Lyapunov theory to (16) and (32), and the interconnection term satisfies $|\mathbf{g}_1(t)| = 1$, the proposed result follows directly from Theorem 7 and Lemma 8 of (Panteley *et al.* 1998). ■

So far, the two first design steps has made it possible for each individual ship to converge to and maintain its assigned formation position relative to the assigned path. The final design step must deal with the synchronization of each formation member with the virtual formation leader, i.e., ensuring the assembly of the formation as a whole.

Step 3: Synchronization Loop Design In this final design step, we determine the required *size* of $\boldsymbol{\alpha}_{\mathrm{v}}$, derived indirectly through $U_{\mathrm{d,m}}$, such that a ship controlled by (13) and (14) with reference signals given by (12) and (42) synchronizes with the formation leader.

Consequently, consider the positive definite and radially unbounded CLF

$$V_{\tilde{\varpi}} \triangleq \frac{1}{2} \tilde{\varpi}^2, \tag{47}$$

where

$$\tilde{\varpi} \triangleq \varpi_{\mathrm{c}} - \varpi_{\mathrm{l}}, \tag{48}$$

and differentiate the CLF with respect to time to get

$$\begin{aligned} \dot{V}_{\tilde{\varpi}} &= \tilde{\varpi} \dot{\tilde{\varpi}} \\ &= \tilde{\varpi} (\dot{\varpi}_{\mathrm{c}} - \dot{\varpi}_{\mathrm{l}}) \\ &= \tilde{\varpi} (z_{\mathrm{c}} + \alpha_{\mathrm{c}} - \dot{\varpi}_{\mathrm{l}}), \end{aligned}$$

where $z_{\mathrm{c}} \triangleq \dot{\varpi}_{\mathrm{c}} - \alpha_{\mathrm{c}}$, and α_{c} represents the desired speed of the collaborator when the mediator has converged to the path, i.e., when $\boldsymbol{\xi} = \mathbf{0}$. Hence, we have that

$$\dot{V}_{\tilde{\varpi}} = \tilde{\varpi}\left(\frac{U_{\mathrm{d,m}}}{|\mathbf{p}_{\mathrm{c}}'|} - \frac{U_{\mathrm{l}}}{|\mathbf{p}_{\mathrm{l}}'|}\right) + \tilde{\varpi} z_{\mathrm{c}},$$

which becomes equal to

$$\dot{V}_{\tilde{\varpi}} = -k_{\tilde{\varpi}} \frac{\tilde{\varpi}^2}{\sqrt{\tilde{\varpi}^2 + \triangle_{\tilde{\varpi}}^2}} + \tilde{\varpi} z_{\mathrm{c}} \tag{49}$$

when choosing

$$U_{\mathrm{d,m}} = |\mathbf{p}_{\mathrm{c}}'|\left(\frac{U_{\mathrm{l}}}{|\mathbf{p}_{\mathrm{l}}'|} - k_{\tilde{\varpi}} \frac{\tilde{\varpi}}{\sqrt{\tilde{\varpi}^2 + \triangle_{\tilde{\varpi}}^2}}\right), \tag{50}$$

where $\triangle_{\tilde{\varpi}} \in [\triangle_{\tilde{\varpi},\,\min}, \infty\rangle$, $\triangle_{\tilde{\varpi},\,\min} > 0$, and where

$$k_{\tilde{\varpi}} = \sigma \frac{U_{\mathrm{l}}}{|\mathbf{p}_{\mathrm{l}}'|},\ \sigma \in \langle 0, 1] \tag{51}$$

ensures that $U_{\mathrm{d,m}}$ satisfies Assumption A.3 since

$$U_{\mathrm{d,m}} = U_{\mathrm{l}}\left(1 - \sigma \frac{\tilde{\varpi}}{\sqrt{\tilde{\varpi}^2 + \triangle_{\tilde{\varpi}}^2}}\right)\frac{|\mathbf{p}_{\mathrm{c}}'|}{|\mathbf{p}_{\mathrm{l}}'|}. \tag{52}$$

Then, expand z_{c} to get

$$\begin{aligned} z_{\mathrm{c}} &= \dot{\varpi}_{\mathrm{c}} - \alpha_{\mathrm{c}} \\ &= \frac{U_{\mathrm{d,m}}(\cos\chi_{\mathrm{r}} - 1) + \gamma \tilde{s}}{|\mathbf{p}_{\mathrm{c}}'|}, \end{aligned} \tag{53}$$

where

$$(\cos\chi_{\mathrm{r}} - 1) = \frac{\triangle_{\tilde{\mathrm{e}}} - \sqrt{\tilde{e}^2 + \triangle_{\tilde{\mathrm{e}}}^2}}{\sqrt{\tilde{e}^2 + \triangle_{\tilde{\mathrm{e}}}^2}}, \tag{54}$$

such that the system dynamics of $\tilde{\varpi}$ and $\boldsymbol{\xi}$ can be written

$$\Sigma_3 : \dot{\tilde{\varpi}} = f_3(t, \tilde{\varpi}) + \mathbf{g}_3(t, \boldsymbol{\xi})^{\top}\boldsymbol{\xi} \tag{55}$$

$$\Sigma_4 : \dot{\boldsymbol{\xi}} = \mathbf{f}_4(t, \boldsymbol{\xi}), \tag{56}$$

which is a cascaded system where the synchronization subsystem ($\tilde{\varpi}$) is perturbed through the interconnection vector

$$\mathbf{g}_3(t, \boldsymbol{\xi}) = \frac{1}{|\mathbf{p}_{\mathrm{c}}'|}\left[\gamma, U_{\mathrm{d,m}} \frac{\triangle_{\tilde{\mathrm{e}}} - \sqrt{\tilde{e}^2 + \triangle_{\tilde{\mathrm{e}}}^2}}{\tilde{e}\sqrt{\tilde{e}^2 + \triangle_{\tilde{\mathrm{e}}}^2}}, \mathbf{0}_{1\times 2}\right]^{\top}, \tag{57}$$

which is well-defined since

$$\lim_{\tilde{e}\to 0} \frac{\triangle_{\tilde{\mathrm{e}}} - \sqrt{\tilde{e}^2 + \triangle_{\tilde{\mathrm{e}}}^2}}{\tilde{e}\sqrt{\tilde{e}^2 + \triangle_{\tilde{\mathrm{e}}}^2}} = 0. \tag{58}$$

Note that the complete cascade structure is completely modular in the sense that the control subsystem ($\mathbf{z}_{\mathrm{g}}$) excites the guidance subsystem ($\tilde{\boldsymbol{\varepsilon}}$), which in turn excites the synchronization subsystem ($\tilde{\varpi}$).

By considering $\boldsymbol{\zeta} \triangleq \left[\tilde{\varpi}, \boldsymbol{\xi}^{\top}\right]^{\top}$, we can now state the following main theorem:

Theorem 1. The equilibrium point $\boldsymbol{\zeta} = \mathbf{0}$ is rendered UGAS/ULES under assumptions A.1-A.2 when applying (13-14) with reference signals (12) and (42) employing (52).

Proof. Since the origin of system Σ_4 is shown to be UGAS/ULES in Proposition 2, the origin of the unperturbed system Σ_3 (i.e., when $\boldsymbol{\xi} = \mathbf{0}$) is trivially shown to be UGAS/ULES by applying standard Lyapunov theory to (47) and (49), and the interconnection term satisfies $|\mathbf{g}_3(t, \boldsymbol{\xi})| < |\mathbf{p}_{\mathrm{p}}'|_{\min}^{-1}\left(\gamma^2 + \left(\frac{U_{\mathrm{l,max}}}{\triangle_{\tilde{\mathrm{e}},\,\min}}\right)^2\right)^{1/2}$, the proposed result follows directly from Theorem 7 and Lemma 8 of (Panteley *et al.* 1998). ■

If every formation member satisfies the conditions of Theorem 1, the formation control problem (6) is solved.

3. DISCUSSION

The guided scheme can also be extended to handle underactuated ships due to its output space of linear velocity and heading, where the heading can either be independently controlled (fully actuated case) or dedicated to control the orientation of the linear velocity (underactuated case). Hence, keeping the control subsystem unchanged, a purposeful redesign of the guidance and synchronization subsystems enables underactuated operations. In fact, when the scenario entails straight-line paths and no environmental disturbances, a redesign is not necessary if

$$\psi_{\mathrm{d}} = \chi_{\mathrm{d}}, \tag{59}$$

i.e., the desired heading is assigned as the desired orientation of the linear velocity.

The specific version of the guided scheme that has been presented in this paper is decentralized in the sense that no coordination variables are communicated between the formation members. Hence, the loop is open at the leader-follower level, i.e., the leader propagates without feedback from the followers. Consequently, while impervious to single-point failure, the formation suffers from graceful degradation, i.e., members who cannot keep up with the leader fall out of formation. However, they will still be able to follow their assigned formation positions relative to the path. Thus, this decentralized scheme could be classified as involving tactical (i.e., local/individual) path following, but strategic (i.e., global/formation-wide) trajectory tracking. An alternative solution involves path following at both the tactical and strategic levels, where the leader receives formation-wide feedback from the followers (perhaps applying such information through a consensus-based algorithm). Hence, strategic path following values spatial aspects over temporal requirements (i.e., the most important task is to maintain the formation composition), while the opposite is true for strategic trajectory tracking (i.e., the formation composition can be sacrificed if some of the members cannot satisfy their required temporal constraints). Strategic trajectory tracking would typically be chosen for dedicated military operations since such endeavors usually have tight temporal constraints and inherently involve radio silence.

4. CASE STUDY: FULLY ACTUATED SHIPS

To illustrate the transient motion behavior associated with the proposed scheme, a computer simulation is carried out in which three fully actuated ships assemble and maintain a V-shaped formation along a sinusoidal path while being exposed to a constant environmental force. Specifically, the desired path is parameterized as $x_{\mathrm{p}}(\varpi) = 10\sin(0.1\varpi)$ $[m]$ and $y_{\mathrm{p}}(\varpi) = \varpi$ $[m]$; the environmental force acts from due north with a size of 1 N; the ship parameters are taken from Cybership 2, a 1:70 scale model of an offshore

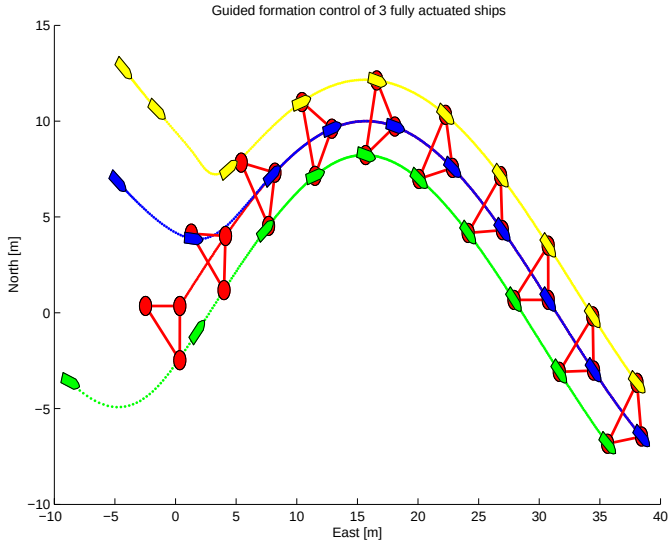

Fig. 3. The transient motion behavior of 3 fully actuated ships that assemble and maintain a V-shaped formation along a sinusoid while exposed to a constant environmental disturbance acting from the north.

supply vessel (Skjetne *et al.* 2004); the control gains and parameters are chosen as $k_{\psi,\mathrm{i}} = 10$, $\mathbf{K}_{\nu,\mathrm{i}} = 10\mathbf{I}$, $\mathbf{\Gamma}_\mathrm{i} = \mathbf{I}$, $\gamma_\mathrm{i} = 100$, $\triangle_{\mathrm{e,i}} = \triangle_{\tilde{\varpi},\mathrm{i}} = 1$ and $\sigma_\mathrm{i} = 0.9$, $\forall i \in \mathcal{I} = \{1, 2, 3\}$; and the speed of the virtual leader is fixed at $U_\mathrm{l} = 0.25$ $[m/s]$. Figure 3 illustrates the transient behavior of the formation members as they assemble and maintain a V-shaped formation defined by $\boldsymbol{\varepsilon}_{\mathrm{f},1} = [-2, -2]^\top$, $\boldsymbol{\varepsilon}_{\mathrm{f},2} = [0, 0]^\top$ and $\boldsymbol{\varepsilon}_{\mathrm{f},3} = [-2, 2]^\top$.

5. CONCLUSIONS

This paper has addressed the topic of formation control for fully actuated ships. A guided formation control concept was developed within a leader-follower framework by means of a modular design procedure, inspired by integrator backstepping and theory on nonlinear time-varying cascades. The three-step design procedure involved the creation of control, guidance, and synchronization laws for each formation member. Also, a key novelty of the approach was the derivation of guidance laws applicable to off-path traversing of curved paths. The helmsman-like transient motion behavior associated with the scheme was finally illustrated through a computer simulation involving three fully actuated ships.

REFERENCES

Aguiar, A. P., R. Ghabcheloo, A. Pascoal, C. Silvestre, J. Hespanha and I. Kaminer (2006). Coordinated path-following of multiple underactuated autonomous vehicles with bidirectional communication constraints. In: *Proceedings of the ISCCSP'06, Marrakech, Morocco.*

Arrichiello, F., S. Chiaverini and T. I. Fossen (2006). Formation control of underactuated surface vessels using the null-space-based behavioral control. In: *Proceedings of the IROS'06, Beijing, China.*

Breivik, M., M. V. Subbotin and T. I. Fossen (2006). Guided formation control for wheeled mobile robots. In: *Proceedings of the 9th ICARCV, Singapore.*

Encarnação, P. and A. Pascoal (2001). Combined trajectory tracking and path following: An application to the coordinated control of autonomous marine craft. In: *Proceedings of the 40th IEEE CDC, Orlando, Florida, USA.*

Fiorelli, E., N. E. Leonard, P. Bhatta, D. Paley, R. Bachmayer and D. M. Fratantoni (2004). Multi-AUV control and adaptive sampling in Monterey Bay. In: *Proceedings of the AUV'04, Sebasco, Maine, USA.*

Fossen, T. I. (2002). *Marine Control Systems: Guidance, Navigation and Control of Ships, Rigs and Underwater Vehicles.* Marine Cybernetics.

Fossen, T. I., A. Loría and A. Teel (2001). A theorem for UGAS and ULES of (passive) nonautonomous systems: Robust control of mechanical systems and ships. *International Journal of Robust and Nonlinear Control* **11**, 95–108.

Fossen, T. I., M. Breivik and R. Skjetne (2003). Line-of-sight path following of underactuated marine craft. In: *Proceedings of the 6th IFAC MCMC, Girona, Spain.*

Ihle, I.-A. F., J. Jouffroy and T. I. Fossen (2005). Formation control of marine surface craft using Lagrange multipliers. In: *Proceedings of the 44th IEEE CDC, Seville, Spain.*

Krstić, M., I. Kanellakopoulos and P. V. Kokotović (1995). *Nonlinear and Adaptive Control Design.* John Wiley & Sons Inc.

Kumar, V., Leonard, N. E. and Morse, A. S., Eds.) (2005). *Cooperative Control.* Vol. 309 of *Lecture Notes in Control and Information Sciences.* Springer-Verlag.

Kyrkjebø, E. and K. Y. Pettersen (2006). Leader-follower dynamic synchronization of surface vessels. In: *Proceedings of the 7th IFAC MCMC, Lisbon, Portugal.*

Lapierre, L., D. Soetanto and A. Pascoal (2003). Coordinated motion control of marine robots. In: *Proceedings of the 6th IFAC MCMC, Girona, Spain.*

Panteley, E., E. Lefeber, A. Loría and H. Nijmeijer (1998). Exponential tracking of a mobile car using a cascaded approach. In: *Proceedings of the IFAC Workshop on Motion Control, Grenoble, France.*

Papoulias, F. A. (1991). Bifurcation analysis of line of sight vehicle guidance using sliding modes. *International Journal of Bifurcation and Chaos* **1**(4), 849–865.

Pavlov, A., E. Børhaug, E. Panteley and K.Y. Pettersen (2007). Straight line path following for formations of underactuated surface vessels. In: *Proceedings of the 7th IFAC NOLCOS, Pretoria, South Africa.*

Pettersen, K. Y., Gravdahl, J. T. and Nijmeijer, H., Eds.) (2006). *Group Coordination and Cooperative Control.* Vol. 336 of *Lecture Notes in Control and Information Sciences.* Springer-Verlag.

Skjetne, R., Ø. N. Smogeli and T. I. Fossen (2004). A nonlinear ship manoeuvering model: Identification and adaptive control with experiments for a model ship. *Modeling, Identification and Control* **25**(1), 3–27.

Skjetne, R., S. Moi and T. I. Fossen (2002). Nonlinear formation control of marine craft. In: *Proceedings of the 41st IEEE CDC, Las Vegas, Nevada, USA.*

Sørdalen, O. J. and O. Egeland (1995). Exponential stabilization of nonholonomic chained systems. *IEEE Transactions on Automatic Control* **40**(1), 35–49.

G. Straight-Line Target Tracking for Unmanned Surface Vehicles

Modeling, Identification and Control, Vol. 29, No. 4, 2008, pp. 131–149

Straight-Line Target Tracking for Unmanned Surface Vehicles

Morten Breivik [1] Vegard E. Hovstein [2] Thor I. Fossen [1,3]

[1] *Centre for Ships and Ocean Structures, Norwegian University of Science and Technology, NO-7491 Trondheim, Norway. E-mail:* morten.breivik@ieee.org

[2] *Maritime Robotics, NO-7010 Trondheim, Norway. E-mail:* vegard.hovstein@maritimerobotics.com

[3] *Department of Engineering Cybernetics, Norwegian University of Science and Technology, NO-7491 Trondheim, Norway. E-mail:* fossen@ieee.org

Abstract

This paper considers the subject of straight-line target tracking for unmanned surface vehicles (USVs). Target-tracking represents motion control scenarios where no information about the target behavior is known in advance, i.e., the path that the target traverses is not defined apriori. Specifically, this work presents the design of a motion control system which enables an underactuated USV to track a target that moves in a straight line at high speed. The motion control system employs a guidance principle originally developed for interceptor missiles, as well as a novel velocity controller inspired by maneuverability and agility concepts found in fighter aircraft literature. The performance of the suggested design is illustrated through full-scale USV experiments in the Trondheimsfjord.

Keywords: Target Tracking, Unmanned Surface Vehicles, High Speed Motion, Underactuation, Constant Bearing Guidance, Velocity Control System, Full-Scale Experiments

1 Introduction

Since a main pillar of the Norwegian economy is related to oil and gas production, a principal research motivation concerns the commercial offshore market, where unmanned vehicle technology is expected to play a key role in future hydrocarbon exploration and exploitation. Additional applications include surveillance of territorial waters, protection of offshore installations, support of oil and gas activities in Arctic regions, environmental monitoring, and data collection operations aiding marine harvest policies. The use of unmanned vehicles can contribute to reduced personnel costs, improved personnel safety, widened weather window of operations, increased operational precision, and more environmentally friendly activities.

When people hear about such vehicles today, they mostly think about either unmanned aerial vehicles (UAVs), unmanned underwater vehicles (UUVs), or unmanned ground vehicles (UGVs). Little attention has been paid to unmanned surface vehicles (USVs). In fact, only last year did the US Navy release its first USV Master Plan (Navy, 2007), where a USV is defined as a vehicle which displaces water at rest and operates with near continuous contact with the water surface, capable of unmanned operations with varying degrees of autonomy.

However, USVs have actually been developed and operated since World War II, but mostly as drone boats for mine clearance and firing practice. It is only during the last decade that they have been considered for more advanced operations. A majority of the USVs currently under development are found in the US, and the technology is mainly developed for naval purposes. In par-

ISSN 1890–1328

ticular, the only industrial-level USVs today are found within the naval segment, mainly for intelligence, surveillance, and reconnaissance (ISR) applications. Most scientific USVs are just experimental platforms, and no applications currently exist in the commercial market. Details about the history, current status, and possible future development of USVs can be found in (Portmann et al., 2002), (Brown, 2004), (Hook, 2006), (Caccia, 2006), (Corfield and Young, 2006), (Bertram, 2008), and (Withington, 2008).

As most other unmanned vehicles, USVs are typically envisioned for use in so-called dirty, dull, and dangerous operations. USV technology harbors a great potential for a number of qualities, including possibilities for new vehicle designs and new concepts of operation. Regarding vehicle designs, current USVs are mostly small, boat-like vehicles that have been adapted from manned vessels originally designed to accommodate human occupants. However, such limitations need not apply to unmanned vehicles (Cooper et al., 2002), which, e.g., can be designed as semi-submersibles for improved stealth and platform stability.

Furthermore, given that USVs are typically small, fast and highly maneuverable vehicles with a large power-to-weight ratio, new motion control concepts must be developed to take advantage of such properties. Traditionally, motion control systems have been developed for fairly large vessels that are not designed for both rapid and precise maneuvering, especially since they spend most of their time in transit through open waters. State-of-the-art solutions for these typically small power-to-weight ratio vessels include course-keeping and course-changing autopilots that provide them with the ability to carry out relatively slow maneuvers (Fossen, 2002). Such autopilots do not suffice for many USV purposes.

Moreover, USVs might cooperate with other unmanned vehicles such as UAVs and UUVs to form large heterogeneous communication and surveillance networks that are able to provide unique situational awareness capabilities. In fact, USVs are unique in the sense that they are able to communicate with vehicles both above and below the sea surface at the same time, capable of acting as relays between underwater vehicles and vehicles operating on land, in the air, or in space. They can also be used to augment the capability of manned surface vessels performing various survey tasks by attaching themselves in purposeful geometric patterns around the manned vessels in order to increase their spatio-temporal survey capacity. Such formation control applications require advanced motion control systems with collision avoidance (CA) functionality. In turn, CA functionality requires both sense and avoid abilities, i.e., access to both global and local information about the environment, as well as superior maneuverability through powerful actuators. Collision avoidance systems for USVs are reported by Benjamin et al. (2006), Larson et al. (2007), and Loe (2008).

Figure 1: One example of an industrial-level USV is the remotely controlled Protector, developed by Rafael of Israel. This vehicle is a 9 m long rigid-hulled inflatable boat equipped with water jet propulsion that enables operations of up to 20 m/s (i.e., approximately 40 $knots$).

In any case, the future prosperity of USV applications depends on the development of a legal framework that renders possible unmanned operations in traditionally manned areas. Operational possibilities within the current framework of the International Maritime Organization (IMO) are reported in (Gibbons and Wilson, 2008), while future inspiration can be sought from ongoing work that is performed in the US regarding UAVs (DeGarmo and Nelson, 2006).

The main contribution of this paper is the development of a motion control system which facilitates high-speed target tracking for underactuated USVs. Specifically, the suggested motion control system consists of two main subsystems, i.e., a guidance system and a velocity control system. The guidance system employs a missile technique known as constant bearing guidance to calculate a desired velocity which enables the USV to track a moving target, while the velocity control system consists of speed and steering controllers that make the actual USV velocity adhere to the desired velocity commanded by the guidance system. The result is a simple yet advanced motion control system which requires a minimum of system identification and tuning tests to be carried out. Full-scale experiments involving an underactuated USV and a target moving in a straight line at high speed are used to illustrate the performance of the proposed motion control scheme.

2 Motion Control Fundamentals

This section introduces some fundamental motion control concepts, including operating spaces, vehicle actuation properties, motion control scenarios, as well as the motion control hierarchy. The material is adapted from (Breivik and Fossen, 2008).

2.1 Operating Spaces

To enable purposeful definitions of motion control scenarios it is necessary to distinguish between different operating spaces. In this regard, the two most fundamental operating spaces are the *work space* and the *configuration space*. The work space is also known as the operational space (Sciavicco and Siciliano, 2002), and represents the physical space in which a vehicle moves. On the other hand, the configuration space, also known as the joint space (Sciavicco and Siciliano, 2002), is constituted by the set of variables sufficient to specify all points of a rigid-body vehicle in the work space (LaValle, 2006). Each configuration variable is called a degree of freedom (DOF).

2.2 Vehicle Actuation Properties

The type, amount, and distribution of vehicle thrust devices and control surfaces, hereafter commonly referred to as actuators, determine the actuation properties of a vehicle. We mainly distinguish between two qualitatively different actuation properties, namely *full actuation* and *underactuation*. A fully actuated vehicle is able to independently control the motion of all its DOFs simultaneously, while an underactuated vehicle is not. Thus, an underactuated vehicle is generally unable to achieve arbitrary tasks in its configuration space. However, it will be able to achieve tasks in the work space as long as it can freely project its main thrust in this space, e.g., through a combination of thrust and attitude control. In fact, this principle is the mode by which most vehicles that move through a fluid operate, from missiles to ships. Even if these vehicles had the ability to roam the work space with an arbitrary attitude, they would usually expend an unnecessary amount of energy by doing so. In practice, most vehicles are underactuated in their configuration space at high speeds, and are forced to maneuver in an energy-efficient manner. Ships are typically underactuated above $1.5-2\ m/s$ ($3-4\ knots$) since the actuators that facilitate full actuation are ineffective above such speeds (Kongsberg Maritime, 2006).

2.3 Motion Control Scenarios

In the traditional control literature, motion control scenarios are typically divided into the following categories: *point stabilization*, *trajectory tracking*, and *path following*. More recently, the concept of *maneuvering* has been added to the fold as a means to bridge the gap between trajectory tracking and path following (Skjetne et al., 2004a). These scenarios are often defined by motion control objectives that are given as configuration-space tasks, which are best suited for fully actuated vehicles. Also, the scenarios typically involve desired motion that has been defined apriori in some sense. Little seems to be reported about tracking of target points for which only instantaneous motion information is available. However, in (Breivik and Fossen, 2008), both apriori and non-apriori scenarios are considered, and all the motion control objectives are given as work-space tasks. Thus, the scenarios cover more broadly, and are also suited for underactuated vehicles. Specifically, these scenarios encompass:

- *Target tracking*: The control objective is to track the motion of a target that is either stationary (similar to point stabilization) or that moves such that only its instantaneous motion is known, i.e., such that no information about the future target motion is available. Thus, in this case it is impossible to separate the spatio-temporal constraint associated with the target into two separate constraints.

- *Path following*: The control objective is to follow a predefined path, which only involves a spatial constraint. No restrictions are placed on the temporal propagation along the path.

- *Path tracking*: The control objective is to track a target that moves along a predefined path (similar to trajectory tracking). Consequently, it is possible to separate the target-related spatio-temporal constraint into two separate constraints. Still, this scenario can be viewed as a target-tracking scenario and handled with target-tracking methods, thus disregarding any apriori path information that is available.

- *Path maneuvering*: The control objective is to employ knowledge about vehicle maneuverability constraints to feasibly negotiate (or optimize the negotiation of) a predefined path. Path maneuvering thus represents a subset of path following, but is less constrained than path tracking since spatial constraints always take precedence over temporal constraints. Path-maneuvering methods can also be used to handle path-tracking scenarios.

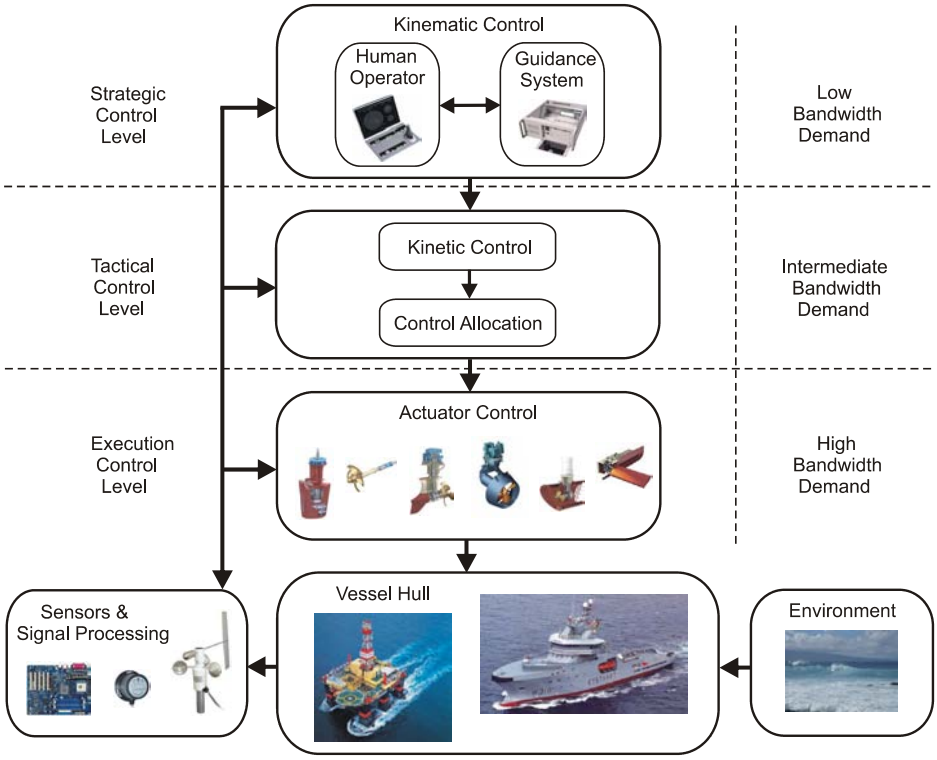

Figure 2: The motion control hierarchy of a marine surface vessel nominally consists of strategic, tactical, and execution levels of control. Additional levels are required to achieve full autonomy.

The work in this paper is concerned with the target-tracking scenario. Specifically, the motion control objective is to track a target which moves at high speed, and for which no future motion information is available. The only accessible target information is its instantaneous position and velocity.

2.4 Motion Control Hierarchy

The purpose of a motion control system is to enable a vehicle to fulfill its assigned motion control objective, and can be conceptualized to involve at least three control levels in a hierarchical structure. Figure 2 illustrates the typical components of a marine motion control system, encompassing strategic, tactical, and execution levels of control (Valavanis et al., 1997). All the involved building blocks represent autonomy-enabling technology, but more instrumentation and additional control levels are required to attain full autonomy.

At the top, we find the strategic control level. Also termed the kinematic control level, it is responsible for prescribing vehicle velocity commands needed to achieve motion control objectives in the work space. Thus, in this paper, kinematic control is equivalent to work-space control, and kinematic controllers are referred to as guidance laws. This level purely considers the geometric aspects of motion, without reference to the forces and moments that generate such motion.

Next, the tactical level encompass kinetic controllers, which do consider how forces and moments generate vehicle motion. These controllers are typically designed by model-based methods, and must handle both parametric model uncertainties and environmental disturbances. For underactuated vehicles, they must actively employ the vehicle attitude as a means to achieve the velocities prescribed by the guidance module. The intermediate control level also contains a control allocation block which distributes the kinetic control commands among the various vehicle actuators.

At the bottom, the individual actuator controllers constitute the execution level, ensuring that the actuators behave as requested by the intermediate control module, and ultimately that the vehicle moves as prescribed by the guidance laws.

This paper focuses on the strategic and tactical control levels, and proposes corresponding guidance and velocity control systems that enable an underactuated USV to fulfill a target-tracking motion control objective. Note that having well-functioning tactical- and execution-level controllers, strategic-level controllers can be exchanged in a modular manner to achieve different motion control objectives.

3 Motion Control System Design

Only a handful of papers currently deal with motion control system design for USVs. These include (Ebken et al., 2005), where motion control technology originally developed for UGVs is used to rapidly achieve basic motion control functionality for USVs, including modes for remote control and waypoint navigation; (Majohr and Buch, 2006), which details the development of a small USV intended to carry out high-precision survey operations in shallow waters, employing a steering controller based on traditional autopilot design methods; (Doucy and Ghozlan, 2008), where qualitative descriptions of advanced motion control capabilities for USVs are given, including dynamic positioning, wave management, obstacle avoidance, and fleet control; (Caccia et al., 2008a), which shows how conventional motion control techniques can be applied to make a small USV equipped with only a GPS antenna and a compass perform auto-heading, auto-speed, and straight-line path-following tasks; and (Naeem et al., 2008), where an LQG-based autopilot is proposed for a USV intended for environmental monitoring and pollutant tracking. Common features of these works are that they employ traditional control techniques and mostly consider low-speed operations in calm water.

So far, no results seem to have been reported on high-speed target-tracking for underactuated vessels. Precision control for target-tracking scenarios is currently achieved by dynamic positioning systems that require fully actuated vessels and thus concerns low speeds (Sørensen et al., 2001). As an attempt to improve this situation, the development of a novel motion control system for an underactuated USV whose assignment is to track a high-speed target is detailed in the following. The proposed design combines a well-known guidance technique with a novel velocity control system consisting of surge speed and yaw rate controllers. Literature on missile guidance, fighter aircraft, and marine vehicles has inspired the approach, which inherently takes saturation limits in the actuator system into account. The suggested design is illustrated for a small planing monohull made from aluminum designated the Kaasbøll USV, which was the first test platform of the Trondheim-based company Maritime Robotics.

3.1 Guidance System

Guidance represents a fundamental methodology which transcends specific vehicle applications (Draper, 1971), and is concerned with the transient motion behavior related to the achievement of motion control objectives (Shneydor, 1998). For this reason, guidance laws are typically stated at a kinematic level, only considering the fundamental geometric aspects of the scenarios of interest. In what follows, three missile guidance techniques applicable to target-tracking scenarios are presented, and the material is adapted from (Breivik and Fossen, 2008).

Representing a kinematic vehicle by its planar position $\mathbf{p}(t) \triangleq [x(t), y(t)]^\top \in \mathbb{R}^2$ and velocity $\mathbf{v}(t) \triangleq \mathrm{d}\mathbf{p}(t)/\mathrm{d}t \triangleq \dot{\mathbf{p}}(t) \in \mathbb{R}^2$, stated relative to some stationary reference frame, and denoting the position of the target by $\mathbf{p}_\mathrm{t}(t) \triangleq [x_\mathrm{t}(t), y_\mathrm{t}(t)]^\top \in \mathbb{R}^2$, the control objective of a target-tracking scenario can be stated as

$$\lim_{t\to\infty} (\mathbf{p}_\mathrm{t}(t) - \mathbf{p}(t)) = \mathbf{0}, \tag{1}$$

where $\mathbf{p}_\mathrm{t}(t)$ is either stationary or moving by a (nonzero and bounded) velocity $\mathbf{v}_\mathrm{t}(t) \triangleq \dot{\mathbf{p}}_\mathrm{t}(t) \in \mathbb{R}^2$.

Also, let the speed of the kinematic vehicle be denoted $U(t) \triangleq |\mathbf{v}(t)| \triangleq \sqrt{\dot{x}(t)^2 + \dot{y}(t)^2} \geq 0$, while the course angle is denoted $\chi(t) \triangleq \mathrm{atan2}\,(\dot{y}(t), \dot{x}(t)) \in \mathbb{S} \triangleq [-\pi, \pi]$, where $\mathrm{atan2}\,(y, x)$ is the four-quadrant version of $\arctan\,(y/x) \in \langle -\pi/2, \pi/2 \rangle$. Correspondingly, the speed and course of the target are denoted $U_\mathrm{t}(t)$ and $\chi_\mathrm{t}(t)$, where $U_\mathrm{t}(t) \in \langle 0, \infty \rangle$.

Concerning tracking of moving targets, the missile guidance community commonly refers to the object that is supposed to destroy another object as either a missile, an interceptor, or a pursuer. Conversely, the threatened object is typically called a target or an evader. In the following, the neutral designations interceptor and target will be used when presenting 3 fundamental guidance strategies, namely line of sight, pure pursuit, and constant bearing. These guidance strategies are referred to as the classical guidance laws, and the associated geometric principles are illustrated in Figure 3.

3.1.1 Line of Sight Guidance

Line of sight (LOS) guidance is classified as a three-point guidance scheme since it involves a (typically stationary) reference point in addition to the interceptor and the target. The LOS denotation stems from the fact that the interceptor is supposed to achieve an intercept by constraining its motion along the line of sight between the reference point and the target. LOS guidance has typically been employed for surface-to-air missiles, often mechanized by a ground station which illuminates the target with a beam that the guided missile is supposed to ride, also known as beam-rider guidance. The LOS guidance principle is illustrated in Figure 3, where the associated velocity command is represented by a vector pointing to the left of the target.

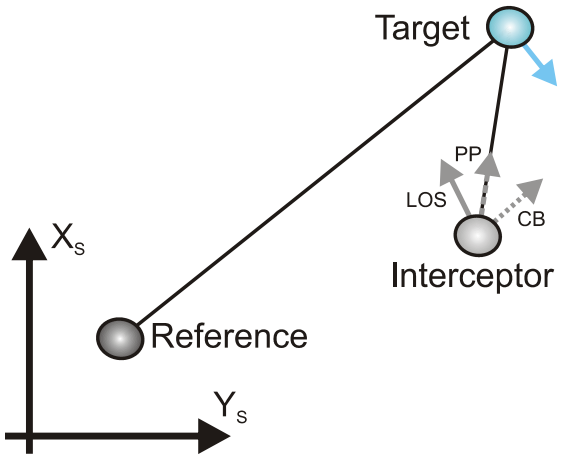

Figure 3: The interceptor velocity commands associated with the classical guidance principles line of sight (LOS), pure pursuit (PP), and constant bearing (CB).

3.1.2 Pure Pursuit Guidance

Pure pursuit (PP) guidance belongs to the two-point guidance schemes, where only the interceptor and the target are considered in the engagement geometry. Simply put, the interceptor is supposed to align its velocity along the line of sight between the interceptor and the target. This strategy is equivalent to a predator chasing a prey in the animal world, and very often results in a tail chase. PP guidance has typically been employed for air-to-surface missiles. The PP guidance principle is represented in Figure 3 by a vector pointing directly at the target.

3.1.3 Constant Bearing Guidance

Constant bearing (CB) guidance is also a two-point guidance scheme, with the same engagement geometry as PP guidance. However, in a CB engagement the interceptor is supposed to align the *relative* interceptor-target velocity along the line of sight between the interceptor and the target. This goal is equivalent to reducing the LOS rotation rate to zero such that the interceptor perceives the target at a constant bearing, closing in on a direct collision course. CB guidance is often referred to as parallel navigation, and has typically been employed for air-to-air missiles. Also, the CB rule has been used for centuries by mariners to avoid collisions at sea; steering away from a situation where another vessel approaches at a constant bearing. Thus, guidance principles can just as well be applied to avoid collisions as to achieve them. The CB guidance principle is indicated in Figure 3 by a vector pointing to the right of the target.

The most common method of implementing CB guidance is to make the rotation rate of the interceptor velocity directly proportional to the rotation rate of the interceptor-target LOS, which is widely known as proportional navigation (PN). However, CB guidance can also be implemented through the direct velocity assignment

$$\mathbf{v}(t) = \mathbf{v}_{\mathrm{t}}(t) + \mathbf{v}_{\mathrm{a}}(t), \tag{2}$$

where $\mathbf{v}_{\mathrm{a}}(t)$ is the velocity with which the interceptor approaches the target, for example chosen as

$$\mathbf{v}_{\mathrm{a}}(t) = \kappa(t)\frac{\tilde{\mathbf{p}}(t)}{|\tilde{\mathbf{p}}(t)|} \tag{3}$$

since CB guidance is considered. Here,

$$\tilde{\mathbf{p}}(t) \triangleq \mathbf{p}_{\mathrm{t}}(t) - \mathbf{p}(t) \tag{4}$$

is the interceptor-target line-of-sight vector, $|\tilde{\mathbf{p}}(t)| = \sqrt{\tilde{\mathbf{p}}(t)^\top \tilde{\mathbf{p}}(t)} \geq 0$ is the Euclidean length of this vector, and $\kappa(t) > 0$ can be chosen as

$$\kappa(t) = U_{\mathrm{a,max}}(t)\frac{|\tilde{\mathbf{p}}(t)|}{\sqrt{\tilde{\mathbf{p}}(t)^\top \tilde{\mathbf{p}}(t) + \triangle_{\tilde{\mathrm{p}}}^2}}, \tag{5}$$

where $U_{\mathrm{a,max}}(t) > 0$ specifies the maximum approach speed toward the target, and $\triangle_{\tilde{\mathrm{p}}} > 0$ influences the transient interceptor-target behavior. This particular implementation of CB guidance seems to first have been suggested in (Breivik et al., 2006), and later also used in (Breivik and Fossen, 2007).

The direct velocity assignment (2) means that in addition to assigning the target speed, which nullifies the relative velocity flow between the interceptor and the target, a relative approach velocity is assigned along the interceptor-target line-of-sight vector to ensure a smooth rendezvous, bounded by the maximum approach speed of $U_{\mathrm{a,max}}(t)$ for large $|\tilde{\mathbf{p}}(t)|$ relative to $\triangle_{\tilde{\mathrm{p}}}$. The concept is illustrated in Figure 4, where it can also be seen that CB guidance becomes equal to PP guidance for a stationary target, i.e., the basic difference between the two guidance schemes is whether the target velocity is used as a kinematic feedforward or not. This difference is vital for underactuated vehicles, which cannot change the direction of their velocity faster than they can turn.

For our application, we only consider moving targets, i.e., targets with positive speed $U_{\mathrm{t}}(t) \geq U_{\mathrm{t,min}} > 0$. Thus, we choose to employ constant bearing guidance, implemented through (2) with (3) and (5), such that

$$\mathbf{v}(t) = \mathbf{v}_{\mathrm{t}}(t) + U_{\mathrm{a,max}}(t)\frac{\tilde{\mathbf{p}}(t)}{\sqrt{\tilde{\mathbf{p}}(t)^\top \tilde{\mathbf{p}}(t) + \triangle_{\tilde{\mathrm{p}}}^2}}, \tag{6}$$

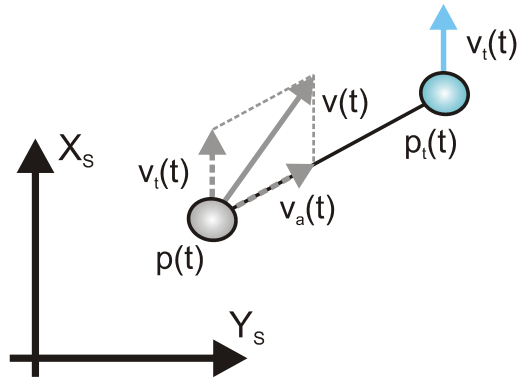

Figure 4: The direct velocity assignment associated with CB guidance.

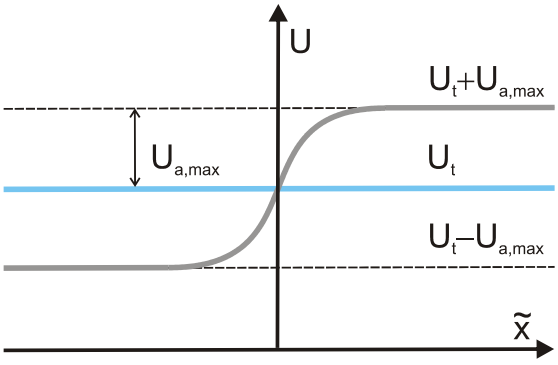

Figure 5: Interceptor speed assignment for movement along the x-axis.

which means that the target will be pursued at a maximum speed of $U_{\mathrm{t}}(t)+U_{\mathrm{a,max}}(t)$, which ramps down to $U_{\mathrm{t}}(t)$ when the interceptor-target distance decreases below $\triangle_{\tilde{\mathrm{p}}}$ toward zero and rendezvous. In this regard, the choice of $\triangle_{\tilde{\mathrm{p}}}$ becomes essential since this parameter explicitly shapes the speed transition between pursuit and rendezvous. For example, too small a value might give too sharp a transition. Figure 5 illustrates the associated speed assignment as a function of interceptor-target distance for movement purely along the x-axis.

This guidance strategy is well suited for underactuated vehicles since an overshoot in position merely reduces the commanded speed below $U_{\mathrm{t}}(t)$ instead of commanding an instantaneous 180 degree turn in the velocity, as would be the case for the pure pursuit strategy. Since the minimum commanded speed is equal to $U_{\mathrm{t}}(t) - U_{\mathrm{a,max}}(t)$, we must choose $U_{\mathrm{a,max}}(t) < U_{\mathrm{t}}(t)$ to ensure steerability through forward motion at all times. Specifically, a suitable choice could be

$$U_{\mathrm{a,max}}(t) = \zeta U_{\mathrm{t}}(t),\ \zeta < 1 \tag{7}$$

assuming that the interceptor has a speed advantage over the target, i.e., such that $U_{\max} > U_{\mathrm{t}}(t) + U_{\mathrm{a,max}}(t) = (1+\zeta)U_{\mathrm{t}}(t)$ at all times.

Finally, note that for a real vehicle, the velocity (6) cannot be assigned directly and achieved instantaneously, but rather represents a desired velocity $\mathbf{v}_{\mathrm{d}}(t)$ which the vehicle must attain through the use of a velocity control system, whose design is the topic of the next section.

3.2 Velocity Control System

This section details the development of a velocity control system that enables an underactuated USV to achieve the velocity command (6) required to attain the target-tracking motion control objective (1). Hence, denoting the velocity error as

$$\tilde{\mathbf{v}}(t) \triangleq \mathbf{v}_{\mathrm{d}}(t) - \mathbf{v}(t), \tag{8}$$

where $\mathbf{v}_{\mathrm{d}}(t)$ is equal to (6) and $\mathbf{v}(t)$ is the actual USV velocity, the velocity control objective becomes

$$\lim_{t\to\infty} \tilde{\mathbf{v}}(t) = \mathbf{0}. \tag{9}$$

In particular, since we consider underactuated USVs, the velocity controller is decomposed into a surge speed controller and a yaw rate controller in a polar coordinate fashion. The design is illustrated for a vehicle named the Kaasbøll USV, and the principal goal is to develop a simple yet advanced velocity control system which requires a minimum of system identification and tuning tests to be carried out.

3.2.1 The Kaasbøll USV

The USV that was used as a test platform for the experiments reported in this paper is a modified Kaasbøll 19 boat, which is a 5.75 m (19 $feet$) planing monohull made of aluminum produced by Kaasbøll Boats from Hitra near Trondheim, Norway. A width of 2.12 m ensures sufficient space for two people manning the center console of the boat during sea trials. The USV is equipped with an off-the-shelf Evinrude 50 E-Tec outboard engine providing 50 hp, which gives it a top speed of about 10 m/s (approximately 20 $knots$) in calm water with two people aboard. This propulsion solution corresponds to a propeller and rudder actuator setup, which means that the USV is unactuated in sway. The navigation system relies on a Seapath 20 NAV solution made by Kongsberg Seatex, which replaces several vessel instruments with a single navigation package that outputs position, heading, velocity, and rate of turn (Kongsberg Seatex, 2006). The USV is also equipped with an onboard computer (OBC)

Figure 6: The Kaasbøll USV operating in the Trondheimsfjord.

that provides a rapid prototyping environment with Matlab/Simulink-compliant software. Execution-level proportional controllers ensure that the E-Tec engine responds effectively to throttle commands in the region $\tau_c \in [-100\%, 100\%]$ and rudder commands in the region $\delta_c \in [-0.2618\ rad, 0.2618\ rad]$. The fully equipped USV is shown in Figure 6. Due to safety considerations and requirements from the port authorities in Trondheim, all motion control experiments in the Trondheimsfjord are performed with at least two persons aboard the USV.

3.2.2 Modeling Considerations

The availability of mathematical models of marine vessels are essential for both control design and simulation study purposes. A standard 3 DOF dynamic model, representing the horizontal surge, sway, and yaw modes, can be found in (Fossen, 2002), and consists of the kinematics

$$\dot{\boldsymbol{\eta}} = \mathbf{R}(\psi)\boldsymbol{\nu}, \tag{10}$$

and the kinetics

$$\mathbf{M}\dot{\boldsymbol{\nu}} + \mathbf{C}(\boldsymbol{\nu})\boldsymbol{\nu} + \mathbf{D}(\boldsymbol{\nu})\boldsymbol{\nu} = \boldsymbol{\tau} + \mathbf{R}(\psi)^\top \mathbf{b}, \tag{11}$$

where $\boldsymbol{\eta} \triangleq [x, y, \psi]^\top \in \mathbb{R}^2 \times \mathbb{S}$ represents the earth-fixed pose (i.e., position and heading); $\boldsymbol{\nu} \triangleq [u, v, r]^\top \in \mathbb{R}^3$ represents the vessel-fixed velocity; $\mathbf{R}(\psi) \in SO(3)$ is the transformation matrix

$$\mathbf{R}(\psi) \triangleq \begin{bmatrix} \cos\psi & -\sin\psi & 0 \\ \sin\psi & \cos\psi & 0 \\ 0 & 0 & 1 \end{bmatrix} \tag{12}$$

that transforms from the vessel-fixed frame to the earth-fixed frame; $\mathbf{M}$ is the inertia matrix; $\mathbf{C}(\boldsymbol{\nu})$ is the centrifugal and coriolis matrix; while $\mathbf{D}(\boldsymbol{\nu})$ is the hydrodynamic damping matrix. The system matrices satisfy the properties $\mathbf{M} = \mathbf{M}^\top > 0$, $\mathbf{C} = -\mathbf{C}^\top$ and $\mathbf{D} > 0$. The vessel-fixed propulsion forces and moment is represented by $\boldsymbol{\tau}$, while $\mathbf{b}$ represents low-frequency, earth-fixed environmental disturbances. Details concerning this model can also be found in (Skjetne et al., 2004b) and (Fossen, 2005).

Most papers considering nonlinear motion control for underactuated marine surface vessels typically use some variant of the model (10)-(11), and assume that the model parameters are either perfectly known or known with only a small degree of uncertainty, see, e.g., (Breivik and Fossen, 2004), (Børhaug and Pettersen, 2005), (Do and Pan, 2006), (Fredriksen and Pettersen, 2006), and (Aguiar and Hespanha, 2007). In practice, it can be quite hard to obtain the parameter values required to populate (11), especially with regard to the hydrodynamic damping matrix. Furthermore, the model is only valid for displacement vessels that operate in a certain part of the speed regime, and does not hold for semi-displacement or planing vessels operating at a large Froude number. This number is a dimensionless parameter defined as

$$Fn \triangleq \frac{U}{\sqrt{Lg}}, \tag{13}$$

where U is the vessel speed, L is the submerged vessel length, and g is the acceleration of gravity (Faltinsen, 2005). According to Fossen (2005), the stated 3 DOF model is only valid for $Fn \leq 0.3$, which corresponds to a speed of only 2.25 m/s for the USV under consideration. However, such a vehicle can operate at much larger Froude numbers, even into the planing region, which is defined for $Fn \geq 1.0 - 1.2$.

A notable exception to the conventional model-based

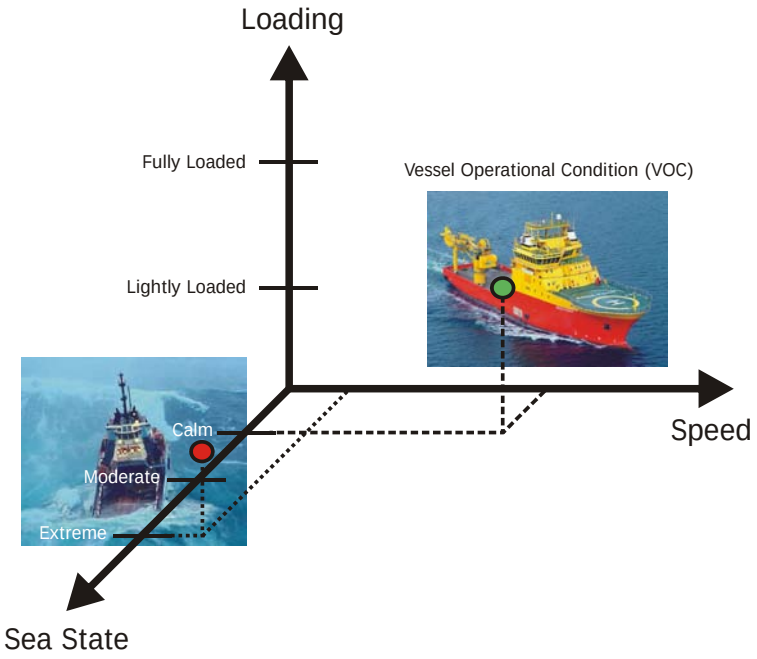

Figure 7: The main axes of speed, sea state, and loading constituting the vessel operational condition (VOC) space. Adapted from (Perez et al., 2006).

approach is reported in (Caccia et al., 2008b), where a more control-oriented scheme is suggested. Likewise, we do not use the kinetic model (11) in our design, but employ a more straightforward approach inspired by concepts from literature on fighter aircraft. This scheme is detailed in the following.

3.2.3 Maneuverability and Agility

The terms maneuverability and agility are defined in several different ways in literature on fighter aircraft (Paranjape and Ananthkrishnan, 2006), where they are essential for describing close-combat fighting abilities. Similarly, we want to employ such concepts when developing velocity control systems for high-powered USVs. In particular, we choose to subscribe to the definitions used by Beck and Cord (1995), where maneuver performance is defined as a measure of steady maneuver capability and agility is defined as a measure of the ability to transition between steady maneuvers. Consequently, the relevant maneuver states of a surface vehicle include the surge speed u, the sway speed v, and the yaw rate r. These variables determine how fast the vessel can move on the sea surface, i.e., traverse the pose space. The agility of a vessel then describes how fast it can transition between its maneuver states. Various tests can be carried out to determine the maneuverability and agility of a vehicle, and in the following such tests and their results are reported for the Kaasbøll USV.

Maneuverability Tests Several factors determine the maneuverability of a vehicle, but the most important one for control purposes is the relationship between the actuator inputs and the maneuver states. All actuators are ultimately controlled by either a voltage or a current signal, such that their capacity can be conveniently represented in the range $[-100\%, 100\%]$ (when abstracting away the actual signal range), where 100% represents maximum input. For a vehicle whose actuator setup corresponds to that of having a stern-mounted propeller and rudder, tests can be carried out in which the control signal for both actuators are applied in steps to cover their entire signal range while simultaneously recording the steady response of the maneuver states. Then, by using, e.g., least-squares curve fitting to the obtained data sets, analytic relationships between the control inputs and the maneuver states can be achieved. The result will ultimately constitute a 5-dimensional surface - a maneuver map - in the combined input (propeller, rudder) and output (surge, sway, and yaw speeds) space, which is the input-output surface that the vessel nominally will be able to traverse.

Furthermore, the tests should be carried out in ideal conditions, i.e., for minimal environmental disturbances (such as wind, waves, and currents) and for nominal loading conditions. The results can then be used to design a feedforward controller that will be able to achieve any allowable set of speeds by simply

allocating the required control inputs derived from the maneuver map. Feedback terms must also be added to take care of any discrepancies between the nominal maneuver map and the actual situation, resulting, e.g., from changing environmental conditions or off-nominal loading conditions. Hence, the feedforward terms handle operations in the nominal part of the vessel operational condition (VOC) space, while the feedback terms enlarge this operational area by adding robustness against modeling errors, parametric uncertainties, and disturbances. See Figure 7 for an illustration of the main axes in the VOC space.

Since we only consider straight-line target-tracking scenarios, it is not necessary to derive a maneuver map which includes the rudder input and the sway and yaw outputs. Hence, we only consider the relationship between the throttle input and the surge output. Accordingly, the USV maneuverability tests consisted of applying throttle inputs from 0% to 100% in steps of 10% for zero rudder, and recording the corresponding steady-state surge speeds. Negative throttle was not considered relevant.

The tests showed that a throttle input of less than 40% was barely recognizable on the surge speed output, which means that the range $0-40\%$ in practice constitutes a dead band. Also, for throttle above 80%, the USV transitioned from the displacement region into the semi-displacement and planing regions, where it is much harder to achieve precision control of the speed. Consequently, we only consider operation within the throttle region $40-80\%$, which corresponds to surge speeds of $1.6-4.8\ m/s$. Then, by declaring that 30% throttle corresponds to zero surge speed, and by using the steady-state output (surge speed) data vector

$$\mathbf{u} = [0, 1.6, 2.3, 3.2, 3.9, 4.8]^\top \tag{14}$$

with the corresponding scaled input (throttle) data vector

$$\boldsymbol{\sigma} = [0, 0.2, 0.4, 0.6, 0.8, 1]^\top, \tag{15}$$

the following analytical relationship was obtained through least-squares curve fitting against a third order polynomial

$$\sigma(u) = -0.0078u^3 + 0.0720u^2 + 0.0428u - 0.0017, \tag{16}$$

which is valid for zero rudder and positive surge speeds. Figure 8 illustrates the maneuver map encapsulated by (16), and shows its correspondence with the data from (14) and (15). As can be seen, this input-output relationship comes close to being linear for high speeds, which is due to the fact that the nonlinear effects of the throttle input mainly competes with the nonlinear effects of the hydrodynamic damping at such speeds.

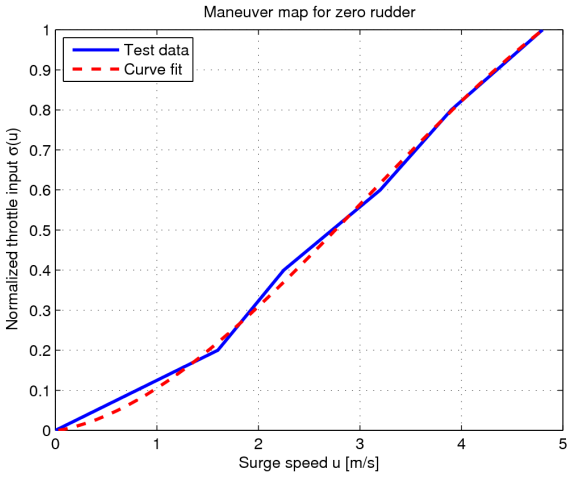

Figure 8: The maneuver map obtained through steady-state USV experiments.

Also, note that the relationship between $\sigma(u) \in [0, 1]$ and the actual throttle $\tau(\sigma(u))$ is equal to

$$\tau(\sigma(u)) = 100\,(0.5\sigma(u) + 0.3) \tag{17}$$

since $\sigma(u) = 0$ corresponds to 30% throttle and $\sigma(u) = 1$ corresponds to 80% throttle. Thus, (16) and (17) tells us that if a surge speed of $3.2\ m/s$ is desired, a throttle of 60% must be applied. For control design purposes, any desired surge speed value that is within the speed range of the maneuver map nominally constitutes a feasible value.

Agility Test One way to determine the maximum agility of a vehicle is to record the response of the maneuver states to steps in the control inputs from 0% to 100%. Such step response analysis determines how fast the vehicle is able to move in the maneuver space. For our vehicle, the agility test was performed as a step in the throttle for zero rudder, which resulted in a surge speed response as shown in the top part of Figure 9. The figure shows two distinct regions of behavior, i.e., one region where the speed climbs fast to $5\ m/s$ (displacement region) and another where it increases more slowly up toward $10\ m/s$ (semi-displacement to planing regions). As already mentioned, it was decided to just consider speeds below $5\ m/s$ ($10\ knots$) since it is very difficult to precision control the vehicle speed outside the displacement region without installing additional control surfaces. Hence, the maximum USV speed $U_{\max}$ was set to $5\ m/s$.

The bottom part of Figure 9 shows the surge speed response in the displacement region together with an approximation. This approximation is not achieved by

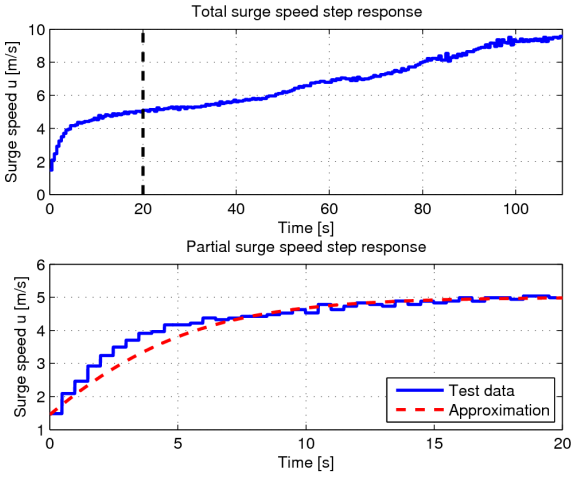

Figure 9: Top: Complete surge speed step response. Bottom: Actual and approximated displacement region responses.

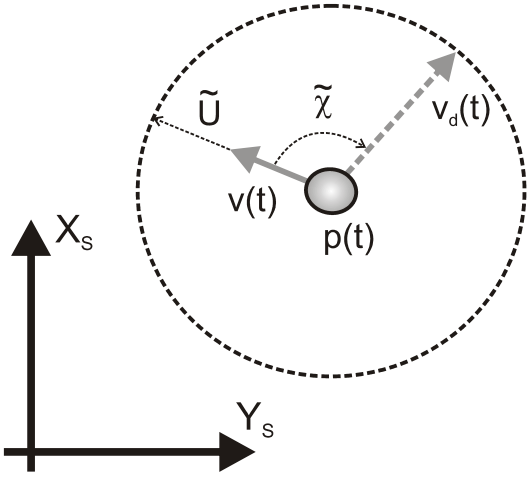

Figure 10: A polar coordinate decomposition of the velocity error $\tilde{\mathbf{v}}(t)$ into a speed error $\tilde{U}$ and a course error $\tilde{\chi}$.

using a low-pass filter with a time constant, as is common when approximating step responses, but rather as a sigmoid-like tanh function with a dynamic input state, i.e., as

$$u(t) = \triangle_{\mathrm{u}} \tanh\left(\frac{\rho(t)}{\triangle_{\mathrm{u}}}\right), \tag{18}$$

where $\dot{\rho}(t) = \alpha(t)$ with $\rho(0) = \triangle_{\mathrm{u}} \tanh^{-1}\left(\frac{u(0)}{\triangle_{\mathrm{u}}}\right)$, and $\triangle_{\mathrm{u}} > 0$ is a scaling variable that renders the tanh function magnitude-invariant, as opposed to a low-pass filter implementation, which is not magnitude-invariant. The variable $\alpha(t)$ thus represents an agility parameter indicating how fast transitions can be made between maneuver states, and the specific value of $\alpha(t)$ obtained through a step-response test involving zero to maximum control input then represents the maximum attainable agility $\alpha_{\max}$, i.e., $\alpha(t) \in \langle 0, \alpha_{\max}]$. This maximum value embeds information about all the dynamic phenomena occurring between the actuator control input and the navigation system output (e.g., motor dynamics, actuator dynamics, vessel-ocean dynamics, sensor dynamics, etc.) without the need for detailed modeling of these intermediate dynamic systems. Specifically, the maximum agility parameter corresponding to Figure 9 was found to be $\alpha_{\max} = 0.7$, while $\triangle_{\mathrm{u}} = 5$ equals the considered speed range. For control design purposes, any speed reference signal corresponding to an $\alpha(t)$ below $\alpha_{\max}$ nominally constitutes a feasible signal rate-wise.

3.2.4 Surge Speed Controller

Since we are dealing with an underactuated USV, the sway speed $v(t)$ cannot be directly controlled. Consequently, the desired velocity commanded by the guidance system must be divided between surge speed and yaw rate controllers in a polar coordinate fashion. Such a scheme means that the surge speed controller becomes responsible for controlling the size of the USV velocity $\mathbf{v}(t)$ while the yaw rate controller is responsible for controlling the direction of the velocity, see Figure 10. Note that the desired velocity $\mathbf{v}_{\mathrm{d}}(t)$ in this figure corresponds to the assigned velocity $\mathbf{v}(t)$ in Figure 4.

Denoting the speed (velocity size) error as

$$\tilde{U}(t) \triangleq U_{\mathrm{d}}(t) - U(t), \tag{19}$$

where $U_{\mathrm{d}}(t) \triangleq |\mathbf{v}_{\mathrm{d}}(t)|$ with $\mathbf{v}_{\mathrm{d}}(t)$ as in (6), the objective of the speed control becomes

$$\lim_{t\to\infty} \tilde{U}(t) = 0, \tag{20}$$

which we need to rewrite in terms of a corresponding control objective for the surge speed. Since $U(t) = |\mathbf{v}(t)| = \sqrt{u(t)^2 + v(t)^2}$ and (20) states that our goal is to have $U(t) \to U_{\mathrm{d}}(t)$, we get that $\sqrt{u(t)^2 + v(t)^2} \to U_{\mathrm{d}}(t)$ or equivalently that $u(t) \to \sqrt{U_{\mathrm{d}}(t)^2 - v(t)^2}$. Hence, we define a desired surge speed as

$$u_{\mathrm{d}}(t) \triangleq \sqrt{U_{\mathrm{d}}(t)^2 - v(t)^2}, \tag{21}$$

which is valid when assuming $U_{\mathrm{d}}(t) \geq |v(t)|$ at all times. This assumption is highly realistic since in practice $|v(t)|$ is just a small fraction of $U(t)$ for straight-line

motion at high speeds. Then denoting the surge speed error as

$$\tilde{u}(t) \triangleq u_{\mathrm{d}}(t) - u(t) \tag{22}$$

with $u_{\mathrm{d}}(t)$ as in (21), the objective of the surge speed controller becomes

$$\lim_{t\to\infty} \tilde{u}(t) = 0, \tag{23}$$

which together with an appropriate control objective for the yaw rate controller will enable the fulfillment of the target-tracking control objective (1).

However, the surge speed controller should not use $u_{\mathrm{d}}(t)$ directly as a reference signal. To ensure both static and dynamic feasibility in the computation of such a reference, information obtained from the maneuverability and agility tests can be employed in the following way:

1. The reference must always be constrained within the range of the maneuver map since it is not physically possible to track a speed that is larger than $U_{\max}$, which is the speed that corresponds to a maximum throttle input.

2. The reference must not change faster than what conforms to the maximum agility parameter $\alpha_{\max}$.

Consequently, when supplied a desired speed $U_{\mathrm{d}}(t) \leq U_{\max}$, corresponding to $u_{\mathrm{d}}(t) \leq u_{\max}$ when adjusting for the sway speed, a feasible reference both magnitude- and rate-wise can be computed by

$$u_{\mathrm{r}}(t) = u_{\max} \tanh\left(\frac{\rho_{\mathrm{r}}(t)}{u_{\max}}\right), \tag{24}$$

where $u_{\max}$ represents the maximum attainable surge speed, and the dynamics of $\rho_{\mathrm{r}}(t)$ is given by

$$\dot{\rho}_{\mathrm{r}}(t) = \alpha(t) \tanh\left(\frac{k_{\mathrm{p},\tilde{\rho}}\tilde{\rho}(t)}{\alpha(t)}\right), \tag{25}$$

where $\alpha(t) \in \langle 0, \alpha_{\max}]$, $k_{\mathrm{p},\tilde{\rho}} > 0$, $\tilde{\rho}(t) \triangleq \rho_{\mathrm{d}}(t) - \rho_{\mathrm{r}}(t)$ where

$$\rho_{\mathrm{d}}(t) = u_{\max} \tanh^{-1}\left(\frac{u_{\mathrm{d}}(t)}{u_{\max}}\right) \tag{26}$$

corresponds to the desired surge speed $u_{\mathrm{d}}(t)$, and with

$$\rho_{\mathrm{r}}(0) = u_{\max} \tanh^{-1}\left(\frac{u(0)}{u_{\max}}\right) \tag{27}$$

accounting for the initial surge speed $u(0)$. Thus, $u_{\mathrm{r}}(t)$ functions as a feasibility filter between $u(t)$ and $u_{\mathrm{d}}(t)$, starting in $u(0)$ and tracking $u_{\mathrm{d}}(t)$ constrained by $\alpha(t) \leq \alpha_{\max}$. This filter is structurally identical with (18) and ensures feasible operation at all times by relying on recorded maneuverability and agility data embedded in $u_{\max}$ and $\alpha_{\max}$. Specifically, while (24) ensures maneuverability compliance, (25) ensures agility compliance. It is then the responsibility of the velocity control system to make $u(t)$ track $u_{\mathrm{r}}(t)$ such that (23) is fulfilled for a feasible $u_{\mathrm{d}}(t)$. However, if $u_{\mathrm{d}}(t)$ is infeasible somehow (either statically, dynamically, or both), it cannot be tracked in any case.

Having obtained the maneuver map constituted by Figure 8, a feasible reference speed $u_{\mathrm{r}}(t)$ can ideally be gained simply by commanding the throttle input corresponding to $\sigma(u_{\mathrm{r}}(t))$, which is a pure feedforward control assignment. Naturally, such an assignment can only result in satisfactory performance for conditions similar to those for which the maneuver tests were performed. Consequently, feedback must also be added as part of the control strategy in order to achieve robustness against curve-fitting errors, off-nominal conditions, and disturbances. Hence, consider the following surge speed controller

$$c(u_{\mathrm{r}}(t), \bar{u}(t)) = \sigma(u_{\mathrm{r}}(t)) + k_{\mathrm{p},\bar{\mathrm{u}}}\bar{u}(t) + k_{\mathrm{i},\bar{\mathrm{u}}} \int_0^t \bar{u}(\tau)\mathrm{d}\tau, \tag{28}$$

where

$$\bar{u}(t) \triangleq u_{\mathrm{r}}(t) - u(t) \tag{29}$$

with $u_{\mathrm{r}}(t)$ as in (24) and $k_{\mathrm{p},\bar{\mathrm{u}}} > k_{\mathrm{i},\bar{\mathrm{u}}} > 0$. This controller thus consists of a feedforward term based on the maneuver map (16) and a PI feedback control term for robust and tight surge speed control. The corresponding throttle command becomes

$$\tau_{\mathrm{c}}(u_{\mathrm{r}}(t), \bar{u}(t)) = 100\left(0.5c(u_{\mathrm{r}}(t), \bar{u}(t)) + 0.3\right), \tag{30}$$

which help ensure that

$$\lim_{t\to\infty} \bar{u}(t) = 0, \tag{31}$$

and thus that the surge speed control objective (23) can be feasibly fulfilled.

3.2.5 Yaw Rate Controller

As previously mentioned, the role of the yaw rate controller is to make the direction of the USV velocity match the direction of the desired velocity commanded by the guidance system. Thus, denoting the course (velocity direction) error as

$$\tilde{\chi}(t) \triangleq \chi_{\mathrm{d}}(t) - \chi(t) \tag{32}$$

where $\chi_{\mathrm{d}}(t) \triangleq \operatorname{atan2}(\dot{y}_{\mathrm{d}}(t), \dot{x}_{\mathrm{d}}(t))$ represents the desired course angle associated with $\mathbf{v}_{\mathrm{d}}(t)$ and $\chi(t) = \operatorname{atan2}(\dot{y}(t), \dot{x}(t))$ represents the actual USV course angle, the objective of the course control becomes

$$\lim_{t\to\infty} \tilde{\chi}(t) = 0, \tag{33}$$

which together with the control objective for the surge speed controller (23) enables the fulfillment of the target-tracking control objective (1).

However, we do not calculate $\tilde{\chi}(t)$ according to (32) by using the explicit course angles. To avoid possible wraparound problems associated with such a method, $\tilde{\chi}(t)$ can be calculated directly by employing cross- and inner-product information about the velocities $\mathbf{v}_\mathrm{d}(t)$ and $\mathbf{v}(t)$. Specifically, we can extract $\sin(\tilde{\chi}(t))$ information from the cross product $\mathbf{v}(t) \times \mathbf{v}_\mathrm{d}(t)$ and $\cos(\tilde{\chi}(t))$ information from the inner product $\mathbf{v}(t)^\top \mathbf{v}_\mathrm{d}(t)$ for use in the direct calculation

$$\tilde{\chi}(t) = \mathrm{atan2}\left(\sin(\tilde{\chi}(t)), \cos(\tilde{\chi}(t))\right), \tag{34}$$

see Figure 10. This method of deriving $\tilde{\chi}(t)$ is unorthodox and does not seem to have been reported in the marine literature before.

Since the considered target-tracking scenario only involves straight-line motion, the yaw rate controller does not require any feedforward terms, and thus no corresponding maneuverability and agility tests need to be performed. Consequently, the commanded rudder angle input can simply be chosen as the pure PI feedback controller

$$\delta_\mathrm{c}(\tilde{r}(t)) = k_{\mathrm{p},\tilde{\mathrm{r}}}\tilde{r}(t) + k_{\mathrm{i},\tilde{\mathrm{r}}}\int_0^t \tilde{r}(\tau)\mathrm{d}\tau \tag{35}$$

with $k_{\mathrm{p},\tilde{\mathrm{r}}} > k_{\mathrm{i},\tilde{\mathrm{r}}} > 0$ and

$$\tilde{r}(t) \triangleq r_\mathrm{d}(t) - r(t), \tag{36}$$

where

$$r_\mathrm{d}(t) = r_{\mathrm{a,max}} \tanh\left(\frac{k_{\mathrm{p},\tilde{\chi}}\tilde{\chi}(t)}{r_{\mathrm{a,max}}}\right) \tag{37}$$

is employed as the desired yaw rate, with $r_{\mathrm{a,max}}$ representing the maximum yaw rate at which $\chi(t)$ is allowed to approach $\chi_\mathrm{d}(t)$, and $k_{\mathrm{p},\tilde{\chi}} > 0$ shaping this approach. Hence, (37) ensures that $\chi(t)$ will rendezvous with $\chi_\mathrm{d}(t)$ in a controlled manner, while the smoothness of the approach depends on $k_{\mathrm{p},\tilde{\chi}}$. Figure 11 shows how the desired yaw rate varies as a function of this gain, i.e., a large value results in a steep approach and vice versa.

Far from a traditional autopilot, the suggested yaw rate controller employs no explicit information about the USV heading angle $\psi(t)$, and controls $\tilde{\chi}(t)$ in a cascaded manner through inner loop control of $\tilde{r}(t)$.

3.3 Total Motion Control System

Summarizing the guidance and velocity control system development, we arrive at Figure 12. This figure illustrates the total motion control system resulting from the proposed designs of the previous sections. As can be seen, this paper contributes at the strategic and tactical levels of control, ultimately issuing throttle and rudder commands for the execution-level proportional

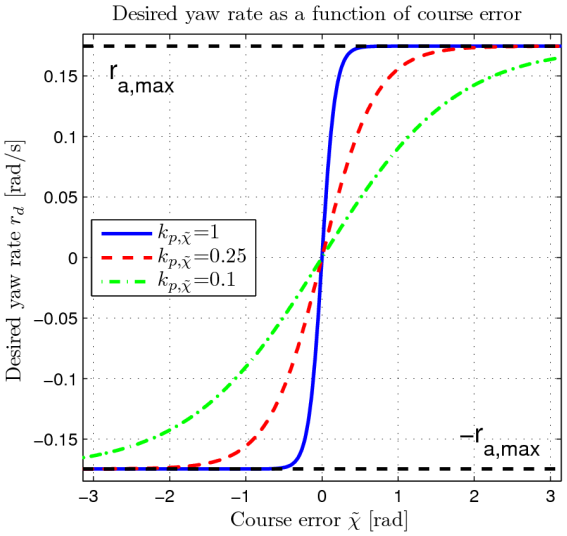

Figure 11: Profile of desired yaw rate as a function of course error for varying $k_{\mathrm{p},\tilde{\chi}}$.

controllers governing the USV outboard engine. The developed motion control system enables underactuated USVs to track high-speed targets, especially those moving in a straight line. Its potential is illustrated through full-scale experiments in the next section.

4 Full-Scale Experimental Results

On Friday 1 August 2008, full-scale experiments were carried out in the Trondheimsfjord where the Kaasbøll USV was supposed to track the position of a virtual target travelling in a straight line at high speed. The environmental conditions during these experiments were far from the ideal conditions that were present on the day when the maneuverability and agility tests were carried out. Specifically, the ocean was visually estimated to be in sea state 3 (Faltinsen, 1990), which is pretty rough for a small vessel such as the Kaasbøll USV. Also, the wind was blowing at around 3.5 m/s with gusts up to 6.5 m/s during the experiments. These conditions were certainly right to test the developed motion control system and explore its performance and robustness.

In the particular experiment detailed here, the virtual target started about 90 m to the northeast of the USV, moving due north in a straight line at a speed of $U_\mathrm{t} = 3$ m/s. The USV started at rest with an initial heading of 145 deg. It was allowed a maximum approach speed of $U_{\mathrm{a,max}} = 1$ m/s with which to intercept the target, i.e., allowed to move with a maximum total speed of $U_\mathrm{t} + U_{\mathrm{a,max}} = 4$ $m/s < U_{\max}$. Also, the USV was allowed a maximum approach yaw rate

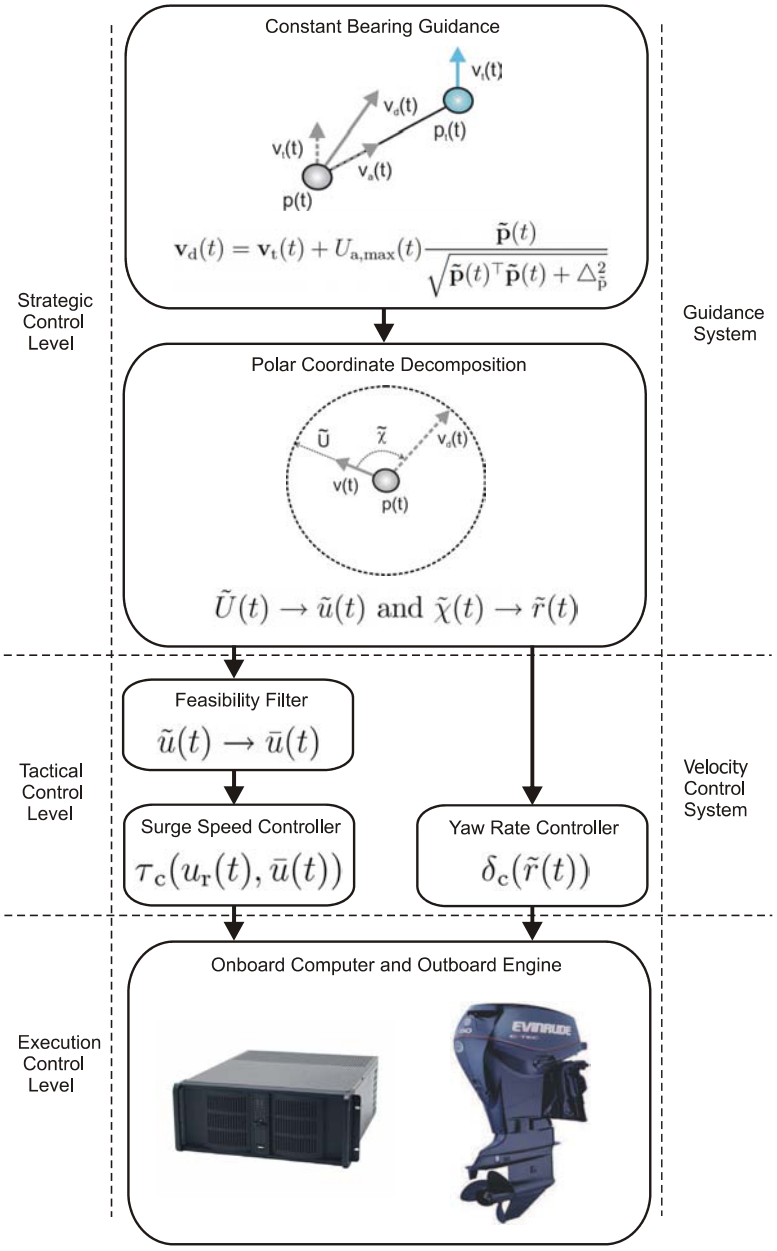

Figure 12: An illustration of the proposed motion control system capable of achieving high-speed target tracking for underactuated USVs. By replacing the guidance system components, other motion control scenarios can also be handled.

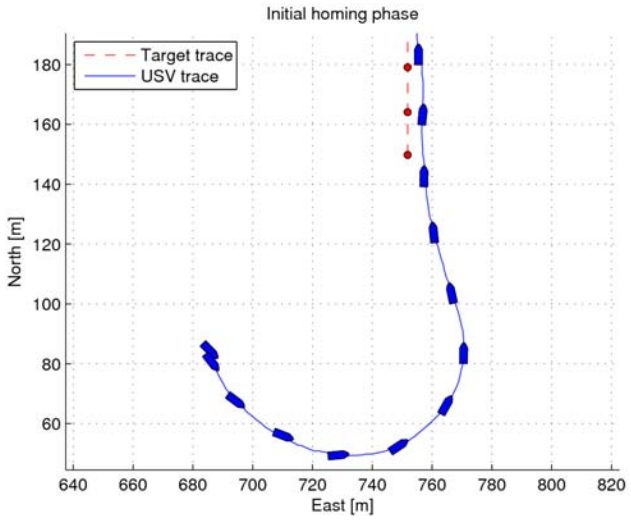

Figure 13: The USV is maneuvering onto an intercept course with the target.

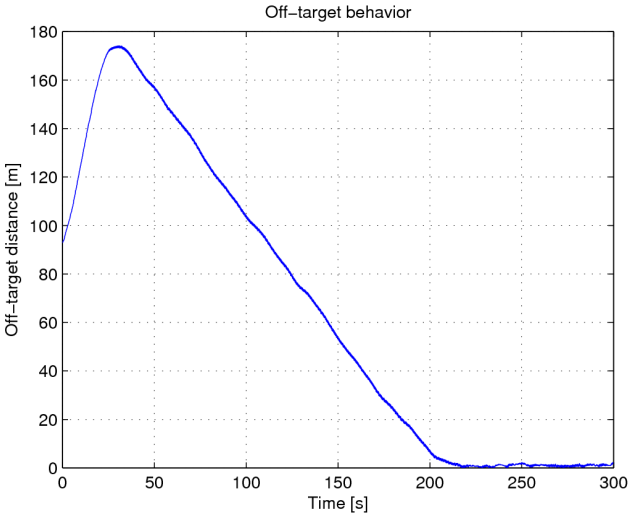

Figure 15: The distance to the target initially increases until the USV begins to move in the target direction and then finally converges smoothly to zero.

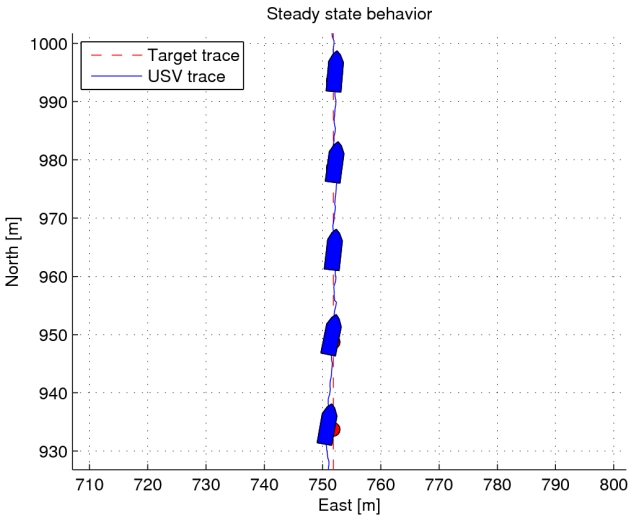

Figure 14: The USV has intercepted the target.

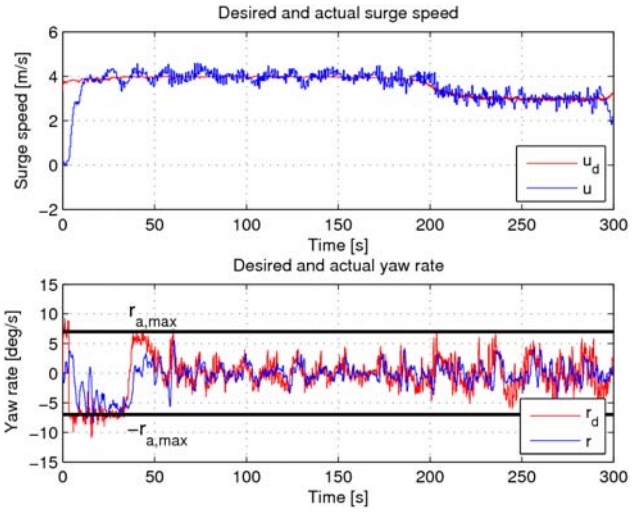

Figure 16: Top: The surge speed response of the Kaasbøll USV. Bottom: The yaw rate is seen to remain within the bounds of $r_{\mathrm{a,max}}$.

of $r_{\mathrm{a,max}} = 0.122\ rad/s$ (equivalent to 7 deg/s) with which to align its velocity with the desired velocity. Furthermore, the guidance system employed $\triangle_{\tilde{\mathrm{p}}} = 10$ m, the surge speed reference filter used $\alpha = 0.4 < \alpha_{\max}$ and $k_{\mathrm{p},\tilde{\rho}} = 10$, the surge speed controller gains were chosen as $k_{\mathrm{p},\tilde{\mathrm{u}}} = 0.5$ and $k_{\mathrm{i},\tilde{\mathrm{u}}} = 0.05$, while the yaw rate controller employed $k_{\mathrm{p},\tilde{\chi}} = 0.5$ and the same PI gains as the surge speed controller.

Figure 13 shows the initial response of the USV as it powers up from rest and starts homing in on the target. The intercept approach appears natural and smooth. Figure 14 shows the steady-state performance of the USV after it has intercepted the target. The time evolution of the off-target distance $|\tilde{\mathbf{p}}(t)|$ is shown in Figure 15. As can be seen, the distance increases in the beginning while the USV is turning to achieve its intercept course. After about 30 seconds, the USV has finished turning and the distance to the target decreases with 1 m/s until intercept takes place after approximately 220 seconds. The top part of Figure 16 shows that the surge speed quickly achieves 4 m/s and then starts to track the reference speed with about 0.5 m/s accuracy, which is acceptable given the sea state of the experiment. Also, the bottom part of Figure 16 shows that the yaw rate is kept within the limitation of 7 deg/s and tracks the reference well given the environmental conditions. Furthermore, Figure 17 shows that the commanded throttle and rudder are well within their bounds, while Figure 18 shows how the target-tracking response becomes less tight with a smaller $r_{\mathrm{a,max}} = 0.087\ rad/s$ (equivalent to 5 deg/s). The green lines of this figure represent the line-of-sight vector between the USV and its target, illustrating how the application of constant bearing guidance leads to stabilization of the LOS angle, and also why the approach sometimes is referred to as parallel navigation. In sum, these results show that the USV motion control system performs very well despite tough conditions.

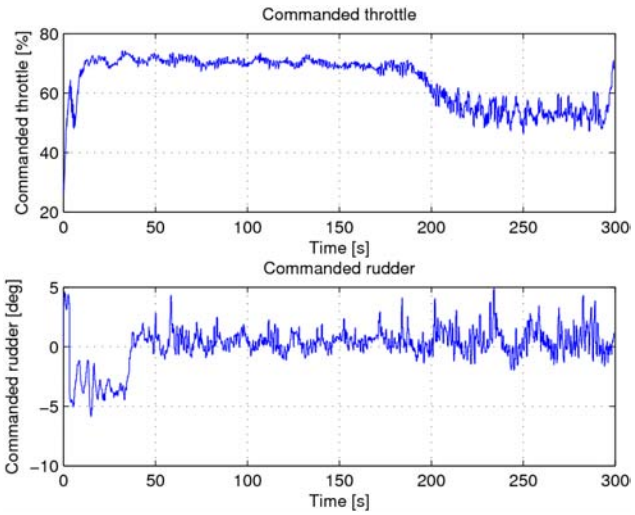

Figure 17: The commanded actuator inputs remain well within their bounds.

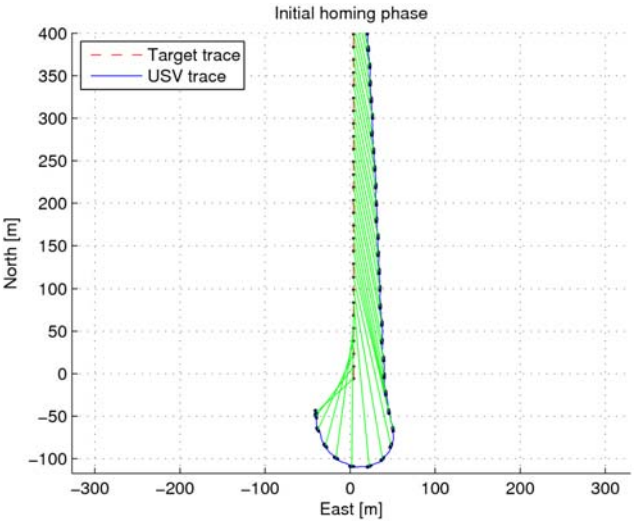

Figure 18: An alternate intercept run with less tight motion control.

5 Conclusions and Further Work

This paper has addressed the subject of straight-line target tracking for unmanned surface vehicles (USVs). Specifically, the work presented the design of a motion control system that enables an underactuated USV to track a target which moves in a straight line at high speed. The motion control system includes a guidance law originally developed for interceptor missiles, as well as a new type of velocity control which is inspired by maneuverability and agility concepts found in literature on fighter aircraft. In fact, several novel concepts were introduced in the design, and its performance was successfully illustrated through full-scale target-tracking experiments in the Trondheimsfjord.

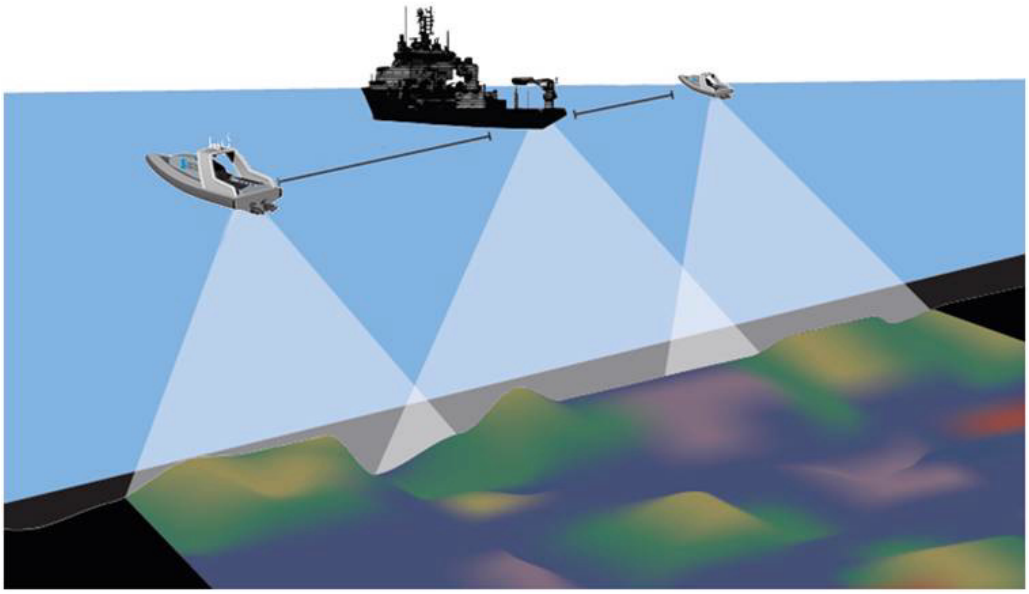

Figure 19: USV-assisted seabed mapping entails faster and cheaper operations since the capacity of the main survey vessel is augmented by that of a fleet of USVs. Courtesy of Maritime Robotics.

This work represents a first step toward the development of new motion control systems that take advantage of the maneuvering abilities of small and high-powered USVs.

Further work includes extending the current motion control system to also handle circular target motion, which involves performing additional maneuverability and agility tests to find the maneuver map between the rudder input and the yaw rate output for feedforward use in the yaw rate controller. Such an enhanced motion control system can for instance be used to achieve formation control with a group of underactuated USVs tracking the motion of a manned leader vessel which has a specific geometric formation pattern associated with it, see Figure 19.

Acknowledgments

This work was supported by the Norwegian Research Council through the Centre for Ships and Ocean Structures and through the MAROFF grant 175977: Unmanned Surface Vehicle. The authors would like to thank the reviewers for their constructive comments, while a special thanks goes to Arild Hepsø, Eirik E. Hovstein, and Stein Johansen at Maritime Robotics for their help with the full-scale experiments. This paper is a tribute to the Kaasbøll USV that was used in the experiments, but which has since been dismantled and replaced by other test platforms.

References

Aguiar, A. P. and Hespanha, J. P. Trajectory-tracking and path-following of underactuated autonomous vehicles with parametric modeling uncertainty. *IEEE Transactions on Automatic Control*, 2007. 52(8):1362–1379.

Beck, J. A. and Cord, T. J. A framework for analysis of aircraft maneuverability. In *Proceedings of the AIAA Atmospheric Flight Mechanics Conference, Baltimore, Maryland, USA*. 1995 .

Benjamin, M. R., Leonard, J. J., Curcio, J. A., and Newman, P. M. A method for protocol-based collision avoidance between autonomous marine surface craft. *Journal of Field Robotics*, 2006. 23(5):333–346.

Bertram, V. Unmanned surface vehicles - A survey. In *Skibsteknisk Selskab, Copenhagen, Denmark*. 2008 .

Breivik, M. and Fossen, T. I. Path following for marine surface vessels. In *Proceedings of the OTO'04, Kobe, Japan*. 2004 .

Breivik, M. and Fossen, T. I. Applying missile guidance concepts to motion control of marine craft. In *Proceedings of the 7th IFAC CAMS, Bol, Croatia*. 2007 .

Breivik, M. and Fossen, T. I. Guidance laws for planar motion control. In *Proceedings of the CDC'08, Cancun, Mexico*. 2008 .

Breivik, M., Strand, J. P., and Fossen, T. I. Guided dynamic positioning for fully actuated marine surface vessels. In *Proceedings of the 6th IFAC MCMC, Lisbon, Portugal*. 2006 .

Brown, N. Not just a remote possibility: USVs enter the fray. *Jane's Navy International*, 2004. 109(1):14–19.

Børhaug, E. and Pettersen, K. Y. Cross-track control for underactuated autonomous vehicles. In *Proceedings of the CDC-ECC'05, Seville, Spain*. 2005 .

Caccia, M. Autonomous surface craft: Prototypes and basic research issues. In *Proceedings of the MED'06, Ancona, Italy*. 2006 .

Caccia, M., Bibuli, M., Bono, R., and Bruzzone, G. Basic navigation, guidance and control of an unmanned surface vehicle. *Autonomous Robots*, 2008a. 25(4):349–365.

Caccia, M., Bruzzone, G., and Bono, R. A practical approach to modeling and identification of small autonomous surface craft. *IEEE Journal of Oceanic Engineering*, 2008b. 33(2):133–145.

Cooper, S. L., Newborn, D. A., and Norton, M. R. New paradigms in boat design: An exploration into unmanned surface vehicles. In *Proceedings of the AUVSI Unmanned Systems, Lake Buena Vista, Florida, USA*. 2002 .

Corfield, S. J. and Young, J. M. Unmanned surface vehicles - Game changing technology for naval operations. In G. N. Roberts and R. Sutton, editors, *Advances in Unmanned Marine Vehicles*, pages 311–328. The Institution of Electrical Engineers, 2006.

DeGarmo, M. and Nelson, G. M. Prospective unmanned aerial vehicle operations in the future national airspace system. In *Proceedings of the 4th AIAA ATIO Forum, Chicago, Illinois, USA*. 2006 .

Do, K. D. and Pan, J. Underactuated ships follow smooth paths with integral actions and without velocity measurements for feedback: Theory and experiments. *IEEE Transactions on Control Systems Technology*, 2006. 14(2):308–322.

Doucy, O. and Ghozlan, F. Advanced functions for USV. In *Proceedings of the ATMA International Autonomous Surface Ship Symposium, Paris, France*. 2008 .

Draper, C. S. Guidance is forever. *Navigation*, 1971. 18(1):26–50.

Ebken, J., Bruch, M., and Lum, J. Applying unmanned ground vehicle technologies to unmanned surface vehicles. In *Proceedings of SPIE 5804: Unmanned Ground Vehicle Technology VII, Orlando, Florida, USA*. 2005 .

Faltinsen, O. M. *Sea Loads on Ships and Offshore Structures*. Cambridge University Press, 1990.

Faltinsen, O. M. *Hydrodynamics of High-Speed Marine Vehicles*. Cambridge University Press, 2005.

Fossen, T. I. *Marine Control Systems: Guidance, Navigation and Control of Ships, Rigs and Underwater Vehicles*. Marine Cybernetics, 2002.

Fossen, T. I. A nonlinear unified state-space model for ship maneuvering and control in a seaway. *Journal of Bifurcation and Chaos*, 2005. 15(9):2717–2746.

Fredriksen, E. and Pettersen, K. Y. Global κ-exponential way-point maneuvering of ships: Theory and experiments. *Automatica*, 2006. 42(4):677–687.

Gibbons, T. D. and Wilson, P. A. Operating a remotely controlled yacht at very large distances. In *Proceedings of the ATMA International Autonomous Surface Ship Symposium, Paris, France*. 2008 .

Hook, D. J. Development of unmanned surface vehicles. In *Proceedings of the World Maritime Technology Conference, London, UK*. 2006 .

Kongsberg Maritime. Kongsberg K-Pos DP dynamic positioning system. 2006. Report no. 301093/B.

Kongsberg Seatex. Datasheet Seapath 20 NAV. 2006.

Larson, J., Bruch, M., Halterman, R., Rogers, J., and Webster, R. Advances in autonomous obstacle avoidance for unmanned surface vehicles. In *Proceedings of the AUVSI Unmanned Systems North America, Washington D.C., USA*. 2007 .

LaValle, S. M. *Planning Algorithms*. Cambridge University Press, 2006.

Loe, Ø. A. G. *Collision Avoidance for Unmanned Surface Vehicles*. Master's thesis, Norwegian University of Science and Technology, 2008.

Majohr, J. and Buch, T. Modelling, simulation and control of an autonomous surface marine vehicle for surveying applications Measuring Dolphin MESSIN. In G. N. Roberts and R. Sutton, editors, *Advances in Unmanned Marine Vehicles*, pages 329–351. The Institution of Electrical Engineers, 2006.

Naeem, W., Xu, T., Sutton, R., and Tiano, A. The design of a navigation, guidance, and control system for an unmanned surface vehicle for environmental monitoring. *Proceedings of the Institution of Mechanical Engineers, Part M: Journal of Engineering for the Maritime Environment*, 2008. 222(2):67–79.

Navy, U. S. The Navy unmanned surface vehicle (USV) master plan. 2007.

Paranjape, A. A. and Ananthkrishnan, N. Combat aircraft agility metrics - A review. *Journal of Aerospace Sciences and Technologies*, 2006. 58(2):1–12.

Perez, T., Sørensen, A. J., and Blanke, M. Marine vessel models in changing operational conditions - A tutorial. In *Proceedings of the 14th IFAC SYSID, Newcastle, Australia*. 2006 .

Portmann, H. H., Cooper, S. L., Norton, M. R., and Newborn, D. A. Unmanned surface vehicles: Past, present, and future. *Unmanned Systems*, 2002. 20(5):32–37.

Sciavicco, L. and Siciliano, B. *Modelling and Control of Robot Manipulators*. Springer-Verlag London Ltd., 2002.

Shneydor, N. A. *Missile Guidance and Pursuit: Kinematics, Dynamics and Control*. Horwood Publishing Ltd., 1998.

Skjetne, R., Fossen, T. I., and Kokotović, P. V. Robust output maneuvering for a class of nonlinear systems. *Automatica*, 2004a. 40(3):373–383.

Skjetne, R., Smogeli, Ø. N., and Fossen, T. I. A nonlinear ship manoeuvering model: Identification and adaptive control with experiments for a model ship. *Modeling, Identification and Control*, 2004b. 25(1):3–27.

Sørensen, A. J., Leira, B., Strand, J. P., and Larsen, C. M. Optimal setpoint chasing in dynamic positioning of deep-water drilling and intervention vessels. *International Journal of Robust and Nonlinear Control*, 2001. 11:1187–1205.

Valavanis, K. P., Gracanin, D., Matijasevic, M., Kolluru, R., and Demetriou, G. A. Control architectures for autonomous underwater vehicles. *IEEE Control Systems Magazine*, 1997. 17(6):48–64.

Withington, T. No crew onboard! *Armada International*, 2008. 32(3):18–26.

H. Guidance Laws for Autonomous Underwater Vehicles

4

Guidance Laws for Autonomous Underwater Vehicles

Morten Breivik[1] and Thor I. Fossen[1,2]
[1]Centre for Ships and Ocean Structures
[2]Department of Engineering Cybernetics
Norwegian University of Science and Technology
Norway

1. Introduction

About 70% of the surface of the Earth is covered by oceans, and the ocean space represents a vast chamber of natural resources. In order to explore and utilize these resources, humankind depends on developing and employing underwater vehicles, not least unmanned underwater vehicles (UUVs). Today, UUVs encompass remotely operated vehicles (ROVs) and autonomous underwater vehicles (AUVs).

The first ROVs were built in the 1950s, put into commercial use in the 1980s, and are mostly used today by the offshore oil and gas industry to carry out inspection and intervention operations at subsea installations (Antonelli et al. 2008). These vehicles are teleoperated by connection to a surface vessel through an umbilical cable that provides them with power and telemetry. In particular, the dependence on a tether represents a considerable challenge for ROV deepwater operations (Whitcomb 2000).

On the other hand, AUVs are free-swimming vehicles that rely on their own energy supply. The first AUVs were built in the 1970s, put into commercial use in the 1990s, and today are mostly used for scientific, commercial, and military mapping and survey tasks (Blidberg 2001). Developed in cooperation between Kongsberg Maritime and the Norwegian Defence Research Establishment, the HUGIN series represents the most commercially successful AUV series on the world market today (Hagen et al. 2003). HUGIN vehicles have been employed for commercial applications since 1997 and for military applications since 2001. The workhorse HUGIN 3000 has an impressive 60 hours endurance at 4 knots speed with payload sensors running. Currently, the main challenges for AUVs encompass endurance, navigation, communication, and autonomy issues.

Traditionally, ROVs and AUVs have been assigned different tasks due to different strengths and weaknesses, see Fig. 1. In the future, hybrid ROV/AUV designs are expected to bridge the gap between these two main UUV types, utilizing the best of both worlds (Wernli 2000).

Regarding motion control research for UUVs, Craven et al. (1998) give an overview of modern control approaches with an emphasis on artificial intelligence techniques; Roberts & Sutton (2006) treat guidance, navigation, and control issues for unmanned marine vehicles with an emphasis on underwater vehicles; while Antonelli et al. (2008) present a state-of-the-art survey of control-related aspects for underwater robotic systems.

Source: Underwater Vehicles, Book edited by: Alexander V. Inzartsev,
ISBN 978-953-7619-49-7, pp. 582, December 2008, I-Tech, Vienna, Austria

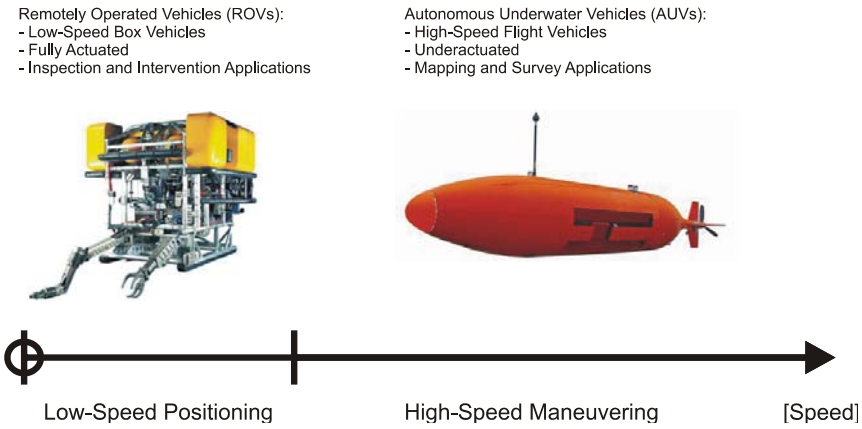

Fig. 1. The two traditional types of UUVs: ROVs and AUVs. These vehicles have different designs and perform different operations in different parts of the speed regime

An essential quality for free-swimming underwater vehicles like AUVs is their ability to maneuver accurately in the ocean space. Motion control is a fundamental enabling technology for such a quality, and every motion control system requires a guidance component. This guidance requirement serves as the main motivation for this work, whose aim is to provide a convenient overview of guidance laws applicable to motion control of AUVs. An extension of (Breivik & Fossen 2008), the exposition is deliberately kept at a basic level to make it accessible for a wide audience. Details and proofs can be found in the references.

1.1 Guidance

According to Shneydor (1998), guidance is defined as: *The process for guiding the path of an object towards a given point, which in general may be moving*. Also, the father of inertial navigation, Charles Stark Draper, states in (Draper 1971) that: *Guidance depends upon fundamental principles and involves devices that are similar for vehicles moving on land, on water, under water, in air, beyond the atmosphere within the gravitational field of earth and in space outside this field*, see Fig. 2. Thus, guidance represents a basic methodology concerned with the transient motion behavior associated with the achievement of motion control objectives.

The most rich and mature literature on guidance is probably found within the guided missile community. In one of the earliest texts on the subject (Locke 1955), a guided missile is defined as: *A space-traversing unmanned vehicle which carries within itself the means for controlling its flight path*. Today, most people would probably think about unmanned aerial vehicles (UAVs) when hearing this definition. However, guided missiles have been operational since World War II (Spearman 1978), and thus organized research on guidance theory has been conducted almost as long as organized research on control theory. The continuous progress in missile hardware and software technology has made increasingly advanced guidance concepts feasible for implementation. Today, missile guidance theory encompass a broad spectrum of guidance laws, namely: classical guidance laws; optimal guidance laws; guidance laws based on fuzzy logic and neural network theory; differential-geometric guidance laws; and guidance laws based on differential game theory.

Fig. 2. Fundamental guidance principles apply from subsea to space

As already mentioned, a classical text on missile guidance concepts is (Locke 1955), while more recent work include (Lin 1991), (Shneydor 1998), (Zarchan 2002), (Siouris 2004), and (Yanushevsky 2008). Relevant survey papers include (Pastrick et al. 1981), (Cloutier et al. 1989), (Lin & Su 2000), and (White & Tsourdos 2001). Also, very interesting personal accounts of the guided missile development during and after World War II can be found in (Haeussermann 1981), (Battin 1982), and (Fossier 1984), while MacKenzie (1990) and Westrum (1999) put the development of guided missile technology into a larger perspective.

The fundamental nature and diverse applicability of guidance principles can be further illustrated through a couple of examples. In nature, some predators are able to conceal their pursuit of prey by resorting to so-called motion camouflage techniques (Mizutani et al. 2003). They adjust their movement according to their prey so that the prey perceive them as stationary objects in the environment. These predators take advantage of the fact that some creatures detect the lateral motion component relative to the predator-prey line of sight far better than the longitudinal component. Hence, approaching predators can appear stationary to such prey by minimizing the relative lateral motion, only changing in size when closing in for the kill. Interestingly, this behavior can be directly related to the classical guidance laws from the missile literature (Justh & Krishnaprasad 2006). Also, such guidance laws have been successfully applied since the early 1990s to avoid computationally-demanding optimization methods associated with motion planning for robot manipulators operating in dynamic environments (Piccardo & Honderd 1991).

2. Motion control fundamentals

This section reviews some basic motion control concepts, including operating spaces, vehicle actuation properties, motion control scenarios, as well as the motion control hierarchy. It concludes with some preliminaries.

2.1 Operating spaces

It is useful to distinguish between different types of operating spaces when considering vehicle motion control, especially since such characterizations enable purposeful definitions of various motion control scenarios. The two most fundamental operating spaces to consider are the *work space* and the *configuration space*.

The work space, also known as the operational space (Sciavicco & Siciliano 2002), represents the physical space (environment) in which a vehicle moves. For a car, the work space is 2-dimensional (planar position), while it is 3-dimensional (spatial position) for an aircraft. Thus, the work space is a position space which is common for all vehicles of the same type.

The configuration space, also known as the joint space (Sciavicco & Siciliano 2002), is constituted by the set of variables sufficient to specify all points of a (rigid-body) vehicle in the work space (LaValle 2006). Thus, the configuration of a car is given by its planar position and orientation, while the configuration of an aircraft is given by its spatial position and attitude.

2.2 Vehicle actuation properties

Every variable associated with the configuration of a vehicle is called a degree of freedom (DOF). Hence, a car has 3 degrees of freedom, while an aircraft has 6 degrees of freedom.

The type, amount, and distribution of vehicle thrust devices and control surfaces, hereafter commonly referred to as actuators, determine the actuation property of a vehicle. We mainly distinguish between two qualitatively different actuation properties, namely *full actuation* and *underactuation*. A fully actuated vehicle is able to independently control all its DOFs simultaneously, while an underactuated vehicle is not. Thus, an underactuated vehicle is generally unable to achieve arbitrary tasks in its configuration space. However, it will be able to achieve tasks in the work space as long as it can freely project its main thrust in this space, e.g., through a combination of thrust and attitude control. In fact, this principle is the mode by which most vehicles that move through a fluid operate, from missiles to ships. Even if these vehicles had the ability to roam the work space with an arbitrary attitude, this option would represent the least energy-efficient alternative.

2.3 Motion control scenarios

In the traditional control literature, motion control scenarios are typically divided into the following categories: *point stabilization*, *trajectory tracking*, and *path following*. More recently, the concept of *maneuvering* has been added to the fold as a means to bridge the gap between trajectory tracking and path following (Skjetne et al. 2004). These scenarios are often defined by motion control objectives that are given as configuration-space tasks, which are best suited for fully actuated vehicles. Also, the scenarios typically involve desired motion that has been defined apriori in some sense. Little seems to be reported about tracking of target points for which only instantaneous motion information is available.

However, in this work, both apriori and non-apriori scenarios are considered, and all the motion control objectives are given as work-space tasks. Thus, the scenarios cover more

broadly, and are also suited for underactuated vehicles. The considered scenarios are defined in the following.

The control objective of a *target-tracking scenario* is to track the motion of a target that is either stationary (analogous to point stabilization) or that moves such that only its instantaneous motion is known, i.e., such that no information about the future target motion is available. Thus, in this case it is impossible to separate the spatio-temporal constraint associated with the target into two separate constraints.

In contrast, the control objective of a *path-following scenario* is to follow a predefined path, which only involves a spatial constraint. No restrictions are placed on the temporal propagation along the path.

However, the control objective of a *path-tracking scenario* is to track a target that moves along a predefined path (analogous to trajectory tracking). Consequently, it is possible to separate the target-related spatio-temporal constraint into two separate constraints. Still, this scenario can be viewed as a target-tracking scenario and handled with target-tracking methods, thus disregarding any apriori path information that is available.

Finally, the control objective of a *path-maneuvering scenario* is to employ knowledge about vehicle maneuverability to feasibly negotiate (or somehow optimize the negotiation of) a predefined path. As such, path maneuvering represents a subset of path following, but is less constrained than path tracking since spatial constraints always take precedence over temporal constraints. Path-maneuvering methods can also be used to handle path-tracking scenarios.

2.4 Motion control hierarchy

A vehicle motion control system can be conceptualized to involve at least three levels of control in a hierarchical structure, see Fig. 3. This figure illustrates the typical components of a marine motion control system, encompassing strategic, tactical, and execution levels of control (Valavanis et al. 1997). All the involved building blocks represent autonomy-enabling technology, but more instrumentation and additional control levels are required to attain fully autonomous operation. An example involves collision avoidance functionality, which demands additional sense and avoid components.

This work is mainly concerned with the highest (strategic) control level of Fig. 3. Termed the kinematic control level, it is responsible for prescribing vehicle velocity commands needed to achieve motion control objectives in the work space. Thus, in this work, kinematic control is equivalent to work-space control, and *kinematic controllers* are referred to as *guidance laws*. This level purely considers the geometrical aspects of motion, without reference to the forces and moments that generate such motion.

Next, the intermediate (tactical) level encompass *kinetic controllers*, which do consider how forces and moments generate vehicle motion. These controllers are typically designed by model-based methods, and must handle both parametric uncertainties and environmental disturbances. For underactuated vehicles, they must actively employ the vehicle attitude as a means to adhere to the velocities ordered by the guidance module. The intermediate control level also contains a *control allocation* block which distributes the kinetic control commands among the various vehicle actuators.

Finally, the lowest (execution) level is constituted by the individual *actuator controllers*, which ensure that the actuators behave as requested by the intermediate control module, and ultimately that the vehicle moves as prescribed by the guidance laws.

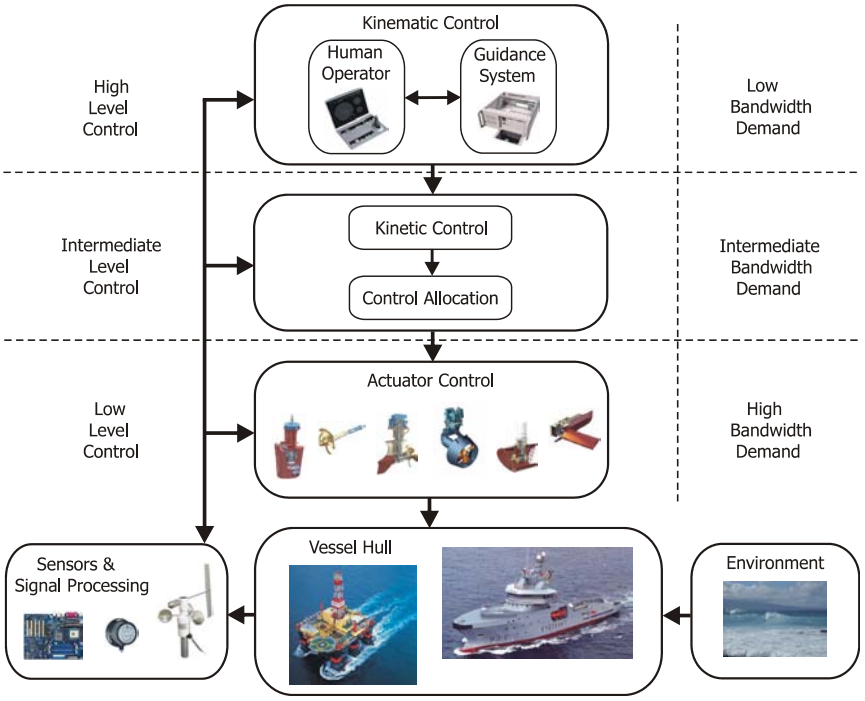

Fig. 3. The motion control hierarchy of a marine surface vessel

2.5 Preliminaries

In the missile literature, guidance laws are typically synonymous with steering laws, assuming that the speed is constant. In this work, guidance laws are either directly prescribed as velocity assignments or partitioned into separate speed and steering laws.

The guidance laws are first introduced in a 2-dimensional framework, where a kinematic vehicle is represented by its planar position $\mathbf{p}(t) \triangleq [x(t), y(t)]^{\mathrm{T}} \in \mathbb{R}^2$ and velocity $\mathbf{v}(t) \triangleq \mathrm{d}\mathbf{p}(t)/\mathrm{d}t \triangleq \dot{\mathbf{p}}(t) \in \mathbb{R}^2$, stated relative to some stationary reference frame. Since most of the AUVs of today are of the survey type, they do not need to perform spatially coupled maneuvers, but typically execute temporally separated planar maneuvers either in the horizontal plane or the vertical plane. Thus, Section 3 and 4 are relevant for such applications. Similar considerations justify the work reported in (Healey & Lienard 1993), (Caccia et al. 2000), and (Lapierre et al. 2003).

In Section 5, the planar methods are extended to a 3-dimensional framework, where a kinematic vehicle is represented by its spatial position $\mathbf{p}(t) \in \mathbb{R}^3$ and velocity $\mathbf{v}(t) \in \mathbb{R}^3$. Results on spatially coupled motion control of AUVs can be found in (Encarnação & Pascoal 2000), (Do & Pan 2003), (Aguiar & Hespanha 2004), (Breivik & Fossen 2005a), (Børhaug & Pettersen 2006), and (Refsnes et al. 2008).

Finally, note that all the illustrations of guidance principles employ the marine convention of a right-handed coordinate system whose z-axis points down.

3. Guidance laws for target tracking

In this section, guidance laws for target tracking are presented. The material is adapted from (Breivik & Fossen 2007).

Denoting the position of the target by $\mathbf{p}_t(t) \triangleq [x_t(t), y_t(t)]^T \in \mathbb{R}^2$, the control objective of a target-tracking scenario can be stated as

$$\lim_{t\to\infty} \left(\mathbf{p}(t) - \mathbf{p}_t(t) \right) = \mathbf{0}, \tag{1}$$

where $\mathbf{p}_t(t)$ is either stationary or moving by a (non-zero and bounded) velocity $\mathbf{v}_t(t) \triangleq \dot{\mathbf{p}}_t(t) \in \mathbb{R}^2$.

Concerning tracking of moving targets, the missile guidance community probably has the most comprehensive experience. They commonly refer to the object that is supposed to destroy another object as either a missile, an interceptor, or a pursuer. Conversely, the threatened object is typically called a target or an evader. Here, the designations interceptor and target will be used.

An interceptor typically undergoes 3 phases during its operation; a launch phase, a midcourse phase, and a terminal phase. The greatest accuracy demand is associated with the terminal phase, where the interceptor guidance system must compensate for the accumulated errors from the previous phases to achieve a smallest possible final miss distance to the target. Thus, 3 terminal guidance strategies will be presented in the following, namely line of sight, pure pursuit, and constant bearing. The associated geometric principles are illustrated in Fig. 4.

Note that while the main objective of a guided missile is to hit (and destroy) a physical target in finite time, we recognize the analogy of hitting (converging to) a virtual target asymptotically, i.e., the concept of asymptotic interception, as stated in (1).

3.1 Line of sight guidance

Line of sight (LOS) guidance is classified as a so-called three-point guidance scheme since it involves a (typically stationary) reference point in addition to the interceptor and the target. The LOS denotation stems from the fact that the interceptor is supposed to achieve an intercept by constraining its motion along the line of sight between the reference point and the target. LOS guidance has typically been employed for surface-to-air missiles, often mechanized by a ground station which illuminates the target with a beam that the guided missile is supposed to ride, also known as beam-rider guidance. The LOS guidance principle is illustrated in Fig. 4, where the associated velocity command is represented by a vector pointing to the left of the target.

3.2 Pure pursuit guidance

Pure pursuit (PP) guidance belongs to the so-called two-point guidance schemes, where only the interceptor and the target are considered in the engagement geometry. Simply put, the interceptor is supposed to align its velocity along the line of sight between the interceptor and the target. This strategy is equivalent to a predator chasing a prey in the animal world, and very often results in a tail chase. PP guidance has typically been employed for air-to-surface missiles. The PP guidance principle is represented in Fig. 4 by a vector pointing directly at the target.

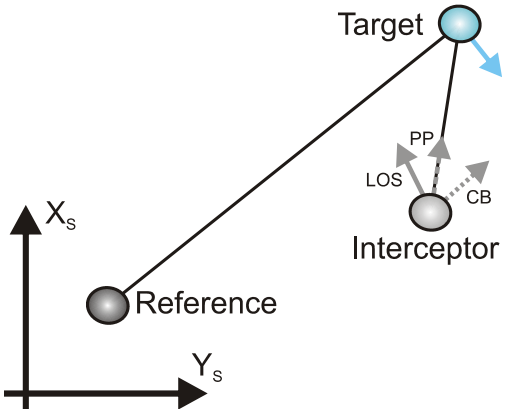

Fig. 4. The interceptor velocity commands that are associated with the classical guidance principles line of sight (LOS), pure pursuit (PP), and constant bearing (CB)

Deviated pursuit guidance is a variant of PP guidance where the velocity of the interceptor is supposed to lead the interceptor-target line of sight by a constant angle in the direction of the target movement. An equivalent term is fixed-lead navigation.

3.3 Constant bearing guidance

Constant bearing (CB) guidance is also a two-point guidance scheme, with the same engagement geometry as PP guidance. However, in a CB engagement, the interceptor is supposed to align the *relative* interceptor-target velocity along the line of sight between the interceptor and the target. This goal is equivalent to reducing the LOS rotation rate to zero such that the interceptor perceives the target at a constant bearing, closing in on a direct collision course. CB guidance is often referred to as parallel navigation, and has typically been employed for air-to-air missiles. Also, the CB rule has been used for centuries by mariners to avoid collisions at sea; steering away from a situation where another vessel approaches at a constant bearing. Thus, guidance principles can just as well be applied to avoid collisions as to achieve them. The CB guidance principle is indicated in Fig. 4 by a vector pointing to the right of the target.

The most common method of implementing CB guidance is to make the rotation rate of the interceptor velocity directly proportional to the rotation rate of the interceptor-target LOS, which is widely known as proportional navigation (PN).

CB guidance can also be implemented through the direct velocity assignment

$$\mathbf{v}(t) = \mathbf{v}_t(t) - \kappa(t)\frac{\tilde{\mathbf{p}}(t)}{|\tilde{\mathbf{p}}(t)|}, \tag{2}$$

where

$$\tilde{\mathbf{p}}(t) \triangleq \mathbf{p}(t) - \mathbf{p}_t(t) \tag{3}$$

is the line of sight vector between the interceptor and the target, $|\tilde{\mathbf{p}}(t)| \triangleq \sqrt{\tilde{\mathbf{p}}(t)^{\mathrm{T}}\tilde{\mathbf{p}}(t)} \geq 0$ is the Euclidean length of this vector, and where $\kappa(t) \geq 0$ can be chosen as

$$\kappa(t) = U_{\mathrm{a,max}} \frac{\left|\tilde{\mathbf{p}}(t)\right|}{\sqrt{\tilde{\mathbf{p}}(t)^{\mathrm{T}}\tilde{\mathbf{p}}(t) + \Delta_{\tilde{\mathrm{p}}}^2}}, \tag{4}$$

where $U_{\mathrm{a,max}} > 0$ specifies the maximum approach speed toward the target, and $\Delta_{\tilde{\mathrm{p}}} > 0$ affects the transient interceptor-target rendezvous behavior.

Note that CB guidance becomes equal to PP guidance for a stationary target, i.e., the basic difference between the two guidance schemes is whether the target velocity is used as a kinematic feedforward or not.

Returning to the example on motion camouflage, it seems that two main strategies are in use; camouflage against an object close by and camouflage against an object at infinity. The first strategy clearly corresponds to LOS guidance, while the second strategy equals CB guidance since it entails a non-rotating predator-prey line of sight.

4. Guidance laws for path scenarios

In this section, guidance laws for different path scenarios are considered, including path following, path tracking, and path maneuvering. Specifically, the guidance laws are composed of speed and steering laws, which can be combined in various ways to achieve different motion control objectives. The speed is denoted $U(t) \triangleq |\mathbf{v}(t)| = \sqrt{\dot{x}(t)^2 + \dot{y}(t)^2} \geq 0$, while the steering is denoted $\chi(t) \triangleq \mathrm{atan2}(\dot{y}(t), \dot{x}(t)) \in \mathbb{S} \triangleq [-\pi, \pi]$, where $\mathrm{atan2}(y, x)$ is the four-quadrant version of $\arctan(y/x) \in \langle -\pi/2, \pi/2 \rangle$.

Path following is ensured by proper assignments to $\chi(t)$ as long as $U(t) > 0$ since the scenario only involves a spatial constraint, while the spatio-temporal path-tracking and path-maneuvering scenarios both require explicit speed laws in addition to the steering laws. The following material is adapted from (Breivik & Fossen 2004a), (Breivik & Fossen 2005b), and (Breivik et al. 2008).

4.1 Steering laws for straight lines

Consider a straight-line path implicitly defined by two waypoints through which it passes. Denote these waypoints as $\mathbf{p}_{\mathrm{k}} \triangleq [x_{\mathrm{k}}, y_{\mathrm{k}}]^{\mathrm{T}} \in \mathbb{R}^2$ and $\mathbf{p}_{\mathrm{k+1}} \triangleq [x_{\mathrm{k+1}}, y_{\mathrm{k+1}}]^{\mathrm{T}} \in \mathbb{R}^2$, respectively. Also, consider a path-fixed reference frame with origin in $\mathbf{p}_{\mathrm{k}}$, whose x-axis has been rotated a positive angle $\alpha_{\mathrm{k}} \triangleq \mathrm{atan2}(y_{\mathrm{k+1}} - y_{\mathrm{k}}, x_{\mathrm{k+1}} - x_{\mathrm{k}}) \in \mathbb{S}$ relative to the x-axis of the stationary reference frame. Hence, the coordinates of the kinematic vehicle in the path-fixed reference frame can be computed by

$$\boldsymbol{\varepsilon}(t) = \mathbf{R}(\alpha_{\mathrm{k}})^{\mathrm{T}}(\mathbf{p}(t) - \mathbf{p}_{\mathrm{k}}), \tag{5}$$

where

$$\mathbf{R}(\alpha_{\mathrm{k}}) \triangleq \begin{bmatrix} \cos\alpha_{\mathrm{k}} & -\sin\alpha_{\mathrm{k}} \\ \sin\alpha_{\mathrm{k}} & \cos\alpha_{\mathrm{k}} \end{bmatrix}, \tag{6}$$

and $\boldsymbol{\varepsilon}(t) \triangleq [s(t), e(t)]^{\mathrm{T}} \in \mathbb{R}^2$ consists of the *along-track distance* $s(t)$ and the *cross-track error* $e(t)$, see Fig. 5. For path-following purposes, only the cross-track error is relevant since

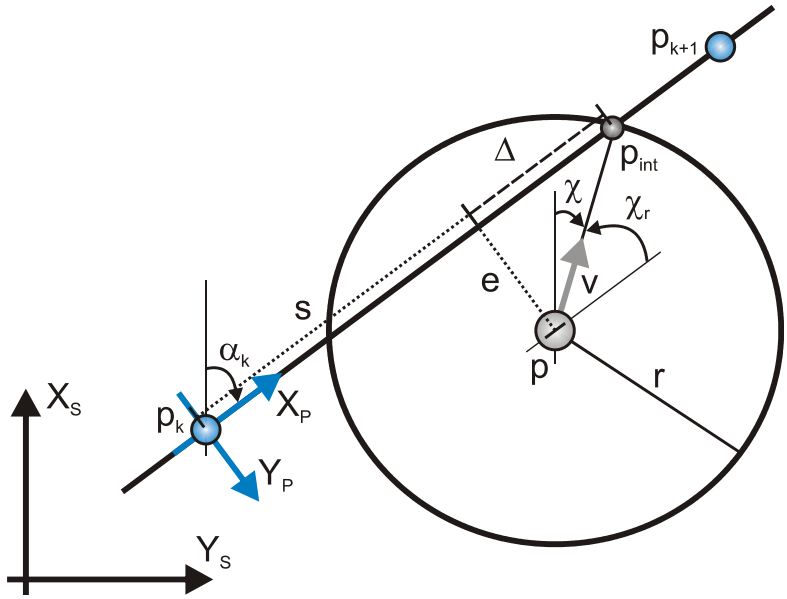

Fig. 5. The main variables associated with steering laws for straight-line paths

$e(t) = 0$ means that the vehicle has converged to the straight line. Expanding (5), the cross-track error can be explicitly stated by

$$e(t) = -(x(t) - x_k)\sin\alpha_k + (y(t) - y_k)\cos\alpha_k, \tag{7}$$

and the associated control objective for straight-line path following becomes

$$\lim_{t\to\infty} e(t) = 0. \tag{8}$$

In the following, two steering laws that ensure stabilization of $e(t)$ to the origin will be presented. The first method is used in ship motion control systems (Fossen 2002), and will be referred to as enclosure-based steering. The second method is called lookahead-based steering, and has links to the classical guidance principles from the missile literature. The two steering methods essentially operate by the same principle, but as will be made clear, the lookahead-based scheme has several advantages over the enclosure-based approach.

4.1.1 Enclosure-based steering

Imagine a circle with radius $r > 0$ enclosing $\mathbf{p}(t)$. If the circle radius is chosen sufficiently large, the circle will intersect the straight line at two points. The enclosure-based strategy for driving $e(t)$ to zero is then to direct the velocity toward the intersection point that corresponds to the desired direction of travel, which is implicitly defined by the sequence in which the waypoints are ordered. Such a solution involves directly assigning

$$\chi(t) = \text{atan2}(y_{\text{int}}(t) - y(t), x_{\text{int}}(t) - x(t)), \tag{9}$$

where $\mathbf{p}_{\text{int}}(t) \triangleq [x_{\text{int}}(t), y_{\text{int}}(t)]^{\text{T}} \in \mathbb{R}^2$ represents the intersection point of interest. In order to calculate $\mathbf{p}_{\text{int}}(t)$ (two unknowns), the following two equations must be solved

$$(x_{\text{int}}(t) - x(t))^2 + (y_{\text{int}}(t) - y(t))^2 = r^2 \tag{10}$$

$$\tan(\alpha_{\text{k}}) = \frac{y_{\text{k+1}} - y_{\text{k}}}{x_{\text{k+1}} - x_{\text{k}}}$$

$$= \frac{y_{\text{int}}(t) - y_{\text{k}}}{x_{\text{int}}(t) - x_{\text{k}}}, \tag{11}$$

where (10) represents the theorem of Pythagoras, while (11) states that the slope of the line between the two waypoints is constant. These equations are solved in the following, temporarily dropping the time dependence of the variables for notational convenience.
Denote the difference between the x- and y-position of the two waypoints as $\Delta x \triangleq x_{\text{k+1}} - x_{\text{k}}$ and $\Delta y \triangleq y_{\text{k+1}} - y_{\text{k}}$, respectively. The equations are first solved analytically assuming that $|\Delta x| > 0$ and secondly for the case $\Delta x = 0$.

Case 1: $|\Delta x| > 0$

Equation (11) results in

$$y_{\text{int}} = \left(\frac{\Delta y}{\Delta x}\right)(x_{\text{int}} - x_{\text{k}}) + y_{\text{k}} \tag{12}$$

when choosing to solve for y_{int}. For simplicity and brevity in the calculations to follow, denote

$$d \triangleq \left(\frac{\Delta y}{\Delta x}\right)$$

$$e \triangleq x_{\text{k}}$$

$$f \triangleq y_{\text{k}}.$$

Writing out (10), yields

$$x_{\text{int}}^2 - 2xx_{\text{int}} + x^2 + y_{\text{int}}^2 - 2yy_{\text{int}} + y^2 = r^2, \tag{13}$$

where

$$y_{\text{int}}^2 = \left(\left(\frac{\Delta y}{\Delta x}\right)(x_{\text{int}} - x_{\text{k}}) + y_{\text{k}}\right)^2$$

$$= (dx_{\text{int}} + (f - de))^2$$

$$= (dx_{\text{int}} + g)^2$$

$$= d^2x_{\text{int}}^2 + 2dgx_{\text{int}} + g^2, \tag{14}$$

where

$$g \triangleq f - de = y_k - \left(\frac{\Delta y}{\Delta x}\right) x_k$$

has been used. Subsequently, consider

$$2yy_{int} = 2y(dx_{int} + g) = 2dyx_{int} + 2gy, \tag{15}$$

such that (14) and (15) inserted into (13) gives

$$(1 + d^2)x_{int}^2 + 2(dg - dy - x)x_{int} + (x^2 + y^2 + g^2 - 2gy - r^2) = 0, \tag{16}$$

which is a standard, analytically-solvable second order equation. Then, denote

$$a \triangleq 1 + d^2$$

$$b \triangleq 2(dg - dy - x)$$

$$c \triangleq x^2 + y^2 + g^2 - 2gy - r^2,$$

from which the solution of (16) becomes

$$x_{int} = \frac{-b \pm \sqrt{b^2 - 4ac}}{2a}, \tag{17}$$

where if $\Delta x > 0$, then $x_{int} = \frac{-b + \sqrt{b^2 - 4ac}}{2a}$, and if $\Delta x < 0$, then $x_{int} = \frac{-b - \sqrt{b^2 - 4ac}}{2a}$. Having calculated x_{int}, y_{int} is easily obtained from (12). Note that when $\Delta y = 0$, $y_{int} = y_k$ $(= y_{k+1})$.

Case 2: $\Delta x = 0$

If $\Delta x = 0$, only equation (10) is valid, which means that

$$y_{int} = y \pm \sqrt{r^2 - (x_{int} - x)^2}, \tag{18}$$

where $x_{int} = x_k$ $(= x_{k+1})$. If $\Delta y > 0$, then $y_{int} = y + \sqrt{r^2 - (x_{int} - x)^2}$, and if $\Delta y < 0$, then $y_{int} = y - \sqrt{r^2 - (x_{int} - x)^2}$. When $\Delta x = 0$, $\Delta y = 0$ is not an option.

4.1.2 Lookahead-based steering

Here, the steering assignment is separated into two parts

$$\chi(e) = \chi_p + \chi_r(e), \tag{19}$$

where

$$\chi_p = \alpha_k \tag{20}$$

is the path-tangential angle, while

$$\chi_r(e) \triangleq \arctan\left(-\frac{e(t)}{\Delta}\right) \tag{21}$$

is a velocity-path relative angle which ensures that the velocity is directed toward a point on the path that is located a *lookahead distance* $\Delta > 0$ ahead of the direct projection of $\mathbf{p}(t)$ onto the path (Papoulias 1991), see Fig. 5.

As can be immediately noticed, this lookahead-based steering scheme is less computationally intensive than the enclosure-based approach. It is also valid for all cross-track errors, whereas the enclosure-based strategy requires $r \geq |e(t)|$. Furthermore, Fig. 5 shows that

$$e^2 + \Delta^2 = r^2, \tag{22}$$

which means that the enclosure-based approach corresponds to a lookahead-based scheme with a time-varying $\Delta(t) = \sqrt{r^2 - e(t)^2}$, varying between 0 (when $|e(t)| = r$) and r (when $|e(t)| = 0$). Only lookahead-based steering will be considered in the following.

4.2 Piecewise linear paths

If a path is made up of n straight-line segments connected by n+1 waypoints, a strategy must be employed to purposefully switch between these segments as they are traversed. In (Fossen 2002), it is suggested to associate a so-called circle of acceptance with each waypoint, with radius $R_{k+1} > 0$ for waypoint $k+1$, such that the corresponding switching criterion becomes

$$(x_{k+1} - x(t))^2 + (y_{k+1} - y(t))^2 \leq R_{k+1}^2, \tag{23}$$

i.e., to switch when $\mathbf{p}(t)$ has entered the waypoint-enclosing circle. Note that for the enclosure-based approach, such a switching criterion entails the additional (conservative) requirement $r \geq R_{k+1}$.

A perhaps more suitable switching criterion solely involves the along-track distance $s(t)$, such that if the total along-track distance between waypoints $\mathbf{p}_k$ and $\mathbf{p}_{k+1}$ is denoted s_{k+1}, a switch is made when

$$(s_{k+1} - s(t)) \leq R_{k+1}, \tag{24}$$

which is similar to (23), but has the advantage that $\mathbf{p}(t)$ does not need to enter the waypoint-enclosing circle for a switch to occur, i.e., no restrictions are put on the cross-track error. Thus, if no intrinsic value is associated with visiting the waypoints, and their only purpose is to implicitly define a piecewise linear path, there is no reason to apply the circle-of-acceptance switching criterion (23).

4.3 Steering for circles

Denote the center of a circle with radius $r_c > 0$ as $\mathbf{p}_c \triangleq [x_c, y_c]^T \in \mathbb{R}^2$. Subsequently, consider a path-fixed reference frame with origin at the direct projection of $\mathbf{p}(t)$ onto the circular

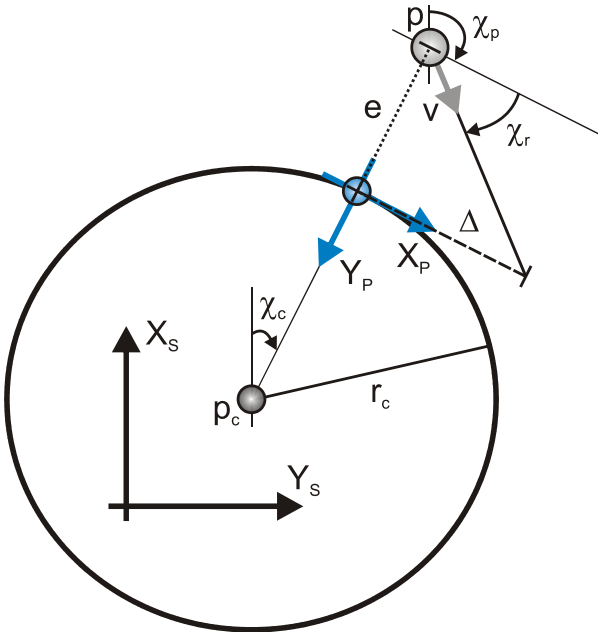

Fig. 6. The main variables associated with steering for circles

path, see Fig. 6. The x-axis of this reference frame has been rotated a positive angle (relative to the x-axis of the stationary reference frame)

$$\chi_{\mathrm{p}}(t) = \chi_{\mathrm{c}}(t) + \lambda\frac{\pi}{2}, \tag{25}$$

where

$$\chi_{\mathrm{c}}(t) \triangleq \operatorname{atan2}\big(y(t) - y_{\mathrm{c}}, x(t) - x_{\mathrm{c}}\big), \tag{26}$$

and $\lambda \in \{-1,1\}$ with $\lambda = -1$ corresponding to anti-clockwise motion and $\lambda = 1$ to clockwise motion. Hence, χ_{p} becomes time-varying for circular (curved) motion, as opposed to the constant χ_{p} associated with straight lines (20). Also, note that (26) is undefined for $\mathbf{p}(t) = \mathbf{p}_{\mathrm{c}}$, i.e., when the kinematic vehicle is located at the circle center. In this case, any projection of $\mathbf{p}(t)$ onto the circular path is valid, but in practice this problem can be alleviated by, e.g., purposefully choosing $\chi_{\mathrm{c}}(t)$ based on the motion of $\mathbf{p}(t)$.

Since the path-following control objective for circles is identical to (8), lookahead-based steering can be employed, implemented by using (19) with (25) instead of (20), and

$$\begin{aligned} e(t) &= r_{\mathrm{c}} - \left|\mathbf{p}(t) - \mathbf{p}_{\mathrm{c}}\right| \\ &= r_{\mathrm{c}} - \sqrt{(x(t) - x_{\mathrm{c}})^2 - (y(t) - y_{\mathrm{c}})^2} \end{aligned} \tag{27}$$

in (21), see Fig. 6. Note that the lookahead distance Δ is no longer defined along the path, but (in general) along the x-axis of the path-fixed frame (i.e., along the path tangential associated with the origin of the path-fixed frame). An along-track distance $s(t)$ can also be computed relative to some fixed point on the circle perimeter if required.

4.4 Steering for regularly parameterized paths

Consider a planar path continuously parameterized by a scalar variable $\varpi \in \mathbb{R}$, such that the position of a point belonging to the path is represented by $\mathbf{p}_{\mathrm{p}}(\varpi) \in \mathbb{R}^2$. Thus, the path is a one-dimensional manifold that can be expressed by the set

$$\mathcal{P} \triangleq \left\{ \mathbf{p} \in \mathbb{R}^2 \mid \mathbf{p} = \mathbf{p}_{\mathrm{p}}(\varpi) \ \forall \ \varpi \in \mathbb{R} \right\}. \tag{28}$$

Regularly parameterized paths belong to the subset of $\mathcal{P}$ for which $\left| \mathbf{p}_{\mathrm{p}}'(\varpi) \right| \triangleq \left| \mathrm{d}\mathbf{p}_{\mathrm{p}}(\varpi) / \mathrm{d}\varpi \right|$ is non-zero and finite, which means that such paths never degenerate into a point nor have corners. These paths include both straight lines (zero curvature) and circles (constant curvature). However, most are paths with varying curvature. For such paths, it is not trivial to calculate the cross-track error $e(t)$ required in (21).

Although it is possible to calculate the exact projection of $\mathbf{p}(t)$ onto the path by applying the so-called Serret-Frenet equations, such an approach suffers from a kinematic singularity associated with the osculating circle of the instantaneous projection point (Samson 1992). For every point along a curved path, there exists an associated tangent circle with radius $r(\varpi) = 1 / c(\varpi)$, where $c(\varpi)$ is the curvature at the path point. This circle is known as the osculating circle, and if at any time $\mathbf{p}(t)$ is located at the origin of the osculating circle, the projected point on the path will have to move infinitely fast, which is not possible. This kinematic singularity effect necessitates a different approach to obtain the cross-track error required for steering purposes. The solution considered here seems to first have been suggested in (Aicardi et al. 1995), then refined and put into a differential-geometric framework in (Lapierre et al. 2003), and finally extended into the form presented below in (Breivik & Fossen 2004b).

Thus, consider an arbitrary path point $\mathbf{p}_{\mathrm{p}}(\varpi)$. Subsequently, consider a path-fixed reference frame with origin at $\mathbf{p}_{\mathrm{p}}(\varpi)$, whose x-axis has been rotated a positive angle (relative to the x-axis of the stationary reference frame)

$$\chi_{\mathrm{p}}(\varpi) = \operatorname{atan2}\left(y_{\mathrm{p}}'(\varpi), x_{\mathrm{p}}'(\varpi) \right), \tag{29}$$

such that

$$\boldsymbol{\varepsilon}(t) = \mathbf{R}(\chi_{\mathrm{p}})^{\mathrm{T}} (\mathbf{p}(t) - \mathbf{p}_{\mathrm{p}}(\varpi)), \tag{30}$$

where $\boldsymbol{\varepsilon}(t) = \left[s(t), e(t) \right]^{\mathrm{T}} \in \mathbb{R}^2$ represents the *along-track* and *cross-track errors* relative to $\mathbf{p}_{\mathrm{p}}(\varpi)$, decomposed in the path-fixed reference frame by

$$\mathbf{R}(\chi_{\mathrm{p}}) = \begin{bmatrix} \cos\chi_{\mathrm{p}} & -\sin\chi_{\mathrm{p}} \\ \sin\chi_{\mathrm{p}} & \cos\chi_{\mathrm{p}} \end{bmatrix}. \tag{31}$$

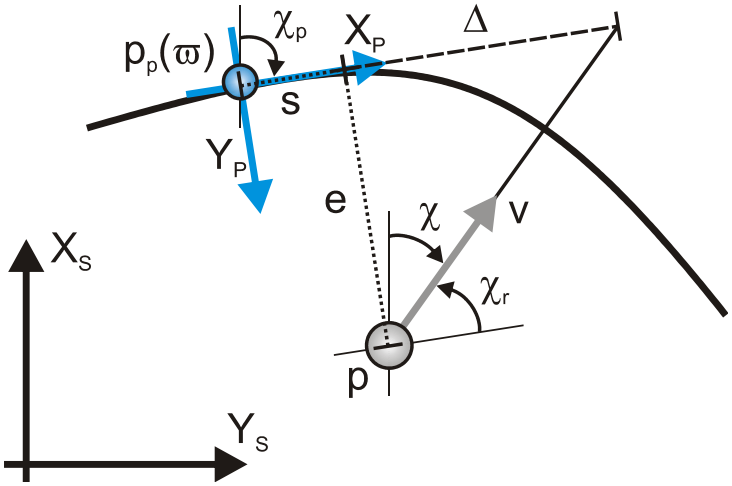

Fig. 7. The main variables associated with steering for regularly parameterized paths

In contrast to (8), the path-following control objective now becomes

$$\lim_{t\to\infty} \boldsymbol{\varepsilon}(t) = \mathbf{0}, \tag{32}$$

and in order to reduce $\boldsymbol{\varepsilon}(t)$ to zero, $\mathbf{p}(t)$ and $\mathbf{p}_{\mathrm{p}}(\varpi)$ can collaborate with each other. Specifically, $\mathbf{p}_{\mathrm{p}}(\varpi)$ can contribute by moving toward the direct projection of $\mathbf{p}(t)$ onto the x-axis of the path-fixed reference frame by assigning

$$\dot{\varpi} = \frac{U(t)\cos\chi_{\mathrm{r}}(e) + \gamma s(t)}{\left|\mathbf{p}_{\mathrm{p}}'(\varpi)\right|}, \tag{33}$$

where $\chi_{\mathrm{r}}(e)$ is given by (21), $\gamma > 0$, and $\left|\mathbf{p}_{\mathrm{p}}'(\varpi)\right| = \sqrt{x_{\mathrm{p}}'(\varpi)^2 + y_{\mathrm{p}}'(\varpi)^2}$. As can be seen, the first element of the numerator represents a kinematic feedforward of the projected speed of $\mathbf{p}(t)$ onto the path tangential, while the second element represents a linear feedback term whose purpose is to reduce the along-track error to zero. Hence, the path-constrained attractor $\mathbf{p}_{\mathrm{p}}(\varpi)$ tracks the motion of $\mathbf{p}(t)$, which steers by the location of $\mathbf{p}_{\mathrm{p}}(\varpi)$ through the cross-track error of (30) by employing (19) with (29) and (21) for $U(t) > 0$. Such an approach suffers from no kinematic singularities, and ensures that $\boldsymbol{\varepsilon}(t)$ is reduced to zero for regularly parameterized paths. To avoid initial transients in $e(t)$, the initial along-track error $s(0)$ can be minimized offline.

4.4.1 Relations to classical guidance laws

Drawing a connection to the classical guidance principles of the missile literature, lookahead-based steering can be interpreted as pure pursuit of the lookahead point. Convergence to $\mathbf{p}_{\mathrm{p}}(\varpi)$ is thus achieved as $\mathbf{p}(t)$ in vain chases a carrot located a distance Δ further ahead along the path tangential. However, in (Papoulias 1992), the lookahead point is suggested to be placed further ahead along the path instead of along the path tangential,

which leads to a steady-state offset in the cross-track error for curved paths. In this case, the velocity of $\mathbf{p}(t)$ cannot be aligned with the velocity of $\mathbf{p}_{\mathrm{p}}(\varpi)$ for zero cross-track error. This distinction is vital for curved paths, but not for straight-line paths, where the path tangential is always directed along the path. Thus, in general, the pursued carrot must be located along the path tangential and not along the path itself. Nevertheless, the along-path approach has been widely reported in the literature, see, e.g., (Ollero & Heredia 1995), (Rankin et al. 1997), and (Castaño et al. 2005).

4.4.2 Off-path traversing of curved paths

In some applications, it can be desirable to perform off-path traversing of regularly parameterized paths. Specifically, off-path traversing of curved paths requires the use of two virtual points to avoid kinematic singularities. This concept was originally suggested in (Breivik et al. 2006), and used for formation control of ships in (Breivik et al. 2008).

4.4.3 Path parameterizations

Although the recently-presented guidance method also can be applied for both straight lines and circles, the analytic, path-specific approaches presented previously are often preferable since they do not require numerical integrations such as (33). However, for completeness, applicable (arc-length) parameterizations of straight lines and circles are given in the following.

Parameterization of straight lines

A planar straight line can be parameterized by $\varpi \in \mathbb{R}$ as

$$x_{\mathrm{p}}(\varpi) = x_{\mathrm{f}} + \varpi \cos\alpha \tag{34}$$

$$y_{\mathrm{p}}(\varpi) = y_{\mathrm{f}} + \varpi \sin\alpha, \tag{35}$$

where $\mathbf{p}_{\mathrm{f}} \triangleq [x_{\mathrm{f}}, y_{\mathrm{f}}]^{\mathrm{T}} \in \mathbb{R}^2$ represents a fixed point on the path (for which ϖ is defined relative to), and $\alpha \in \mathbb{S}$ represents the orientation of the path relative to the x-axis of the stationary reference frame (corresponding to the direction of increasing ϖ).

Parameterization of circles

A planar circle can be parameterized by $\varpi \in \mathbb{R}$ as

$$x_{\mathrm{p}}(\varpi) = x_{\mathrm{c}} + r_{\mathrm{c}} \cos\left(\frac{\varpi}{r_{\mathrm{c}}}\right) \tag{36}$$

$$y_{\mathrm{p}}(\varpi) = y_{\mathrm{c}} + \lambda r_{\mathrm{c}} \sin\left(\frac{\varpi}{r_{\mathrm{c}}}\right), \tag{37}$$

where $\mathbf{p}_{\mathrm{c}} = [x_{\mathrm{c}}, y_{\mathrm{c}}]^{\mathrm{T}} \in \mathbb{R}^2$ represents the circle center, $r_{\mathrm{c}} > 0$ represents the circle radius, and $\lambda \in \{-1, 1\}$ decides in which direction $\mathbf{p}_{\mathrm{p}}(\varpi)$ traces the circumference; $\lambda = -1$ for anti-clockwise motion and $\lambda = 1$ for clockwise motion.

4.5 Speed law for path tracking

As previously stated, the control objective of a path-tracking scenario is to track a target that is constrained to move along a path. Denoting the path-parameterization variable associated with the path-traversing target by $\varpi_t(t) \in \mathbb{R}$, the control objective is identical to (1) with $\mathbf{p}_t(t) = \mathbf{p}_p(\varpi_t(t))$. Here, $\varpi_t(t)$ can be updated by

$$\dot{\varpi}_t = \frac{U_t(t)}{\left|\mathbf{p}_p'(\varpi_t)\right|}, \tag{38}$$

which means that the target point traverses the path with the speed profile $U_t(t) > 0$, which can also be made to vary with ϖ_t.

Naturally, this problem can be solved by the target-tracking methods of Section 3, e.g., through the direct velocity assignment (2). However, by using such methods, all available path information is disregarded, and $\mathbf{p}(t)$ will appear to be "cutting corners" in its pursuit of $\mathbf{p}_p(\varpi_t(t))$, seeing only $\mathbf{p}_t(t)$.

Another approach is to employ the path knowledge that is apriori available, to divide the path-tracking problem into two tasks, i.e., a spatial task and a temporal task (Skjetne et al. 2004). The spatial task was just solved in the previous part, while the temporal task can be solved by employing the speed law

$$U(t) = \left|\mathbf{p}_p'(\varpi)\right| \left(\frac{U_t(t)}{\left|\mathbf{p}_p'(\varpi_t)\right|} - \mu \frac{\tilde{\varpi}(t)}{\sqrt{\tilde{\varpi}(t)^2 + \Delta_{\tilde{\varpi}}^2}} \right), \tag{39}$$

where

$$\tilde{\varpi}(t) \triangleq \varpi(t) - \varpi_t(t), \tag{40}$$

μ can be chosen as

$$\mu = \rho \frac{U_t(t)}{\left|\mathbf{p}_p'(\varpi_t)\right|}, \ \rho \in \langle 0, 1], \tag{41}$$

and where $\Delta_{\tilde{\varpi}} > 0$ specifies the rendezvous behavior toward the target, such that

$$U(t) = U_t(t) \left(1 - \rho \frac{\tilde{\varpi}(t)}{\sqrt{\tilde{\varpi}(t)^2 + \Delta_{\tilde{\varpi}}^2}} \right) \frac{\left|\mathbf{p}_p'(\varpi(t))\right|}{\left|\mathbf{p}_p'(\varpi_t(t))\right|}, \tag{42}$$

which means that the kinematic vehicle speeds up to catch the target when located behind it, and speeds down to wait when located in front of it. Hence, this approach entails a synchronization-law extension of the path-following scenario, where no corners are cut.

4.6 Path maneuvering aspects

The path-maneuvering scenario involves the use of knowledge about vehicle maneuverability constraints to design purposeful speed and steering laws that allow for feasible path negotiation. Since this work only deals with kinematic considerations, such

deliberations are outside of its scope. However, relevant work in this vein include (Sheridan 1966), (Yoshimoto et al. 2000), (Skjetne et al. 2004), (Børhaug et al. 2006), (Subbotin et al. 2006), (Gomes et al. 2006), and (Sharp 2007). Much work still remains to be done on this topic, which represents a rich source of interesting and challenging problems.

4.7 Steering laws as saturated control laws

Rewriting (21) as

$$\chi_{\mathrm{r}}(e) = \arctan\left(-k_{\mathrm{p}} e(t)\right),\ k_{\mathrm{p}} = \frac{1}{\Delta} > 0, \tag{43}$$

it can be seen that the lookahead-based steering law is equivalent to a saturated proportional control law, effectively mapping $e \in \mathbb{R}$ into $\chi_{\mathrm{r}}(e) \in \langle -\pi/2, \pi/2 \rangle$.

As can be inferred from the geometry of Fig. 5, a small lookahead distance implies aggressive steering, which intuitively is confirmed by a correspondingly large proportional gain in the saturated control interpretation. This interpretation also suggests the possibility of introducing, e.g., integral action into the steering law, such that

$$\chi_{\mathrm{r}}(e) = \arctan\left(-k_{\mathrm{p}} e(t) - k_{\mathrm{i}} \int_0^t e(\tau)\mathrm{d}\tau\right), \tag{44}$$

where $k_{\mathrm{i}} > 0$ represents the integral gain. Note that such integral action is not necessary in a purely kinematic setting, but can be particularly useful for underactuated AUVs that can only steer by attitude information, enabling them to follow straight-line paths while under the influence of constant ocean currents even without having access to velocity information. Thus, considering horizontal path following along straight lines, the desired yaw angle can be computed by

$$\psi_{\mathrm{d}}(e) = \alpha_{\mathrm{k}} + \chi_{\mathrm{r}}(e) \tag{45}$$

with $\chi_{\mathrm{r}}(e)$ as in (44). In practice, to avoid overshoot and windup effects, care must be taken when using integral action in the steering law. Specifically, the integral term should only be used when a steady-state off-track condition has been detected.

For those AUVs that do have access to velocity information, temporal integration can be replaced by spatial integration in order to minimize overshoot and windup problems (Davidson et al. 2002), employing

$$\chi_{\mathrm{r}}(e) = \arctan\left(-k_{\mathrm{p}} e(t) - k_{\mathrm{i}} \int_0^s e(\sigma)\mathrm{d}\sigma\right), \tag{46}$$

where for straight-line paths

$$\int_0^s e(\sigma)\mathrm{d}\sigma = \int_0^t e(\tau)\frac{\mathrm{d}\sigma}{\mathrm{d}\tau}\mathrm{d}\tau \tag{47}$$

$$= \int_0^t e(\tau) U(\tau) \cos(\chi(\tau) - \alpha_{\mathrm{k}})\mathrm{d}\tau, \tag{48}$$

which means that integration only occurs when the velocity has a component along the path. Also, derivative action can be added to the steering law in order to obtain a damped transient response toward the path.

5. Guidance laws for 3D scenarios

In this section, guidance laws for 3D motion control scenarios are considered. For spatial target-tracking purposes, the guidance principles of Section 3 remain equally valid, and the velocity assignment (2) is directly applicable for 3D target tracking. However, the steering laws of Section 4 need to be extended. Specifically, in what follows, lookahead-based steering will be put into a spatial framework for regularly parameterized paths, adapted from (Breivik & Fossen 2005b). Note that the path-tracking speed law (42) need not be modified, and can be directly applied to 3D scenarios.

Now, represent the kinematic vehicle by its spatial position $\mathbf{p}(t) \triangleq \left[x(t), y(t), z(t)\right]^{\mathrm{T}} \in \mathbb{R}^3$ and velocity $\mathbf{v}(t) \triangleq \dot{\mathbf{p}}(t) \in \mathbb{R}^3$, stated relative to some stationary reference frame. Also, the speed is represented by $U(t) \triangleq \left|\mathbf{v}(t)\right| = \sqrt{\dot{x}(t)^2 + \dot{y}(t)^2 + \dot{z}(t)^2} \geq 0$, while the steering is characterized by the two angular variables $\chi(t) \triangleq \operatorname{atan2}\left(\dot{y}(t), \dot{x}(t)\right) \in \mathbb{S}$ (the azimuth angle) and $\upsilon(t) \triangleq \operatorname{atan2}\left(-\dot{z}(t), \sqrt{\dot{x}(t)^2 + \dot{y}(t)^2}\right) \in \mathbb{S}$ (the elevation angle). Path following is then ensured by proper assignments to $\chi(t)$ and $\upsilon(t)$ as long as $U(t) > 0$.

Then, consider a spatial path continuously parameterized by a scalar variable $\varpi \in \mathbb{R}$, such that the position of a point belonging to the path is represented by $\mathbf{p}_{\mathrm{p}}(\varpi) \in \mathbb{R}^3$. Thus, the path can be expressed by the set

$$\mathcal{P} \triangleq \left\{ \mathbf{p} \in \mathbb{R}^3 \,|\, \mathbf{p} = \mathbf{p}_{\mathrm{p}}(\varpi) \;\forall\; \varpi \in \mathbb{R} \right\}. \tag{49}$$

Subsequently, consider an arbitrary path point $\mathbf{p}_{\mathrm{p}}(\varpi)$, and define a path-fixed reference frame with origin at this point. Starting with the same orientation as the stationary frame, two consecutive elementary rotations can be performed to arrive at this path-fixed frame. The first is to positively rotate the stationary frame an angle

$$\chi_{\mathrm{p}}(\varpi) = \operatorname{atan2}\left(y_{\mathrm{p}}'(\varpi), x_{\mathrm{p}}'(\varpi)\right) \tag{50}$$

about its z-axis, while the second is to positively rotate the resulting intermediate frame an angle

$$\upsilon_{\mathrm{p}}(\varpi) = \operatorname{atan2}\left(-z_{\mathrm{p}}'(\varpi), \sqrt{x_{\mathrm{p}}'(\varpi)^2 + y_{\mathrm{p}}'(\varpi)^2}\right) \tag{51}$$

about its y-axis. These rotations can also be represented by the rotation matrices

$$\mathbf{R}(\chi_{\mathrm{p}}) \triangleq \begin{bmatrix} \cos\chi_{\mathrm{p}} & -\sin\chi_{\mathrm{p}} & 0 \\ \sin\chi_{\mathrm{p}} & \cos\chi_{\mathrm{p}} & 0 \\ 0 & 0 & 1 \end{bmatrix} \tag{52}$$

and

$$\mathbf{R}(\upsilon_{\mathrm{p}}) \triangleq \begin{bmatrix} \cos\upsilon_{\mathrm{p}} & 0 & \sin\upsilon_{\mathrm{p}} \\ 0 & 1 & 0 \\ -\sin\upsilon_{\mathrm{p}} & 0 & \cos\upsilon_{\mathrm{p}} \end{bmatrix}, \tag{53}$$

respectively. Hence, the full rotation can be represented by

$$\mathbf{R}(\chi_{\mathrm{p}}, \upsilon_{\mathrm{p}}) \triangleq \mathbf{R}(\chi_{\mathrm{p}})\mathbf{R}(\upsilon_{\mathrm{p}}), \tag{54}$$

such that

$$\boldsymbol{\varepsilon}(t) = \mathbf{R}(\chi_{\mathrm{p}}, \upsilon_{\mathrm{p}})^{\mathrm{T}}(\mathbf{p}(t) - \mathbf{p}_{\mathrm{p}}(\varpi)), \tag{55}$$

where $\boldsymbol{\varepsilon}(t) = [s(t), e(t), h(t)]^{\mathrm{T}} \in \mathbb{R}^3$ represents the *along-track*, *cross-track*, and *vertical-track errors* relative to $\mathbf{p}_{\mathrm{p}}(\varpi)$, decomposed in the path-fixed reference frame. The path-following control objective is identical to (32), and $\boldsymbol{\varepsilon}(t)$ can be reduced to zero by assigning an appropriate steering law to the velocity of $\mathbf{p}(t)$ as well as a purposeful collaborative behavior to $\mathbf{p}_{\mathrm{p}}(\varpi)$.

Specifically, the steering law involves

$$\chi_{\mathrm{r}}(e) \triangleq \arctan\left(-\frac{e(t)}{\Delta}\right), \tag{56}$$

which is equivalent to (21) with $\Delta > 0$, used to shape the convergence behavior toward the xz-plane of the path-fixed frame, and

$$\upsilon_{\mathrm{r}}(h) \triangleq \arctan\left(\frac{h(t)}{\sqrt{e(t)^2 + \Delta^2}}\right), \tag{57}$$

used to shape the convergence behavior toward the xy-plane of the path-fixed frame, see Fig. 8. Also, $\mathbf{p}_{\mathrm{p}}(\varpi)$ moves collaboratively toward the direct projection of $\mathbf{p}(t)$ onto the x-axis of the path-fixed reference frame by

$$\dot{\varpi} = \frac{U(t)\cos\chi_{\mathrm{r}}(e)\cos\upsilon_{\mathrm{r}}(h) + \gamma s(t)}{\left|\mathbf{p}_{\mathrm{p}}'(\varpi)\right|}, \tag{58}$$

where $\gamma > 0$ and $\left|\mathbf{p}_{\mathrm{p}}'(\varpi)\right| = \sqrt{x_{\mathrm{p}}'(\varpi)^2 + y_{\mathrm{p}}'(\varpi)^2 + z_{\mathrm{p}}'(\varpi)^2}$. In sum, four angular variables (50), (51), (56), and (57) are used to specify the 3D steering law required for path-following purposes. Fortunately, these variables can be compactly represented by the azimuth angle

$$\chi(\chi_{\mathrm{p}}, \upsilon_{\mathrm{p}}, \chi_{\mathrm{r}}, \upsilon_{\mathrm{r}}) = \operatorname{atan2}\left(f(\chi_{\mathrm{p}}, \upsilon_{\mathrm{p}}, \chi_{\mathrm{r}}, \upsilon_{\mathrm{r}}), g(\chi_{\mathrm{p}}, \upsilon_{\mathrm{p}}, \chi_{\mathrm{r}}, \upsilon_{\mathrm{r}})\right), \tag{59}$$

where

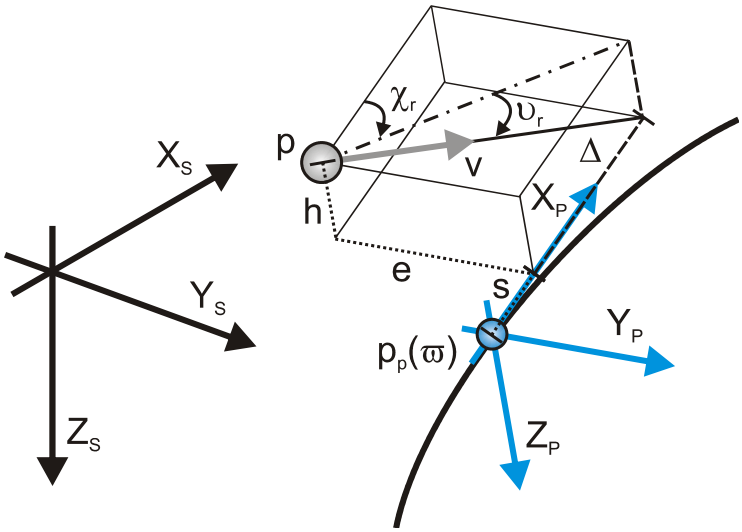

Fig. 8. The main variables associated with steering for regularly parameterized 3D paths

$$f(\chi_p,\upsilon_p,\chi_r,\upsilon_r) = \cos\chi_p \sin\chi_r \cos\upsilon_r - \sin\chi_p \sin\upsilon_p \sin\upsilon_r + \sin\chi_p \cos\upsilon_p \cos\chi_r \cos\upsilon_r \tag{60}$$

and

$$g(\chi_p,\upsilon_p,\chi_r,\upsilon_r) = -\sin\chi_p \sin\chi_r \cos\upsilon_r - \cos\chi_p \sin\upsilon_p \sin\upsilon_r + \cos\chi_p \cos\upsilon_p \cos\chi_r \cos\upsilon_r, \tag{61}$$

and the elevation angle

$$\upsilon(\upsilon_p,\chi_r,\upsilon_r) = \arcsin(\sin\upsilon_p \cos\chi_r \cos\upsilon_r + \cos\upsilon_p \sin\upsilon_r). \tag{62}$$

Through the use of trigonometric addition formulas, it can be shown that (59) is equivalent to (19) in the 2D case, i.e., when $\upsilon_p = \upsilon_r = 0$.

5.1 Path parameterizations

Applicable (arc-length) parameterizations of straight lines and helices are now given.

5.1.1 Parameterization of straight lines

A spatial straight line can be parameterized by $\varpi \in \mathbb{R}$ as

$$x_p(\varpi) = x_f + \varpi \cos\alpha \cos\beta \tag{63}$$

$$y_p(\varpi) = y_f + \varpi \sin\alpha \cos\beta \tag{64}$$

$$z_p(\varpi) = z_f - \varpi \sin\beta, \tag{65}$$

where $\mathbf{p}_\mathrm{f} \triangleq [x_\mathrm{f}, y_\mathrm{f}, z_\mathrm{f}]^\mathrm{T} \in \mathbb{R}^3$ represents a fixed point on the path (for which ϖ is defined relative to), and $\alpha \in \mathbb{S}$ represents the azimuth angle of the path, while $\beta \in \mathbb{S}$ represents the elevation angle of the path (both corresponding to the direction of increasing ϖ).

5.1.2 Parameterization of helices

A helix can be parameterized by $\varpi \in \mathbb{R}$ as

$$x_\mathrm{p}(\varpi) = x_\mathrm{c} + r_\mathrm{c} \cos\left(\frac{\varpi}{\sqrt{2} r_\mathrm{c}}\right) \tag{66}$$

$$y_\mathrm{p}(\varpi) = y_\mathrm{c} + \lambda r_\mathrm{c} \sin\left(\frac{\varpi}{\sqrt{2} r_\mathrm{c}}\right) \tag{67}$$

$$z_\mathrm{p}(\varpi) = z_\mathrm{c} - \frac{\varpi}{\sqrt{2}}, \tag{68}$$

where $\mathbf{p}_\mathrm{c} = [x_\mathrm{c}, y_\mathrm{c}, z_\mathrm{c}]^\mathrm{T} \in \mathbb{R}^3$ represents the origin of the helix center (for which ϖ is defined relative to), $r_\mathrm{c} > 0$ represents the radius of the horizontally-projected circle of the helix, and $\lambda \in \{-1, 1\}$ decides in which direction this horizontally-projected circle is traced; $\lambda = -1$ for anti-clockwise motion and $\lambda = 1$ for clockwise motion. Here, an increase in ϖ corresponds to movement in the negative direction of the z-axis of the stationary frame.

6. Conclusions

This work has given an overview of guidance laws applicable to motion control of AUVs in 2D and 3D. Specifically, considered scenarios have included target tracking, where only instantaneous information about the target motion is available, as well as path scenarios, where spatial information is available apriori. For target-tracking purposes, classical guidance laws from the missile literature were reviewed, in particular line of sight, pure pursuit, and constant bearing. For the path scenarios, enclosure-based and lookahead-based guidance laws were presented. Relations between the guidance laws have been discussed, as well as interpretations toward saturated control.

7. References

Aguiar, A. P. & Hespanha, J. P. (2004). Logic-based switching control for trajectory-tracking and path-following of underactuated autonomous vehicles with parametric modeling uncertainty. In: *Proceedings of the ACC'04, Boston, Massachusetts, USA*

Aicardi, M.; Casalino, G.; Bicchi, A. & Balestrino, A. (1995). Closed loop steering of unicycle-like vehicles via Lyapunov techniques. *IEEE Robotics and Automation Magazine* 2(1), 27—35

Antonelli, G.; Fossen, T. I. & Yoerger, D. R. (2008). Underwater robotics. In: *Springer Handbook of Robotics* (B. Siciliano and O. Khatib, Eds.). pp. 987— 1008. Springer-Verlag Berlin Heidelberg

Battin, R. H. (1982). Space guidance evolution - A personal narrative. *Journal of Guidance, Control, and Dynamics* 5(2), 97—110

Blidberg, D. R. (2001). The development of autonomous underwater vehicles (AUVs); a brief summary. In: *Proceedings of the ICRA'01, Seoul, Korea*

Breivik, M. & Fossen, T. I. (2004a). Path following of straight lines and circles for marine surface vessels. In: *Proceedings of the 6th IFAC CAMS, Ancona, Italy*

Breivik, M. & Fossen, T. I. (2004b). Path following for marine surface vessels. In: *Proceedings of the OTO'04, Kobe, Japan*

Breivik, M. & Fossen, T. I. (2005a). Guidance-based path following for autonomous underwater vehicles. In: *Proceedings of the OCEANS'05, Washington D.C., USA*

Breivik, M. & Fossen, T. I. (2005b). Principles of guidance-based path following in 2D and 3D. In: *Proceedings of the CDC-ECC'05, Seville, Spain*

Breivik, M.; Subbotin, M. V. & Fossen, T. I. (2006). Kinematic aspects of guided formation control in 2D. In: *Group Coordination and Cooperative Control* (K. Y. Pettersen, J. T. Gravdahl and H. Nijmeijer, Eds.). pp. 54—74. Springer-Verlag Heidelberg

Breivik, M. & Fossen, T. I. (2007). Applying missile guidance concepts to motion control of marine craft. In: *Proceedings of the 7th IFAC CAMS, Bol, Croatia*

Breivik, M.; Hovstein, V. E. & Fossen, T. I. (2008). Ship formation control: A guided

leader-follower approach. In: *Proceedings of the 17th IFAC World Congress, Seoul, Korea*

Breivik, M. & Fossen, T. I. (2008). Guidance laws for planar motion control. In: *Proceedings of the CDC'08, Cancun, Mexico*

Børhaug, E. & Pettersen, K. Y. (2006). LOS path following for underactuated underwater vehicle. In: *Proceedings of the 7th IFAC MCMC, Lisbon, Portugal*

Børhaug, E.; Pettersen, K. Y. & Pavlov, A. (2006). An optimal guidance scheme for cross-track control of underactuated underwater vehicles. In: *Proceedings of the MED'06, Ancona, Italy*

Caccia, M.; Bruzzone, G. & Veruggio, G. (2000). Guidance of unmanned underwater vehicles: Experimental results. In: *Proceedings of the ICRA'00, San Francisco, California, USA*

Castaño, A. R.; Ollero, A.; Vinagre, B. M. & Chen, Y. Q. (2005). Synthesis of a spatial lookahead path tracking controller. In: *Proceedings of the 16th IFAC World Congress, Prague, Czech Republic*

Cloutier, J. R.; Evers, J. H. & Feeley, J. J. (1989). Assessment of air-to-air missile guidance and control technology. *IEEE Control Systems Magazine* 9(6), 27—34

Craven, P. J.; Sutton, R. & Burns, R. S. (1998). Control strategies for unmanned underwater vehicles. *Journal of Navigation* 51, 79—105

Davidson, M.; Bahl, V. & Moore, K. L. (2002). Spatial integration for a nonlinear path tracking control law. In: *Proceedings of the ACC'02, Anchorage, Alaska, USA*

Do, K. D. & Pan, J. (2003). Robust and adaptive path following for underactuated autonomous underwater vehicles. In: *Proceedings of the ACC'03, Denver, Colorado, USA*

Draper, C. S. (1971). Guidance is forever. *Navigation* 18(1), 26—50

Encarnação, P. & Pascoal, A. (2000). 3D path following for autonomous underwater vehicle. In: *Proceedings of the CDC'00, Sydney, Australia*

Fossen, T. I. (2002). *Marine Control Systems: Guidance, Navigation and Control of Ships, Rigs and Underwater Vehicles*. Marine Cybernetics

Fossier, M. W. (1984). The development of radar homing missiles. *Journal of Guidance, Control, and Dynamics* 7(6), 641—651

Gomes, P.; Silvestre, C.; Pascoal, A. & Cunha, R. (2006). A path-following controller for the DELFIMx autonomous surface craft. In: *Proceedings of the 7th IFAC MCMC, Lisbon, Portugal*

Haeussermann, W. (1981). Developments in the field of automatic guidance and control of rockets. *Journal of Guidance and Control* 4(3), 225—239

Hagen, P. E.; Størkersen, N. J. & Vestgård, K. (2003). The HUGIN AUVs – Multi-role capability for challenging underwater survey operations. *EEZ International*

Healey, A. J. & Lienard, D. (1993). Multivariable sliding-mode control for autonomous diving and steering of unmanned underwater vehicles. *IEEE Journal of Oceanic Engineering* 18(3), 327—339

Justh, E. W. & Krishnaprasad, P. S. (2006). Steering laws for motion camouflage. *Proceedings of the Royal Society A* 462(2076), 3629—3643

Lapierre, L.; Soetanto, D. & Pascoal, A. (2003). Nonlinear path following with applications to the control of autonomous underwater vehicles. In: *Proceedings of the CDC'03, Maui, Hawaii, USA*

LaValle, S. M. (2006). *Planning Algorithms*. Cambridge University Press

Lin, C.-F. (1991). *Modern Navigation, Guidance, and Control Processing, Volume II*. Prentice Hall, Inc.

Lin, C.-L. & Su, H.-W. (2000). Intelligent control theory in guidance and control system design: An overview. *Proceedings of the National Science Council, ROC* 24(1), 15—30

Locke, A. S. (1955). *Guidance*. D. Van Nostrand Company, Inc.

MacKenzie, D. A. (1990). *Inventing Accuracy: A Historical Sociology of Nuclear Missile Guidance*. MIT Press

Mizutani, A.; Chahl, J. S. & Srinivasan, M. V. (2003). Motion camouflage in dragonflies. *Nature* 423, 604

Ollero, A. & Heredia, G. (1995). Stability analysis of mobile robot path tracking. In: *Proceedings of the IROS'95, Pittsburgh, Pennsylvania, USA*

Papoulias, F. A. (1991). Bifurcation analysis of line of sight vehicle guidance using sliding modes. *International Journal of Bifurcation and Chaos* 1(4), 849—865

Papoulias, F. A. (1992). Guidance and control laws for vehicle pathkeeping along curved trajectories. *Applied Ocean Research* 14(5), 291—302

Pastrick, H. L.; Seltzer, S. M. & Warren, M. E. (1981). Guidance laws for short-range tactical missiles. *Journal of Guidance and Control* 4(2), 98—108

Piccardo, H. R. & Honderd, G. (1991). A new approach to on-line path planning and generation for robots in non-static environments. *Robotics and Autonomous Systems* 8(3), 187—201

Rankin, A. L.; Crane III, C. D. & Armstrong II, D. G. (1997). Evaluating a PID, pure pursuit, and weighted steering controller for an autonomous land vehicle. In: *Proceedings of the SPIE Mobile Robotics XII, Pittsburgh, Pennsylvania, USA*

Refsnes, J. E.; Sørensen, A. J. & Pettersen, K. Y. (2008). Model-based output feedback control of slender-body underactuated AUVs: Theory and experiments. *IEEE Transactions on Control Systems Technology* 16(5), 930—946

Roberts, G. N. & Sutton, R. (2006). *Advances in Unmanned Marine Vehicles*. The Institution of Electrical Engineers

Samson, C. (1992). Path following and time-varying feedback stabilization of a wheeled mobile robot. In: *Proceedings of the ICARCV'92, Singapore*

Sciavicco, L. & Siciliano, B. (2002). *Modelling and Control of Robot Manipulators*. Springer-Verlag London Ltd.

Sharp, R. S. (2007). Application of optimal preview control to speed-tracking of road vehicles. *Proceedings of the Institution of Mechanical Engineers, Part C: Journal of Mechanical Engineering Science* 221(12), 1571—1578

Sheridan, T. B. (1966). Three models of preview control. *IEEE Transactions on Human Factors in Electronics* 7(2), 91—102

Shneydor, N. A. (1998). *Missile Guidance and Pursuit: Kinematics, Dynamics and Control*. Horwood Publishing Ltd.

Siouris, G. M. (2004). *Missile Guidance and Control Systems*. Springer-Verlag New York, Inc.

Skjetne, R.; Fossen, T. I. & Kokotović, P. V. (2004). Robust output maneuvering for a class of nonlinear systems. *Automatica* 40(3), 373—383

Spearman, M. L. (1978). Historical development of worldwide guided missiles. In: *AIAA 16th Aerospace Sciences Meeting, Huntsville, Alabama, USA*

Subbotin, M. V.; Dăcić, D. B. & Smith, R. S. (2006). Preview based path-following in the presence of input constraints. In: *Proceedings of the ACC'06, Minneapolis, Minnesota, USA*

Valavanis, K. P.; Gracanin, D.; Matijasevic, M.; Kolluru, R. & Demetriou, G. A. (1997). Control architectures for autonomous underwater vehicles. *IEEE Control Systems Magazine* 17(6), 48—64

Wernli, R. L. (2000). AUV commercialization – Who's leading the pack?. In: *Proceedings of the OCEANS'00, Providence, Rhode Island, USA*

Westrum, R. (1999). *Sidewinder: Creative Missile Development at China Lake*. Naval Institute Press

Whitcomb, L. (2000). Underwater robotics: Out of the research laboratory and into the field. In: *Proceedings of the ICRA'00, San Francisco, California, USA*

White, B. A. & Tsourdos, A. (2001). Modern missile guidance design: An overview. In: *Proceedings of the IFAC Automatic Control in Aerospace, Bologna, Italy*

Yanushevsky, R. (2008). *Modern Missile Guidance*. CRC Press

Yoshimoto, K.; Katoh, M. & Inoue, K. (2000). A vision-based speed control algorithm for autonomous driving. In: *Proceedings of the AVEC'00, Ann Arbor, Michigan, USA*

Zarchan, P. (2002). *Tactical and Strategic Missile Guidance*. 4th ed.. American Institute of Aeronautics and Astronautics, Inc.

I. Modeling and Control of Underway Replenishment Operations in Calm Water

MODELING AND CONTROL OF UNDERWAY REPLENISHMENT OPERATIONS IN CALM WATER

Renato Skejic[1] **Morten Breivik**[2] **Thor I. Fossen**[2,3] **Odd M. Faltinsen**[2,4]

[1] *MARINTEK,*
NO - 7052 Trondheim, Norway (e-mail: renato.skejic@marintek.sintef.no)

[2] *Centre for Ships and Ocean Structures, Norwegian University of Science and Technology,*
NO - 7491 Trondheim, Norway (e-mail: morten.breivik@ieee.org)

[3] *Department of Engineering Cybernetics, Norwegian University of Science and Technology,*
NO - 7491 Trondheim, Norway (e-mail: fossen@ieee.org)

[4] *Department of Marine Technology, Norwegian University of Science and Technology,*
NO - 7491 Trondheim, Norway (e-mail: odd.faltinsen@ntnu.no)

Abstract: Ship-to-ship operations, such as underway replenishment (UNREP), lightering, etc., entail potentially hazardous situations due to the possibility of collisions between two ships operating in close proximity. In order to ensure safe joint operations with collision avoidance, knowledge of the hydrodynamic interaction loads between the two vessels is highly advantageous. This paper thus considers the hydrodynamic interaction effects between two advancing ships and their maneuvering behaviors in calm water during typical replenishment operations. For this purpose, a unified seakeeping and maneuvering model of two interacting ships based on a two-time scales and modular concept relevant for calm water is employed. The maneuvering module is based on generalized slender-body theory, while calm-water interaction forces and moments between the two ships are estimated using Newman-Tuck theory. Automatic steering and speed control algorithms for both ships are also employed to achieve high-precision and collision-free UNREP maneuvers, which is illustrated through a numerical simulation involving the well-known 'ESSO OSAKA' and 'MARINER' models from the ship literature.

Keywords: Underway replenishment, Calm water, Maneuvering, Hydrodynamic interaction effects, Two–time scale model, Automatic motion control

1. INTRODUCTION

Underway replenishment (UNREP) operations involve cargo transfer between two or more cooperating ships in transit (Miller and Combs, 1999), and represent very important capabilities that enable navies to accomplish global missions. In this context, the task of the so-called guide ship is to maintain steady course and speed while the so-called approach ship moves up alongside the guide to receive, e.g., fuel, munitions, food, and personnel, see Fig. 1. When the two ships start to operate in close proximity, their maneuvering behavior becomes affected by the hydrodynamic interaction loads between them. These loads may cause strong and sudden attraction or repulsion effects between the ships, and the magnitude and duration of the effects depend on the size of the vessels, their lateral and longitudinal separation distance, speeds, wetted hull shapes, water depth, and transverse distance from a channel bank. The interconnection among these variables may initiate a deviation in the desired course of one or both of the ships, creating a possible collision situation which may be further worsened if the involved ships experience significant environmental loads due to waves, wind, and current.

The present study investigates UNREP maneuvers involving two advancing ships in calm water. Hydrodynamic interaction loads are theoretically predicted by Newman-Tuck (1974) theory, which is one among several slender-body theories (such as, e.g., Abkowitz et al. (1970), Dand (1974), Yeung (1978), and Kijima and Yasukawa (1984)) capable of predicting the interaction effects between two bodies in infinite fluid at moderate Froude numbers $Fn \lessapprox 0.2$. These theories are based on potential flow, which means that the viscous effects are not accounted for and that calm-water conditions are assumed.

A unified seakeeping and maneuvering modular model was applied to two ships with forward speed in calm water by Skejic and Faltinsen (2007, 2008) and Skejic (2008). However, to achieve successful simulations of an UNREP maneuver, a unified seakeeping and maneuvering model must also include motion control modules on both ships that are capable of satisfying requirements imposed by the approach and guide ship in a way that mimics, as much as possible, realistic situations in accordance with the international and US Navy regulations (Naval Warfare Publication, 2004).

Using these modules, a numerical simulation of an UNREP maneuver in calm water is presented and discussed later in the text, accounting for the main maneuvering and motion control variables of ship speeds, longitudinal and lateral separation distances, rudder inclination angles, and hydrodynamic interaction effects. These data are shown in

Fig. 1. Two naval ships performing underway replenishment; the guide ship to the left and the approach ship to the right. Courtesy of the US Navy.

order to exemplify the critical stages of an UNREP maneuver, i.e., stages which are potentially dangerous for both ships from a navigational safety point of view.

Recent work concerning UNREP-like formation control issues can be found in (Skjetne, 2005), (Ihle, 2006), (Kyrkjebø, 2007), and (Børhaug, 2008). Unfortunately, these authors do not consider the hydrodynamic interaction effects occurring between the formation members. However, previous work more in the vein of this paper can be found in (Dimmick, 1978) and (Brown, 1983).

2. MATHEMATICAL MODELING

Modeling UNREP maneuvers is achieved by a unified model formulated on two time scales, i.e., a slowly and rapidly varying time scale, respectively related to maneuvering and seakeeping analyses.

The Cartesian right-handed maneuvering body-fixed coordinate systems $O_{Ci}x_{Ci}y_{Ci}$, shown in Fig. 2 with positive z_{Ci} – axis pointing upwards, are used both for the seakeeping and maneuvering problem. Here, index $i \in$ [A, B] represents the approach ship A and the guide ship B, respectively. A transformation between the coordinate frames that define the seakeeping and maneuvering problem is described by Skejic (2008).

The centre of gravity (CG) of each ship is in the origin O_{Ci} of the coordinate system $O_{Ci}x_{Ci}y_{Ci}$, which is located in the lateral symmetry plane of each body. $OX_EY_EZ_E$ is an Earth-fixed coordinate system with positive Z_E – axis pointing upwards. X_i and Y_i are hydrodynamic forces defined positively in the positive x_{Ci} and y_{Ci} directions, respectively. K_i denotes the roll (heel) moment about the x_{Ci} – axis, while N_i is the yaw moment about the z_{Ci} – axis, defined positively as shown in Fig. 2. Furthermore, u_i and v_i are x_{Ci} and y_{Ci} – components of the total ship speed $U_i = \sqrt{u_i^2 + v_i^2}$. The roll angular speed is represented by p_i, while the yaw angular speed is denoted by r_i. Also, ϕ_i, ψ_i, δ_i and $\beta_i \triangleq \text{atan}(-v_i/u_i)$ are respectively the roll (heel), yaw (heading), rudder, and drift angles from the maneuvering analysis. The longitudinal and lateral distances between the CGs of the ships (O_{CA} and O_{CB}) are s and e, respectively, defined in respect to the coordinate system of the guide ship B. The ship lengths between perpendiculars are L_i for $i \in$ [A, B].

The slowly-varying system (1) consistent with the ITTC (1975) nomenclature and used by the maneuvering module represents a modified version of the generalized surge-sway-yaw slender-body theory by Söding (1982), derived from the 6 DOF nonlinear maneuvering equations given by Imlay (1961). One modification relative to Söding (1982) is that coupling with roll is accounted for. A moderate Froude number, i.e., $Fn <\approx 0.2$ is implicitly assumed so that steady wave generation is small.

The maneuvering model is based on a modular concept, which means that the forces and moments in (1) due to rudder (subscript R), resistance R and propulsion T, and nonlinear viscous cross-flow (subscript CF) form the separate modules. Further details about each module are given by Skejic and Faltinsen (2008) and Skejic (2008).

The ship mass, moments and products of inertia within (1) are respectively defined as M, $I_{44} = \widetilde{I}_{44} + Mz_g^2$, $I_{66} = \widetilde{I}_{66}$, $-I_{46} = -\widetilde{I}_{46}$, and $-I_{64} = -\widetilde{I}_{64}$, where the symbol '~' denotes values with respect to the centre of gravity O_C of the maneuvering body–fixed coordinate systems, while $i \in$ [A, B].

$$
\begin{bmatrix} M & 0 & 0 & 0 \\ 0 & M & 0 & 0 \\ 0 & 0 & I_{44}-Mz_g^2 & -I_{46} \\ 0 & 0 & -I_{64} & I_{66} \end{bmatrix}_i \begin{bmatrix} \dot{u} \\ \dot{v} \\ \dot{p} \\ \dot{r} \end{bmatrix}_i + \begin{bmatrix} 0 & -Mr & 0 & 0 \\ 0 & 0 & 0 & Mu \\ 0 & 0 & 0 & 0 \\ 0 & 0 & 0 & 0 \end{bmatrix}_i \begin{bmatrix} u \\ v \\ p \\ r \end{bmatrix}_i =
$$

$$
= \begin{bmatrix} X_{\dot{u}} & 0 & 0 & 0 \\ 0 & Y_{\dot{v}} & Y_{\dot{p}} & Y_{\dot{r}} \\ 0 & K_{\dot{v}} & K_{\dot{p}} & K_{\dot{r}} \\ 0 & N_{\dot{v}} & N_{\dot{p}} & N_{\dot{r}} \end{bmatrix}_i \begin{bmatrix} \dot{u} \\ \dot{v} \\ \dot{p} \\ \dot{r} \end{bmatrix}_i + \begin{bmatrix} 0 & 0 & 0 & 0 \\ 0 & Y_v & Y_p & Y_r \\ 0 & K_v & K_p & K_r \\ 0 & N_v & N_p & N_r \end{bmatrix}_i \begin{bmatrix} u \\ v \\ p \\ r \end{bmatrix}_i +
$$

$$
+ \begin{bmatrix} 0 & -C_{TN}Y_{\dot{v}}r & -Y_{\dot{p}}r & -Y_{\dot{r}}r \\ 0 & 0 & 0 & X_{\dot{u}}u \\ 0 & 0 & 0 & 0 \\ 0 & -X_{\dot{u}}u & 0 & 0 \end{bmatrix}_i \begin{bmatrix} u \\ v \\ p \\ r \end{bmatrix}_i - \begin{bmatrix} 0 & 0 & 0 & 0 \\ 0 & 0 & 0 & 0 \\ 0 & 0 & C_{44} & 0 \\ 0 & 0 & 0 & 0 \end{bmatrix}_i \begin{bmatrix} \int_0^t u dt \\ \int_0^t (v + z_g p + u\psi) dt \\ \phi \\ \psi \end{bmatrix}_i +
$$

$$
+ \begin{bmatrix} X_R \\ Y_R \\ 0 \\ N_R \end{bmatrix}_i + \begin{bmatrix} -R(u)+(1-t)T(u) \\ 0 \\ 0 \\ 0 \end{bmatrix}_i + \begin{bmatrix} 0 \\ Y_{CF} \\ K_{CF} \\ N_{CF} \end{bmatrix}_i + [INT]_i . \qquad (1)
$$

Hydrodynamic interaction sway forces and yaw moments estimated by Newman-Tuck (1974) theory are accounted for by the vector [*INT*], and given as follows:

- for i = A; $[INT]|_{i=\text{A}} = [0\ Y_{AB}\ 0\ N_{AB}]^T$,
- for i = B; $[INT]|_{i=\text{B}} = [0\ Y_{BA}\ 0\ N_{BA}]^T$,

where Y_{AB} stands for the interaction sway force on ship A (approach ship) due to the presence of ship B (guide ship), while N_{AB} stands for the interaction yaw moment on ship A due to the presence of ship B, and vice versa. The positive direction of the interaction loads is defined with the arrows as indicated in Fig. 2.

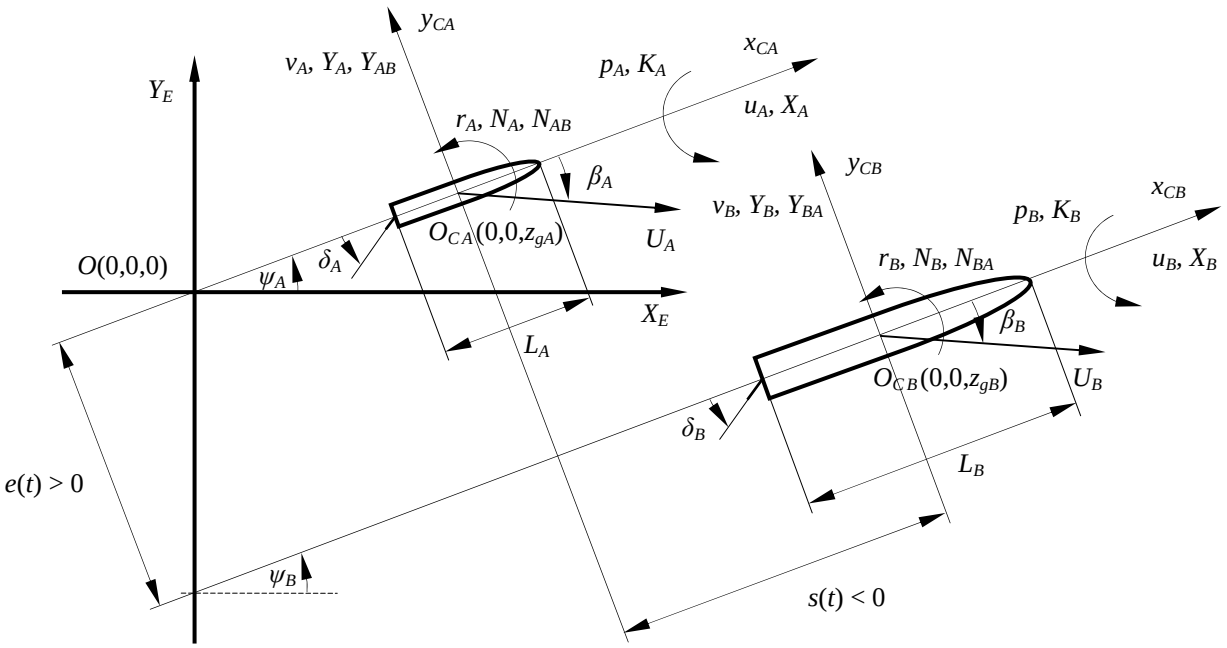

Fig. 2. Coordinate systems for approach ship A and guide ship B.

Let us now focus on the parameters within (1) which are of importance for the UNREP operation analysis. The C_{TN} − nondimensional coefficient is associated with the resistance term $-C_{TN}Y_{\dot{v}}r$ and is an empirical coefficient that modifies the predictions of potential flow theory at moderate speeds. The C_{TN} coefficient in (1) has been selected as 1.0 in the later numerical example of an UNREP maneuver since both ships are moving mainly on a straight course in a joint parallel configuration.

Simulation wise, the maneuvering system (1) is solved with a time integration algorithm based on the 4th-order explicit Runge-Kutta method with constant time steps.

The seakeeping module based on the STF strip theory of Salvesen-Tuck-Faltinsen (1970) generalized to 6 DOF is used to calculate zero encounter-frequency added mass values which are needed to estimate parts of the maneuvering derivatives, see (1).

The vessel positions in the Earth-fixed coordinate system $OX_EY_EZ_E$ (see Fig. 2) can in general be obtained by transformation of the slowly time-varying velocities $(u, v, w, p, q, r)_i$, defined with respect to the maneuvering ship-fixed coordinate systems $O_{Ci}x_{Ci}y_{Ci}$, into the velocities $\left(\dot{X}_E, \dot{Y}_E, \dot{Z}_E, \dot{\Phi}_E, \dot{\Theta}_E, \dot{\Psi}_E\right)_i$, which are defined with respect to the Earth-fixed coordinate system $OX_EY_EZ_E$. The transformation is carried out by using the finite Euler angles matrices and can be expressed as

$$\left[\dot{X}_E \quad \dot{Y}_E \quad \dot{Z}_E \quad \dot{\Phi}_E \quad \dot{\Theta}_E \quad \dot{\Psi}_E\right]_i^T = \boldsymbol{J}_{6\times6_i}\left[u \quad v \quad w \quad p \quad q \quad r\right]_i^T, \tag{2}$$

where $\dot{X}_E$ represents the time derivative dX_E/dt, while $\boldsymbol{J}_{6\times6_i}$ represents the finite Euler angles matrices given as

$$\boldsymbol{J}_{6\times6_i} \triangleq \begin{bmatrix} \boldsymbol{R}_{3\times3} & \boldsymbol{0}_{3\times3} \\ \boldsymbol{0}_{3\times3} & \boldsymbol{S}_{3\times3} \end{bmatrix}_i,$$

where

$$\boldsymbol{R}_{3\times3_i} \triangleq \begin{bmatrix} \cos\psi\cos\theta & -\sin\psi\cos\phi+\cos\psi\sin\theta\sin\phi & \sin\psi\sin\phi+\cos\psi\cos\phi\sin\theta \\ \sin\psi\cos\theta & \cos\psi\cos\phi+\sin\phi\sin\theta\sin\psi & -\cos\psi\sin\phi+\sin\theta\sin\psi\cos\phi \\ -\sin\theta & \cos\theta\sin\phi & \cos\theta\cos\phi \end{bmatrix}_i,$$

$$\boldsymbol{S}_{3\times3_i} \triangleq \begin{bmatrix} 1 & \sin\phi\tan\theta & \cos\phi\tan\theta \\ 0 & \cos\phi & -\sin\phi \\ 0 & \sin\phi/\cos\theta & \cos\phi/\cos\theta \end{bmatrix}_i,$$

and $\boldsymbol{0}_{3\times3_i}$ is the 3x3 zero matrix for $i\in$ [A, B].

3. MOTION CONTROL SYSTEM

UNREP operations are currently performed manually, demanding the very best of helmsmanship. In particular, the hydrodynamic interaction effects appearing when the cooperating ships close in on each other make it difficult to achieve desired inter-vessel spacing by manual course and speed control. However, the required UNREP maneuvers might be automated by developing a purposeful motion control system. Potential benefits include enhanced maneuver precision and increased crew safety. This section considers the development of such a control system, which is used for the simulation reported later.

The motion control system that is illustrated in Fig. 3 ensures operator-specified inter-vessel spacing by automatic course and speed control for an approach ship A attempting to rendezvous with a guide ship B. Requested lateral (transverse) distance e (see Fig. 2) is given as an input to the steering module, which computes the heading control

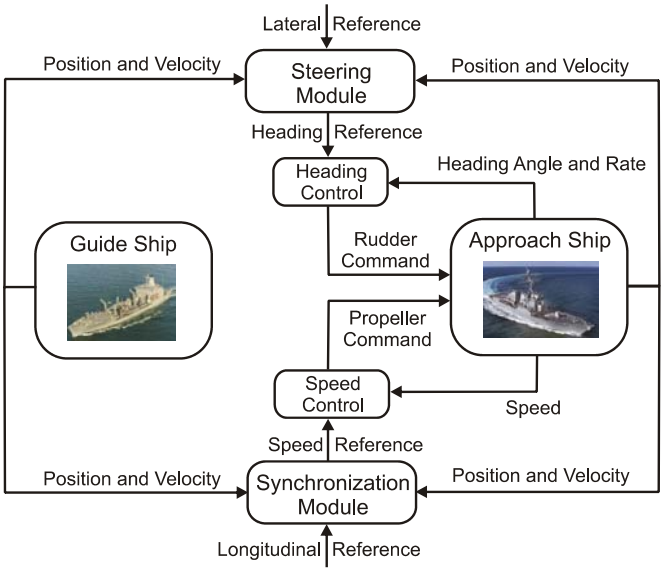

Fig. 3. The main components of a motion control system used by an approach ship taking part in an automated UNREP maneuver; a steering subsystem ensures lateral alignment vis-à-vis the guide ship, while a synchronization subsystem takes care of the required longitudinal alignment.

reference signals enabling lateral alignment. The steering module is an outer-loop controller whose output is fed to an inner-loop heading controller (autopilot) that computes the associated rudder command. Requested longitudinal distance s is given as an input to the synchronization module, which computes the speed control reference signals that ensure longitudinal alignment. The synchronization module is also an outer-loop controller, whose output acts as reference to an inner-loop speed controller that computes the associated propeller command. In sum, inner-loop kinetic controllers work with outer-loop kinematic controllers to perform a specified UNREP maneuver.

In what follows, the CG of the approach ship A is represented by its planar position $\mathbf{p}_A \triangleq \left[X_{E_A}, Y_{E_A} \right]^T \in \mathbb{R}^2$ and velocity $\mathbf{v}_A \triangleq \mathrm{d}\mathbf{p}_A / dt \triangleq \dot{\mathbf{p}}_A \in \mathbb{R}^2$, stated relative to the Earth-fixed coordinate system $OX_EY_EZ_E$ whose X_E – axis points North (see Fig. 2). Using standard notation (Fossen, 2002), the total speed of the approach ship A is then denoted

$$U_A \triangleq \left| \mathbf{v}_A \right| = \sqrt{\dot{X}_{E_A}^2 + \dot{Y}_{E_A}^2} \geq 0 \tag{4}$$

while the course angle is denoted

$$\chi_A \triangleq \operatorname{atan2}\left(\dot{Y}_{E_A}, \dot{X}_{E_A} \right) \in \mathbb{S} \triangleq \left[-\pi, \pi \right], \tag{5}$$

where atan2(y,x) is the four-quadrant version of atan(y,x) $\in \langle -\pi/2, \pi/2 \rangle$. Similarly, the guide ship B is represented by the variables $\mathbf{p}_B$, $\mathbf{v}_B$, U_B, and χ_B.

3.1 Steering subsystem

The outer-loop steering module of the approach ship A utilizes the fact that the guide ship B maintains steady course and speed during the UNREP operation. Such steady course and speed of ship B imply straight-line motion, which can be parameterized by three variables, i.e., two position variables representing a point along the straight-line path and one orientation variable representing the inclination of this path relative to North, i.e., relative to the X_E – axis, see Fig. 2. Hence, these variables can be represented by $\mathbf{p}_B$ and χ_B.

Using the lookahead-based steering law from (Breivik and Fossen, 2008), and specifying the desired inter-vessel lateral spacing as $e_d > 0$, the approach ship A is able to assume a parallel course with the guide ship B by adhering to the desired course angle

$$\chi_{dA} = \chi_B + \chi_r, \tag{6}$$

where χ_B is the course angle of the guide ship B, while

$$\chi_r = \arctan(-\tilde{e} / \Delta) \tag{7}$$

is a relative steering angle which employs knowledge about the cross-track distance to the parallel course which is implicitly defined by e_d. Specifically,

$$\tilde{e} \triangleq e - e_d, \tag{8}$$

where e represents the cross-track distance to the guide ship path, which can be calculated by

$$e = -(X_{E_A} - X_{E_B}) \sin \chi_B + (Y_{E_A} - Y_{E_B}) \cos \chi_B. \tag{9}$$

Also, $\Delta > 0$ represents a tuning parameter in the steering law called the lookahead distance (Papoulias, 1991). This parameter is given in meters and usually takes values between 4 to 5 ship lengths (Healey, 2006).

Since the relationship between the course, heading, and sideslip (drift) angles for a ship is typically given by

$$\chi = \psi - \beta, \tag{10}$$

where β = atan($-v$,u), the desired heading angle must be computed by

$$\psi_{dA} = \chi_{dA} + \beta_A, \tag{11}$$

where χ_{dA} is given by (6).

The inner-loop heading controller is then just chosen as a simple PID control law

$$\delta_A = -k_{p,\tilde{\psi}_A} \tilde{\psi}_A - k_{d,\tilde{\psi}_A} \dot{\tilde{\psi}}_A - k_{i,\tilde{\psi}_A} \int_0^t \tilde{\psi}_A \, dt, \tag{12}$$

where δ_A represents the rudder angle, $\tilde{\psi}_A \triangleq \psi_A - \psi_{dA}$, while ψ_{dA} is given by (11). Also, the time derivative of this angle might be approximated by

$$\dot{\psi}_{dA} \approx \dot{\chi}_{dA} \tag{13}$$

when assuming steady-state conditions, i.e., $\dot{\beta}_A \approx 0$. Furthermore,

$$\dot{\chi}_{dA} = \frac{\dot{X}_{E_A} \sin \chi_B - \dot{Y}_{E_A} \cos \chi_B}{\tilde{e}^2 + \Delta^2} \tag{14}$$

when the guide ship B moves in a straight line, i.e., $\dot{\chi}_B = 0$.

Finally, $k_{d,\tilde{\psi}_A} > k_{p,\tilde{\psi}_A} > k_{i,\tilde{\psi}_A} > 0$ with $k_{d,\tilde{\psi}_A} \approx 5k_{p,\tilde{\psi}_A}$ and $k_{p,\tilde{\psi}_A} \approx 10k_{i,\tilde{\psi}_A}$. Note that (12) inherently assumes the convention that a positive rudder angle gives positive yaw rate, i.e., $\delta_A = -\delta_{rA}$, where δ_{rA} is the real rudder angle.

3.2 Speed subsystem

In addition to assuming a parallel course with the guide ship B (lateral alignment), the approach ship A must also synchronize its motion with the guide ship B along this course (longitudinal alignment). This synchronization can be achieved by commanding a desired total speed U_{dA} for the approach ship A as

$$U_{dA} = U_B + U_{A,max} \frac{s}{\sqrt{s^2 + \Delta_s^2}}, \qquad (15)$$

where U_B is the total speed of the guide ship B, $U_{A,max}$ denotes the maximum total speed with which the approach ship A should approach the guide ship B, and where

$$s = (X_{E_A} - X_{E_B}) \cos \chi_B + (Y_{E_A} - Y_{E_B}) \sin \chi_B \qquad (16)$$

is the along-course distance between the approach ship and the guide ship, see Fig. 2. Also, $\Delta_s > 0$ is a tuning parameter specifying the rendezvous behaviour toward the projection of the guide ship B onto the parallel course defined by e_d, ensuring that the approach ship A smoothly ramps down its total speed to U_B as the along-course distance s goes to zero.

Since the relationship between the total speed, surge speed, and sway speed of a ship is given by $U = \sqrt{u^2 + v^2}$, the desired surge speed must be computed by

$$u_{dA} = \sqrt{U_{dA}^2 - v_A^2}, \qquad (17)$$

where the total speed U_{dA} is given by (15). The inner-loop speed controller is then just chosen as a simple PI control law

$$n_A = -k_{p,\tilde{u}_A} \tilde{u}_A - k_{i,\tilde{u}_A} \int_0^t \tilde{u}_A dt, \qquad (18)$$

where n_A represents the number of propeller revolutions, $\tilde{u}_A \triangleq u_A - u_{dA}$, and u_{dA} is given by (17). Finally, $k_{p,\tilde{u}_A} > k_{i,\tilde{u}_A} > 0$ with $k_{p,\tilde{u}_A} \approx 10k_{i,\tilde{u}_A}$.

Note that in the following case study, the guide ship B is also controlled by a rudder controller such as given in (12) and a propeller controller such as given in (18), albeit with constant course and speed references to keep a steady course and speed.

4. CASE STUDY

The following case study concerns an UNREP maneuver in calm water involving the 'ESSO OSAKA' and 'MARINER' ships studied by the ITTC (1975, 2002) with main particulars according to Fig. 4. It should be noted that further details concerning the propulsion and rudder system for these ships may be found in Skejic and Faltinsen (2008).

	'ESSO OSAKA'	***'MARINER'***
Hull particulars		
Length between perpendiculars, L_{PP}	325.0 m	160.934 m
Breadth, B	53.0 m	23.165 m
Draft (even keel), T	21.79 m	7.468 m
Block coefficient, C_B	0.831	0.61
Displacement	319455.3 t	16800 t
Centre of gravity, CG (x_g, y_g, z_g)	(0, 0, -8.66) m	(0, 0, -2.45) m
Centre of buoyancy, CB (x_b, y_b, z_b)	(0, 0, -10.82) m	(0, 0, -3.48) m
Metacentric height (transverse), G_{MT}	8.014 m	4.551 m
Metacentric height (longitudinal), G_{ML}	331.4 m	191.361 m
Radius of gyration, roll k_{xx}	15.9 m	6.942 m
Radius of gyration, pitch/yaw k_{yy}/k_{zz}	81.25 m	40.233 m
Nominal (design) ship speed, U	16 knots	20 knots

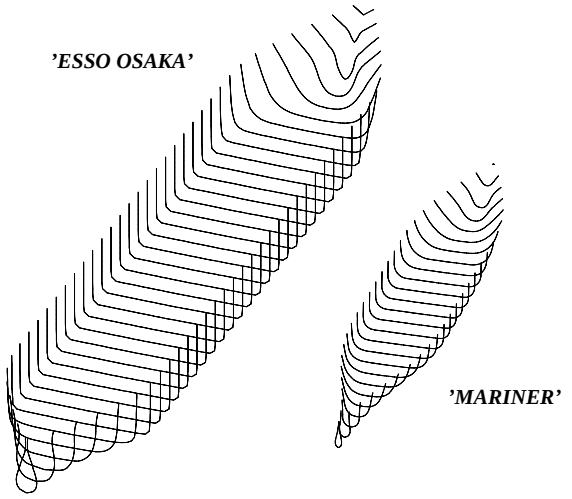

Fig. 4. Principal characteristics of the 'ESSO OSAKA' and 'MARINER' ships with examples of the cross sectional distribution of the submerged part of the hulls at even keel.

Fig. 5 presents the UNREP maneuver in calm water between a smaller approach ship A ('MARINER') and a larger guide ship B ('ESSO OSAKA'). The starting positions of the approach ship A and guide ship B are different, and the motion control module is used on both ships from the beginning of the simulation.

Ship B advances on a straight course with a constant forward speed of 10 knots, while the maximum rendezvous speed of ship A is restricted to 14 knots. The motion control system simultaneously engages speed and rudder controls on the approach ship so that she tries to establish the desired longitudinal distance s = 0 m between the ships, as well as a transverse clearance of $e - 0.5(B_A + B_B) = 40$ m between the facing sides of both hulls, whose value is defined in respect to the coordinate system of ship B. Here, B_A is the beam of the approach ship A, while B_B is the beam of the guide ship B. Hence, $e_d = 0.5(B_A + B_B) + 40$ m.

A worst case scenario entails a collision between the two ships. The motion controllers thus replace the experienced helmsmen and deck crew on both ships to avoid such incidents. As time goes on, approach ship A catches up with the guide ship B at a position of approximately 6500 m with respect to $OX_EY_EZ_E$, see Fig. 5. The relative longitudinal

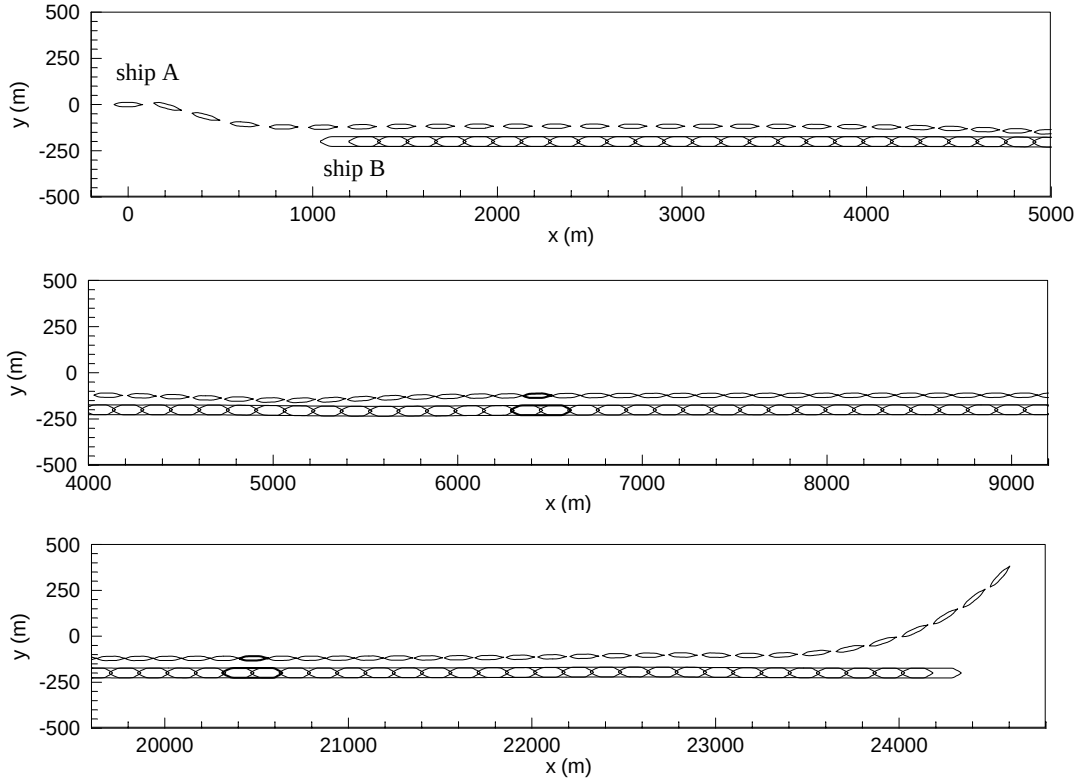

Fig. 5. An UNREP maneuver between the 'MARINER' and 'ESSO OSAKA' ships advancing in calm water. The starting positions: Ship A (0 m, 0 m) and ship B (1200 m, – 200 m). Note that the part of the figure where 9200 m < x < 19600 m is not shown since for that range both ships are on steady course in a parallel abeam configuration.

position s between both ships decreases to zero, i.e., both ships become abeam with zero relative speed ($u_A - u_B$) = 0 m/s for both ships on the desired transversal distance e_d = 0.5(B_A + B_B) + 40 m. Fig. 5 shows the simulated UNREP trajectories for both ships, and the rendezvous maneuver can be seen in the region where 0 m $\leq x <\approx$ 6500 m.

In conjunction with this maneuver, both ships experience hydrodynamic interaction loads. After an initial repulsion phase, the ships encounter an attraction phase where the peak values of interaction sway forces and yaw moments tend to swing the bow of the each ship away from each other. Following this behavior, the hydrodynamic interaction effects are successfully stabilized and the cargo transfer can start.

In Fig. 6, some relevant motion control variables and hydrodynamic interaction loads related to the UNREP maneuver are shown. As can be seen, the rudder actions on both ships are opposing the experienced yaw moments which tend to swing the bow of each ship away from each other. Also, the hydrodynamic interaction loads attain constant behavior during the phase where the transfer operation is in progress, which is reasonable due to the calm-water operational conditions.

The last stage of the UNREP maneuver takes place from a position of about 20500 m, where the approach ship A slowly starts to increase its speed with respect to the guide ship B, which remains at steady speed and course. The possibility of collision increases again since both ships now experience repulsive interaction sway forces and yaw moments pointing in the same direction. Fortunately, the collision risk is reduced to a minimum due to the employed automatic motion control system. Finally, when the relative speed ($u_A - u_B$) between the approach ship A and the guide ship B reaches approximately 1 knot, a rudder on the approach ship A is deflected to the port side so that she actually disengages herself from the parallel straight-line configuration with the guide ship B. This UNREP maneuver resembles quite well a real-life maneuver since it is performed according to the US Navy replenishment rules (Naval Warfare Publication, 2004).

Our discussion related to the above numerical example can be shortly summarized as follows. First of all, the UNREP maneuver in calm water showed that the hydrodynamic interaction loads between two ships estimated with Newman-Tuck (1974) theory cannot be neglected when the two ships are involved in close-proximity maneuvers. We also demonstrated the application of an automatic motion control system. The employment of such a control module has been chosen to exemplify the requirements for experienced helmsmen and deck crews needed to successfully accomplish UNREP operations in either calm water or waves, particularly avoiding any possible collision hazards during such close-proximity maneuvers.

5. CONCLUSIONS

The scenario of two advancing ships involved in close-proximity maneuvers in calm water has been simulated by using a two-time scale unified seakeeping and maneuvering

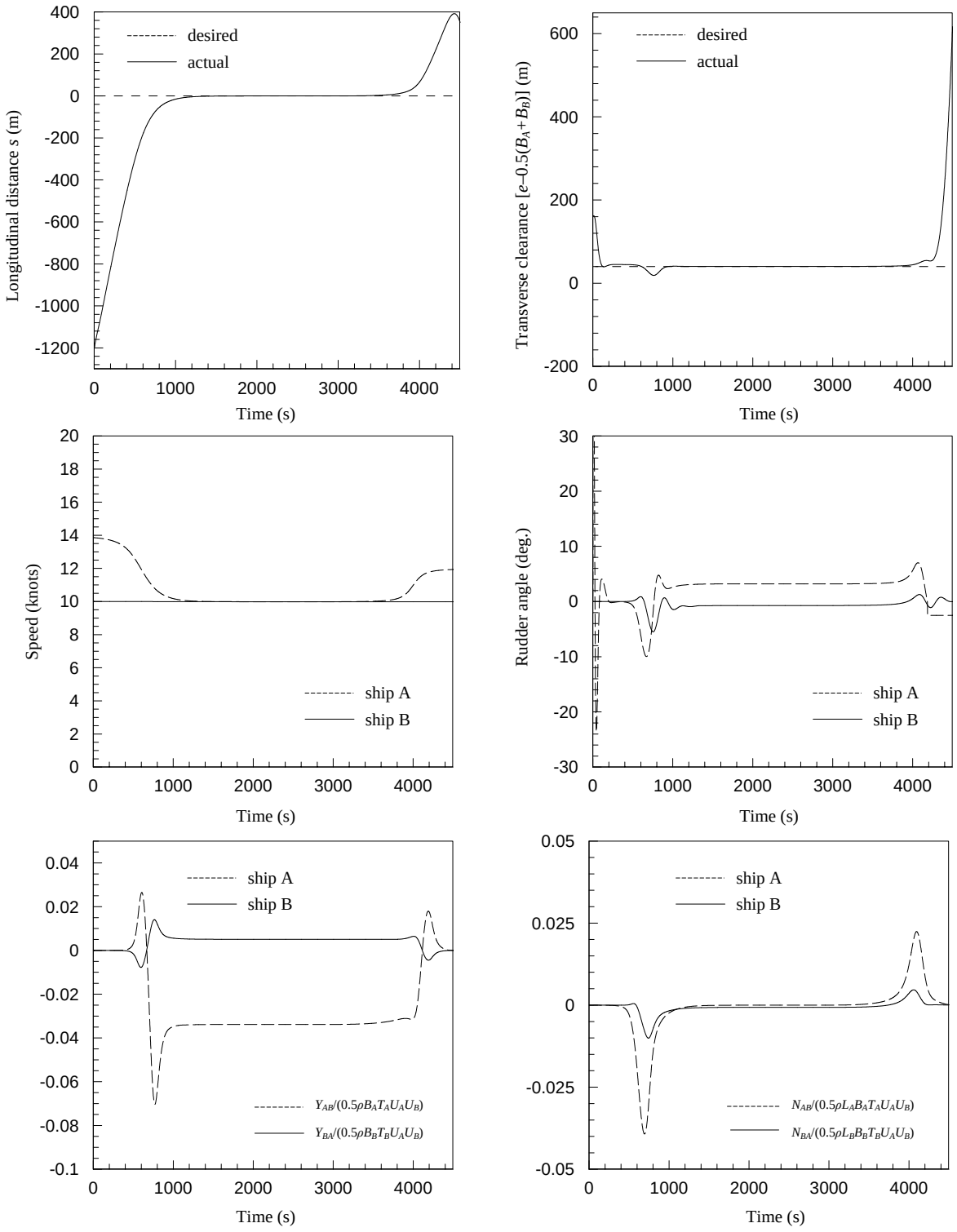

Fig. 6. Basic motion control variables and hydrodynamic interaction loads during the UNREP maneuver between the 'MARINER' and 'ESSO OSAKA' ships advancing in calm water. B_A denotes the beam of the 'MARINER' hull on the main frame, B_B denotes the beam of the 'ESSO OSAKA' hull on the main frame, while 1 knot = 0.5144 m/s.

model of two interacting ships by Skejic and Faltinsen (2007) and Skejic (2008). This model is based on a modular concept which in general accounts for the propulsion and resistance, rudder forces and moments, nonlinear viscous loads, calm-water hydrodynamic interaction loads, and mean second-order wave loads, which are all modelled as separate modules

to allow for the possibility to replace or update the existing numerical procedures in a module without affecting the other modules. The calm-water hydrodynamic interaction loads between the two ships were estimated with Newman-Tuck (1974) far-field theory. Also, the latest theoretical and semi-empirical methods covering the hull, propeller, and rudder interaction effects were used, see Skejic (2008) for details.

Finally, a motion control module involving a guidance system as well as steering and speed controllers was employed for both ships in order to achieve high-precision and collision-free UNREP operations between two advancing ships of different type and size. This module was included to illustrate the critical stages of such operations. Furthermore, an UNREP maneuver was simulated in accordance with the international and US Navy regulations (Naval Warfare Publication, 2004) in order to consider realistic conditions.

Future work will concern UNREP operations in waves to further increase the realism of the simulations and the validity of the motion control system performance. Ultimately, it would be interesting to validate the theoretical two-time scale model with its motion control module for the influence of hydrodynamic interaction loads, waves, and wind for two ships involved in close-proximity maneuvers through experiments with free-running models exposed to similar wave and wind conditions.

REFERENCES

Abkowitz, M.A., G.M. Ashe and R.M. Fortson (1970). Interaction effects of ships operating in proximity in deep and shallow water. In *Proceedings of the 8th Symposium. on Naval Hydrodynamics*, Rome, Italy, pp. 671–691.

Breivik, M. and T.I. Fossen (2008). Guidance laws for planar motion control. In *Proceedings of the 47th IEEE CDC*, Cancun, Mexico, pp. 570–577.

Brown, S.H. and J.G. Dimmick (1983). Simulation analysis of steering control during underway replenishment. *Journal of Ship Research*, 27(4), pp. 236–251.

Børhaug, E. (2008). Nonlinear Control and Synchronization of Mechanical Systems. PhD thesis, Department of Engineering Cybernetics, Norwegian University of Science and Technology, Trondheim, Norway.

Dand, I.W. (1974). Some aspects of maneuvering in collision situations in shallow water. In *Proceedings of the 10th Symposium on Naval Hydrodynamics*, Cambridge, MA, USA, pp. 261–275.

Dimmick, J.G., R. Alvestad and S.H. Brown (1978). Two-block romeo! (Simulation of ship steering control for underway replenishment). In *Proceedings of the 28th IEEE Vehicular Conference*, New York, USA, pp. 382–389.

Fossen, T.I. (2002). *Marine Control Systems: Guidance, Navigation and Control of Ships, Rigs and Underwater Vehicles*. Marine Cybernetics, Trondheim, Norway.

Healey, A.J. (2006). Guidance laws, obstacle avoidance and artificial potential functions. In *Advances in Unmanned Marine Vehicles* (G.N. Roberts and R. Sutton, Eds.), IEE Control Engineering Series 69, pp. 43-66.

Ihle, I.-A. F. (2006). Coordinated Control of Marine Craft. PhD thesis, Department of Engineering Cybernetics, Norwegian University of Science and Technology, Trondheim, Norway.

Imlay, F.H. (1961). The Complete Expressions for Added Mass of a Rigid Body Moving in an Ideal Fluid. DTMB Report 1528, Washington D.C., USA.

ITTC (1975). The Mariner model cooperative test program—correlations and applications. Report of the Manoeuvrability Committee. In *Proceedings of the 14th ITTC*, Ottawa, Canada, pp. 414–427.

ITTC (2002). The specialist committee on *Esso Osaka*. Final report and recommendations to the 23rd ITTC. In *Proceedings of the 23rd ITTC*, Venice, Italy, pp 581–617.

Kijima, K. and H. Yasukawa (1985). Manoeuvrability of ships in narrow waterway. *J. Soc. Naval Architects of Japan*, 23, pp. 25–37.

Kyrkjebø, E. (2007). Motion Coordination of Mechanical Systems: Leader-Follower Synchronization of Euler-Lagrange Systems using Output Feedback Control. PhD thesis, Department of Engineering Cybernetics, Norwegian University of Science and Technology, Trondheim, Norway.

Miller, M.O. and J.A. Combs (1999). The Next Underway Replenishment System. *Naval Engineers Journal*, 111(2), pp. 45–55.

Naval Warfare Publication (2004). Underway Replenishment, NWP 4–01.4 (Formerly NWP 14 (Rev. E)), Department of the US Navy.

Newman, J.N. and E.O. Tuck (1974). Hydrodynamic interaction between ships. In *Proceedings of the 10th Symposium on Naval Hydrodynamics*, Cambridge, MA, USA, pp. 35–70.

Papoulias, F.A. (1991). Bifurcation analysis of line of sight vehicle guidance using sliding modes. *International Journal of Bifurcation and Chaos*, 1(4), pp. 849–865.

Salvesen, N., E.O. Tuck and O.M. Faltinsen (1970). Ship motions and sea loads. *Trans. SNAME*, 78, pp. 250–287.

Skejic, R. and O.M. Faltinsen (2007). A unified seakeeping and maneuvering analysis of two interacting ships. In *Proceedings of the 2nd International Conference on Marine Research and Transportation*, Ischia, Italy, pp. 209–218.

Skejic, R. and O.M. Faltinsen (2008). A unified seakeeping and maneuvering analysis of ships in regular waves. *Journal of Marine Science and Technology*, 13, pp. 371–394.

Skejic, R. (2008). Maneuvering and Seakeeping of a Single Ship and of Two Ships in Interaction. PhD thesis, Department of Marine Technology, Norwegian University of Science and Technology, Trondheim, Norway.

Skjetne, R. (2005). The Maneuvering Problem. PhD thesis, Department of Engineering Cybernetics, Norwegian University of Science and Technology, Trondheim, Norway.

Söding, H. (1982). Prediction of ship steering capabilities. *Schiffstechnik*, 29, pp. 3–29.

Yeung, R.W. (1978). On the interaction of slender ships in shallow water. *J. Fluid Mech.*, 85, pp. 143–159.